

CHARACTERIZATION OF TRANSPORT AND ADSORPTION MECHANISMS IN CHROMATOGRAPHIC MEDIA

zur Erlangung des akademischen Grades eines
DOKTORS DER INGENIEURWISSENSCHAFTEN (Dr.-Ing.)

von der Fakultät für Chemieingenieurwesen und Verfahrenstechnik der
Universität Fridericiana Karlsruhe (TH)
angenommene

DISSERTATION
(Tag der mündlichen Prüfung: 18.12.2009)

von
Dipl.-Biol. (t.o.) Florian Dimer
aus Hannover

Referent: Prof. Dr.-Ing. Jürgen Hubbuch
Koreferent: PD. Dr.-Ing. Matthias Franzreb

Acknowledgments

It is on my heart to pass awards to the following people:

Prof. Dr. Christian Wandrey for the great opportunity to start my PhD thesis in the Institute of Biotechnology 2 at the Research Centre in Juelich and for the great working conditions.

Prof. Dr. Juergen Hubbuch for his personal, scientific and financial support and the freedom he gave me to develop my topic ... and for teaching me how enlightening improvised scientific talks can be.

PD. Dr.-Ing. Matthias Franzreb for taking the time to be the second referee of my thesis.

Dipl. Biotechnol. Annette Berg for countless fruitful talks at a thai restaurant in Aachen, for even more politically incorrect jokes at work and for teaching me how to get up before sunrise, even in summertime.

Dr. Ing. Matthias Wiendahl formerly (and still) known as Matthias Bensch for visualizing the thermodynamics of the chaotropic effect of salts and for spending tremendous amounts of money for making jokes about small people.

Dipl. Ing. Pierre Beugré who taught me how to handle the robotic workstation.

Dr. Ing. Arthur Susanto who was the first (Indonesian) Rhinelander I met and who taught me, that 'Halve Haan' has nothing to do with chicken or other poultry.

Dipl. Ing. Martin Petzold who was the one and only diploma student I had and who helped me getting a handle on orientation determination at changing mobile phase conditions.

Petra Geilenkirchen for helping me getting started with the Äkta and Dipl. Ing. (FH) Esther Knieps Grünhagen for spending hours in the cellar with the confocal laser-scanning microscope.

All members of the Bioseparations Group at the Research Centre in Juelich and later the Biomolecular Separation Science Group at the University of Karlsruhe for the great working atmosphere, for always giving me a helping hand when needed and for introducing to me the concept of the 'Kölner Karneval'.

I also want to thank all my friends that are not mentioned here by name for the good time, especially those that I got to know due to my PhD work.

I would also like to thank my parents. Without their initiative I wouldn't be here, and without their patience, support and the first chemistry kit I would have become a truck driver, which used to be my favorite. Only at a very few incidents during my PhD I sometimes wished I had become one.

Last but not least I would like to thank my girlfriend Alina for coming all the way with me to Karlsruhe and for listening to my (probably) boring scientific monologues at the dinner table. I wouldn't have had such a wonderful time if it wasn't for her.

Abstract

This PhD thesis deals with the two fundamental processes underlying the chromatographic separation of proteins:

- The interaction between a protein molecule and the adsorber surface
- The transport of a protein from the mobile into the stationary phase and inside the stationary phase itself

To characterize the interplay of proteins with an adsorber surface, an analytical procedure was developed, based on the covalent modification of unbound and adsorber-bound lysozyme. Primary amino-groups of lysine residues located on the surface of the protein can chemically react with dye molecules (Cy5). As a result of this labelling reaction, six single-labelled and a small fraction of multi-labelled lysozyme isoforms are generated, one for each of the six lysine residues on the surface of lysozyme. Lysine residues are positively charged under physiological buffer conditions and thus the chemical reaction of one amino group with one negatively charged dye molecule reduces the net charge of the protein by two and also alters the charge distribution. As a result of this, the different forms can be separated on a cation exchanger. The assignment of elution peaks to the different lysozyme variants necessary for quantification of each form was achieved by a combination of mass-spectrometrical analysis of tryptic digests (MALDI-TOF) and electrostatic characterization of the altered charge distribution. By comparing the labelling efficiency of the different lysine residues in the unbound and in the adsorber bound state, possible binding sites could be identified.

In the following different cation exchange materials were investigated: SP Sepharose FF[®], Source 15S[®], SP Sepharose XL[®] and EMD Fractogel SO_3^- [®]. The first material is a standard adsorber based on a hydrophilic polymer backbone. The second material has, in contrast to the first, a hydrophobic polystyrene backbone. The third and the fourth adsorber are grafted materials, in which the ligands are bound to the polymer matrix via long spacers to give them a high flexibility. Their main difference is the ligand density. For SP Sepharose FF[®] two possible main binding sites were found on the surface of the lysozyme molecule, while Source 15S[®] revealed only one binding site. This was ascribed to the hydrophobic backbone of the second material because this binding site showed a significant amount of hydrophobic residues in contrast to the other. These results showed, that the polymer backbone not only contributes to an increased pressure stability of the material but also to the binding of proteins. The two grafted materials showed a multipoint binding mechanism that could only be achieved by the high flexibility of the ligands, offering a reasonable explanation for the often reported high binding affinities of grafted materials. Additionally, the experiments with EMD Fractogel SO_3^- [®] showed a re-orientation of lysozyme molecules with increasing protein density on the surface towards a less space-consuming conformation, giving hints about extremely high binding capacities of grafted materials.

In further experiments the effects of the two main mobile phase parameters were investigated: ionic strength and pH. Both parameters can be varied to achieve elution of bound proteins in ion-exchange chromatography, although the mechanisms for elution are completely different. While increasing the ionic strength by increasing the salt concentration leads to a higher competition between ions and proteins for the charged ligands

on the adsorber surface and additionally to a shielding of the surface charges, an elevated pH changes the net charge and the charge distribution of the protein surface and thus reduces the interaction strength. The individual pK_a values (influenced by the 3D protein structure) of the charged amino acids effect the charge distribution, e.g. not all positively charged residues loose their charge simultaneously at the same pH. Experiments with SP Sepharose FF[®] and SP Sepharose XL[®] showed that the ionic strength did not have an effect on the binding orientation of lysozyme as expected, because increasing the ionic strength does not alter the protein or adsorber properties. An increasing pH had an effect on the equilibrium between the two binding sites found for SP Sepharose FF[®]. At low pH the first binding site was preferred, while at high pH the second binding site prevailed. Both binding sites consist of four positive and one negative charge, but the first binding site looses part of its charge already at low pH, which could explain the changes in the equilibrium between both sites. Due to the flexibility of the ligands no changes were found for SP Sepharose XL[®], both binding sites can simultaneously interact with the adsorber. Surprisingly, the second binding site still showed a positive net charge (according to the titration curves of the individual amino acids) above the isoelectric point of lysozyme (lysozyme has a negative net charge at these pHs) which means, that lysozyme should still bind to a cation exchanger at that pH. This could be approved by experiments up to one pH unit above the pI.

The experimental data about the binding mechanism on SP Sepharose FF[®] were then used to develop a model to be able to predict *in silico* the retention behaviour of a protein at different pH only based on its 3D structure. Molecular dynamic simulation tools can be used to calculate the energy content of complex systems also accounting for the flexible and dynamic nature of biological systems. The AMBER toolbox was used to design the 3D structure of a SP Sepharose FF[®] surface with a size of approximately $100 * 100 \text{ \AA}$ and different ligand densities. The actual chemical structure of the ligands was used for the simulation (rather than a point-charge approximation), which gave the ligands some flexibility. A lysozyme molecule was situated on the center of the surface in a certain orientation. In order to be able to describe pH effects, the charge distribution was adjusted according to the intrinsic pK_a values of the charged amino acids. The total electrostatic energy of the system could be calculated from the simulation results, which became the interaction energy for adsorption after deducting the energies of single component simulations. These simulations were repeated for altogether 62 systematically varied lysozyme orientations to give an interaction landscape for the whole lysozyme surface, including favourable and unfavourable binding orientations. The favourable ones were in good agreement with experimental results. The landscapes were then used to calculate an average interaction energy for each pH. This energy correlated well with experimentally determined retention data (retention times in a linear gradient at pHs between 5 and 12 as a measure for the affinity) for a surface with a ligand spacing of 10 \AA . The same setup was then used to predict the retention behaviour of a second protein *in silico*: Ribonuclease A. The retention volume within a 30 ml long linear gradient could be predicted with an accuracy of 0.4 ml.

The second part of this thesis deals with transport phenomena in chromatographic media for affinity based purifications. Confocal laser-scanning microscopy (CLSM) has proven to be a useful tool to visualize protein transport in spherical chromatographic particles and miniaturized packed columns. Membrane adsorbers, a relatively new form of a

chromatographic adsorber material, has not been studied in detail on a microscopic scale. In a cooperation project with the University of Essen we developed a module that allows to visualize time-resolved and space-resolved protein transport inside a membrane under flow conditions. One major problem when evaluating the images is the irregular shape of the filament network inside the membrane. We were able to measure and mathematically describe space- and time-resolved breakthrough curves in different membrane materials. An interesting finding was, that breakthrough occurred at different time points depending on the location inside the membrane which indicates different linear flow rates at different positions. This could possibly lead to band broadening of elution peaks. We were also able to identify protein binding areas inside the membrane network. These filamentous areas were clearly delimitable from structure-giving cellulose fibers.

In a second cooperation with the University of British Columbia in Vancouver an improved mathematical transport model was developed to describe inner-particle protein transport in spherical adsorbers to model column chromatography. The standard transport model is based on pore diffusion only, and one of the assumption is, that the pore concentration and the stationary phase loading in the center of the particle is greater than 0 as soon as the protein solution reaches the boundary of the particle. This leads to a significant overestimated protein uptake speed which in turn reduces the quality of breakthrough curve predictions. The new model divides the particles into two zones: an outer ring with already adsorbed protein and an empty inner ring. This leads to a better modelling of uptake profiles of single particles calculated from time-resolved confocal laser-scanning images. The new model also included a term that describes a concentration-dependent protein adsorption equilibrium (Langmuir isotherm) and that replaced the old shrinking-core model, in which protein adsorption equilibrium only occurs at the very beginning of the adsorption front, which leads to very sharp adsorption fronts.

Zusammenfassung

Die vorliegende Doktorarbeit beschäftigt sich mit den zwei grundlegenden Prozessen der chromatographischen Trennung von Proteinen:

- Die Wechselwirkung zwischen Proteinmolekül und Adsorberoberfläche
- Dem Transport der Proteine von der mobilen Phase in die stationäre Phase sowie in der stationären Phase selber.

Für die Charakterisierung der Wechselwirkung zwischen Protein und Adsorber wurde zunächst ein analytisches Verfahren entwickelt, welches auf kovalenter Modifizierung von ungebundenem und Adsorber-gebundenem Lysozym beruht. Dabei reagieren Farbstoffmoleküle (Cy5) mit primären Aminogruppen von Lysin-Resten auf der Proteinoberfläche. Bei der Reaktionen können neben mehrfach markierten auch sechs einfach markierte Lysozym Isoformen entstehen (Lysozym trägt sechs Lysine auf der Oberfläche). Da Lysin unter physiologischen Bedingungen positiv geladen ist, hat die Reaktion mit einem negativ geladenen Farbstoffmolekül einen Einfluss sowohl auf die Nettoladung des Konjugats als auch auf die Ladungsverteilung. Dadurch können die markierten Formen auf einem Kationen-Tauscher voneinander getrennt werden. Die Zuordnung der Peaks im Chromatogramm zu der jeweiligen Isoform (also der Markierungsposition), die für eine getrennte Quantifizierung notwendig ist, konnte mit Hilfe einer Kombination aus massenspektrometrischen Analysen von tryptischen Verdaus (MALDI-TOF) und elektrostatischen Berechnung zur Charakterisierung der veränderten Ladungsverteilung erreicht werden. Über einen Vergleich der Markierungseffizienz der einzelnen Lysine für gebundenes und ungebundenes Lysozym konnten Aussagen über mögliche Bindungsstellen gemacht werden.

Es wurden zunächst verschiedene Kationentauscher Materialien untersucht: SP Sepharose FF[®], Source 15S[®], SP Sepharose XL[®] und EMD Fractogel SO_3^- [®]. Bei dem ersten Material handelt es sich um ein Standardadsorber mit einem hydrophilen Agarose Gerüst. Der zweite Adsorber hat ein hydrophobes Polymergerüst aus Polystyrol. Bei dem dritten und vierten Adsorber handelt es sich jeweils um gegraftete Materialien, bei denen die geladenen Liganden über lange Spacer an das Polymergerüst gebunden sind. Für SP Sepharose FF[®] wurden zwei mögliche Bindestellen auf der Lysozymoberfläche gefunden, auf Source 15S[®] nur eine der beiden. Dies konnte auf das hydrophobe Polystyrol Gerüst zurückgeführt werden, da eine der Bindungsstellen einen relativ großen hydrophoben Bereich aufweist. Dies hat gezeigt, dass das Polymergerüst nicht nur einen Einfluss auf die Druckstabilität hat, sondern ebenfalls auf das Bindungsverhalten. Im Gegensatz dazu wurde auf beiden gegrafteten Adsorbieren eine simulatene Bindung beider Bindestellen festgestellt, die nur durch die hohe Liganden-Flexibilität erreicht werden kann, und die erklärt, warum gegraftete Materialien in vielen Fällen stärkere Bindungen eingehen als Standardmaterialien. Außerdem haben die Experimente für EMD Fractogel SO_3^- gezeigt, dass sich die Lysozym Moleküle mit zunehmender Protein Dichte auf der Oberfläche umorientieren, um eine platzsparendere Orientierung einzunehmen, was eine mögliche Erklärung für die oft zitierte hohe Bindungskapazität gegrafteter Materialien liefert.

In weiteren Experimenten wurde der Einfluss der beiden wichtigsten Parameter der mobilen Phase untersucht: Ionenstärke und pH Wert. Beide Parameter können variiert werden, um an Ionentauschern gebundene Proteine zu eluieren, der Mechanismen ist

allerdings grundlegend verschieden. Während eine Erhöhung der Ionenstärke durch Salzzugabe zu einer Erhöhung der Konkurrenz um die geladenen Liganden des Adsorbers führt, und so die gebundenen Proteine verdrängt, bewirkt ein steigender pH Wert eine Veränderung der Ladungsverteilung auf der Proteinoberfläche. Die unterschiedlichen pK_a Werte der einzelnen Aminosäuren bewirken, dass z.B. nicht alle positiv geladenen Aminosäuren gleichermaßen ihre Ladung verlieren, wenn sich der pH Wert erhöht. Experimente mit SP Sepharose FF[®] und SP Sepharose XL[®] haben gezeigt, dass die Ionenstärke keinen Einfluss auf die Bindungsorientierung hat, was durchaus zu erwarten war, da die Salzzugabe weder die Protein- noch die Adsorbereigenschaften verändert. Eine pH Wert Erhöhung bewirkte bei SP Sepharose FF[®] eine Verschiebung des Gleichgewichts zwischen den beiden gefundenen Bindungsorientierungen. Beide Bindestellen weisen vier positive und eine negative Ladung auf, die erste Bindestelle verliert jedoch schon bei relativ niedrigen pH Werten einen Teil ihrer positiven Ladung, was die Gleichgewichtsverschiebung erklärt. Da die Liganden auf SP Sepharose XL[®] flexibel sind, können sie mit beiden Bindungsstellen gleichzeitig interagieren, eine Umorientierung wurde nicht gefunden. Interessanterweise zeigte vor allem die zweite Bindungsstelle jenseits des isoelektrischen Punkts von Lysozym noch positive Ladungen (abgeleitet aus den Titrationskurven der beteiligten Aminosäuren), was bedeuten würde, dass Lysozym auch jenseits des pI, also bei negativer Nettoladung, noch Bindung an einen Kationentauscher (also eine ebenfalls negativ geladene Oberfläche) aufweisen müßte. Anhand von Experimenten konnte dies für einen pH Wert bestätigt werden, der ca. eine pH Einheit über dem pI lag.

Die Daten aus den Experimenten mit SP Sepharose FF[®] wurden anschließend verwendet, um ein Modell zu entwickeln, mit dessen Hilfe man *in silico* nur auf Basis der 3D Struktur von Proteinen deren Adsorptionsverhalten bei unterschiedlichen pH Werten abschätzen kann. Zur Berechnung des Energieinhalts komplexer Systeme können Moleküldynamik Simulationstools verwendet werden. Mit Hilfe des AMBER Pakets wurde ein 3D Model einer SP Sepharose FF Oberfläche mit einer Größe von ca. $100 * 100 \text{ \AA}$ mit verschiedenen Ligandendichten erstellt. Dabei entsprach die Modelstruktur der verwendeten Liganden der tatsächlichen chemischen Struktur (keine Vereinfachung durch Reduktion auf Punktladungen), was ihnen eine gewisse Flexibilität gab. Im Zentrum der Oberfläche wurde ein Lysozym Molekül in einer bestimmten Orientierung plaziert. Um pH Effekte simulieren zu können, wurde die Ladungsverteilung auf dem Lysozym mit Hilfe der pK_a Werte der einzelnen Aminosäuren angepaßt. Mit Hilfe der Moleküldynamik Simulation konnte dann die elektrostatische Gesamtenergie des Systems berechnet werden, von der anschließend die Energien der Einzelkomponenten-Systeme subtrahiert wurden, um die Energie der Interaktion zu berechnen. Dies wurde für insgesamt 62 verschiedene, systematisch variierte Orientierungen wiederholt, so dass mehrere Interaktions-Diagramme für die gesamte Lysozym Oberfläche jeweils für verschiedene pH Werte erstellt werden konnte. Aus diesen Diagrammen lassen sich in Abhängigkeit vom pH Wert Bereiche auf der Oberfläche erkennen, die bevorzugt eine Bindung mit dem Adsorber eingehen. Diese bevorzugten Orientierungen entsprachen den zuvor experimentell bestimmten Orientierungen. Aus jedem Diagramm wurde anschließend eine mittlere elektrostatische Interaktionsenergie berechnet, die mit dem Elutionsverhalten korreliert werden konnte (genauer: mit dem Elutionszeitpunkt von Lysozym in einem linearen Elutionsgradienten für den jeweiligen pH als Maß für die Affinität). Für einen Abstand von 10 \AA zwischen den einzelnen Liganden wurde eine sehr guter lineare Korrelation für alle pH Werte zwischen

5 und 12 erreicht. Genau wie die oben erwähnten theoretischen Betrachtungen über die Protonierung der beiden Bindestellen, läßt sich durch dieses Modell eine Bindung von Lysozym an SP Sepharose FF bei einem pH Wert jenseits des isoelektrischen Punkts vorrausgesagt. Die Simulationen wurden dann mit Ribonuclease A (einem zweiten Modellprotein) wiederholt, um dessen Retentionsverhalten *in silico* abschätzen zu können. Es gelang so mit Hilfe der aus den Simulationen berechneten mittleren elektrostatischen Interaktionsenergie das Retentionsvolumen in einem 30 ml langen linearen Gradienten mit einer Abweichung von 0.4 ml vorauszusagen.

Der zweite Teil der Arbeit beschäftigt sich mit Transport Phänomenen in der Chromatographie. Die konfokale Laser-Scanning Mikroskopie hat sich bereits in der Vergangenheit als nützlich erwiesen, um Protein Transport in sphärischen chromatographischen Partikeln und miniaturisierten chromatographischen Säulen zu visualisieren. Wenig untersuchte Systeme stellen dabei die relativ neuen Membranadsorber da. Deshalb wurde in Kooperation mit der Universität Essen ein Modul entwickelt, mit dem man erstmals den Transport und die Adsorption von fluoreszenz-markiertem Protein, in diesem Fall von Lysozym, in verschiedenen Membranadsorbentern zeitaufgelöst und unter Fluss beobachten kann. Ein wesentliches Problem bei der Bildauswertung stellt die unregelmäßige Struktur der Membran da. Trotz der Schwierigkeiten konnten ortaufgelöste Durchbruchkurven aufgezeichnet und mit Hilfe eines mathematischen Modells beschrieben werden. Auffällig war hierbei, das im Gegensatz zu gepackten Säulen der Zeitpunkt des Durchbruchs nicht über den gesamten Durchmesser der Membran gleich war, sondern dass es scheinbar Bereiche gab, in denen die effektive Flussrate höher war als in anderen, was zu einer Peak Verbreiterung bei der Elution führen kann. Außerdem konnten Bereiche identifiziert werden, die hauptsächlich für die Bindung von Lysozym verantwortlich waren. Diese filamentösen Bereiche konnten klar von den strukturgebenden makroporösen Cellulosefasern abgegrenzt werden.

In einer weiteren Kooperation mit der University of British Columbia in Vancouver wurde der intrapartikuläre Proteintransport in sphärischen Adsorber Partikel näher untersucht, um ein verbessertes mathematisches Modell zur Simulation von Säulenchromatographie zu entwickeln. Das gängige Transportmodell nimmt an, dass der Transport im Partikel alleine durch sogenannte Porendiffusion stattfindet. Eine der Randbedingungen ist, dass die Protein Konzentration in den Poren im Zentrum des Partikels sowie die Proteinbeladung des Adsorbenters im Zentrum des Partikels ungleich 0 ist, sobald der Partikel mit der Proteinlösung in Kontakt tritt. Diese Annahme führt dazu, dass die Aufnahmegeschwindigkeit im Modell zu hoch ist, was dazu führt, dass Durchbruchkurven nicht exakt modelliert werden können. Das neue Modell teilt den Partikel in zwei Zonen: eine äußere Zone, in der bereits Protein vorhanden ist, und eine innere, proteinfreie Zone. Dies führt zu einer wesentlich besseren Beschreibung von zeitaufgelösten Bild-Daten, die mittels eines konfokalen Laser-Scanning Mikroskops von einzelnen Partikeln aufgenommen wurden. Desweiteren beinhaltet das neue Modell einen Term zur Beschreibung eines konzentrationsabhängigen Adsorptionsgleichgewichts (Langmuir Isotherme) für die Bindung der Proteine an den Adsorber. Dieses Modell ersetzt das Shrinking Core Modell, in welchem das Adsorptionsgleichgewicht nicht konzentrationsabhängig ist, und Adsorption deshalb nur an Adsorptionsfront stattfindet, was zu einer sehr scharfen Adsorptionsfront führt.

Contents

1	Introduction	12
1.1	Chromatography	13
1.1.1	Batch chromatography	15
1.1.2	Packed bed chromatography	16
1.2	Driving forces for adsorption	17
1.2.1	Van der Waals forces	17
1.2.2	Electrostatic forces	18
1.2.3	H-bonds and hydrophobic forces	19
1.2.4	Other Forces	19
1.2.5	Implications for adsorption phenomena in chromatography	19
1.3	Adsorption models	20
1.3.1	Langmuir model	20
1.3.2	Steric mass action model	20
1.3.3	Available area model	21
1.4	Transport models	22
1.4.1	Mass balance equations	23
1.4.2	Model complexity	25
1.5	Chromatographic adsorber materials: Ion Exchange Chromatography (IEC)	26
1.5.1	Geometry	26
1.5.2	Ligand and backbone chemistry	28
2	Research Proposal	29
3	Publications & Manuscripts	31
	A novel approach to characterize the binding orientation of lysozyme on ion-exchange resins	32
	Effects of ionic strength and mobile phase pH on the binding orientation of lysozyme on different ion-exchange adsorbents	50
	3D Structure-based Protein Retention Prediction for Ion-Exchange Chromatography	72
	Detailed analysis of membrane adsorber pore structure and protein binding by advanced microscopy	92
	A novel two-zone protein uptake model for affinity chromatography and its application to the description of elution band profiles of proteins fused to a family 9 cellulose binding module affinity tag	115
4	Conclusion & Outlook	143
5	References	145
6	Curriculum Vitae	160

1 Introduction

It started in 1901 with the russian botanist Michail Semjonovitsch Tswett, who first used a packed column with calcium carbonate to separate green chlorophylls from yellow carotinoids, which gave chromatography its name. Two years later he published the first manuscript with the title "About a New Category of Adsorption Phenomena and their Application for Biochemical-Analysis" which was translated into english and republished in 1989 (Tswett, 1989). Reading this paper the main task of establishing a chromatographic process in those days becomes clear: Tswett studied more than 100 different adsorber materials and a whole variety of loading and elution conditions. Tswett already noticed, that there is an obvious link between particle porosity and binding capacity and that the composition of the solvent in the mobile phase has a great influence on the binding ability of the target substances.

It took another 50 years for the first application of size exclusion chromatography in an industrial process, and in the 1970s ion-exchange chromatography was first used commercially in the production process of insulin (Curling, 2007). Since then chromatographic resins have evolved, column technology has advanced and separation processes have been optimized, but the main tasks are the same as a hundred years ago: to find the most suitable resin and mobile phase conditions for an efficient separation. And still, publications dealing with the optimization of chromatographic processes could end with the same remarks Tswett concluded his publication with in 1903: "Without any doubt further investigation on the mechanism of adsorption would lead to the perfection of its analytical application. The empirical determination of the adsorption properties of different substances [...] would lead to the elaboration of certain adsorption-analytical approaches for various practical problems." Statistics show that one in every four new pharmaceuticals is based on a biomolecule (*e.g.* recombinant protein, monoclonal antibody or nucleic acid based) (Walsh, 2005). The demands for efficient purification processes have to be met, and the biopharmaceutical market is still growing with an expected size of \$70 billion by the end of the decade (Walsh, 2006). A lot of knowledge about the mechanisms underlying chromatography was gained over the past decades and there is a whole variety of descriptive models available for retention, the most prominent ones for ion-exchange chromatography will be explained in detail later. But still, purely mechanistical models are rare and this is a strong indicator for a lack of understanding of what is happening during a chromatographic separation.

In the first part of my work I want to shed some light on adsorption phenomena in ion-exchange chromatography and discuss the influence of mobile phase composition on the general binding mechanism of proteins. Starting with the development of an assay to measure binding orientations of lysozyme under changing experimental conditions, the effects of different adsorber materials and their geometries on the binding mechanism will be discussed. I will show, that in some cases ion-exchange adsorbers do not only separate proteins on the basis of their charge. Some experiments will provide insights into the effects of mobile phase pH and ionic strength on protein binding. I will also show that molecular dynamic simulations, when set up carefully, can offer a good tool (and also a mechanistical model) to access adsorption energies based solely on 3D structures of proteins. These simulations also gave hints about what makes different adsorbers unique in their selectivity although many of them have chemically similar ligands. The second

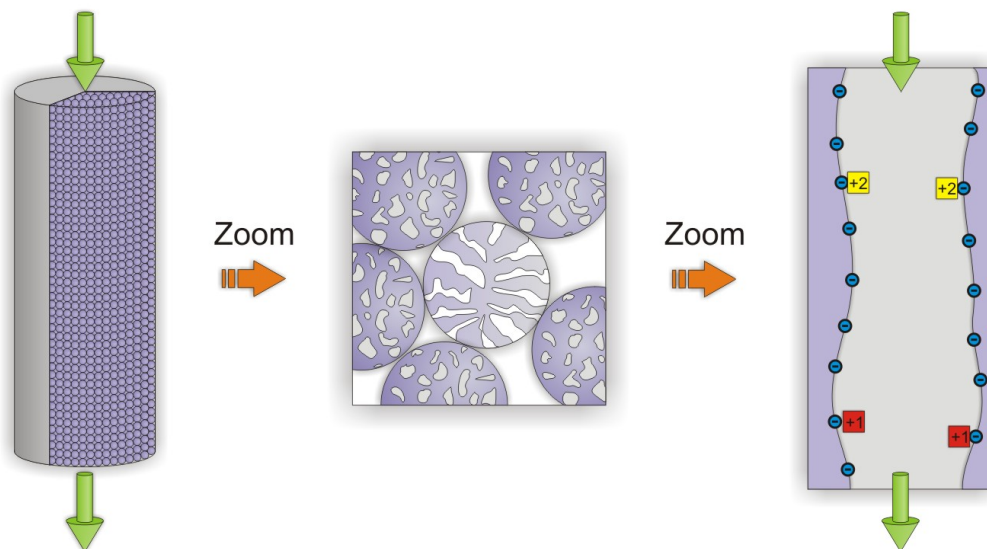


Figure 1: Schematic of cation-exchange chromatography: from macroscopic view of the column to a microscopic view of the adsorber surface. Green arrows indicate flow directions of the mobile phase. The red and yellow squares represent molecules with a different charged state.

part of my work deals with transport mechanisms in different chromatographic materials. In some way characterizing the transport seems easier, because it can be visualized and quantified using for example a confocal laser-scanning microscope (CLSM). But optical phenomena such as light attenuation (Susanto *et al.*, 2006) can make it a difficult task, especially in irregular shaped materials such as membrane adsorbers. In a cooperation project between the University Essen and our group, a membrane module was engineered to enable imaging of protein transport inside a membrane stack. In a second project with The University of British Columbia in Vancouver a mathematical transport model for affinity chromatography was validated with data from microscopic scale experiments in single particles using confocal laser-scanning microscopy as well as macroscopic-scale experiments in packed columns on a standard liquid chromatography system.

1.1 Chromatography

There are several modes chromatography can be applied in: size exclusion chromatography (SEC), ion-exchange chromatography (IEC), hydrophobic interaction chromatography (HIC), affinity chromatography and mixed-mode chromatography. In general, the mode determines the physical basis for the separation of the substances, e.g. the separation in size-exclusion chromatography is according to the hydrodynamic radius of the molecules. Different adsorber materials are usually classified according to the chemical composition of their ligands, i.e. an adsorber carrying functional SO_3^- groups belongs to the family of ion-exchange materials (and the subfamily of cation-exchangers) that separate proteins according to their charged state. In this PhD thesis, mainly ion-exchange and affinity adsorbers are used, and thus focus on these two techniques is laid.

Fig. 1 shows a schematic of different scales of a packed chromatographic column. Chromatographic separations in an industrial as well as an analytical scale are usually

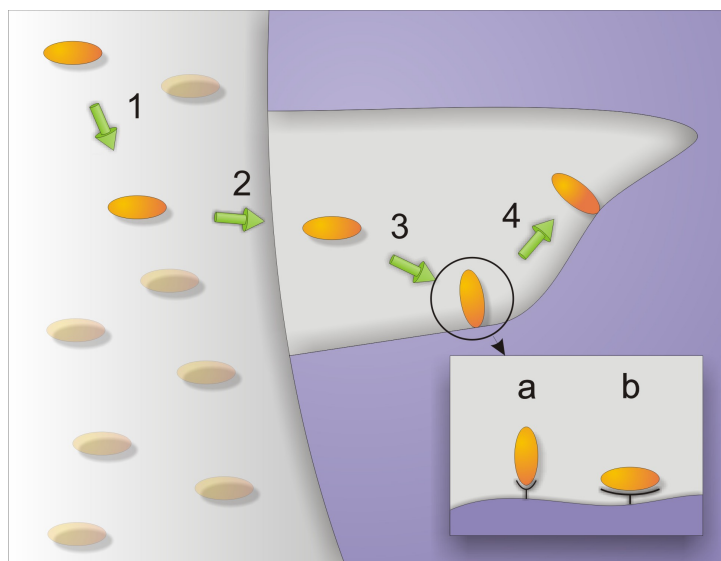


Figure 2: Sequence of typical transport and adsorption phenomena in chromatographic media: 1. Convection and dispersion, 2. Filmdiffusion, 3. Porediffusion and adsorption (a + b), and 4. Surface diffusion.

performed in packed columns. The mobile phase is being applied from the top at a constant linear flow rate. Inside the column, the adsorber particles are packed into a fixed bed. In most cases, the particles are spherical, but there are other materials with irregular shaped particles as well. Depending on the specified use of the column (preparative or analytical purposes), the size of the particles can vary between one and a few hundred μm . The actual separation takes place on the surface of the adsorber, where the protein molecules interact with the ligands and in some cases with the polymer backbone (refer to the results section). Due to diverse degrees of interaction, different molecules have different dwell times in the particles and thus different retention times. To improve the performance of adsorbers, the particles have a high porosity increasing the total available surface area. The only exception is size exclusion chromatography. In that mode the interaction of proteins with the adsorber is unwanted. Protein molecules of different size have a different available particle volume: for small proteins the accessible particle volume is bigger and thus their dwell time inside the particles is longer than for bigger molecules. Fig. 2 shows the general transport and adsorption phenomena as they appear in the mobile phase, at the border of mobile and stationary phase, and inside the stationary phase. Most phenomena occur independent from the work mode (batch or continuous chromatography, will be discussed later), although they can vary in their value. Convection and dispersion occur in the mobile phase either due to an applied flow or due to mixing. The particle-pores are filled with buffer as well but there is no convective buffer exchange between mobile phase and particle-pores, equalization between concentrations is only achieved by a process called film diffusion, and the proteins inside the pores are transported via pore diffusion, before they can interact and bind to the adsorber surface. The mechanism of surface diffusion, which includes a movement of protein molecules along the adsorber surface in the bound state is controversially discussed in literature, but due to reasons of completeness, this mechanism will also be discussed later.

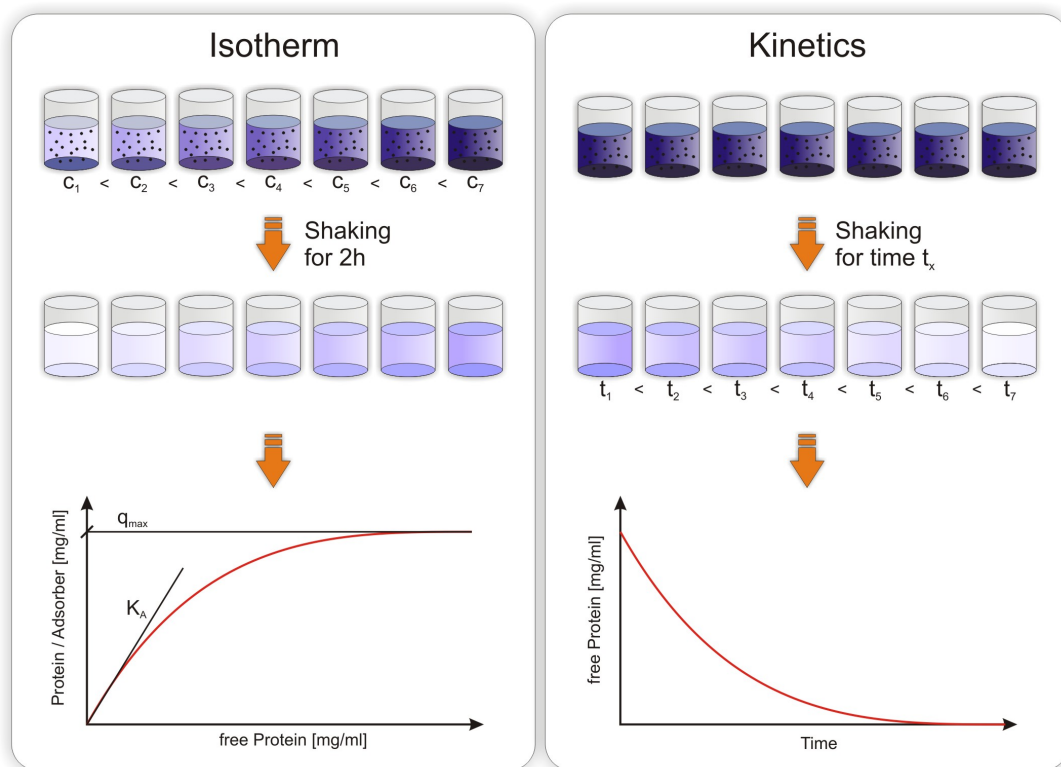


Figure 3: Scheme for the generation of isotherms (left) and uptake kinetics (right).

1.1.1 Batch chromatography

The simplest way to characterize different adsorber materials offers batch chromatography. In this work mode, a certain amount of chromatographic adsorber resin is incubated with a protein solution at a fixed mobile phase composition (buffer type and concentration, pH, ionic strength, etc.).

In case of an isotherm measurement, different starting concentrations of the protein solution are used (schematics shown left in fig. 3), while the amount of adsorber and the total volume for the reaction are kept constant. The adsorber-protein mixture is incubated for 2h under constant mixing to reach an equilibrium between bound and unbound protein. When measuring the unbound protein concentration after incubation, the particle loading q can be calculated according to:

$$q = \frac{(c_0 - c_{eq}) * V_{mob}}{V_{ads}} \quad (1)$$

With c_0 being the protein starting concentration, c_{eq} the final concentration of unbound protein, V_{mob} the total volume of mobile phase and V_{ads} the adsorber volume. When plotting q over c_{eq} , the data can be fitted using the Langmuir equation:

$$q = \frac{K_a * q_{max} * c_{eq}}{1 + K_a * c_{eq}} \quad (2)$$

which allows the determination of two parameters, that are characteristic for the protein-adsorber combination under the used experimental conditions:

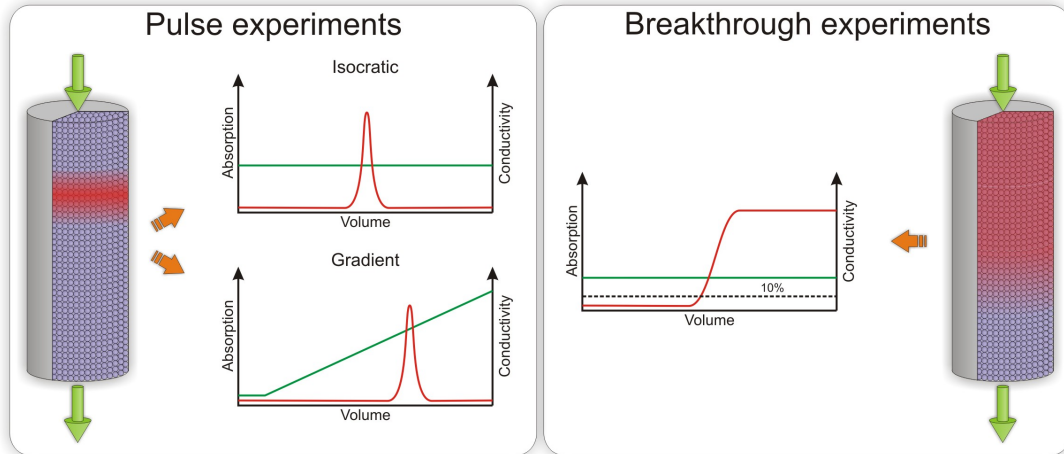


Figure 4: Commonly used experiments to characterize adsorber-resin combinations and experimental conditions in packed bed chromatographic runs.

1. q_{max} : the saturation of the isotherm which is the maximum protein binding capacity of the adsorber
2. K_a : equilibrium constant for the adsorption, which is a measure for the affinity of the protein

In fact, this is the simplest model for chromatography with a physical basis allowing the calculation of particle loadings with a given protein starting concentration in the mobile phase under the assumption that the experimental conditions (pH, ionic strength, buffer concentration, etc.) are the same.

In case of a kinetic measurement, the same protein starting concentration is used for all experiments, but the incubation time is different. While for an isotherm measurement it is important that equilibrium between mobile and stationary phase is reached, for a kinetic measurement the incubation time is different for all samples (see fig. 3), allowing for the determination of the uptake and binding speed of a given adsorber-protein combination.

These two experimental setups are often used to determine suitable conditions for the separation of two or more components. If e.g. two components a and b are to be separated, the isotherm for component a should be almost rectangular with a high maximum binding capacity, should have a high K_a value indicating a strong interaction between protein and adsorber and a fast binding kinetics, while the isotherm for the component b should have a low maximum binding capacity, a low K_a and slow binding kinetics.

1.1.2 Packed bed chromatography

Although batch chromatography offers a way to characterize adsorber materials, it does not represent the same conditions found in a packed chromatographic column. This becomes clearer by looking at single particles. In a batch mode experiment, all particles 'see' the same protein concentration in the mobile phase, and upon protein adsorption the concentration of unbound protein decreases. Besides, due to the long incubation time protein adsorption can reach equilibrium. In a column experiment, the situation is

more complex, e.g. for a pulse experiment with a short injection of protein solution, a gaussian shaped peak is proceeding through the column leading to a flowrate dependent contact time of varying protein concentration. Typical experiments to characterize protein/adsorber combinations under varying experimental conditions are shown in fig. 4. Pulse injections of protein solution followed by either an isocratic elution or a gradient elution can be used to determine the binding strength of a protein. In a breakthrough experiment the column is loaded with a protein solution until protein leaves the bottom outlet of the column. A typical value to characterize the breakthrough capacity is given by a 10% breakthrough. This point can be used to calculate the dynamic binding capacity of the column under process-like conditions.

1.2 Driving forces for adsorption

In the following chapter, the main driving forces for the interaction of matter will be briefly described, without going to much into the details of their mathematical description. A mix of these forces actually leads to protein adsorption, but the actual contribution of each force strongly depends on the kind of chromatographic material used, even for materials belonging to the same class of chromatographic materials (e.g. ion-exchange materials), as becomes apparent when reading the results and discussion part of this work.

1.2.1 Van der Waals forces

This force is responsible for the general non-covalent attraction of atoms and molecules even when they are neutral. The Van der Waals forces can generally be splitted into three different forces: the Keesom force between two dipoles, the Debye force between a dipole and a polarizable molecule and the London force between two polarizable molecules. The latter is often referred to as the real Van der Waals force. The strength of VdW interactions is usually in the range of 1 kJ/mol (0.24 kcal/mol) and declines with $1/r^6$, which makes it a rather weak and short-ranged force. The general idea of the VdW force arises from quantum mechanical considerations. Each electron surrounding the core of an atom has a certain probability to be found at a spatial position within its orbital according to the wave function $\psi(\vec{r})$ and thus the center of the charge distribution has a certain probability of not being located in the core of the atom. As a result the atom is an oscillating dipole which can interact with other temporary or permanent dipoles. Dealing with VdW forces is generally complicated as the interaction depends on the geometry of the interacting species, e.g. for two point atoms the VdW energy can be calculated as:

$$F_{VdW} = -\frac{C}{r^6} \quad (3)$$

where C is a constant for the atom-atom interaction and r is the distance between the atoms. The VdW energy for the interaction between two surfaces must be calculated differently:

$$F_{VdW} = -\frac{A}{12\pi D^2} \quad (4)$$

where A is the Hamaker constant and D is the distance between the surfaces. In molecular dynamics simulations the interaction energy is often calculated by the Lennard-Jones

potential:

$$E(r) = \epsilon \left[\left(\frac{r_0}{r} \right)^{12} - 2 \left(\frac{r_0}{r} \right)^6 \right] \quad (5)$$

where r_0 is the equilibrium separation between the particles, r is the distance and ϵ a characteristic energetic constant. The negative (attractive) term is the VdW energy and the positive (repulsive) term is the hard sphere force, that results from the Pauli principle and that adds an energy penalty whenever electron-filled orbitals overlap. The Leonard-Jones potential has an energetical minimum at the equilibrium distance r_0 .

1.2.2 Electrostatic forces

In contrast to the Van der Waals energy which is an attracting force, the interaction between charges can be attractive or repulsive, depending on the sign of the charges. This electrostatic interaction can be found between point charges (ion-ion), between a point charge and a dipole (or multipole) and between dipoles (or multipoles). The Coulomb's law describes the first case, the ion-ion interaction:

$$E_C = \frac{q_1 q_2}{4\pi\epsilon\epsilon_0 r} \quad (6)$$

where q_1 and q_2 are the number of charges, r is the distance, ϵ is the dielectric permittivity and ϵ_0 is the dielectric permittivity of free space. From this equation it becomes obvious that electrostatic interactions are long-ranged forces, in case of ion-ion interactions the force decays with $1/r$, while ion-dipole and dipole-dipole interactions decay with $1/r^2$ and $1/r^3$ respectively. Higher order electrostatic interactions (quadrupolar, etc.) provide only small contributions in biological systems. In general, electrostatic forces play a major role in the interaction between biopolymers, such as DNA, RNA and proteins because typical energies are in the range of 500 kJ/mol (120 kcal/mol). These systems usually include ions and thus shielding can occur. Whenever a charged object is put into a liquid, an electrical double layer is formed. The first layer represents the surface charge of the object. The second layer is formed by counter-ions that are attracted by the charged surface. These ions lead to a significant shielding of the surface charge. This double layer theory helps to simplify the calculation of electrostatic forces: rather than including every counterion in the calculation a modified potential can be used to account for the shielding effect. The most prominent way to deal with small ions in solutions without explicitly including them in the calculations offers the Poisson equation for electrostatics, which relates the electrostatic potential to the free ion concentration in a dielectric:

$$\epsilon_r \epsilon_0 \frac{d^2\psi}{dx^2} = -\rho_{freeion} \quad (7)$$

where ϵ_r is the relative permittivity of the dielectric, in which the ions are embedded. The Poisson equation can be combined with the Boltzmann distribution in order to be able to calculate potentials, electric fields and counterion densities at any spatial position in the system. The Boltzmann distribution in this case describes the distribution of different energetical states of the counterions in the system at a certain temperature. The Poisson-Boltzmann equation has the form:

$$\frac{d^2\psi}{dx^2} = -\frac{ze\rho}{\epsilon_r\epsilon_0} e^{-ze\psi/kT} \quad (8)$$

where z is the charge, k is the Boltzmann constant and ϕ is the potential.

1.2.3 H-bonds and hydrophobic forces

Hydrogen bonds play an important role in all systems that include biomolecules, especially in aqueous buffers, although their energy contribution (10-40 kJ/mol or 2.5-10 kcal/mol) is usually smaller than the contribution by electrostatic forces. They are the driving force of the self-assembly of protein structures and membranes, and they usually involve a strongly polar proton donor group (OH, NH, SH, etc.) and an electronegative proton acceptor atom. But H-bonds not only stabilize polar structures, they are also the driving force for a shielding of apolar surface areas by the formation of ordered clathrate structures by water molecules around these areas. This entropy change is proportional to the apolar surface area, and thus the solvation energy of a biomolecule is proportional to the size of apolar surface patches. As a result of this entropic effect, hydrophobic areas of different molecules can attract each other, driven by a gain in entropy. For molecular dynamics simulations, these H-bond effects are difficult to account for, due to their high flexibility (e.g. water molecules in a clathrate structure can be exchanged as the structure is not very rigorous) and due to their variability (e.g. a single oxygen atom can form H-bonds with more than one H atom at the same time).

1.2.4 Other Forces

There are a few other forces that will only be briefly discussed here, since they play only a minor role in this work. These forces are entropically driven, such as the depletion force that occurs when proteins are surrounded by a solution containing polymers. The protein molecules experience an attracting force when the distance between them becomes small and the polymer molecules are excluded from this volume fraction. By reducing this excluded volume fraction (attraction between the molecules), the entropy in the system increases and this increase leads to an attractive force. This effect is often used in protein crystallization because it drives proteins out of solution.

Another entropically driven force occurs for polymer-grafted surfaces that are stabilized by the bound polymers. In a good solvent the polymers extend into the solvent giving them a certain flexibility. Whenever two such surfaces (e.g. of two colloids in solution) approach each other, the polymer flexibility decreases leading to a reduced entropy and thus a repulsive force between the surfaces. The range of this effect strongly depends on the molecular weight of the grafted polymers. In a bad solvent, the polymer brush collapses onto the surface and no longer extends into the solvent and the polymers can no longer stabilize the surface.

1.2.5 Implications for adsorption phenomena in chromatography

From a thermodynamical point of view when trying to understand the adsorption of a molecule onto a surface, the exact geometry of the system is of great importance, since all the described forces show distance-dependent decay. Some of the forces are long-ranged, such as the electrostatic interaction between charges that decays with $1/r$, some are short ranged such as the VdW interactions that decay with $1/r^6$. One can easily imagine that especially for macromolecules such as proteins or DNA, the orientation of a molecule

towards its interacting partner is thus of great importance if not crucial for a detailed understanding of the energetics of the interaction.

1.3 Adsorption models

There are different models available to describe and characterize protein adsorption in chromatography, the most frequently used ones will be discussed here briefly. All these models facilitate the prediction of protein binding behaviour to some degree, depending on the complexity of the model, but they are all semi-empirical, meaning that the model parameters have to be determined empirically, but have a physical relevance.

1.3.1 Langmuir model

As already described earlier, the Langmuir model is the general model to describe protein adsorption at given experimental conditions. Though it is the most widely used in biochromatography, the assumptions it is based on do not apply for preparative chromatography:

1. Adsorption takes place in a single layer.
2. All binding sites on the adsorber are equal in their affinity towards the protein.
3. No interaction between bound protein molecules.

The Langmuir model has two parameters: the maximum binding capacity q_{max} and the equilibrium constant K_a . Both parameters can be determined by measuring a binding isotherm. The major drawback of this model is, that the parameters are only valid for the exact same experimental conditions the isotherm was determined at and does not allow predictions for other conditions, such as ionic strength. And although there is an extended version of the Langmuir model for multi-component systems, the determination of multi-component isotherms is rather difficult and its predictive power is limited (Cano *et al.*, 2007).

1.3.2 Steric mass action model

The semi-empirical SMA model was developed in 1992 by Brooks and Cramer (Brooks and Cramer, 1992). Fig. 5 illustrates the influence of the binding orientation, that is taken into consideration in this model. This model uses three parameters to describe the interaction between the protein and the adsorber:

1. ν : Characteristic charge of the protein, that is a measure for the number of interaction points upon binding. The characteristic charge is not equal to the net charge.
2. σ : Steric factor, that describes the number of ligands that are blocked upon binding but do not contribute to the binding event.
3. K_a : Equilibrium constant, that is a measure for the affinity between adsorber and protein.

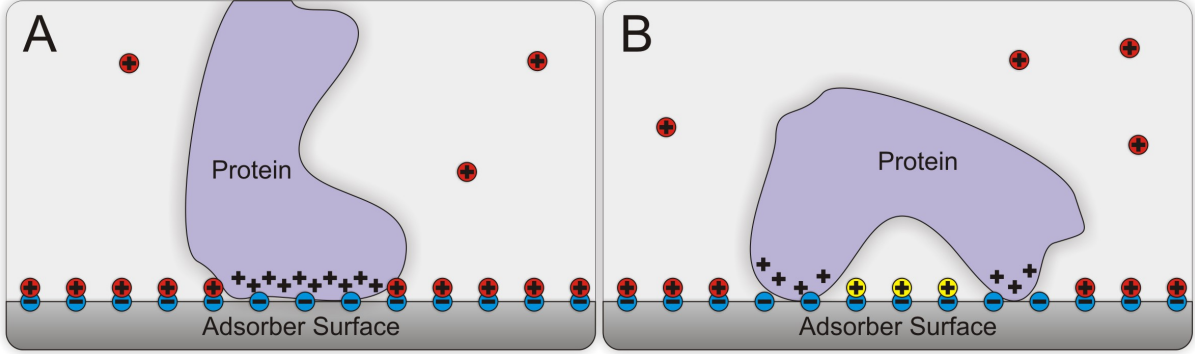


Figure 5: Different protein orientations on a cation exchanger according to the SMA model. *red*: counter ions, *yellow*: blocked counter ions, *blue*: ligands.

This model was specifically developed for multi-component systems because it includes a way of accessing the space consumption of each component. The equilibrium constant K_a can be written as

$$K_a = \left(\frac{q_{prot}}{c_{prot}} \right) \left(\frac{c_{ion}}{\bar{q}_{ion}} \right) \quad (9)$$

where q_{prot} is the bound protein concentration, c_{prot} is the unbound protein concentration, c_{ion} is the salt concentration in the mobile phase and \bar{q}_{ion} is the total amount of ions available for exchange. The number of blocked ligands/counter ions is

$$q_{blocked} = \sigma * q_{prot} \quad (10)$$

Electroneutrality requires that

$$\bar{q}_{ion} - (\sigma + \nu) * q_{prot} = 0 \quad (11)$$

The parameter determination can be done in different ways, one would be the measurement of at least three isotherms at different ionic strengths. This model, in contrast to the Langmuir model allows protein retention prediction at different ionic strength (and thus also for gradient elution) and for multi-component systems due to the fact, that the three parameters are independent of the salt concentration. The main limitation of this model is that the parameters are not independent of pH and thus do not allow predictions for a changed pH.

1.3.3 Available area model

In 2004, Bosma and Wesselingh developed a new model to describe protein adsorption using only two parameters (Bosma and Wesselingh, 2004). Fig. 6 shows a scheme taken from their publication. In this model proteins are represented by discs on the surface of an adsorber. These discs use a certain amount of area χ and cannot overlap, so a second molecule can only bind in a distance bigger than the radius of the disc. This leads to an excluded area ϵ . No center of another protein with the same size can be located within this excluded area. The space left is the available area α . The model is based on the following assumptions:

1. At equilibrium, adsorption and desorption rates are equal.

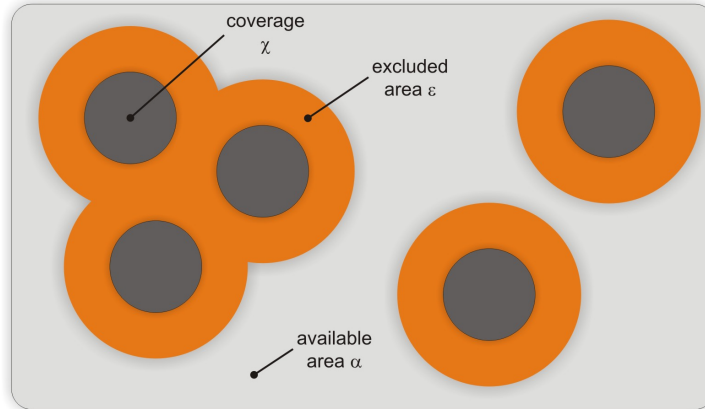


Figure 6: Schematics of the parameters used in the available area model that describes protein adsorption based on the space consumption of proteins.

2. The desorption rate is proportional to the surface coverage (same as Langmuir).
3. The adsorption rate is proportional to the mobile phase concentration (same as Langmuir) but also to the available area.

Based on these assumption, the following equation can be obtained

$$c = K \frac{\chi}{\alpha} \quad (12)$$

where K is an equilibrium constant, and c is the mobile phase concentration. There is also a relation between α and χ which depends on the degree of surface coverage. For low coverage the relation can be expressed as

$$\alpha = (1 - \chi)^4 \quad (13)$$

At high surface coverage the relation could only be found by numerical simulations which resulted in

$$\alpha = \left(1 - \frac{\chi}{\chi_{max}}\right)^{(4+5.5\chi^2)\chi_{max}} \quad (14)$$

Interestingly the numerical simulations revealed a maximum coverage (χ_{max}) of 54.7%. The advantage of this model is that it can be used for different modes of chromatography. In contrast to the SMA model which was specifically developed to describe ion-exchange chromatography, the available area model can be combined with other adsorption models empirically or fundamentally accessing the effects of ionic strength and pH on the adsorption constant (Bosma and Wesselingh, 1998a, Roth *et al.*, 1996, Roush *et al.*, 1994, Stahlberg *et al.*, 1991).

1.4 Transport models

One of the main tasks models are industrially used for is the optimization of chromatographic separation problems with a minimum number of experiments. In order to optimize a process *in silico* at least the most important steps need to be included in the

model. In the previous section we dealt with models for the adsorption of proteins onto adsorber surfaces, the focus of this section will be on the question of how the protein molecules are transported through the column and into the particles. The complexity of protein transport mechanisms included in chromatographic models can strongly vary, depending on the accessible computational power, the available amount of information about the chromatographic system (column and packing parameters, protein parameters, etc.) and the desired accuracy of the simulation results. In general the following transport mechanisms can be found in models:

- Convection: usually only in the mobile phase, except for macroporous materials
- Dispersion
- Film diffusion: Mass transfer from the mobile phase into the stationary phase
- Pore diffusion: Mass transfer inside the stationary phase
- Surface diffusion: Mass transfer along the adsorber surface

When modelling chromatographic processes, a number of assumptions have to be made:

1. The packed bed is homogenously packed with spherical particles of constant diameter
2. Fluid density and viscosity are constant
3. Size-exclusion effects are not taken into account so the available pore volume is the same for all solute molecules
4. Radial effects in the column are neglected, so the models are actually one-dimensional (in the mobile phase only the direction of flow x and in the stationary phase the radial position r)

1.4.1 Mass balance equations

The fundamental basis of any chromatographic model is the mass balance for the molecules in the mobile phase, the stationary phase and in the adsorbed state. Fig. 7 shows a scheme for the different fluxes from the column scale on the left down to the scale of single pores on the right.

The general mass balance for the accumulation of a component i in a differential volume dV can be written as

$$\frac{\delta}{\delta t} [m_{acc,i}(x,t)] = \dot{m}_{conv,i}^x(x,t) - \dot{m}_{conv,i}^{x+dx}(x,t) + \dot{m}_{disp,i}^x(x,t) - \dot{m}_{disp,i}^{x+dx}(x,t) - \dot{m}_{mt,i}(x,t) \quad (15)$$

where \dot{m}_{conv} is the convective flux, \dot{m}_{disp} is the dispersive flux and \dot{m}_{mt} is the mass transfer flux into the particles. The flux into the particles is equal to the overall accumulation of component i in the adsorber:

$$\frac{\delta}{\delta t} (\bar{m}_{acc,ads,i}) = \dot{m}_{mt,i} \quad (16)$$

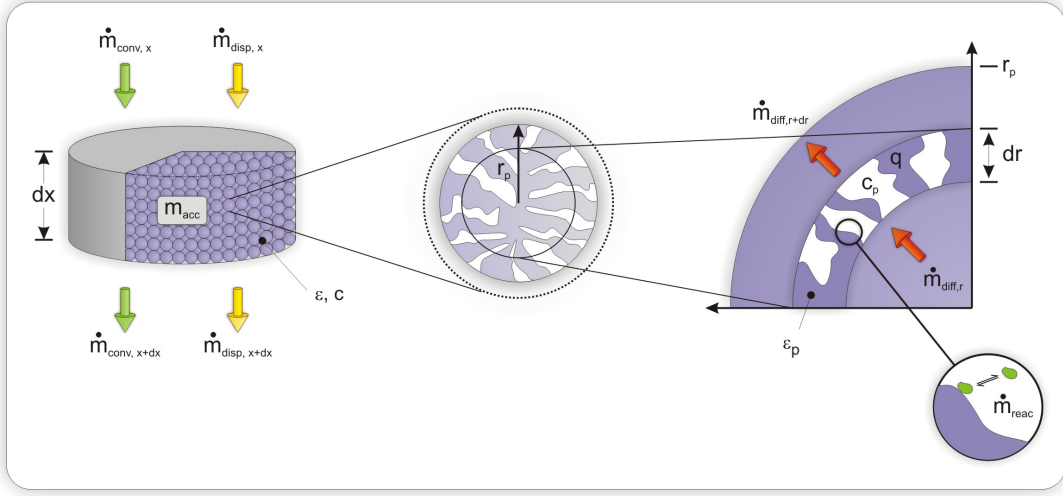


Figure 7: Mass fluxes in chromatographic models for the mobile phase on the left and the stationary phase on the right. Adopted from (Schmidt-Traub, 2005).

The fluxes inside the stationary phase can be splitted into pore diffusion, surface diffusion and a kinetic term for the adsorption:

$$\frac{\delta}{\delta t} (m_{acc,pore,i}) = -\frac{\delta}{\delta r} (\dot{m}_{diff,pore,i}) dr - \dot{m}_{reac,i} \quad (17)$$

$$\frac{\delta}{\delta t} (m_{acc,solid,i}) = -\frac{\delta}{\delta r} (\dot{m}_{diff,solid,i}) dr + \dot{m}_{reac,i} \quad (18)$$

To be able to work with these mass balances, the equations need to be based on concentrations and therefore different volumes have to be introduced. The total differential volume dV_c of a column element with a cross section A_c and a length dx is the sum of the mobile phase volume dV_{int} and the adsorber volume dV_{ads} :

$$dV_c = A_c dx = dV_{int} + dV_{ads} \quad (19)$$

The mobile phase volume and the adsorber volume can be expressed as a function of the total column porosity ϵ :

$$dV_{int} = \epsilon A_c dx \quad (20)$$

$$dV_{ads} = (1 - \epsilon) A_c dx \quad (21)$$

The same applies for the pore volume:

$$dV_{pore} = \epsilon_p dV_{ads} = \epsilon_p (1 - \epsilon) A_c dx \quad (22)$$

$$dV_{solid} = (1 - \epsilon_p) dV_{ads} = (1 - \epsilon_p) (1 - \epsilon) A_c dx \quad (23)$$

By introducing the mobile phase concentration c_i , the mean overall adsorber loading \bar{q}_i^* , the mean pore concentration $\bar{c}_{p,i}$ and the mean solid loading \bar{q}_i , the mass balance equations can be written as follows:

$$m_{acc,i} = c_i dV_{int} = c_i \epsilon A_c dx \quad (24)$$

$$\bar{m}_{acc,ads,i} = \bar{q}_i^* dV_{ads} = \bar{q}_i^* (1 - \epsilon) A_c dx \quad (25)$$

$$\bar{m}_{acc,pore,i} = \bar{c}_{p,i} dV_{pore} = \bar{c}_{p,i} \epsilon_p (1 - \epsilon) A_c dx \quad (26)$$

$$\bar{m}_{acc,solid,i} = \bar{q}_i dV_{solid} = \bar{q}_i (1 - \epsilon_p) (1 - \epsilon) A_c dx \quad (27)$$

The overall adsorber loading is equal to the sum of the pore concentration and the solid loading:

$$\bar{q}_i^* = \epsilon_p \bar{c}_{p,i} + (1 - \epsilon_p) \bar{q}_i \quad (28)$$

The equations that can be used to i.e. model the pore diffusion will be discussed later in the introduction to the last publication.

1.4.2 Model complexity

In the following I will briefly discuss the different levels of complexity that can be used to model chromatography, starting with the simplest model. This description is based on a chapter of the book 'Preparative Chromatography' by Prof. Dr. Schmidt-Traub (Schmidt-Traub, 2005). The aim of this section is to give the reader an insight into modelling of chromatographic processes, it does not make the claim to be complete.

1. Equilibrium Model

This model only accounts for convective transport in the mobile phase of the column and the thermodynamic equilibrium for adsorption, and is thus the simplest possible model. It neglects axial dispersion as well as mass transfer from the mobile phase into the stationary phase and inside the stationary phase. Protein adsorption/desorption equilibrium is assumed to be reached instantaneously. As a result of this, the concentration within the adsorber particle is constant and not a function of the particle radius. This model was mainly used to understand the influence of the isotherm shape on the elution behaviour of proteins in column experiments (Lapidus and Amundson, 1952, Vandemter *et al.*, 1956), because it allows to calculate a retention time of a component i according to:

$$t_{R,i}(c_i) = t_0 \left(1 + \frac{1 - \epsilon_t}{\epsilon_t} \frac{\delta q_i}{\delta c_i} \Big|_{c_i} \right) \quad (29)$$

where t_0 is the dead time of the column and ϵ_t the total porosity. Rhee *et al.* (Rhee *et al.*, 1970) and Helfferich (Helfferich and Whitley, 1996) made analytical solutions available for multi-component systems based on Langmuir isotherms. For these systems, an additional term for the concentration dependence of both isotherms is used, describing the influence of one component on the propagation speed of the other component in a concentration dependent manner.

2. Equilibrium Dispersive Model

This model is more complex than the first one and is often used for the optimization of chromatographic systems (Felinger and Guiochon, 1992a,b, Jacobson *et al.*, 1992a,b). This model includes a term for axial dispersion in the mobile phase. In many models, the effects of some parameters are lumped into one. In this model all parameters leading to peak broadening are lumped into the axial dispersion coefficient D_{ax} , which is only affected by the column packing quality, although peak broadening has numerous sources: pore diffusion, surface diffusion, mass transport into the particle, flow velocity, etc. This coefficient was first introduced by van Deemter (Vandemter *et al.*, 1956). This model shows a good agreement especially for very efficient columns with a plate number $N \gg 100$.

3. Transport Dispersive Model

This model belongs to the family of lumped rate models, that all include a second parameter describing rate limitations apart from axial dispersion. Only the adsorption equilibrium, convection and film transfer resistance are considered to be rate limiting. The film transfer resistance parameter is actually a lumped parameter including all internal and external mass transfer resistances. Other than the axial dispersion coefficient, this lumped parameter is not depending on the interstitial fluid velocity. Since this model includes a transport resistance into the stationary phase, there need to be two mass balance equations: one for the mobile phase

$$\frac{\delta c_i}{\delta t} + u_{int} \frac{\delta c_i}{\delta x} + \frac{1 - \epsilon}{\epsilon} \left[\epsilon_p \frac{\delta c_{p,i}}{\delta t} + (1 - \epsilon_p) \frac{\delta q_i}{\delta t} \right] = D_{ax} \frac{\delta^2 c_i}{\delta x^2} \quad (30)$$

and for the stationary phase

$$\epsilon_p \frac{\delta c_{p,i}}{\delta t} + (1 - \epsilon_p) \frac{\delta q_i}{\delta t} = k_{eff,i} \frac{3}{r_p} (c_i - c_{p,i}) \quad (31)$$

where k_{eff} is the lumped transfer resistance parameter. It is obvious that the driving force for the transport into the stationary phase is the concentration gradient between mobile phase (c_i) and the surface of the adsorber ($c_{p,i}$).

4. General Rate Model

This is the most complex model, because it includes at least two other mass resistance terms besides the axial dispersion term to describe mass transfer. These two terms can combine convection in the mobile phase, film transfer from the mobile into the stationary phase, pore diffusion in the stationary phase, binding kinetics and surface diffusion in many different ways. I will not go into detail here, because there are many different modifications of the general rate model.

1.5 Chromatographic adsorber materials: Ion Exchange Chromatography (IEC)

1.5.1 Geometry

There are numerous different adsorber geometries that can be used to achieve the separation of molecules, some of them designed for analytical purposes only (i.e. monolithic materials, small-sized non-porous spherical particles) and some of them for preparative scale purifications (i.e. macroporous spherical beads, grafted materials, membrane adsorbers). In the following, the most common geometries will be introduced.

1. Monolithic columns

By reading the previous section about modelling of chromatographic systems it becomes clear, that some transport phenomena (especially the slow process of diffusional transfer from the mobile phase into the pore volume) can lead to significant band broadening, and band broadening reduces the resolution of a column because peaks 'meld' together and baseline separation is more difficult to achieve. Besides

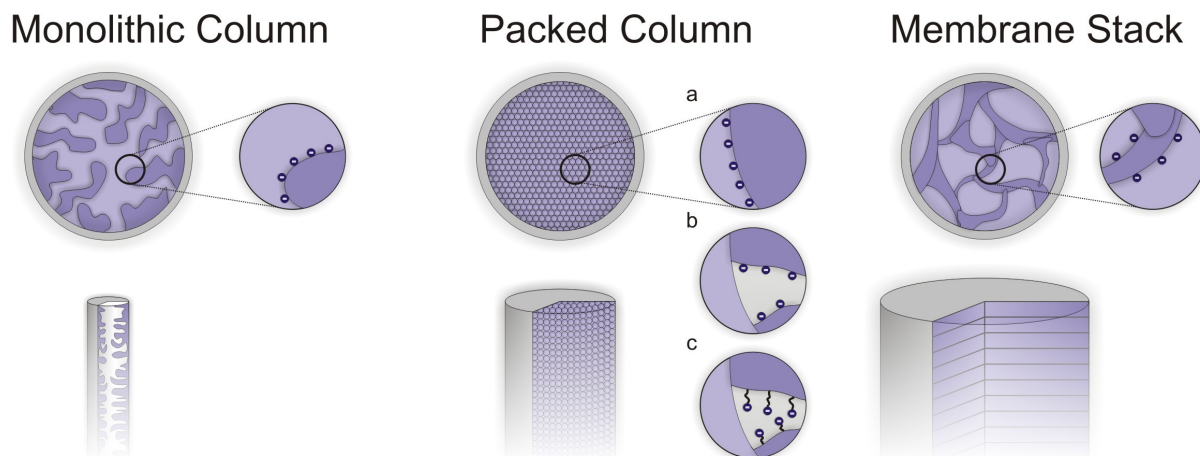


Figure 8: Different adsorber geometries: *Left:* Monolithic column with one continuous skeleton and one interconnected flow path. *Middle:* Packed column with spherical particle. *a.* non-porous *b.* standard material *c.* grafted material. *Right:* Membrane stack with fibers and macropores.

band broadening, the slow mass transfer also reduces the maximum flow velocity and increases analytical time. Monolithic columns are different from packed bed columns because they are not made from spherical particles, but from one piece of solid that possesses an interconnected skeleton and interconnected flow paths. Monolithic columns are usually made out of organic polymers (Tanaka and Kobayashi, 2003) with a total diameter between $20 \mu\text{m}$ and 8 mm and a total porosity of $60 - 70 \%$. With this column type, $100,000 - 220,000$ theoretical plates m^{-1} have been reported (Tanaka and Kobayashi, 2003). Due to the small diameter of the monolithic columns, their use is limited to analytical applications.

2. Packed bed columns with spherical particles

There is a wide range of adsorbers in the form of spherical particles available, most likely dozens if not hundreds, and it is still the most common way to do chromatography. The adsorbers differ in their particle size, porosity, ligand density, surface geometry and of course ligand and backbone chemistry (which will be subject of the next section). As already mentioned, one of the major effects for band broadening is the mass transfer from the mobile phase into the pores of the particles. To minimize this drawback, analytical resins have a drastically reduced particle size of only a few μm and are, in some cases, not porous. In most cases, these analytical resins have a rigid and incompressible backbone to allow high flow rates and a high pressure drop to increase analytical speed and efficiency. For preparative resins, the particles are often in the range of $100 \mu\text{m}$ or more to reduce back pressure. Some resins were especially designed for the purification of large proteins, so-called macro-porous adsorbers allowing convective mass transfer from the mobile phase into the particles often at the cost of reducing the binding capacity due to a decreased surface to volume ratio. One way to increase the performance of spherical particles is to introduce a polymer-grafted surface, where the ligands are bound to the adsorber surface via flexible spacer arms with a length of a few hundred Å. This increases the maximum binding capacity and often the strength of binding.

3. Membrane adsorbers

A relatively new development in the field of downstream processing is the family of membrane adsorbers. These adsorbers consist of a microporous filament support network either made of cellulose, polyethersulfone or polyvinylidene fluoride or by copolymerization of two functional monomers that can be activated with basically all ligand chemistries that are used for spherical particles (Boi, 2007). The idea for the development of such adsorbers was to facilitate purification steps with high flow rates without limiting mass transfer resistances and it also offers all advantages of disposable membrane cartridges (good batch to batch reproducibility, easy sanitation, etc.). The major drawback, as for all non-porous materials, is the low maximum binding capacity. For this reason, membrane adsorbers are most often used towards the end of a purification process for trace-impurity removal and polishing.

1.5.2 Ligand and backbone chemistry

The ligand chemistry for cation exchangers is rather simple. There are only two types of negatively charged groups commonly used: $-SO_3^-$ for strong cation exchangers and $-COO^-$ for weak cation exchangers. The difference between these two groups is their protonation state at different pH. The $-SO_3^-$ group has low pK_a of around 1.2 which means that its charged state is more or less independent of the mobile phase pH, at least in the physiological range. The $-COO^-$ group has a significantly higher pK_a around 5 which makes its degree of protonation a function of mobile phase pH.

The ligands are usually attached to the adsorber surface via aliphatic, non-cyclic carbon hydrid chains. For non grafted materials, this can range from single $-CH_2-$ groups (e.g. Source 15S[®] resin) up to $-CH_2CHOHCH_2OCH_2CH_2CH_2-$ groups (e.g. SP Sepharose FF[®]). For grafted materials, usually long dextrane chains are used, that carry multiple ligands to increase the ligand density and to give the ligands a higher flexibility (e.g. SP Sepharose XL[®]). The exact geometry of these grafted materials is unclear, e.g. it is only a theory that the polymer brushes collapse and become more or less unflexible at very low ionic strength.

In contrast to the ligands, the polymer backbone chemistry is more diverse, especially in the field of analytical chromatography. The standard material is the polysaccharide agarose usable only for mediocre flow rates due to its compressibility and its low pressure stability (3 bar according to the manufacturer). Other polymers such as the hydrophobic polystyrene and divinyl benzene (used for Source 15S[®]) show a significant higher pressure stability of up to 180 bar (according to the manufacturer), and are thus often used in combination with small particle sizes in analytical columns that generate very high back pressures at mediocre flow rates. Other popular materials that are more hydrophilic are methacrylate (used for all Toyopearl[®] materials) and silica gels (for all TSK-Gels[®] and most monolithic columns).

2 Research Proposal

After reading the introduction it becomes evident that the separation of proteins is a challenging task, no matter the scale: industrial purification or analytical lab scale. Especially challenging are chromatographic steps with complex protein mixtures (for capture steps often a few hundreds if not thousands of proteins) and with different forms of post-translationally modified proteins, that often show very similar chromatographic behaviour. In these cases, process conditions need to be optimized: adsorber material, binding buffer composition and pH, gradient shape and so on. In the past decades or so, this was usually done by manual empirical screenings of a very limited parameter space in order to achieve a reasonable separation in a reasonable amount of time. In the last few years, high-throughput screening (HTS) techniques became very popular, to efficiently decrease development times. The extended parameter space used in these screenings leads to processes that are closer to the real optimal conditions and the robustness of the resulting process can be increased due to the extended knowledge obtained through the high data density. The major drawback of these HTS techniques is the material consumption. Especially in early stage process development, the amount of available material is limited and a pre-screening *in silico* could reduce the experimental efforts. That is the reason why mathematical modelling becomes more and more popular to support the traditional process development. Besides, these models can help to understand the mechanisms underlying chromatographic separation.

When looking at the available models that can be used to analyze, describe and predict chromatographic behaviour for ion-exchange chromatography it is evident that there is a lack of mechanistical models: most models describe the effects of e.g. a changed mobile phase composition on an empirical basis through the use of model parameters. These model parameters have to be determined experimentally, which can be time-consuming and, in some cases, very difficult because the parameter estimation is mostly done with pure substances. When this work started, the aim was to find a way to predict the retention behaviour of modified proteins, that are very similar in shape and size, like for example post-translationally modified proteins. Initially this seemed to be easier than the establishment of a model for completely different proteins. A suitable model system was already available: chemically modified variants of lysozyme with attached dye molecules. This system was first used on protein transport studies with single adsorber particles in confocal laser-scanning microscopy, where native lysozyme is mixed with labelled forms in order to visualize protein uptake. People assumed for years that both species behave the same in an ion-exchange resin. When we found out that they do not, a suitable model system was found and after being able to separate and quantify the different labelled isoforms the aim of the work was extended to a more detailed study of adsorption mechanisms in general followed by the development of a mechanistic model which is able to predict protein retention on the basis of 3D structure information.

The most difficult part in modelling chromatographic behaviour is the adsorber material itself because it is hard to find and parametrize those adsorber properties that are crucial for protein uptake, transport and binding. Hence for most empirical models protein and adsorber specific properties are lumped together and the determined parameters are specific for a certain protein/adsorber combination. Thus the major advantage of a mechanistical model is, besides providing a more detailed understanding, that it usu-

ally includes individual sets of parameters for each component (e.g. chemical structure of protein and adsorber) and thus allows an easy transfer to other separation problems without the need of making additional experiments. A lot of work has been done in the field of protein transport, especially for the standard chromatographic adsorber materials, probably due to the fact that general transport phenomena in liquids have been known and characterized for a rather long time (in chromatography mostly convection and diffusion). The adsorption process is more difficult to understand on account of the complex chemical nature and dynamic structure of protein molecules and adsorber surfaces. For that reason mechanistical models for the adsorption are rare to find.

3 Publications & Manuscripts

1. *A novel approach to characterize the binding orientation of lysozyme on ion-exchange resins*

Florian Dimer, Jürgen Hubbuch

Journal of Chromatography A, 1149 (2007) 312

This paper describes the establishment of the analytics needed for determining the binding orientation of lysozyme on different adsorber materials. It includes a description of the chemical modification of unbound and adsorber-bound lysozyme, the chromatographic separation of the six resulting mono-labelled isoforms and the identification of the labelling position of each lysozyme isoform. It also includes first results with two different adsorber materials: Source 15S and EMD Fractogel SO_3^- .

2. *Effects of ionic strength and mobile phase pH on the binding orientation of lysozyme on different ion-exchange adsorbents*

Florian Dimer, Martin Petzold, Jürgen Hubbuch

Journal of Chromatography A, 1194 (2008) 1121

This paper investigates the effects of mobile phase composition on the binding orientation of lysozyme on two different adsorber materials: SP Sepharose FF and SP Sepharose XL and the binding sites are discussed in detail. Ionic strength did not show any significant effect on either of the adsorbents, while an increasing pH lead to a re-orientation of the molecules on one of the adsorbents.

3. *3D Structure-based Protein Retention Prediction for Ion-Exchange Chromatography*

Florian Dimer, Jürgen Hubbuch

submitted to Journal of Chromatography A

This paper discusses the usage of Molecular Dynamic (MD) simulations for the assessment of adsorption energies for the binding of lysozyme to an SP Sepharose FF surface model at different pH and for different ligand spacings. It includes the generation of the 3D structure for the surface and the overall setup of the simulations. Experimentally determined binding orientations could be confirmed and a good correlation of the calculated adsorption free energies was found, allowing for the prediction of the retention time of ribonuclease A.

4. *Detailed analysis of membrane adsorber pore structure and protein binding by advanced microscopy*

Jun Wang, Florian Dimer, Jürgen Hubbuch, Mathias Ulbricht

Journal of Membrane Science 320 (2008) 456

This article shows the development of a module that can be used to visualize protein transport inside membrane adsorber materials in a time- and space resolved manner under flow conditions on a confocal laser-scanning microscope. Filamentous structures responsible for protein binding could clearly be distinguished from structure-forming cellulose fibers and dynamic breakthrough curves were determined at different locations inside the membrane.

5. *A novel two-zone protein uptake model for affinity chromatography and its application to the description of elution band profiles of proteins fused to a family 9 cellulose binding module affinity tag*

Mojgan Kavooosi, Nooshafarin Sanaie, Florian Dimer, Jürgen Hubbuch, Douglas G. Kilburn, Charles A. Haynes

Journal of Chromatography A, 1160 (2007) 137

In this manuscript a new transport model for inner-particle transport is introduced and compared to time-resolved confocal laser-scanning microscopy images of single adsorber particles. In contrast to older models, this model splits the particles in two zones: an protein filled out shell and an empty inner core. This significantly improved the modelling of breakthrough curves. It also includes a term to describe protein adsorption as a concentration dependent process (in agreement with the Langmuir model) in contrast to an older shrinking core model.

A NOVEL APPROACH TO CHARACTERIZE THE BINDING ORIENTATION OF LYSOZYME ON ION-EXCHANGE RESINS

Florian Dismer, Juergen Hubbuch*

Institute of Biotechnology 2, Research Centre Juelich, 52425 Juelich, Germany

** Corresponding author. Tel.: +49 2461 616044; fax: +49 2461 613870. E-mail address: j.hubbuch@fz-juelich.de (J. Hubbuch).*

Abstract

Much work has been done to qualify and quantify chromatographic adsorption and transportation mechanisms in different adsorber materials. An important aspect in all studies is the understanding of the binding mechanism between protein and resin on a molecular level in order to optimize processes on the level of adsorber design. We established a method to determine the binding orientation of lysozyme for different materials under various experimental conditions enabling us to observe changes in the mode of adsorption. We varied the protein load of two different adsorber types, Source 15S, a conventional cation exchange resin and EMD Fractogel SO₃, a tentacle-type cation exchanger. We found similar preferential binding sites for the interaction between lysozyme and the surface of these adsorbers at low surface coverage, however, the tentacle adsorber exhibited multi-point binding whereas the binding on Source was limited to one binding site only. With increasing protein density on the surface, lysozyme rotates from a space-consuming side-on to a space-saving end-on orientation on Fractogel, explaining a higher maximum binding capacity for Fractogel. This re-orientation could not be observed for Source.

Keywords: Fluorescent labelling; Protein orientation; Tentacle adsorbers; Chromatography; Surface interaction

1 Introduction

Ion-exchange chromatography is a widely used method to separate molecules depending on charge. Much research has been done to increase the basic understanding of the underlying mechanisms of adsorption and desorption [1] especially the characterization of different adsorber resins [2–6] with regard to their static and dynamic capacities, their chromatographic resolution and the effects of counterions on the retention behaviour of proteins [7–9]. But only little is known so far about the localization and orientation of protein molecules on the adsorber surface on a molecular basis especially for ion exchange materials. In the past few years, the quality of electrostatic calculations using protein continuum electrostatics improved significantly providing an *in silico* approach to predict protein orientations on charged surfaces. Latour and co-workers [10] choose such an approach to predict the orientation of lysozyme, focusing on different adsorber surfaces with varying degrees of hydrophobicity. For the interaction with charged surfaces they found only one possible orientation, whereas for hydrophobic interaction there seemed to be multiple possible ways of binding. Kim and Somorjai [11] tried to experimentally determine the binding of lysozyme, BSA and fibrinogen on hydrophilic and hydrophobic surfaces using visible sum frequency generation (SFG) vibrational spectroscopy as a function of protein concentration. By SFG vibrational spectroscopy, changes in the binding orientation can be estimated by determining the relative orientation of methyl group carrying amino acids, but absolute orientations could not be derived. The authors found that for lysozyme adsorption onto hydrophilic surfaces, the orientation is not a function of the protein concentration, whereas for BSA and fibrinogen the protein molecules seemed to tilt at higher protein concentrations. Hearn and co-workers [12] studied binding of Cyt c and bGH to reversed-phase materials using tryptic digestion of bound protein molecules followed by elution and RP-HPLC analysis of the fragments. Although this method is suitable for reversed-phase materials with a strong interaction between protein and adsorber surface, it is probably not optimal under ion-exchange conditions. This method is also limited to relatively specific binding conditions, namely the optimum conditions for the enzymatic digestion following adsorption and provides relatively limited information about the protein orientation. A third approach used was to identify surface areas crucial for the interaction between protein molecules and adsorber surfaces by characterizing the chromatographic behaviour of recombinant proteins differing in only one or more amino acids. Yao and Lenhoff [13] investigated different cytochrome c variants and calculated free energies for the interaction between the protein and the adsorber surface, using energy-minimized 3D models based on the structure of native cytochrome c. By calculating these interaction free energies, Yao and Lenhoff found a favourable binding site of cytochrome c which correlated well with the experimental data. This work gave a first impression of the surface areas being involved in the interaction of a protein with the adsorber on a molecular level, again pointing out that not only the net charge of a protein plays an important role for its retention, but also the charge distribution on the surface of the molecule. Although this method is suitable for cytochrome c, it is difficult to establish for other proteins, because multiple variants of the protein are needed for such an investigation, differing in only a small number of residues. To gain enough useful information from the experiments resulting in a good prediction of the binding orientation, the variations of the amino acid composition on the surface of the protein have to be distributed evenly

on the surface. There remains always the question whether or not the changes in the 3D structure of the protein can be predicted well enough by energy-minimization procedures due to the fact, that the structure of a protein is only available for the native form. It is also not possible to determine the effects of experimental parameters, such as an increasing protein density on the adsorber surface. In the present work, we developed an easy-to-use method to determine the orientation of lysozyme as a model protein, bound to the surface of Source 15 S as an example of a conventional cation exchange adsorber and EMD Fractogel SO₃ as an example of a tentacle-type adsorber as a function of the amount of protein bound to the adsorber surface. In general, we compared random labelling of specific surface groups of lysozyme with the respective degree of labelling when bound to the surface. By combining a specific dye-labelling reaction and the subsequent analysis of the labelling degrees of the various surface groups it was possible to determine the binding orientation of lysozyme on both adsorber types for different loading states of the resin. The identification and quantification of the various labelled isoforms was performed by analytical cation exchange chromatography. Electrostatic calculations in combination with MALDI-TOF experiments were used to establish and validate the analytical methods. Due to the robustness of this method, other experimental parameters, such as ionic strength, pH, counter-ion type and adsorber material can be varied easily, and their effects on the binding mechanism can be evaluated.

2 Materials and methods

2.1 Materials

Hen egg white lysozyme (L-6876) was purchased from Sigma (St. Louis, MO). Source 15 S, Sephadex-G10 and Cy5 were obtained from GE Healthcare (Uppsala, Sweden), EMD Fractogel SO₃ was purchased from Merck (Darmstadt, Germany). Source 15 S is a porous, spherical cation exchange adsorber material with a polystyrene base matrix and negatively charged SO₃⁻ ligands. The particles have approximately a size of 15 μm. EMD Fractogel SO₃ consists of spherical particles with a synthetic methacrylate base matrix and a diameter between 40 and 90 μm. The ligands are again SO₃⁻ groups, but in this case bound to the surface via spacers, that are bound to hydroxyl groups on the surface, giving the ligands a higher flexibility. Cy5 is an activated monoreactive NHS ester used as a fluorescent dye with a molecular weight of 791 Da. It can be covalently attached to lysine residues on the surface of proteins and is often used in fluorescence microscopy techniques such as confocal laser scanning microscopy to make proteins visible.

2.2 Apparatus

Both gel filtration and ion-exchange chromatography were carried out on an A kta basic 10 HPLC system using Tricorn 5/50 as well as Xk16/20 columns (GE Healthcare Freiburg, Germany). Centrifugation was carried out on a Heraeus Biofuge Pico microcentrifuge (Kendro Lyboratory Products, Langenselbold, Germany). Protein and dye concentrations were determined on a Cary 50 UV/Visible spectrophotometer (Varian Inc., Palo Alto, CA). Peak areas were evaluated with the Unicorn 5.0 software package (GE Healthcare, Freiburg, Germany).

2.3 Protein labelling reaction

A lysozyme solution at various concentrations ranging up to 2.6 mg/ml were first incubated with a defined volume of 8 μ l adsorber material in a total volume of 2ml working buffer (sodium phosphate buffer, 6 mM, pH 7 [14]). Different lysozyme concentrations were used to obtain different protein loading states of the resin. After incubation for 2 h on an Eppendorf shaker (Hamburg, Germany) at 1000 rpm, the samples were centrifuged at 13,000 rpm for 5 min and the supernatant was analyzed in the photometer at 280 nm to determine the amount of bound protein. The resin particles were washed twice with 500 μ l working buffer. Particles were re-suspended in 500 μ l working buffer and an amount of Cy5 dye was added depending on the amount of bound protein, keeping a constant dye to protein ratio of 20 μ g dye/mg lysozyme. As a reference, a sample of 500 μ l of a 1 mg/ml lysozyme solution was labelled under the same conditions to give the labelling efficiency for the various surface groups under optimal accessibility. The labelling reaction was stopped after 30 min by spinning down the particles and discarding the supernatant. To analyze the samples, the protein was eluted from the resin by washing the resin repeatedly with 200 μ l of a 0.5M sodium chloride solution for 30 min each time, until the washing solution was free of protein. After elution, fractions were pooled and the buffer was changed back to the buffer used for LC analytics by gel filtration. All experiments and analysis were performed in duplicates and showed similar results.

Degree of labelling (DoL): The obtained average number of labels attached to a protein or a group of proteins (i.e. proteins found in after elution) during the conjugation procedure.

Labelling efficiency: The fraction of labels attached to a specific lysine residue in relation to the total amount of labels covalently attached during the conjugation procedure.

2.4 LC analytics

Samples were analyzed using a Tricorn 5/50 column packed with 1ml Source 15 S material. 200 μ l sample were applied to the column and eluted with a gradient ranging from 20% buffer B (10mM sodium phosphate, 500 mM ionic strength adjusted with sodium chloride, pH 7.0) to 50% buffer B over 30 column volumes. The absorption of the labelled protein was continuously measured at 280 and 650 nm and peak areas were determined using the evaluation tool of the Unicorn 5.0 software (GE Healthcare Freiburg, Germany), a software package used to control the chromatographic system and to evaluate chromatograms in terms of retention time, peak area and peak symmetry.

2.5 Electrostatic calculations

In a first step, the accessible surface of lysozyme was calculated using the Molecular Surface package by M. Connolly based on ideas by Lee and Richards [15]. Therefore, a hard-sphere model of the protein is created using 3D structural information about the locations of atoms within the protein molecule. Each atomic sphere is given by the van der Waals radius of the atom. Then, a sphere with approximately the radius of the molecule or group, which is supposed to interact with the protein, is rolled over the surface, generating the accessible surface area of the protein. Areas of the hard-sphere model, which cannot be reached by the probe sphere are areas that are not accessible

to the target molecule or group. The structural information for lysozyme was retrieved from the RCSB Protein Data Bank (PDB-ID: 132 1). The probe size was set to 3.0 Å, approximately the size of the functional group on the surface of Source 15 S material (used for the LC analytics). The surface area was then transformed into distinct coordinate points using the same software. Besides the coordinates defining each point, information about the size of the surface area represented by every coordinate point was generated. Surface points within a distinct radius around every positively charged atom (belonging to lysine or arginine residues) on the surface were used for electrostatic calculations. For these calculations, the freely accessible web based tool Protein continuum electrostatics (PCE) was used [16], based on the MEAD (macroscopic electrostatics with atomic detail) package developed by Bashford [17]. This tool calculates electrostatic potential values via finite difference solution to the Poisson-Boltzmann equation at distinct coordinates, specified by the user. The calculated potential at each coordinate together with the surface area information was then used to calculate a mean electrostatic potential for each positively charged atom and its surrounding surface area.

For each Cy5 molecule covalently bound to lysozyme, the net charge of the protein is reduced by 2. To calculate the altered charge distribution on the surface of the molecule, the change of the local charge at the Cy5 bound lysine residue was simulated by reducing the local charge (point charge) from +1 to -1 as well. Any possible structural changes caused by the bound Cy5 molecule were neglected.

2.6 Calculation of surface coverage

After the incubation of lysozyme with different adsorbers, the protein concentration in the supernatant was determined to calculate the amount of bound protein. From these data, maximum binding capacities and binding equilibrium constants were obtained by fitting the data with a Langmuir model. The surface coverage (SC) was then calculated using the following equation:

$$SC = \frac{q}{q_{max}} * 100 [\%] \quad (1)$$

A surface coverage value of 100% refers to the fluid phase conditions used here, although at the pH and the ionic strength of the buffer used for the experiments, a binding capacity close the maximum capacity should be achieved.

3 Results and discussion

3.1 Lysozyme

All proteins dealt with in this work are variants of lysozyme labelled at different lysine residues resulting in a slightly altered charge distribution on the surface. The structure of lysozyme is shown in Fig. 1. Lysozyme is a protein with a size of about 14.3 kDa consisting of 129 residues with a pI of 11.3 and is thus positively charged at pH 7.0. The

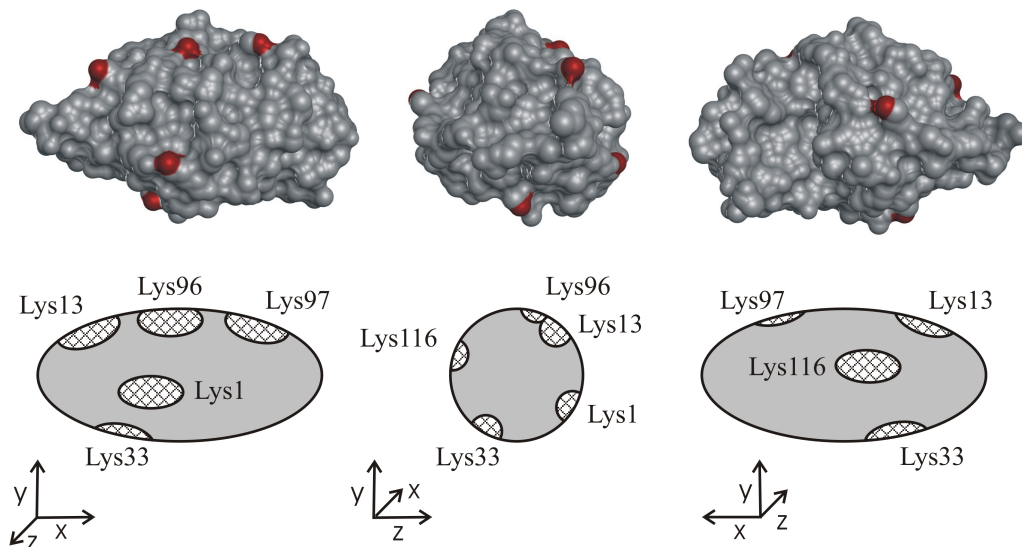


Figure 1: Lysozyme structure (A) with the six lysine residues and schematic drawings (B). The three orientations shown here were created by rotating the molecule around the y-axis in 90° steps.

positive charge carrying residues are 6 lysines and 11 arginines that together with the 9 negatively charged residues result in a positive net charge at pH 7.0.

3.2 LC analytics

Fig. 2 shows a chromatogram of the separation of various forms of lysozyme generated during a random labelling procedure. Each peak of the elution chromatogram represents one of the variants being labelled at a different lysine residue. By comparing the peak areas of the absorption for A280 and A650 the absorption maximum of Cy5 the labelling degree of each form can be calculated. Here the degree of labelling (DoL) is defined as the obtained average number of labels attached to a protein molecule or a group of proteins (i.e. proteins found in an elution peak) during the conjugation procedure. In an earlier study it could be shown by MALDI-TOF analysis that peak 6 and peak 3 expressed a DoL of approximately 1 representing lysozyme being labelled at lysine 97 and lysine 33, respectively [18]. Peak 1 represents lysozyme with a DoL of approximately 2 with lysine 33 and lysine 97 as the most probable labelling positions. The lysozyme in peak 8 shows no absorption at 650 nm and refers to the native, unlabelled form. Baseline separation could not be achieved for all lysozyme variants under the conditions used nevertheless peak areas were determined manually where appropriate. Note, that all the mono labelled forms have approximately the same net charge.

3.3 Electrostatic prediction of the elution sequence

Several parameters influence the protein retention in ion-exchange chromatography, including short-range van der Waals (VDW) interactions, long-range electrostatic interactions and under certain conditions hydrophobic interactions between the protein and the adsorber. Under low salt conditions as used here, hydrophobic interaction can be

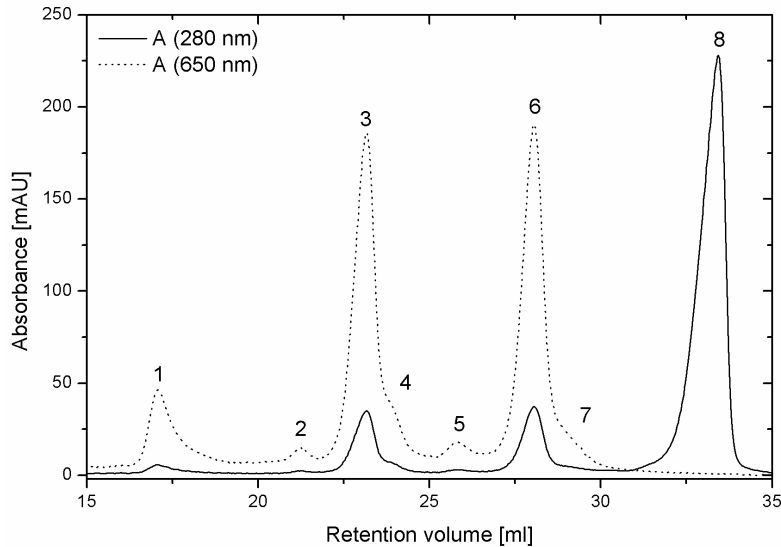


Figure 2: Chromatographic purification of labelled lysozyme, showing the absorption of lysozyme at 280 nm (-) and Cy5 at 650 nm (- -) in the eluate. The A650 to A280 ratio demonstrates that peak 1 is a double labelled lysozyme. Peaks 2-7 are mono labelled isoforms, peak 8 is the native molecule.

neglected. Roth et al. [19] calculated the hydrophobic interaction of lysozyme and hydrophilic polyethylenimine-adsorbers and found it to be comparatively small. The short-range VDW interactions depend mostly on the size of the protein [20], which is for all lysozyme variants approximately the same (with Cy5 having a molecular weight of only 789 Da compared to 14.3 kDa for native lysozyme) and can thus be neglected as well, leaving electrostatic interactions as the driving force for the separation of proteins sharing great structural homologies. A very detailed description of these different forces and their effects on retention of proteins in ion-exchange chromatography as well as the suitability of the solution of the Poisson-Boltzmann equation can be found in a review by Jan Stahlberg [21]. Earlier publications showed that proteins of similar or equal net charge can often be separated by ion-exchange chromatography [7, 22], indicating that the net charge alone is not sufficient to explain chromatographic retention. The reliability of predictions regarding the retention behaviour of charged biomolecules improved by correlating the charge density of a protein with its retention time rather than the net charge [23] and further improved when the charge distribution was taken into account using 3D structure information of proteins [22, 24]. Calculations of charge distributions on the surface of proteins were also successfully used to predict the salt dependency of protein adsorption onto charged surfaces by Stahlberg and co-workers [25].

In order to identify the labelling position of all forms that could be separated or identified on a Source 15 S column, (see Fig. 2) changes in the charge distribution and average electrostatic potential of different variants were correlated to the obtained elution series. The correlation was based on the prerequisite that only changes in the electrostatic potential distribution account for changes in the retention behaviour and anchored by the average electrostatic potential of the three variants where the surface position of Cy5 was identified earlier [18] and the native form eluting last (see Fig. 2 Peak 1, 3, 6, 8).

Previous studies of Haggerty and Lenhoff [22] showed that the probe radius used to calculate the accessible surface of a protein molecule can significantly influence the results

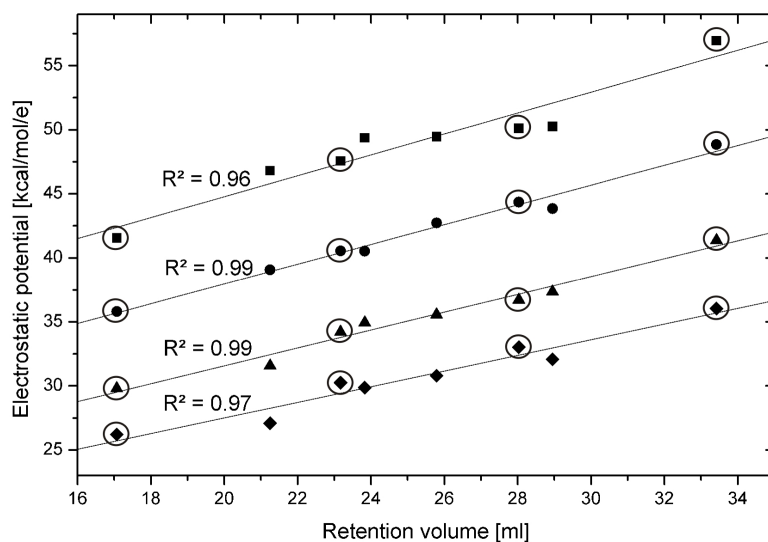


Figure 3: Linear fitting of calculated electrostatic potentials vs. the retention volume of each isoform for patches with 3 Å (■), 4 Å (●), 5 Å (▲) and 6 Å (◆) radius. The linear fit for 5 Å revealed the best results. The lysozyme variants identified with MALDI TOF are marked (○).

of the potential calculations. Usually a probe radius of 1.4 Å is used when calculating the protein surface accessible to water molecules. By using a probe radius of 3.0 Å, which refers to the size of a ligand on the surface of a Source 15 S adsorber, we tried to take the structural properties of the adsorber into account with the additional effect of simplifying the surface to some degree. The charge distribution was accounted for by calculating the mean potential not only for the charge carrying atoms, but for patches of different size surrounding these atoms. Patches were used because it was assumed, that not only the point charges are responsible for the interaction with the adsorber surface, but also the residues located in close proximity to the charges, e.g. a positive charge has a higher affinity to a negatively charged surface when being surrounded by uncharged residues than it has when having a negatively charged residue located next to it. The change of the local charge at the labelling position showed that the electrostatic potential changes not only close to the location where the local charge changes, but also at residues located in greater distance. The calculated mean potential for a patch with a radius of 5 Å around lys1 for example changes from +2.7 kcal/mol/e for native lysozyme down to +2.0 kcal/mol/e in case of a Cy5 molecule bound at lys96, although lys1 is located almost 20 Å away from lys96, which is almost half of the length of the lysozyme molecule. By the use of patches rather than single charge-carrying atoms, negative charges and thus the charge distribution are also accounted for by reducing the mean potential of the patch, which represents a possible interaction site of protein and adsorber. Fig. 3 shows the linear regression of the retention volume of each lysozyme variant and the calculated mean potential for different patch sizes. The total electrostatic potential decreases with increasing patch size due to the fact that the positive charge is located at the centre of each patch surrounded by uncharged or negatively charged residues. The best fit was found for a patch radius of 4 and 5 Å, showing an R^2 of 0.99. As also shown in Fig. 3, the elution sequence of peaks 3 and 4 as well as peaks 6 and 7 cannot be predicted using only the electrostatic potential due to the very small differences in the potentials

of these isoforms. For 4 and 6 Å patch radius, the potentials of peak 4 and 7 are lower than the potentials of the peaks 3 and 6, respectively. Only together with the MALDI TOF data, the exact elution sequence could be determined, represented by a patch size of 5 Å. The elution sequence obtained from the linear fit is as follows, starting with the lowest retention volume: lys33&97, lys13, lys33, lys96, lys116, lys97, lys1 and native lysozyme. It should be mentioned here that due to the simplifications made, our model is not suitable to predict retention volumes in general. It is only applicable when comparing the retention behaviour of variants of the same protein and acts as a basis for the following discussion of lysozyme orientation.

3.4 Binding parameters for Source 15 S and EMD Fractogel SO₃

The maximum binding capacity under the conditions described above determined in the same experimental run as the labelling efficiencies discussed later were $q_{max} = 114$ mg/ml for Source 15 S and $q_{max} = 178$ mg/ml for EMD Fractogel SO₃. The K_a values were $K_a = 166.9$ ml/mg for Source 15 S and $K_a = 249.2$ ml/mg for EMD Fractogel SO₃, indicating that the tentacle-type adsorber had both higher static binding capacity and higher binding affinity than the conventional adsorber, although previous publications showed, that the ionic capacity is lower for EMD Fractogel SO₃ than for Source 15 S [26]. A possible explanation for that is discussed below.

3.5 Evaluation of binding orientation and orientation changes

The outcome of a labelling reaction is a statistical effect influenced by the reactivity and accessibility of the respective reaction partners, in our case the lysine residues and the respective fluorescent molecules. The difference between the labelling sites i.e. lysine residues on the protein surface is the reactivity and accessibility towards the conjugation reaction. These differences arise from the three dimensional structure and amino acid composition of the protein. The principle hypothesis behind our study lies in the relative change of the labelling efficiency obtained for different lysine residues on the surface of the lysozyme molecule. The labelling efficiency is represented by the fraction of each labelled isoform relatively to the total amount of labelled molecules, e.g. a labelling efficiency of 35% for Lys97 means, that 35% of all labelled lysozyme molecules have a dye molecule covalently attached to position Lys97 (see

Fig. 4). The labelling efficiency of a certain lysine residue is a relative term and is thus independent of the total amount of labelled molecules. This said an important factor when interpreting the results is the ratio between protein accessible for a reaction and dye used for the labelling reaction. In general an excess of dye molecules leading to a complete labelling of all lysines accessible would provide the clearest signal. This approach is, however, experimentally not feasible due to costs and the influence on adsorption conditions caused by the dye when present in such a high excess. We thus opted for a constant and rather low dye to protein ratio for the conjugation procedure. Note, the total amount of proteins labeled remains widely constant, only the distribution changes and thus labelling efficiencies can increase and decrease. A change in labelling efficiency upon binding is thus the result of a reduced accessibility of highly reactive sites leaving more

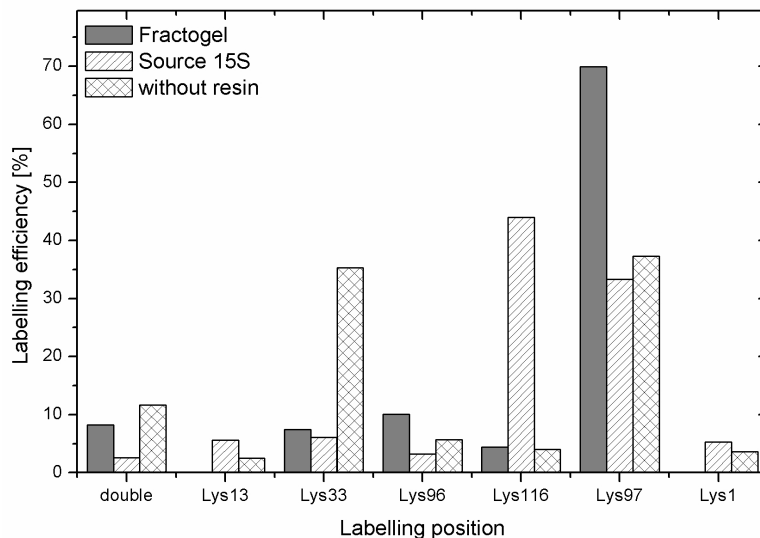


Figure 4: Fraction of each labelled form after labelling of lysozyme in the bound state at low surface coverage (28% for Source 15 S and 18% for EMD Fractogel SO₃) compared with lysozyme labelled under normal conditions in the absence of resin.

dye as reaction partner for the formerly less reactive sites. Variations in the labelling efficiency of these low reactive sites caused by such a decrease provide further indications on orientation and sterical hindrance due to neighbouring molecules. Under the given experimental conditions, the order of lysine reactivity of lysozyme in free solution starting with the highest reactivity is Lys97, Lys33 > Lys1, Lys96, Lys116 > Lys13 (see Fig. 4). During the analysis of our results we decided changes of about 5% or less to be not significant enough to allow a sound interpretation. With an increasing inner particle protein concentration, the total amount of labelled lysozyme (Degree of labelling) and consequently the composition of labelled lysozyme forms changes in the range of a few percent. The reason for this lies probably in the locally higher protein concentration during the conjugation reaction caused by the increasing surface coverage (data not shown). Additionally, with a sterical hindrance of one or more labelling positions, the labelling efficiency might increase slightly at other positions due to a newly adjusted chemical equilibrium for the labelling reaction without actual changes in the binding orientation.

3.6 Binding orientation on Source 15 S

Fig. 4 shows the distribution of lysozyme variants after labelling in the bound state at relatively low surface coverage (28% for Source 15 S and 18% for EMD Fractogel) compared to the labelling efficiency of the reference samplerandom labelling of lysozyme in free solution. For lysozyme bound to Source 15 S, the fraction of labelled lys33 is reduced significantly from 35.3% to 6.1% indicating that the binding interface of lysozyme is located close to lys33. This is in agreement to molecular simulations addressing lysozyme binding on a charged surface [27] which further indicate that next to lys33, lys1 is also involved in the binding. The latter explaining why the labelling efficiency of lys1 does not increase as a result of the sterical hindrance of lys33. Taking this into account, the molecule is tilted slightly around the x-axis, thus sterically hindering the labelling

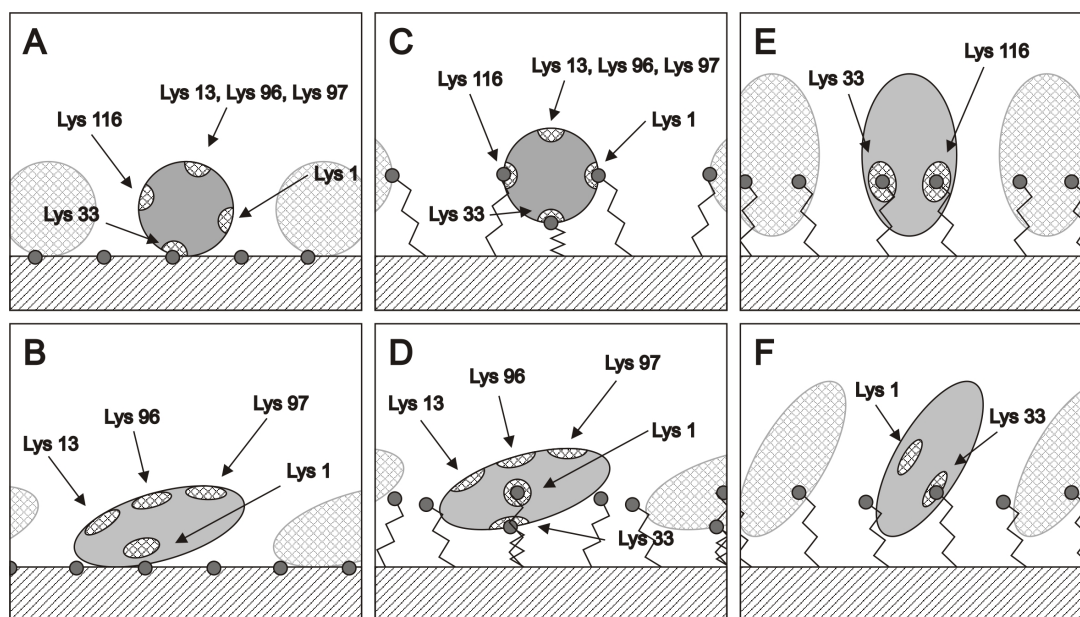


Figure 5: Possible orientations of lysozyme on Source 15 S for high surface coverage (A) front view and (B) side view and on EMD Fractogel SO₃ for low surface coverage (C) front view and (D) side view and for high surface coverage (E) front view and (F) side view.

reaction at both locations (see Fig. 5 A

showing the front view and B showing the side view). As a result of the hindrance and thus dye available to other lysine residues, the freely accessible lys116 is labelled more efficiently (from 4.0% in the unbound state to 44% in the bound state). The fraction of labelled lys97 remains about the same, still contributing significantly to the total amount of labelled protein, indicating that lys97 is also freely accessible. The reason why lys116 is preferred over lys97 in this case might be connected to reactivity changes caused by the adsorption on the solid surface. There are further no significant changes for lys13 and lys96. For an increasing surface coverage of the adsorber, bringing the lysozyme molecules bound to the adsorber into closer proximity, the fraction of labelled lys116 located at the right hand site of the molecule decreases down to 17.9% (see Fig. 6) probably due to steric hindrance by adjacent molecules (see Fig. 5A and B). At the same time the fraction of labelled lys97 increases suggesting that this position is still freely accessible. Besides the significant decrease at lys116, a minor increase of the fraction of labelled lys1 is observable (from 5.3% to 10.7%). Altogether the data suggest that changes of the labelling efficiency in this case result highly probable from sterical hindrance of neighbouring molecules and thus there are no orientational changes with increasing protein density adsorbed to Source 15 S.

3.7 Binding orientation on EMD Fractogel SO₃

Similar to the results for Source 15 S, lys33 is close to the favourable binding interface of lysozyme on EMD Fractogel SO₃. The fraction of labelled lys33 is reduced down to 7.4% (see Fig. 3). Interestingly, the main increase is not found for lys116 (as it was for Source 15 S) but for lys97, which did not significantly change when lysozyme was bound to Source 15 S. Both positions on the left and on the right side of the lysozyme molecule (lys1

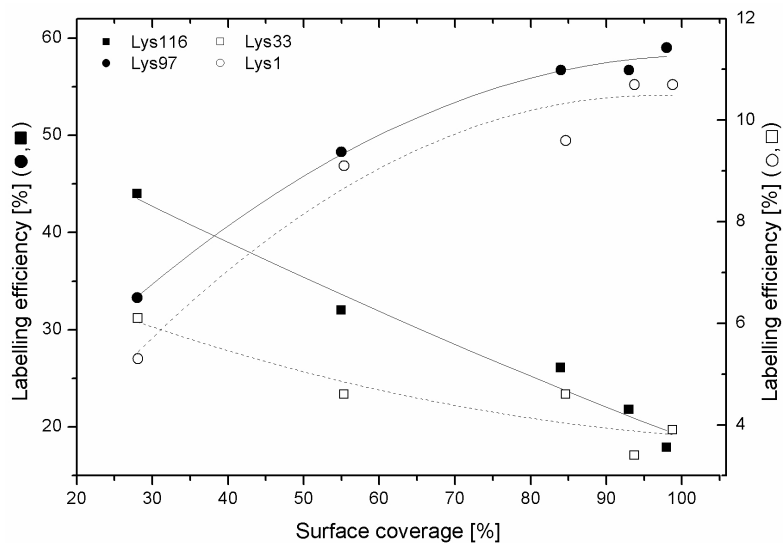


Figure 6: Changes in the lyszyme-variant composition after labelling of bound lyszyme with increasing loading of the resin (Source 15 S). The solid symbols refer to the scale of the left y-axis, the empty symbols to the scale of the right y-axis.

and lys116) are apparently not accessible, resulting in an increased labelling efficiency at position lys97. Lys1 is not labelled at all at low surface coverage. This could either be explained by a multi-point interaction involving lys1, lys33 and lys116 (see Fig. 5C and D) or sterical hindrance due to the lyszyme orientation. EMD Fractogel SO₃ is a tentacle-type adsorber with ligands being attached to flexible spacer arms with a length of approximately 200 Å, reaching into the pores. Due to the flexibility of the ligands it is possible, that the lyszyme molecule is bound at more than one site, supporting the fact that the K_a for EMD Fractogel is roughly 1.5 times higher than the K_a for Source 15 S.

With increasing surface coverage, lys1 becomes available for labelling (up to about 20% of the total labelled protein, see Fig. 7), suggesting a re-orientation of the molecules, also Fig. 6. Changes in the lyszyme-variant composition after labelling of bound lyszyme with increasing loading of the resin (Source 15 S). The solid symbols refer to the scale of the left y-axis, the empty symbols to the scale of the right y-axis. supported by the significantly decreasing labelling efficiency at lys97 (from 73.7% down to 55%). One explanation is a rotation around the x-axis, destroying the interaction between lys1 and the adsorber. Lys97 would tilt towards the adsorber surface resulting in a sterical hindrance of the labelling reaction by neighbouring molecules. This explanation, however, is less favourable due to the fact, that there is no obvious driving force for such a rotation. A second explanation is a rotation around the z-axis (see Fig. 5 E and F), resulting in a more or less end-on orientation of the lyszyme molecule. In this way lys97 is sterically hindered as well by neighbouring molecules. Apparently the interaction between lys1 and the adsorber is reduced, so lys1 becomes partly available for the labelling reaction. The driving force for this re-orientation is probably a decreased size of the surface area needed by bound lyszyme resulting in an increased binding capacity. Thinking of lyszyme as an ellipsoid-shaped molecule, and taking into account its dimensions, the surface area covered by lyszyme in a complete end-on orientation is about 2-times smaller, explaining the higher maximum binding capacity of EMD Fractogel SO₃ (in our experiments about

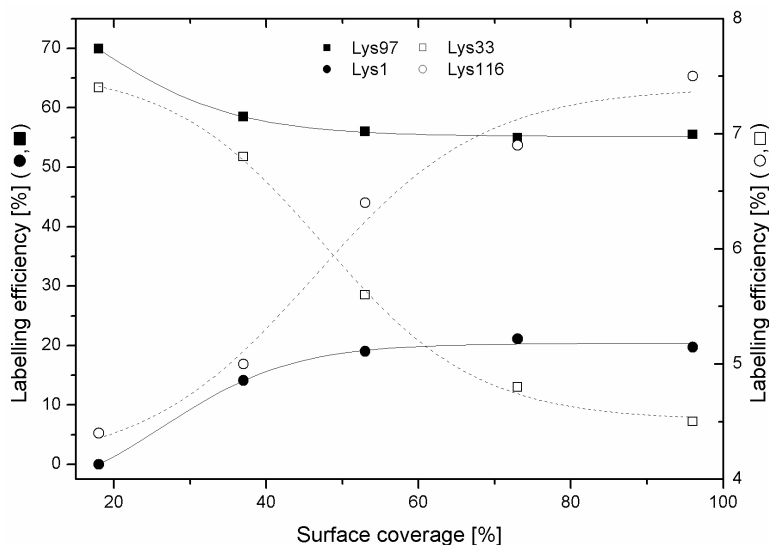


Figure 7: Changes in the lysozyme-variant composition after labelling of bound lysozyme with increasing loading of the resin (EMD Fractogel SO₃). The solid symbols refer to the scale of the left y-axis, the empty symbols to the scale of the right y-axis.

1.6- times higher than Source 15 S), although the ionic capacity of Source 15 S is about 1.5 times higher than that of EMD Fractogel SO₃ [26]. Wu and Walters [28] investigated the effects of increasing ligand density of adsorbers on the capacity and the retention of proteins. They determined Z parameters for the binding of lysozyme to adsorbers with varying ligand densities. The Z parameter represents the amount of interaction sites between the adsorber and a protein involved in the binding. For low but increasing ligand densities, they found increasing Z values indicating differences in the binding mechanism up to a critical ligand density. Further increase did not result in an increased Z value. In our case, the higher ligand density of Source 15 S expressed by the higher ionic capacity cannot be efficiently used by the side-on bound lysozyme molecules, whereas the flexible ligands of EMD Fractogel SO₃ allow an end-on orientation of lysozyme reducing the surface area covered by each lysozyme molecule and thus the amount of covered ligands and allowing a more efficient use of ligands. Earlier publications already indicated that tentacle-type adsorbers might have an increased affinity due to multi-point interactions with proteins [5, 29–34], and that the binding capacity is generally higher compared to conventional adsorbers [5].

References

- [1] J. S. Fritz, Early milestones in the development of ion-exchange chromatography: a personal account, *Journal of Chromatography A* 1039 (1-2) (2004) 3–12.
- [2] C. Chang, A. M. Lenhoff, Comparison of protein adsorption isotherms and uptake rates in preparative cation-exchange materials, *J Chromatogr A* 827 (2) (1998) 281–93.

-
- [3] E. Boschetti, P. Girot, L. Guerrier, B. Andre, [chromatographic sorbents for the preparative separation of proteins], *Ann Pharm Fr* 51 (6) (1993) 299–306.
- [4] H. Chen, C. Horvath, High-speed high-performance liquid chromatography of peptides and proteins, *J Chromatogr A* 705 (1) (1995) 3–20.
- [5] P. DePhillips, A. M. Lenhoff, Determinants of protein retention characteristics on cation-exchange adsorbents, *J Chromatogr A* 933 (1-2) (2001) 57–72.
- [6] P. DePhillips, I. Lagerlund, J. Farenmark, A. M. Lenhoff, Effect of spacer arm length on protein retention on a strong cation exchange adsorbent, *Anal Chem* 76 (19) (2004) 5816–22.
- [7] W. Kopaciewicz, F. E. Regnier, Mobile phase selection for the high-performance ion-exchange chromatography of proteins, *Anal Biochem* 133 (1) (1983) 251–9.
- [8] W. Kopaciewicz, F. E. Regnier, A system for coupled multiple-column separation of proteins, *Anal Biochem* 129 (2) (1983) 472–82.
- [9] A. N. Hodder, M. I. Aguilar, M. T. Hearn, High-performance liquid chromatography of amino acids, peptides and proteins. lxxxix. the influence of different displacer salts on the retention properties of proteins separated by gradient anion-exchange chromatography, *J Chromatogr* 476 (1989) 391–411.
- [10] Y. Sun, W. J. Welsh, R. A. Latour, Prediction of the orientations of adsorbed protein using an empirical energy function with implicit solvation, *Langmuir* 21 (12) (2005) 5616–26.
- [11] J. Kim, G. A. Somorjai, Molecular packing of lysozyme, fibrinogen, and bovine serum albumin on hydrophilic and hydrophobic surfaces studied by infrared-visible sum frequency generation and fluorescence microscopy, *J Am Chem Soc* 125 (10) (2003) 3150–8.
- [12] M. I. Aguilar, D. J. Clayton, P. Holt, V. Kronina, R. I. Boysen, A. W. Purcell, M. T. W. Hearn, Rp hplc binding domains of proteins, *Analytical Chemistry* 70 (23) (1998) 5010–5018.
- [13] Y. Yao, A. M. Lenhoff, Electrostatic contributions to protein retention in ion-exchange chromatography. 1. cytochrome c variants, *Anal Chem* 76 (22) (2004) 6743–52.
- [14] T. Herrmann, M. Schroder, J. Hubbuch, Generation of equally sized particle plaques using solid-liquid suspensions, *Biotechnology Progress* 22 (3) (2006) 914–918.
- [15] B. Lee, F. M. Richards, Interpretation of protein structures - estimation of static accessibility, *Journal of Molecular Biology* 55 (3) (1971) 379.
- [16] M. A. Miteva, P. Tuffery, B. O. Villoutreix, Pce: web tools to compute protein continuum electrostatics, *Nucleic Acids Res* 33 (Web Server issue) (2005) W372–5.

- [17] D. Bashford, Macroscopic electrostatic models for protonation states in proteins, *Front Biosci* 9 (2004) 1082–99.
- [18] C. Teske, R. Simon, A. Niebisch, J. Hubbuch, Changes in retention behaviour of fluorescently labeled proteins during ion-exchange chromatography caused by different protein surface labeling positions, *Biotechnology and Bioengineering* accepted.
- [19] C. M. Roth, J. E. Sader, A. M. Lenhoff, Electrostatic contribution to the energy and entropy of protein adsorption, *Journal of Colloid and Interface Science* 203 (1) (1998) 218–221.
- [20] C. M. Roth, K. K. Unger, A. M. Lenhoff, Mechanistic model of retention in protein ion-exchange chromatography, *Journal of Chromatography A* 726 (1-2) (1996) 45–56.
- [21] J. Stahlberg, Retention models for ions in chromatography, *Journal of Chromatography A* 855 (1) (1999) 3–55.
- [22] L. Haggerty, A. M. Lenhoff, Relation of protein electrostatics computations to ion-exchange and electrophoretic behavior, *Journal of Physical Chemistry* 95 (3) (1991) 1472–1477.
- [23] L. A. Haff, L. G. Fagerstam, A. R. Barry, Use of electrophoretic titration curves for predicting optimal chromatographic conditions for fast ion-exchange chromatography of proteins, *Journal of Chromatography* 266 (AUG) (1983) 409–425.
- [24] A. M. Lenhoff, Contributions of surface-features to the electrostatic properties of rough colloidal particles, *Colloids and Surfaces A* 87 (1) (1994) 49–59.
- [25] E. Hallgren, F. Kalman, D. Farnan, C. Horvath, J. Stahlberg, Protein retention in ion-exchange chromatography: effect of net charge and charge distribution, *Journal of Chromatography A* 877 (1-2) (2000) 13–24.
- [26] N. Tugcu, S. M. Cramer, The effect of multi-component adsorption on selectivity in ion exchange displacement systems, *Journal of Chromatography A* 1063 (1-2) (2005) 15–23.
- [27] A. Steudle, Personal communication.
- [28] D. L. Wu, R. R. Walters, Effects of stationary phase ligand density on high-performance ion-exchange chromatography of proteins, *Journal of Chromatography* 598 (1) (1992) 7–13.
- [29] W. Kopaciewicz, M. A. Rounds, F. E. Regnier, Stationary phase contributions to retention in high-performance anion-exchange protein chromatography - ligand density and mixed-mode effects, *J. Chromatogr.* 318 (2) (1985) 157–172.
- [30] R. Janzen, K. K. Unger, W. Muller, M. T. W. Hearn, Adsorption of proteins on porous and nonporous poly(ethyleneimine) and tentacle-type anion-exchangers, *Journal of Chromatography* 522 (1990) 77–93.

-
- [31] J. R. Xie, M. I. Aguilar, M. T. W. Hearn, High-performance liquid-chromatography of amino-acids, peptides and proteins .138. adsorption of horse heart cytochrome-c onto a tentacle-type cation-exchanger, *Journal of Chromatography A* 691 (1-2) (1995) 263–271.
- [32] J. R. Xie, M. I. Aguilar, M. T. W. Hearn, Studies on the adsorption capacities of proteins with a tentacle-type ion-exchanger and their relationship to the stoichiometric retention parameter $z(c)$, *Journal of Chromatography A* 711 (1) (1995) 43–52.
- [33] F. W. Fang, M. I. Aguilar, M. T. W. Hearn, High-performance liquid chromatography of amino acids, peptides and proteins .93. influence of temperature on the retention behaviour of proteins in cation-exchange chromatography, *Journal of Chromatography A* 729 (1-2) (1996) 49–66.
- [34] F. W. Fang, M. I. Aguilar, M. T. W. Hearn, High-performance liquid chromatography of amino acids, peptides and proteins .96. temperature-induced changes in the bandwidth behaviour of proteins separated with cation-exchange adsorbents, *Journal of Chromatography A* 729 (1-2) (1996) 67–79.

EFFECS OF IONIC STRENGTH AND
MOBILE PHASE PH ON THE BINDING
ORIENTATION OF LYSOZYME ON
DIFFERENT ION-EXCHANGE ADSORBENTS

Florian Dimer, Martin Petzold, Juergen Hubbuch*

Institute of Biotechnology 2, Research Centre Juelich, 52425 Juelich, Germany

* Corresponding author. Tel.: +49 2461 616044; fax: +49 2461 613870. E-mail address: j.hubbuch@fz-juelich.de (J. Hubbuch).

Abstract

Chromatography is the most widely used technique for the purification of biopharmaceuticals in the biotech industry. Surprisingly, process development is often still based on empirical studies or experience; recently high-throughput screening stations are employed to minimize development time and to improve screening quality. Still, experimental effort remains high and a more detailed understanding of adsorption mechanisms on a molecular level underlying chromatographic separation could help in the future to select and design chromatography steps in silico. In this study, we focused on the elucidation of protein orientation upon adsorption onto a chromatographic resin. We identified two characteristic binding sites of lysozyme on SP Sepharose Fast Flow and one multipoint interaction of lysozyme with SP Sepharose XL. Increasing ionic strength did not significantly influence the binding, whereas changes in the mobile phase pH led to a re-orientation on SP Sepharose FF. This phenomenon agrees well with theoretical considerations, including a detailed description of the surface charge distribution with changing pH and linear elution experiments, giving an idea why proteins are often retained on ion-exchange materials beyond their isoelectric point.

Keywords: Ion exchange chromatography; Binding mechanism; Lysozyme; Ionic strength; Mobile phase pH; Characteristic charge

1 Introduction

Chromatographic separation is one of the most important separation method in downstream processing and constitutes an essential component in the industrial purification of biomolecules. In the recent decades, the principles of adsorption and desorption in the context of chromatography have been investigated in increasing detail, aiming for a better understanding of the molecular processes. Significant progress was made by applying computer simulation methods with structural information about the target molecule and the chromatography matrix [1–5]. In ion-exchange chromatography (IEC), charge distribution was identified to play an important role in the retention behaviour of a molecule [6]. Therefore, *in silico* approaches should take both the molecule geometry and the correct arrangement of charged groups on the surface into account [7, 8]. With detailed knowledge about the predominant patches of matrix interaction on the molecule surface, protein retention can be described mechanistically and effects of changed process parameters on the retention behaviour could become predictable. Chromatographic separation could be optimized *in silico* on the level of adsorbent selection and even design and process steps could be improved. Although much effort has been made in computer simulation of protein binding, experimental confirmation of the proposed sites of interaction is either lacking or only obtained with the help of elaborate procedures such as Fourier transform infrared spectroscopy (FTIR), that in most cases only detects changes in the molecule orientation rather than the absolute orientation.

Gill et al. [9–11] studied the effect of site-directed mutations on the adsorption behaviour of rat cytochrome b5 on an anion exchange matrix. The authors neutralized charged residues by replacement with other amino acids. A significant reduction of the Z number (number of charged interactive binding sites between protein surface and stationary phase support [1]) and adsorption affinity led to identification of a preferred chromatographic contact region. The method was unfavourable with regard to its complex nature and the risk of changing the 3D protein structure by introducing two or more substitutions at once.

A similar approach was made by Fausnaughpollitt et al. [12] who compared seven avian lysozyme variants with similar three-dimensional structure that contained several amino acid substitutions across their surface. Variation of retention behaviour was experimentally tested for three different modes of adsorption, namely immuno-affinity chromatography (IAC), hydrophobic interaction chromatography (HIC) and IEC. For all three modes, chromatographic contact regions were identified in which amino acid substitutions had an effect on the retention of the molecule. However, for IEC that region was comparably large and not clearly defined since amino acid alteration at multiple sites influenced retention. Similar experiments were conducted by Chicz and Regnier [13, 14] for subtilisin variants also applying reversed-phase chromatography.

Protein adsorption is a complex process which depends on a number of factors in addition to the ones mentioned above. The effect of lysozyme concentration on a negatively charged silica surface (surface coverage) on the molecule orientation was investigated by Daly et al. [15]. Employing total internal reflection fluorescence (TIRF), the authors found that, depending on the lysozyme surface concentration, a two-stage re-orientation occurs. Additionally, the influence of ionic strength and shear rate were examined.

The present work is based on a method introduced earlier by the authors [16] and

aims for a description of protein orientation in dependence of a large set of parameters. In the course of the previous work, we determined main contact regions on the surface of hen egg white lysozyme during adsorption onto two different strong cation exchangers with the help of Cy5, a lysine-specific fluorescent dye. The surface of lysozyme contains six evenly distributed lysine residues. By comparing the reactivity of each lysine residue for unbound lysozyme with adsorbent-bound lysozyme, conclusions about the sterical hindrance of certain lysine residues upon binding to the surface and thus the protein orientation on the stationary phase were possible.

While in the former experiments only the surface coverage of the matrix and the type of adsorbent (conventional versus tentacle-type) were varied, the present paper covers ionic strength and pH of the mobile phase as additional parameters. The buffers salt concentration is known to influence the interaction affinity and thus the retention of proteins [17–19], which led for example to the widely accepted non-stoichiometric steric mass action model of Brooks and Cramer [20] that provides a mechanistic understanding of proteinadsorbent interaction under different salt concentrations. In this model, binding of a protein leads to a shielding of a number of binding sites on the adsorbent surface that is usually higher than the characteristic charge of this protein, giving an idea about the space consumption of a protein in the bound state and thus some information about orientational changes. The degree of steric shielding is described by a steric factor, which does not depend on the ionic strength of the mobile phase, although the direct experimental proof for the effects of the salt concentration on the binding orientations remained more or less unexplored.

In contrast to that, the pH directly influences the charge distribution on the surface of a protein due to the differences in the intrinsic pK_a values of all charged amino acids and thus influences the affinity between protein and adsorbent surface by changing the protein properties. Interestingly, there are only a few publications dealing with the effect of the mobile phase pH on chromatographic retention and resolution [21–26][2126] and again only a few of these offer some kind of mechanistic explanation for the experimental findings, e.g. the fact that some proteins are retained on ion-exchange materials beyond their pI, where the net charge of the protein equals the charge of the adsorbent surface. With the present work, we want to shed some light on these findings by taking a detailed look at the identified binding sites and by relating the characteristic charge of a protein as described by the SMA model to the charge of these binding sites, pointing out the fact that characteristic charge and net charge of a protein correlate only to some degree. In this respect, our previous paper [16] acts as a base for discussions on analytical methods used and specifically the results obtained for adsorbent Source 15 S mentioned throughout the present paper.

2 Materials and methods

2.1 Materials

Hen egg white lysozyme (L-6876) from Sigma (St. Louis, MO, USA) was dissolved in the respective working buffer at various concentrations. All salts including 1M NaOH for pH adjustment were purchased from Merck (Darmstadt, Germany). The two adsorbent materials analyzed (SP Sepharose Fast Flow and SP Sepharose XL) were obtained from

GE Healthcare (Uppsala, Sweden), as well as Source 15 S for the analytical column. Both SP Sepharose adsorbents share the same backbone (porous 6% cross-linked agarose) and are equal in size (average diameter 90 μm) and pore size distribution. While the standard-type adsorbent SP Sepharose has an open pore network (sulphopropyl ligands are directly attached to the pore walls), the tentacle-type adsorbent SP Sepharose XL carries the ligands on long flexible dextran chains, which fill the particle pores. In contrast to the experiments previously performed with Source 15 S and EMD Fractogel SO_3 [16], the two adsorbent types tested are more comparable, not only with regard to particle and pore size, but also in terms of their backbone chemistry. The previously tested adsorbent type Source 15 S was different from all other analyzed types by having a hydrophobic base matrix. Cy5 fluorescent dye (PA 15104), used for the protein labeling reaction, was purchased from GE Healthcare (Uppsala, Sweden).

2.2 Adsorption isotherms on robotic platform

Protein binding onto 13.4 μL adsorbent samples (aliquots made with plaque device by Atoll, Germany) was performed in triplicate in 1.2mL deep well plates (Abgene, UK), using 20 different concentrations. Pipetting, incubation and centrifugation was automatically conducted on a Tecan Evo 200 robotic platform (Crailsheim, Germany). For protein binding, the plate was shaken at 1500 rpm for 2 h on a Variomag Teleshake 4 MTP shaker (H + P Labortechnik, Oberschleiheim, Germany). For the ionic strength experiments, a 10 mM sodium phosphate ground buffer was used and the ionic strength was adjusted by adding sodium chloride. Then the pH was adjusted to pH 7. For the pH experiments the following buffers were used: 10 mM citrate buffer (pH 5), phosphate buffer (pH 7), carbonate buffer (pH 9), glycine (pH 11) or NaOH (pH 12).

After equilibrium was reached, the plates were centrifuged for 10 min at 1000 rpm in a Rotanta 46 RSC centrifuge (Hettich, Tuttlingen, Germany), supernatant was transferred into 96 well UVstar plates (Greiner, Frickenhausen, Germany) and A280 was measured with a Genios Pro microplate UVVIS reader (Tecan, Crailsheim, Germany). Adsorption isotherms were then generated.

2.3 Protein labeling

Eight adsorbent samples covering a protein surface coverage range of 20100% were transferred in duplicate into AcroPrep 96 filter plates 0.45 μm GHP (Pall, Ann Arbor, MI, USA). The term surface coverage is calculated as Q/Q_{max} with the Q_{max} coming from the best binding conditions for each individual adsorbent. It is thus a relative data on protein density within the adsorbent. When conducting experiments with varying ionic strength Q_{max} is derived from the data set using 10 mM sodium phosphate, while for pH experiments Q_{max} is derived from the data set using pH 7. The term surface coverage was introduced, because in previous experiments we found the protein orientation on some adsorbents to be a function of the protein density and thus the distance between protein molecules on the surface. When comparing different binding conditions for one adsorber, it is thus necessary to establish a relationship between each individual particle load and a global maximum binding capacity. Washing with working buffer, incubation with Cy5 fluorescent dye and elution was all performed manually inside the filter plate wells, using

a multipipette. For washing, the particles were flushed one to three times with 300 μL of 10 mM sodium phosphate buffer (ionic strength (IS) = 19 mM), pH 7, minimizing the chance of unwanted protein desorption (at this ionic strength, no measurable amount of protein elutes). Cy5 labeling was then done in a 300 μL mixture of the respective working buffer (10mM sodium phosphate, pH 7, IS adjusted with NaCl) and Cy5 in a constant dye to protein ratio of 20 μg dye/mg protein (cf. [16]). The top and bottom of the filter plate were sealed with tape pads (3M, St. Paul, MN, USA) and adhesive tape, respectively, and the plate was shaken for 30 min at 1500 rpm. Before the labeled protein was desorbed, unbound material was washed off by flushing the particles three times with 10 mM sodium phosphate, pH 7. The effect of the labeling buffer composition and pH on the outcome of the isoform mixture was also investigated. The first experimental setup included labeling under the same conditions used for protein binding, except for pH 12 (at this pH the labeling is not possible). In the second experimental setup the labeling was performed at pH 7 independent from the binding conditions. Both setups showed qualitatively the same results, but differed in the absolute values. Due to the fact, that the pH showed significant effect on the efficiency of the labeling reaction especially at high pH, we decided to label at pH 7, although we were aware of the risk that the protein orientation might slightly change during labeling. In fact, the worst case scenario in this respect and clear indicator would be that labeling at pH 7 results in the same binding orientation for all experimental pH, which we did not observe.

2.4 Elution

For protein desorption, elution buffer (10 mM sodium phosphate, pH 7, with 0.5 M NaCl) was used. The loaded particles were repeatedly incubated with 300 μL elution buffer and shaken for 20 min at 1500 rpm. The eluate was collected by centrifuging the filter plate, being stacked onto a standard polystyrene microplate, flat bottom (Greiner, Frickenhausen, Germany). Steps were repeated until the eluate of all samples turned clear (46 runs in average); fractions with an A_{650} (absorbance maximum of Cy5 dye) of higher than 0.35 were collected for analytical chromatography.

2.5 Analytical column chromatography

The pooled eluates of each adsorbent sample were transferred into 0.3 mL microvials PP (VWR, Langenfeld, Germany). For samples of higher protein concentration, the eluate was diluted two- to fivefold with 10mM sodium phosphate buffer, pH 7. This helped to improve the peak resolution by reducing the amount of material applied. Also, buffer exchange by gel filtration, as done in [16], could be omitted. Gradient elution chromatography was performed exactly as outlined in [16] on an Akta Basic 10 FPLC system with a Tricorn 5/50 column. Sample application was done automatically with an A-900 autosampler (both GE Healthcare, Uppsala, Sweden), using a 450 μL sample loop (205 μL sample + 245 μL transport fluid (water)). Sodium phosphate (10 mM), pH 7 (standard working buffer), was used as buffer A, buffer B contained 0.5 M NaCl in addition. After column equilibration and sample loading, an elution gradient was applied that ranged from 0 to 55% buffer B in 55 column volumes. During all steps, a flow rate of 0.5 mL/min was applied. For every buffer pH and ionic strength tested, a reference

probe was prepared with Cy5 bound to unadsorbed (native) lysozyme at 0.33 mg/mL in the dye to protein ratio stated.

2.6 Data evaluation

The FPLC software package Unicorn 5.0 (GE Healthcare, Uppsala, Sweden) was used for method setup, run control and curve evaluation. Peak areas beneath the A_{280} (protein) and A_{650} (dye) curves were determined and the relative area of each A_{650} peak was calculated according to [16], with the difference that the peak of doubly labeled protein, if present, was ignored. For a detailed description of the data evaluation procedure, please refer to [16].

2.7 Theoretical considerations

For protonation state calculations, the HendersonHasselbalch equation was used.

$$pH = pK_a + \log \frac{c(A^-)}{c(HA)} \quad (1)$$

The intrinsic pK_a values were calculated using the PCE (protein continuum electrostatics) web tool [27] and a 3D structure of lysozyme (PDB-ID: 132l).

2.8 Retention experiments

To determine the pH dependent strength of interaction of lysozyme with SP Sepharose FF and SP Sepharose XL, retention experiments were conducted. Lysozyme solutions were prepared at pH 5, 7, 9, 11 or 12 using 10 mM citrate buffer (pH 5), phosphate buffer (pH 7), carbonate buffer (pH 9), glycine (pH 11) or NaOH (pH 12). The columns used were 1 ml prepacked columns (Atoll, Germany), separation was performed on the same A kta system as described for the analytics. Sample loading (240 μ L, 3 mg/mL lysozyme) was followed by two-column volumes wash with buffer A (10 mM, buffer type depending on pH). The elution was done with a linear gradient from 0 to 100% buffer B (10 mM buffer + 0.5 M NaCl) over 50 column volumes. The conductivity at the point of elution was used to determine the strength of interaction between adsorbent and protein.

2.9 Electrostatic calculations

To calculate the electrostatic potential of the protein surface, the Connolly surface needed to be converted into distinct coordinate points. This surface is created by rolling a spherical probe with a distinct radius over the protein structure to describe the accessible surface area rather than the surface area given by the atom radii. Surface areas were assigned to each of these points. The PCE tool by Miteva et al. [28] was used to calculate the potentials at these distinct coordinate points using the 3D structure of lysozyme. For the calculation of the mean surface potential, the surface area that was assigned to each coordinate point was used together with the information about the potential at this coordinate.

Table 1: Langmuir parameters of adsorption isotherms generated with SP Sepharose FF and XL at pH 7 with different ionic strengths

IS (mM)	SP Sepharose FF		SP Sepharose XL	
	K_a (mg/mL)	Q_m (mg/mL)	K_a (mg/mL)	Q_m (mg/mL)
19	100.8	113.3	3223.9	203.6
50	91.6	95.7	52.5	184.3
100	14.7	82.9	11.8	147.5

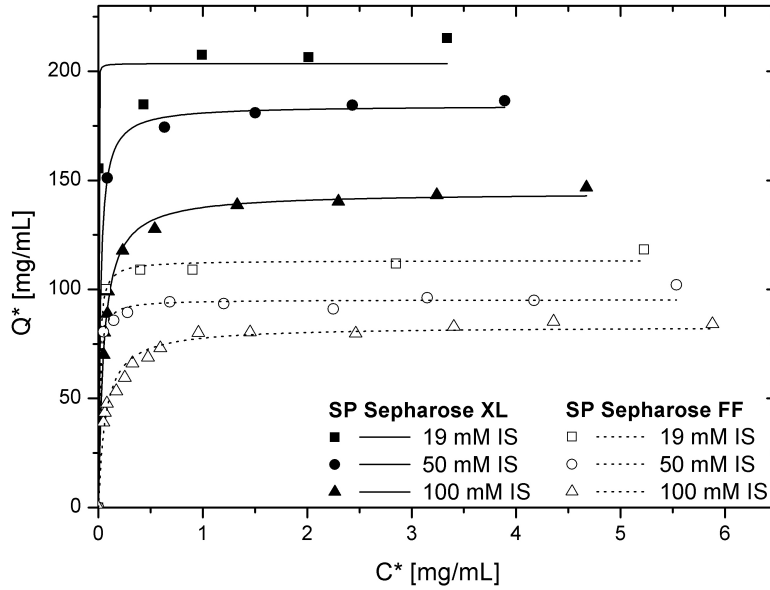


Figure 1: Isotherms for SP Sepharose FF and XL at different ionic strengths. All data sets were fitted with the Langmuir model, parameters can be found in Table 1.

3 Results and discussion

3.1 Binding isotherms

All obtained adsorption isotherms (Fig. 1) after incubation of protein and adsorbent were fitted with the Langmuir model, using Eq. (2). The relationship between the association constant K_a and the dissociation constant K_d is shown in Eq. (3).

$$Q^* = Q_m * \frac{c^*}{K_d + c^*} \quad (2)$$

$$K_a = \frac{1}{K_d} \quad (3)$$

Q^* is the protein concentration on the stationary phase at equilibrium, Q_m the maximum capacity (in mg protein per mL packed bed). c^* represents the equilibrium concentration of protein in the mobile phase. The fitting parameters Q_m and K_a for lysozyme binding to SP Sepharose FF and SP Sepharose XL with varying IS are summarized in Table 1. The results are as expected; for increasing ionic strength, the maximum capacity of the adsorbent decreases, as well as the protein affinity (association constant).

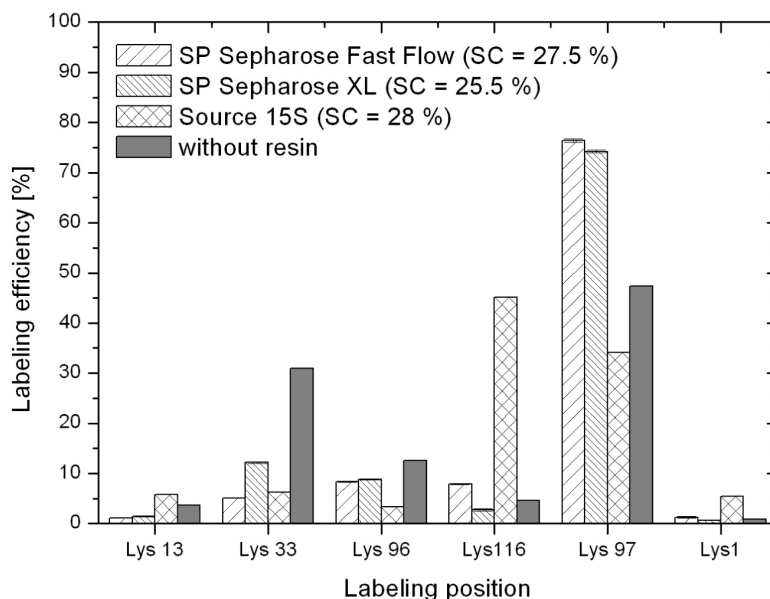


Figure 2: Comparison of the labeling patterns of lysozyme bound to SP Sepharose FF, SP Sepharose XL, Source 15 S and of unbound lysozyme, all incubated at low ionic strength (19 mM) at pH 7 and for low surface coverage as indicated. Source 15 S results from [16].

The capacities decrease due to the increased competition of Na^+ for binding sites on the adsorbent surface. The binding capacities of the tentacle adsorbent are about twice as high as those of SP Sepharose FF. This was observed by many authors and is generally explained by the flexibility of the network, which allows a more effective usage of the binding sites.

3.2 Initial binding orientation on different stationary phases

In all the following models we suggest for the binding of lysozyme, the adsorbent surface is assumed to be flat. Although this might not hold true when looking at the surface in a macroscopic scale, but when looking at it on the scale of single protein molecules this description of the adsorbent surface might be close to reality. The label distribution obtained with Source 15 S cation exchange particles at 28% surface coverage by Dismer and Hubbuch [16] was compared to results obtained with SP Sepharose FF and SP Sepharose XL at similar conditions (pH, ionic strength, surface coverage). In Fig. 2, the label distribution for the three adsorbent types and, as a reference, for unbound protein is shown.

The labeling efficiency (LE) of one lysine residue is the relative occurrence of a lysozyme isoform labeled at that particular site when incubated with the dye Cy5, represented by its relative peak area. All conclusions about protein orientation have to be made by comparison to the labeling efficiency in the unbound state of lysozyme. An increase or decrease of the labeling efficiency of one site can be explained by changes in the accessibility of that site for the dye molecules. The labeling reaction itself is a statistical process, in which mainly singly labeled isoforms are generated. Thus, increasing sterical hindrance at one lysine residue caused by the adsorbent surface upon binding or by neighboring protein molecules would result in a decreased labeling efficiency at this

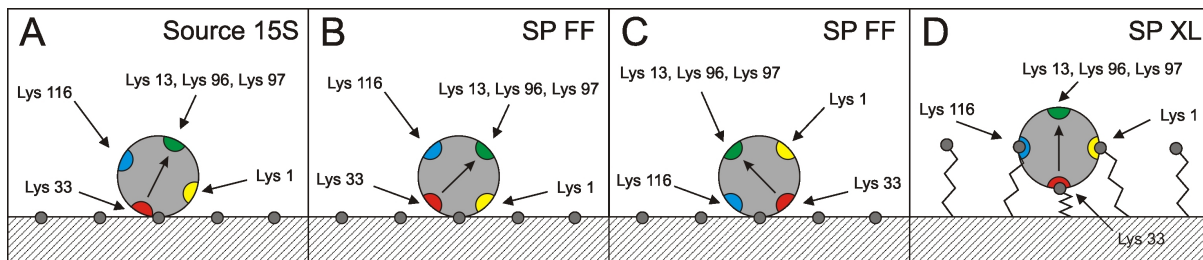


Figure 3: Suggested orientations of lysozyme on Source 15 S, SP Sepharose FF and SP Sepharose XL at low to intermediate degrees of surface coverage $\sim 25\%$) when incubated in 19mM ionic strength buffer. The arrow is for the purpose of better understanding. (A) Binding site on Source 15 S; (B and C) 2 binding sites on SP Sepharose FF; (D) one multipoint binding site on SP Sepharose XL.

surface position.

In the recent publication [16], an orientation of lysozyme on the standard-type adsorbent Source 15 S was determined. Position lys33 was identified to be part of the most prevalent site of interaction between adsorbent and protein due to its significantly reduced labeling efficiency in the bound state. For relatively low surface coverage, lys116 had a high LE which was significantly reduced at high protein densities on the adsorbent surface due to neighboring protein molecules. The proposed binding orientation is shown in Fig. 3A.

In the case of SP Sepharose FF, the labeling efficiency decrease at lys33 (by 25%) indicates the presence of a major binding site in that region. However, the different labeling pattern suggests a more complex scenario which comprises two important interaction sites. A second binding region between lysozyme and SP Sepharose FF is most probably located near the labeling site lys116, which, in striking contrast to Source 15 S, remains at a low level of labeling efficiency when compared to the native protein.

The presence of two major binding sites is supported by the highest labeling efficiency of lys97, making up a fraction of more than 75%. The region around lys97 can, therefore, be regarded as the only area that is fully exposed to the mobile phase when lysozyme is bound to SP Sepharose FF. The example of Source 15 S showed that two lysine residues of high labeling efficiency (lys97 and lys116) are obtained if only one major protein-adsorbent binding site exists.

Electrostatic potential calculations were performed using the PCE tool by Miteva et al. [28] and the protein structure 132L of hen egg white lysozyme from the RCSB Protein Data Bank [29]. The aim was to identify those surface area patches of lysozyme that show the highest positive mean electrostatic potential as these would probably be the regions that interact with the negatively charged ligands of the adsorbent. By definition, these patches had a size of about 80 \AA^2 (5 \AA radius). Table 2 lists the amino acids located in the center of one of these 5 patches with the highest mean potential and indicates their location in reference to the known lysine residues.

According to Table 2, regions of high positive charge density are between lys1 and lys33, around lys13 and around lys116. The first and latter support the two predominant protein orientations suggested above. Instead of lys33 as the center of the first binding site, the more probable position is between lys1 and lys33. The labeling efficiency of lys1 is negligible for both bound and unbound protein, thus, its participation in the adsorbent binding is likely. Although lys13 is a region of high positive charge density, its role

Table 2: Ten patches with the highest mean electrostatic potential (patch size $\sim 80 \text{ \AA}^2$). For each patch, the amino acid roughly located in the center is given, the exact center is specified by the atom number.

Amino acid	Atom no.	Mean potential [kcal/(mol*e)]	Location
Lys1	5	5.51	
Lys13	97	4.85	
Lys116	898	4.81	
Arg128	988	4.74	Near Lys13
Ile124	956	4.55	Near Lys13
Ser86	668	4.21	Near Lys1
Val2	16	4.10	Between Lys1 & Lys33
Arg5	36	4.08	Between Lys1 & Lys33
Cys6	48	3.78	Between Lys1 & Lys33
Phe38	301	3.75	Between Lys1 & Lys33

as a site of protein adsorbent interaction is supposedly small. Lys97 is located in close proximity to lys13 on the same side of the molecule and would be labeled less efficiently if the region around lys13 was part of a binding site.

Fig. 3B and C schematically depict the two most probable binding orientations of lysozyme on SP Sepharose FF. The first orientation (B) incorporates adsorption via the region between lys1 and lys33; the second (C) is characterized by a binding site between lys116 and lys33. The probability of this binding site is higher than that of one with lys116 in the center, since the predominantly labeled residue lys97 is more exposed to the mobile phase. Both illustrated orientations allow the high labeling efficiency at lys97 that is observed during the experiments with SP Sepharose FF. Inconsistent with this theory are the slightly decreased labeling efficiencies of lys13 and lys96. Both amino acids are located on the same side of the protein as lys97 and should, therefore, be more accessible for Cy5 molecules as well. A possible explanation for this observation could be changes in the reactivity of functional groups upon adsorption, as already suggested by Dismer and Hubbuch [16].

At first sight, the differences between SP Sepharose FF and Source 15 S (Fig. 3) are remarkable since both share the same type of ligands, namely sulphopropyl groups connected to the matrix by C_6 spacers. However, considering the adsorbent backbone, Source 15 S has a polystyrene base matrix, while the matrix of SP Sepharose FF is made of cross-linked agarose. The difference between the two is that polystyrene in contrast to agarose is characterized by significant hydrophobicity. That means that in the case of Source 15 S presumably two modes of adsorption contribute to the binding of lysozyme while for the interaction of lysozyme with SP Sepharose FF only electrostatic interaction plays a significant role. Fig. 4 illustrates the location of hydrophobic regions on a three-dimensional model of the protein.

It can be seen that a high density of patches is located between lys1 and lys33, whereas in the vicinity of lys116 the number is much lower. This observation would explain why a binding site around lys116 could not be identified for Source 15 S. Since a

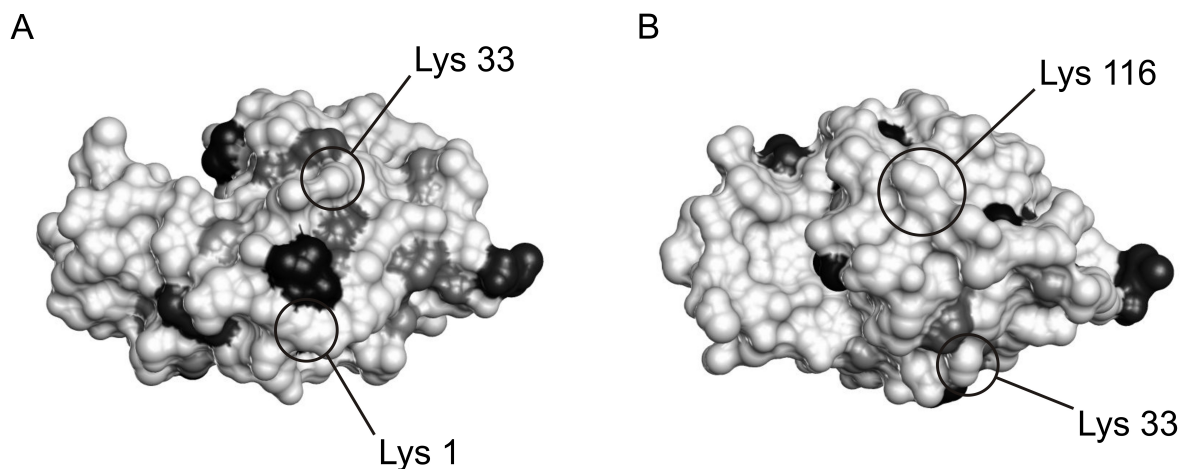


Figure 4: Location of hydrophobic areas on the lysozyme surface. The hydrophobicity ranges from low hydrophobicity coloured in white to high hydrophobicity coloured in black according to Kyte and Doolittle [30]. **(A)** Binding site between lys1 and lys33; **(B)** binding site between lys33 and lys116. Pictures made with Chimera [31].

proteinadsorbent interaction via the lys1lys33 region is much stronger, no binding occurs via the less hydrophobic region around lys116. Previous experiments [16] showed, that for Source 15 S the labeling efficiency and thus the accessibility of lys116 was significantly increased when bound to the surface (see Fig. 2), especially for low surface coverage. With increasing protein density on the surface, the labeling efficiency decreased by about 25%. A likely explanation for that is, that with increasing protein density the protein molecules on the surface come into closer proximity of each other leading to a sterical hindrance of the lysine residues located on both sides of the molecule.

Looking at the tentacle-type adsorbent SP Sepharose XL (Fig. 3D), the labeling pattern is similar to that of SP Sepharose FF. Lys33 is labeled 7% more efficiently, lys116 5% less efficiently. Further similarities could be detected when comparing the result to that obtained at low to intermediate surface coverage degrees with EMD Fractogel SO₃, a second tentacle-type adsorbent tested in the previous study [16]. For EMD Fractogel SO₃, a multipoint binding mechanism was proposed, which incorporates lys1, lys33 and lys116 as simultaneous binding sites, enabled by the flexible dextran tentacles carrying the ligands. Because of the high similarities of the two labeling patterns and the structural analogies (tentacles of similar length, comparable ligands), the same multipoint interaction scheme is concluded for SP Sepharose XL. The influence of pH on the binding orientations on SP Sepharose FF and XL, that is discussed later, provides further evidence for this multipoint interaction.

3.3 Influence of surface protein density

In Fig. 5, the labeling patterns of SP Sepharose FF and SP Sepharose XL at varying degrees of surface coverage are shown. Other than expected when considering the previous results with Source 15 S or EMD Fractogel SO₃ [16], no significant changes of the labeling efficiencies were observed. For Source 15S, the decrease of the relative amount of the lys116 isoform was explained by a reduced accessibility of this lysine located on the side

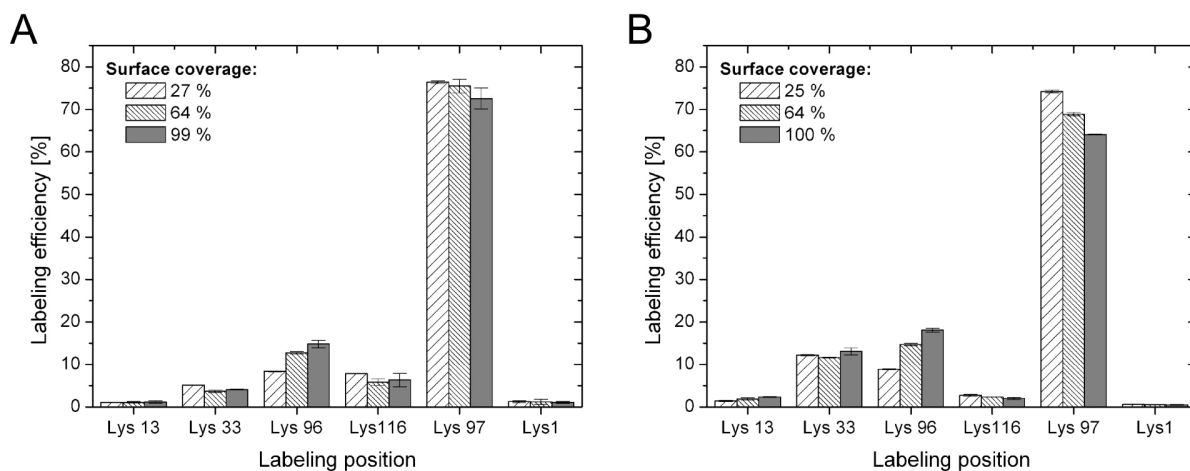


Figure 5: Labeling pattern of lysozyme bound to (A) SP Sepharose FF and (B) SP Sepharose XL at varying surface coverage of the stationary phase at 19mM ionic strength. From eight surface coverage degrees tested, only three are shown for reasons of clearness.

of the molecule by neighboring bound molecules. This could not be concluded from the SP Sepharose FF results, which might be explained by the fact that lys116 is part of one binding interface. The only variation of the labeling patterns is for both adsorbent types observable at positions lys96 (steady increase) and lys97 (steady decrease). It was found that the variation at these two residues is linked to the constant increase of the degree of labeling (DoL), being the amount of labeled molecules relative to the total amount of molecules) with increasing surface coverage. Although the aim was to retain a constant DoL by keeping a constant dye to protein ratio during the labeling reaction, the higher dye concentration in probes with high SC inevitably led to a higher labeling degree. E.g., for SP Sepharose FF, the DoL was below 5% for low surface coverage degrees and $\sim 25\%$ for about 100% SC. Experiments with equally loaded adsorbent particles and varying dye concentrations (a fixed dye to protein ratio but a changed reaction volume) revealed that only the labeling efficiencies of lys96 and lys97 are a function of the dye concentration (data not shown). With increasing dye concentration, the labeling efficiency of lys97 decreases while the efficiency of lys96 increases to the same degree; the other lysine residues remain unchanged. The reason for that probably lies in the chemical nature of each individual labeling reaction, and is not well understood.

Therefore, a re-orientation of lysozyme on SP Sepharose FF and SP Sepharose XL with increasing surface coverage could be excluded. A re-orientation with increasing surface coverage that was found for EMD Fractogel SO_3 (also a grafted adsorbent with flexible ligands) was caused by protein-protein interactions at high protein density on the adsorbent surface. Such a re-orientation could not be found for SP Sepharose XL leading to the assumption that apparently the protein density on the surface is lower, eventually caused by a lower ligand density.

3.4 Changing ionic strength

By adding sodium chloride, the ionic strength of the equilibration buffer (10 mM sodium phosphate, pH 7) was altered. In addition to the standard buffer, which had an ionic

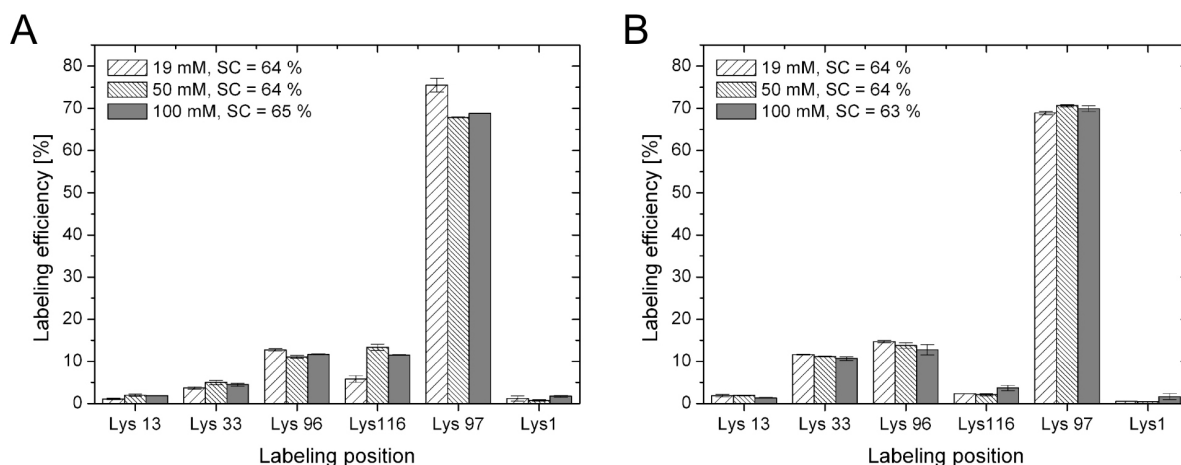


Figure 6: Labeling pattern of lysozyme bound to (A) SP Sepharose FF and (B) SP Sepharose XL at varying ionic strength of the binding buffer. Representative samples with a constant, intermediate surface coverage of about 64% are chosen for comparison.

strength of 19 mM, two buffers were prepared with 50 and 100 mM IS, respectively. The labeling efficiency results are shown in Fig. 6. In the case of SP Sepharose FF, only a slight variation of labeling efficiency is observable at positions lys116 and lys97. With a change from low salt buffer (19 mM IS) to medium salt (50 mM IS), the efficiency at lys116 is increased by about 7%, while at lys97 a decrease of about the same extent is observed. A further increase to 100 mM IS does not result in any significant change for either lysine residue. Altered reactivity of these lysine residues caused by the change of salt concentration is rather unlikely as the effect is also negligible for protein bound to SP Sepharose XL and for unbound protein (data not shown). It is possible that upon an ionic strength increase from 19 to 50 mM, protein bound to SP Sepharose FF via the region between lys33 and lys116 is slightly tilted, making position lys116 more accessible for Cy5 dye molecules. In general, the higher salt concentration leads to a decreased overall proteinadsorbent affinity (cf. isotherms). Potentially, regions of lower affinity are dissociated first, which, in fact, could lead to a slight re-orientation, as characterized by the altered labeling pattern.

In the case of SP Sepharose XL, the labeling pattern is constant over the whole range of buffer salt concentration tested. The orientation of lysozyme bound via the proposed highly affine multipoint interactions apparently not affected by the salt content of the buffer.

3.5 pH effects on charge distribution

Lysozyme has a total of 29 charged groups located on the surface of the molecule: 11 arginines, 6 lysines, 1 histidine, 7 aspartic acids, 2 glutamic acids, the N- and the C-terminus, which can all be protonated or deprotonated depending on the pH of the solution and their intrinsic pK_a . The pK_a value depends on the neighboring amino acids and thus on the molecular structure. The basic amino acids (arginine, lysine and histidine) are either positively charged when protonated or uncharged when deprotonated. For the acidic residues (aspartic and glutamic acid) the protonated form is uncharged

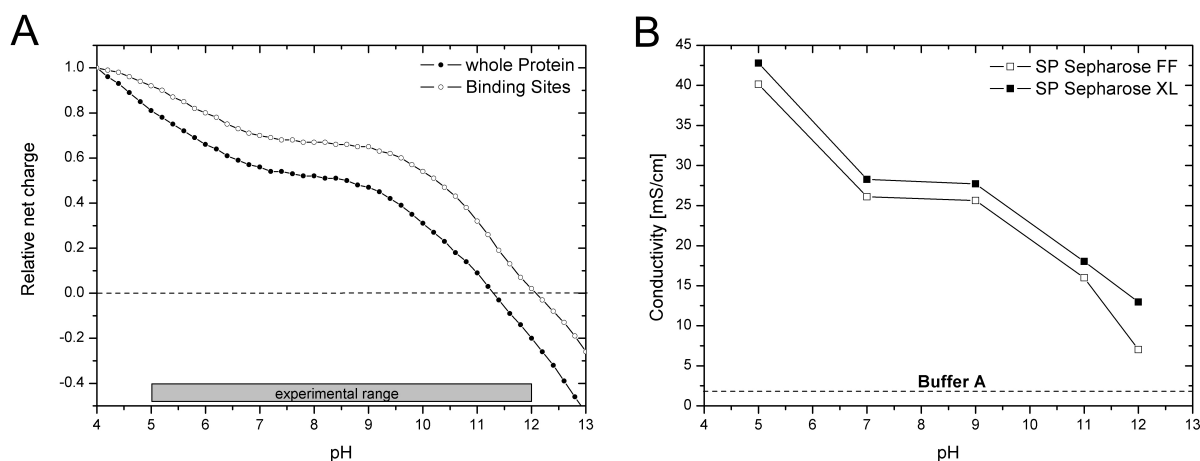


Figure 7: (A) Calculated relative net charge of the whole protein (●) and only for both binding sites (○). The experimental working range is indicated. (B) Gradient elution experiments with lysozyme at different pH. The conductivity on the y-axis is the conductivity at point of elution. The dashed line indicates the conductivity of buffer A, the gradient range was 0-100% buffer B. The column was washed with two-column volumes buffer A after injection before gradient elution.

while the unprotonated form carries a negative charge. Using the intrinsic pK_a values, the net charge of lysozyme at a certain pH can be calculated. The result of such a calculation for lysozyme (according to Bashford [27]) is shown in Fig. 7A. The diagram depicts the relative net charge of lysozyme with increasing pH of the mobile phase. The net charge decreases with a plateau region between pH 7 and pH 9, where the charge of the molecule is more or less stable. The isoelectric point was identified to be at 11.3, where the net charge of the molecule is 0 (in good agreement with experimental data [32]). Linear gradient elution experiments have shown (see Fig. 7B) that the protein affinity to the adsorbent, measured by the conductivity at point of elution, decreases as well with increasing pH. The shapes of these curves for both adsorbents and the relative net charge curve look very much alike, showing the same plateau between pH 7 and pH 9. In this region, a change of the pH has apparently only little effect on protein retention. A notable difference is that the protein shows significant retention at pH 12, which is above the isoelectric point (meaning that protein and adsorbent are both negatively charged). This phenomenon was observed and documented before, e.g. by Yamamoto and Ishihara [21], indicating that the net charge of a protein is not a perfectly suitable parameter to describe protein retention in ion-exchange chromatography. To find an explanation for such a behaviour on a molecular level, we took a more detailed look at the binding sites that were discussed above and are shown in Fig. 8. Both binding sites consist of four positive and one negative charge at low pH. The individual titration curves for the amino acids located within

the binding sites are shown in Fig. 9. In the experimental range of investigated pH, all acidic residues remain unprotonated and all arginine residues protonated, not changing the charge state of either one of the binding sites. A change of protonation was however observed for the lysine residues and especially for the N-terminus of lysozyme, which is located in the area of the first binding site (between lys1 and lys33). While the N-terminus is almost completely protonated at pH 5, it loses its positive charge above pH 6.

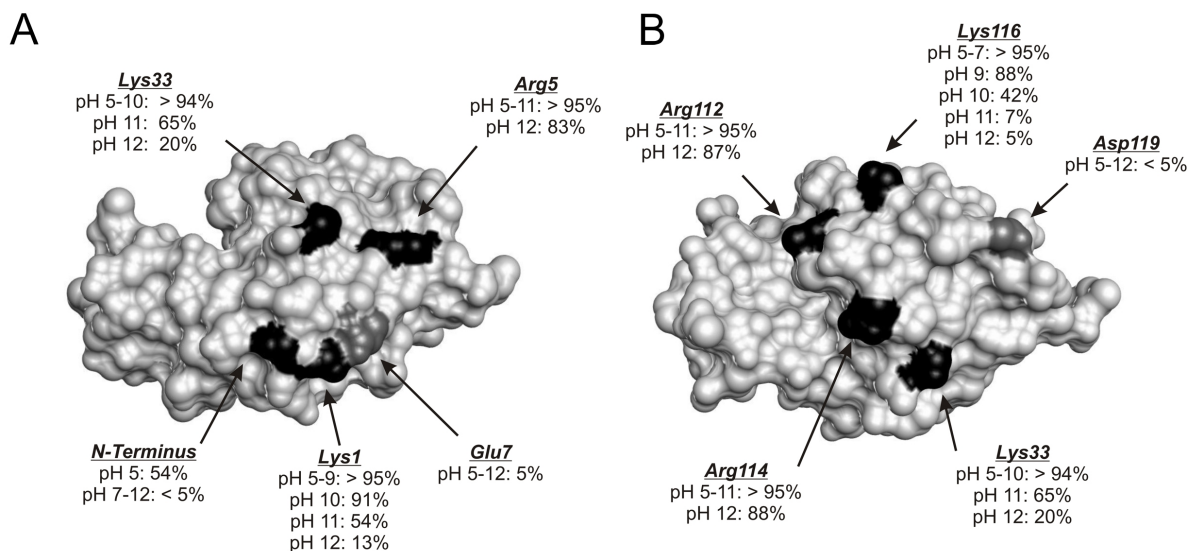


Figure 8: Binding domains of lysozyme. Positively charged amino acids are black, negatively charged amino acids are gray. The values below each residue indicate the degree of protonation. (A) First binding site between lys1 and lys33; (B) Second binding site between lys33 and lys116. Pictures made with Chimera [31].

By knowing the residues involved in both binding sites, we were able to calculate the net charge for only these binding sites rather than for the whole protein molecule. This charge would be similar to the characteristic charge parameter from the steric mass action model published by Brooks and Cramer [20]. The relative binding site charge with increasing pH is shown in Fig. 7A. Obviously, the shape of this curve is similar to the curve for the net

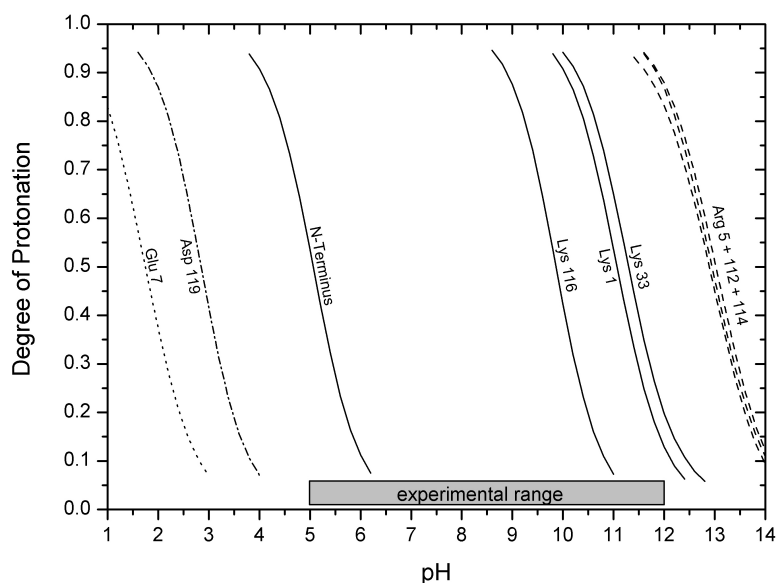


Figure 9: Calculated titration curves for the amino acids involved in either one of the binding sites. For arginine, lysine and the N-terminus, protonation results in a gain of positive charge, for glutamic and aspartic acid protonation leads to a loss of negative charge.

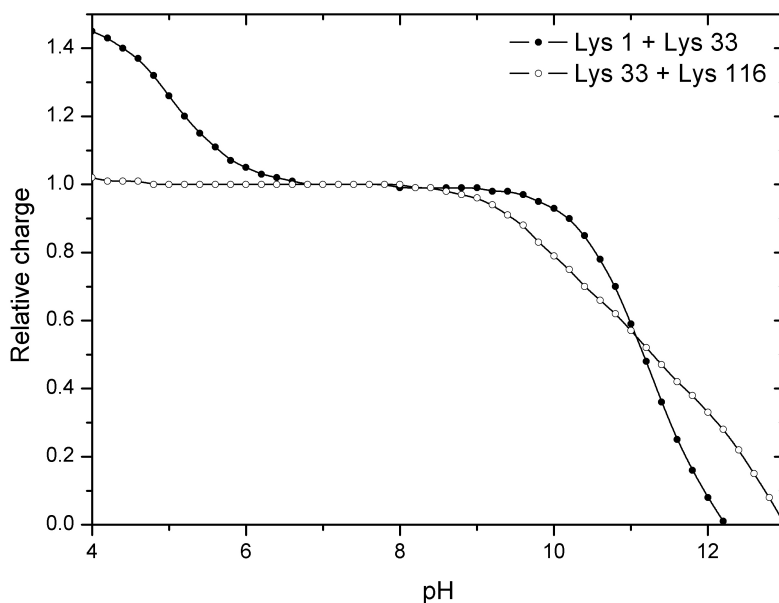


Figure 10: Relative charge of both binding sites with increasing pH. The charge is relative to the charge at neutral pH 7.

charge of the whole molecule but the isoelectric point is significantly shifted from 11.3 to 12.1, giving a first idea why protein retention was observed at pH 12 on both adsorbents. Fig. 10 shows the charge of both individual binding sites in relation to the charge at neutral pH. The charge of the second binding site (lys33 + lys116) remains constant up until pH 9, while the charge of the first binding site (lys1 + lys33) significantly decreases between pH 5 and pH 6 due to the deprotonation of the N-terminus. At pH > 11 the charge of the second binding site dominates and is positively charged until pH 13, again giving a good explanation why retention can be observed beyond the pI of 11.3. If the two binding sites found at pH 7 really co-exist, the equilibrium between the two binding sites would be pH dependent due to the fact that with increasing pH, the charge of each binding site changes individually. At low pH, one would expect favoured binding via the first binding site, which would shift towards the second binding site at higher pH.

3.6 pH effects: experimental results

Binding orientations were investigated for a relatively high surface coverage of about 65-70%, which was chosen for all pH. The highest maximum binding capacity ($q_{max} = 141.2$ mg/mL), which was obtained at pH 5 was set to 100% surface coverage, and was chosen as a reference point for all other pH. All isotherms were almost rectangular, even at pH 12. Fig. 11A shows the labeling efficiency of 4 singly labeled isoforms with increasing mobile phase pH during protein binding. Note that for a surface coverage of about 65-70%, the bound lysozyme molecules are relatively tightly packed on the surface and sterical hindrance might occur by neighboring molecules.

The experimental results for SP Sepharose FF confirm what was expected from the theoretical considerations discussed in the previous section (see Fig. 11A and Fig. 12). At low pH, the binding mechanism is dominated by the first binding site (lys1 + lys33). As a result, the accessibility of lys1 and thus the fraction of the isoform labeled at this position

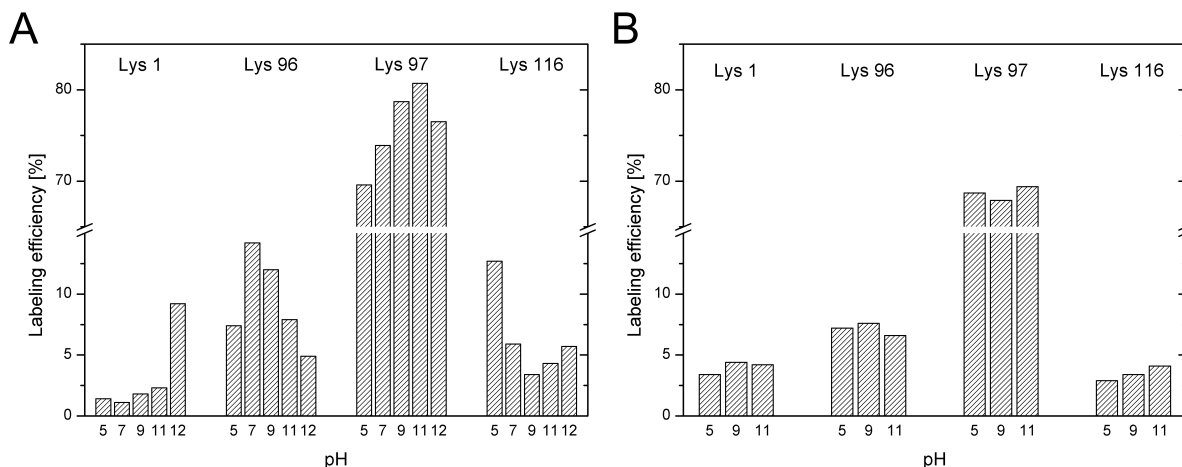


Figure 11: Relative amounts of labeled residues lys1, lys96, lys97 and lys116 at different pH when labeled in the bound state for (A) SP Sepharose FF and (B) SP Sepharose XL.

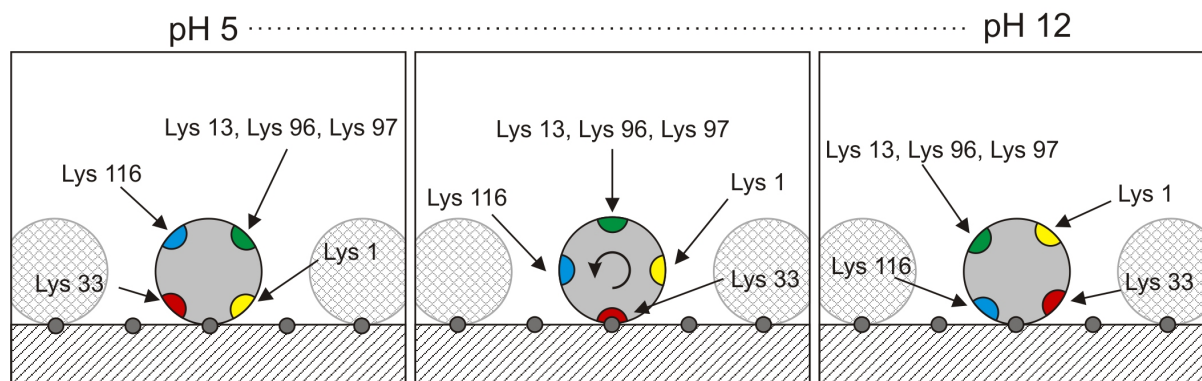


Figure 12: Lysozyme binding model on SP Sepharose FF with increasing pH. The molecule rotates from the lys1 + lys33 interface towards the lys33 + lys116.

is relatively low. Lys116 is located on the upper side of the molecule, pointing away from the adsorbent and, thus, showing significant accessibility. As the pH increases, the accessibility of lys116 decreases as it moves closer to the adsorbent surface. At the same time, lys96 and lys97 move further away from neighboring molecules and the adsorbent surface and their accessibility increases. This rolling mechanism continues with increasing pH, until at pH 12, lys1 moves to the upper part of the molecule, suddenly becoming accessible for the dye molecules. Note, that at this pH the first binding site is almost uncharged, while the second binding site still carries positive charges.

Fig. 11B shows the labeling efficiencies for lysozyme bound to SP Sepharose XL, a grafted adsorbent. For this adsorbent type, no significant changes could be found with increasing pH. It should be mentioned that the binding capacity at pH 12 was too low to allow the analysis of the labeling pattern; the amount of bound protein was below the detection limit after labeling and elution.

Keeping in mind that a multipoint interaction was discussed for SP Sepharose XL earlier in this paper (similar to the binding of lysozyme to EMD Fractogel SO₃ as published before [16]), it is reasonable that no changes in this binding mechanism occur with increasing pH. The ligands on the adsorbent surface show a sufficient flexibility to interact

simultaneously with both binding sites, independent from pH, as long as both binding sites are positively charged.

4 Conclusions

By investigating the binding orientations of lysozyme on SP Sepharose FF, we were able to identify differences in the binding mechanism when compared to the results for Source 15 S acquired earlier. These changes are due to the influence of the adsorbent backbones, which seem to have a significant effect on the interaction between protein and adsorbent surface, at least in the case of lysozyme. Two different binding sites were found for SP Sepharose FF solely driven by electrostatic interaction. For Source 15 S, an additional hydrophobic component of the interaction was identified, leading to only one main binding site. We also determined the binding of lysozyme to SP Sepharose XL, a grafted adsorbent. For this adsorbent, a multipoint interaction of the highly flexible ligands was proposed, similar to the binding mechanism identified earlier for EMD Fractogel SO₃. However, no re-orientation of the protein molecules with increasing density on the adsorbent surface was observed as we did for EMD Fractogel SO₃. One possible explanation would be a lower ligand density on SP Sepharose FF and, thus, less protein-protein interaction at maximum protein loading of the adsorbent.

We then investigated the effects of mobile phase ionic strength and pH on the lysozyme binding orientation on both adsorbents. We found that the binding mechanism remains widely unchanged up to an ionic strength of about 100 mM, which is in good agreement with the SMA model by Brooks and Cramer [20]. Two parameters in this model give an idea about the binding orientation of proteins: the characteristic charge and the steric hindrance factor. A change of the binding mechanism always involves a change of either one or both parameters. These parameters were found to be independent of ionic strength [20], but not independent of pH [21]. Indeed, we also found changes in the binding mechanism for SP Sepharose FF, where the protein orientations shift from one binding site at low pH towards a second binding site at high pH, all in good agreement with the theoretical charge distribution on the protein surface and linear gradient elution experiments at different pH. By identification of these two binding sites, lysozyme retention beyond the isoelectric point could be explained, also in agreement with the assumption made by Brooks and Cramer that the characteristic charge of a protein is not equal to the net charge. For SP Sepharose XL, we were not able to detect differences in the binding mechanism. This could be explained by a multipoint interaction where the flexibility of the ligands allows simultaneous interaction with both binding sites independent of mobile phase pH.

References

- [1] A. N. Hodder, K. J. Machin, M. I. Aguilar, M. T. W. Hearn, High-performance liquid-chromatography of amino-acids, peptides and proteins .101. identification and characterization of coulombic interactive regions on sperm whale myoglobin by high-performance anion-exchange chromatography and computer-graphic analysis, *Journal of Chromatography* 507 (1990) 33–44.

-
- [2] Y. Yao, A. M. Lenhoff, Electrostatic contributions to protein retention in ion-exchange chromatography. 1. cytochrome c variants, *Analytical Chemistry* 76 (22) (2004) 6743–6752.
- [3] Y. Yao, A. M. Lenhoff, Electrostatic contributions to protein retention in ion-exchange chromatography. 2. proteins with various degrees of structural differences, *Analytical Chemistry* 77 (7) (2005) 2157–2165.
- [4] B. J. Yoon, A. M. Lenhoff, Computation of the electrostatic interaction energy between a protein and a charged surface, *Journal of Physical Chemistry* 96 (7) (1992) 3130–3134.
- [5] J. Zhou, S. F. Chen, S. Y. Jiang, Orientation of adsorbed antibodies on charged surfaces by computer simulation based on a united-residue model, *Langmuir* 19 (8) (2003) 3472–3478.
- [6] D. J. Barlow, J. M. Thornton, The distribution of charged groups in proteins, *Biopolymers* 25 (9) (1986) 1717–1733.
- [7] D. Asthagiri, A. M. Lenhoff, Influence of structural details in modeling electrostatically driven protein adsorption, *Langmuir* 13 (25) (1997) 6761–6768.
- [8] F. Carlsson, E. Hyltner, T. Arnebrant, M. Malmsten, P. Linse, Lysozyme adsorption to charged surfaces. a monte carlo study, *Journal of Physical Chemistry B* 108 (28) (2004) 9871–9881.
- [9] D. S. Gill, D. J. Roush, R. C. Willson, Adsorption heterogeneity and thermodynamic driving forces in anion-exchange equilibria of cytochrome-b(5), *Journal of Colloid and Interface Science* 167 (1) (1994) 1–7.
- [10] D. S. Gill, D. J. Roush, K. A. Shick, R. C. Willson, Microcalorimetric characterization of the anion-exchange adsorption of recombinant cytochrome b(5) and its surface-charge mutants, *Journal of Chromatography A* 715 (1) (1995) 81–93.
- [11] C. O. Gill, J. Bryant, The presence of escherichia-coli, salmonella and campylobacter in pig carcass dehairing equipment, *Food Microbiology* 10 (4) (1993) 337–344.
- [12] J. Fausnaughpollitt, G. Thevenon, L. Janis, F. E. Regnier, Chromatographic resolution of lysozyme variants, *Journal of Chromatography* 443 (1988) 221–228.
- [13] R. M. Chicz, F. E. Regnier, Single amino-acid contributions to protein retention in cation-exchange chromatography - resolution of genetically engineered subtilisin variants, *Analytical Chemistry* 61 (18) (1989) 2059–2066.
- [14] R. M. Chicz, F. E. Regnier, Microenvironmental contributions to the chromatographic behavior of subtilisin in hydrophobic-interaction and reversed-phase chromatography, *Journal of Chromatography* 500 (1990) 503–518.
- [15] S. M. Daly, T. M. Przybycien, R. D. Tilton, Coverage-dependent orientation of lysozyme adsorbed on silica, *Langmuir* 19 (9) (2003) 3848–3857.

- [16] F. Dismer, J. Hubbuch, A novel approach to characterize the binding orientation of lysozyme on ion-exchange resins, *Journal of Chromatography A* 1149 (2) (2007) 312–320.
- [17] W. R. Melander, Z. Elrassi, C. Horvath, Interplay of hydrophobic and electrostatic interactions in bio-polymer chromatography - effect of salts on the retention of proteins, *Journal of Chromatography* 469 (1989) 3–27.
- [18] V. Noinville, C. Vidalmadjar, B. Sebille, Modeling of protein adsorption on polymer surfaces - computation of adsorption potential, *Journal of Physical Chemistry* 99 (5) (1995) 1516–1522.
- [19] I. Mazsaroff, L. Varady, G. A. Mouchawar, F. E. Regnier, Thermodynamic model for electrostatic-interaction chromatography of proteins, *Journal of Chromatography* 499 (1990) 63–77.
- [20] C. A. Brooks, S. M. Cramer, Steric mass-action ion-exchange - displacement profiles and induced salt gradients, *Aiche Journal* 38 (12) (1992) 1969–1978.
- [21] S. Yamamoto, T. Ishihara, Resolution and retention of proteins near isoelectric points in ion-exchange chromatography. molecular recognition in electrostatic interaction chromatography, *Separation Science and Technology* 35 (11) (2000) 1707–1717.
- [22] G. Malmquist, U. H. Nilsson, M. Norrman, U. Skarp, M. Stromgren, E. Carredano, Electrostatic calculations and quantitative protein retention models for ion exchange chromatography, *Journal of Chromatography A* 1115 (1-2) (2006) 164–186.
- [23] J. C. Bosma, J. A. Wesselingh, ph dependence of ion-exchange equilibrium of proteins, *Aiche Journal* 44 (11) (1998) 2399–2409.
- [24] S. Bouhallab, G. Henry, E. Boschetti, Separation of small cationic bioactive peptides by strong ion-exchange chromatography, *Journal of Chromatography A* 724 (1-2) (1996) 137–145.
- [25] Q. S. Shi, Y. Zhou, Y. Sun, Influence of ph and ionic strength on the steric mass-action model parameters around the isoelectric point of protein, *Biotechnology Progress* 21 (2) (2005) 516–523.
- [26] M. A. Hashim, K. H. Chu, P. S. Tsan, Effects of ionic-strength and ph on the adsorption equilibria of lysozyme on ion-exchangers, *Journal of Chemical Technology and Biotechnology* 62 (3) (1995) 253–260.
- [27] D. Bashford, Macroscopic electrostatic models for protonation states in proteins, *Front Biosci* 9 (2004) 1082–99.
- [28] M. A. Miteva, P. Tuffery, B. O. Villoutreix, Pce: web tools to compute protein continuum electrostatics, *Nucleic Acids Res* 33 (Web Server issue) (2005) W372–5.
- [29] H. M. Berman, J. Westbrook, Z. Feng, G. Gilliland, T. N. Bhat, H. Weissig, I. N. Shindyalov, P. E. Bourne, The protein data bank, *Nucleic Acids Research* 28 (1) (2000) 235–242.

-
- [30] J. Kyte, R. F. Doolittle, A simple method for displaying the hydropathic character of a protein, *Journal of Molecular Biology* 157 (1) (1982) 105–132.
- [31] E. F. Pettersen, T. D. Goddard, C. C. Huang, G. S. Couch, D. M. Greenblatt, E. C. Meng, T. E. Ferrin, Ucsf chimera - a visualization system for exploratory research and analysis, *Journal of Computational Chemistry* 25 (13) (2004) 1605–1612.
- [32] P. G. Righetti, G. Tudor, K. Ek, Isoelectric points and molecular-weights of proteins - a new table, *Journal of Chromatography* 220 (2) (1981) 115–194.

3D STRUCTURE-BASED PROTEIN RETENTION PREDICTION FOR ION-EXCHANGE CHROMATOGRAPHY

Florian Dimer, Juergen Hubbuch*

*Institute of Engineering in Life Sciences, Section IV: Biomolecular Separation Science,
University of Karlsruhe (TH), 76131 Karlsruhe, Germany*

** Corresponding author. Tel.: +49 721 608-2557; fax: +49 721 608-6240. E-mail address:
juergen.hubbuch@kit.edu*

in preparation for Journal of Chromatography A

Abstract

The interest in understanding fundamental mechanisms underlying chromatography drastically increased over the past decades resulting in a whole variety of mostly semi-empirical models describing protein retention. Experimental data about the molecular adsorption mechanisms of lysozyme on different chromatographic ion-exchange materials were used to develop a mechanistical model for the adsorption of lysozyme onto a SP Sepharose FF surface based on molecular dynamic simulations (temperature controlled NVT simulations) with the Amber software package using a force-field based approach with a continuum solvent model. The ligand spacing of the adsorbent surface was varied between 10 and 20 Å. With a 10 Å spacing it was possible to predict the elution order of lysozyme at different pH (also explaining why lysozyme showed significant retention at pH12, which is beyond the pI) and to confirm *in silico* the pH-dependent orientation of lysozyme towards the surface that was reported earlier. The energies of adsorption at different pH values were correlated with linear gradient elution experiments and this correlation was used to predict the retention volume of ribonuclease A in the same experimental setup only based on its 3D structure properties. The study presents a strong indication for the validity of the assumption, that the ligand density of the surface is one of the key parameters with regard to the selectivity of the adsorbent, suggesting that a high ligand density leads to a specific interaction with certain binding sites on the protein surface, while at low ligand densities the net charge of the protein is more important than the actual charge distribution.

Keywords: protein dynamics, adsorption energies, binding orientation, lysozyme, retention volume prediction, ribonuclease A

1 Introduction

Chromatography is the most important technique in downstream processing of biotechnological products. Although it has been used extensively over the past decades, the understanding of the underlying fundamental mechanisms is still limited, especially when it comes to adsorption mechanisms on a molecular level. Studies about the effects of mobile phase composition on the retention behaviour of proteins - especially in ion exchange chromatography - resulted in semi-empirical models aiming at the prediction of retention time under changing experimental conditions. One of the most popular models in this regard is the steric mass-action model (SMA) by Brooks and Cramer [1], followed by other models, such as the available area model by Bosma and Wesselingh [2, 3] or the stoichiometric displacement model by Regnier *et al.* [4–6]. All these models require the determination of protein and adsorbent specific parameters. Although these parameters are all empirically defined, they have an underlying physical relevance. For example, the SMA model uses the three parameter ionic capacity, describing the number of available ligands in the adsorbent resin, the steric hindrance factor, describing the amount of space the bound protein blocks on the adsorbent surface, and the characteristic charge, describing the number of interaction site between the protein and the adsorbent surface.

The predictive power of the SMA model - as well as most other approaches - is based however on the underlying assumption that the binding mechanism remains unchanged [7–11]. With a change in the mobile phase pH, the charge distribution on the surface of the protein changes, which in return might change protein surface interactions, specifically the site on the protein mainly responsible for binding [12]. As models fail to account for changes on the protein molecular level, there are approaches such as quantitative structure-property relationship (QSPR) to include these effects [13–15]. These approaches use structural descriptors together with a statistical evaluation of experiments to establish a link between protein properties and the retention behaviour. Yang *et al.* [13] for example treated proteins at different pH values as distinct molecules in order to allow retention time prediction at different pH. Nevertheless, the training of this model required a data set of >250 experiments.

Besides these semi-empirical approaches, there are also mechanistical models available to describe protein retention on ion-exchange materials. Roth & Lenhoff [16] investigated the adsorption of lysozyme onto a charged surface *in silico* by calculating the electrostatic and van der Waals energies for the interaction already in 1993. Due to the limitations in the computational speed at that time, they used a sphere representation of lysozyme with the net charge located at the center of the sphere for most of their calculations. In their studies, this showed to be a valid assumption, allowing them to demonstrate the effects of ionic strength on the affinity of lysozyme. In 1991 Stahlberg [17] published a paper dealing with the relationship between the Gibbs free energy and the retention factor for proteins on charged surfaces. In this work, the interaction between the protein molecule and the adsorbent surface was simplified by using two charged surfaces differing in their charge density. In 1992 he extended his model by addition of van der Waals forces [18]. In 1999 he wrote a detailed review article [19] about retention models in ion chromatography, mainly focusing on small molecules, but also including a chapter about charged macromolecules. With the increase of computational speed during the last years it is now possible to perform simulations of the dynamics of proteins in solution

rather than static calculations. This development clearly has a potential to reach a higher level of understanding and insights into protein-surface interactions [20–24]. In this paper modelling approaches were built on a detailed mechanistical understanding of the adsorption behaviour of lysozyme onto a SP Sepharose FF adsorbent surface at varying pH determined experimentally and published earlier [12, 25]. These experimental results were used to construct an adequate adsorbent surface model of SP Sepharose FF *in silico* to perform molecular dynamic simulations and to access adsorption energies at different pH and for different proteins.

In the presented approach, the interaction between an adsorber surface (SP Sepharose FF) and two proteins (lysozyme and ribonuclease A) was characterized by MD simulations. The simulations were temperature controlled (NVT type simulations) and without boundary conditions, meaning that the surface had a limited size and was not periodically repeated. The force-field used for the simulations was the *ff03* force field developed by Duan *et al.* [26], which is a modified version of the *ff99* force-field by Wang *et al.* [27], both general force-fields for MD simulations with proteins and nucleic acids. All simulations were performed using a generalized Born continuum solvent model initially implemented by Onufriev *et al.* [28]. In a first step, a simplified model for the adsorber surface was constructed, meaning that the polymer backbone (namely agarose) was not included in the model. The charge carrying ligands of the adsorbent were designed according to their chemical structure. To fix the ligands in space, which is necessary for building a surface-like structure, a positional restraint energy in the form of:

$$E_{restraint,i} = k(\Delta x_i)^2 \quad (1)$$

was applied to i atoms, where k is the weight of positional restraint energy (which was set to $+1.0 \text{ kcal}/(\text{mol}\cdot\text{\AA})$) and Δx is the difference between the actual Cartesian coordinates of the restrained atom i and its reference position. For each ligand molecule, the atom that would normally be covalently attached to the polymer backbone of the adsorbent surface and the next two atoms were restrained, and the above described restrained energy was applied to each of these atoms throughout the whole simulation. Although the surface of a real adsorbent particle would probably not be planar from a macroscopic point of view, on the scale of a single protein molecule this assumption should be acceptable. This surface models allows for a certain flexibility of the ligands due to their chemical structure, accounting for experimental findings by DePhillips *et al.* [29] who found a significant influence of the spacer length on the retention behaviour of proteins. Three different ligand spacings were chosen: 10, 15 and 20 Å (defining the distance to the next ligand in x and y direction in the surface plane). After generating the surface, it was a highly ordered structure. For the starting structure of the surface to be more realistic and to validate whether or not the starting conformation of the surface had any influence on the course of the simulation, a short MD simulation was run with the surface to generate three different starting structures for the actual MD simulation with surface and protein.

In a second step, these three surfaces were used to generate three surface-protein ensembles. The center of mass of the protein molecule (either lysozyme or ribonuclease A) was brought above the center of the surface, and the distance between the protein and the nearest ligand was adjusted to 5 Å. A MD simulation was performed (20 ps) for each ensemble in order to extract the different energies of the ensemble: bond-, angle-,

dihedral-, van der Waals-, electrostatic- and restraint-energy. To be able to calculate the energies caused by adsorption for different protein orientations, the MD simulations were repeated for altogether 62 different, systematically varied protein orientations to screen the whole protein surface for possible interaction sites (for detailed information see the materials and methods section). For such a screening it was of great importance, that a) the protein does not change its orientation in the course of the simulation, and b) the protein does not change its distance to the surface. Therefore the backbone atoms (imido-N, C_α and carbonyl-C) of the protein were restrained in the same way as described above for the surface ligands. The MD simulation results for all three different starting structures for each protein orientation were compared to determine the effects of the starting conformation on the MD simulation. The different energies were plotted versus the protein orientation (defined by two rotation angles) into interaction plot which revealed favourable and unfavourable binding sites and were correlated with experimental data about binding orientations. Average electrostatic interaction energies were calculated from the gathered data and correlated with retention experiments. All MD simulations were performed for different pH values. To estimate the effect of the pH on the charge distribution and net charge of the protein, protonation states of all charged amino acids were calculated and considered in the MD simulations. An empirical correlation between electrostatic interaction energy and retention behaviour was then used to estimate the retention behaviour of a second model protein (ribonuclease A) only based on the 3D structure of the molecule.

2 Materials and methods

2.1 Gradient elution experiments

Hen egg white lysozyme (L-6876) and ribonuclease A from Sigma (St. Louis, MO, USA) was dissolved in the respective working buffer at various concentrations. All salts including 1M NaOH for pH adjustment were purchased from Merck (Darmstadt, Germany). The adsorbent material analyzed (SP Sepharose Fast Flow) was obtained from GE Healthcare (Uppsala, Sweden). To determine the pH dependent strength of interaction of lysozyme with SP Sepharose FF, retention experiments were conducted. Lysozyme solutions were prepared at pH 5-12 using 10 mM citrate buffer (pH 5), phosphate buffer (pH 7), carbonate buffer (pH 9), glycine (pH 11) or NaOH (pH 12). The columns used were 1 ml prepacked columns (Atoll, Germany), separation was performed on an Akta system purchased from GE Healthcare (Uppsala, Sweden). Sample loading (240 μL, 3 mg/mL lysozyme) was followed by two column volumes wash with buffer A (10 mM, buffer type depending on pH). The elution was done with a linear gradient from 0 to 100% buffer B (10 mM buffer + 0.5 M NaCl) over 30 column volumes. The conductivity at the point of elution was used to determine the strength of interaction between adsorbent and protein.

2.2 Adsorber surface construction

The chemical structure of the ligand is available on the homepage of the manufacturer (www.gehealthcare.com):



In a real adsorbent particle, the ligand is coupled to the agarose matrix via an oxygen atom. Due to the fact, that the polymer matrix was not included in the model, an additional C-atom was added to represent the coupling point. The 3D structure of the ligand was created using ANTECHAMBER, a tool provided with the AMBER 9 package, a commonly used package for molecular mechanics [30, 31]. The ligands were then distributed evenly to give a quadratic surface of at least 100 Å size in both directions, which is approximately 2-times the size of lysozyme. Three different spacings between ligands were used to generate three different surfaces: 10 Å, 15 Å and 20 Å (the spacing defines the distance to the next ligand in x- and y- direction within the surface plane). To keep the ligands in a layer and to avoid a breakdown of the surface during the simulation, the Cartesian coordinates of the first three atoms of each ligand (C₃, O and C₁) were restrained by a harmonic potential of the form mentioned above (see eq.1 with $k = +1.0$ kcal/mol*Å²) during all simulations. This means that only the part of the ligand, that would be attached to the polymer backbone of the adsorbent is fixed in space, but the part carrying the charge (which is the part interacting with the protein) remains flexible.

2.3 Protein structure preparation

For the dynamic simulations with lysozyme (PDB-ID: 132L) [32, 33] and ribonuclease A (PDB-ID: 1FS3) [33, 34] at different pH values, the internal pK_a of lysine, arginine, histidine, glutamic acid and aspartic acid were calculated using the PCE (protein continuum electrostatics) web tool [35]. The charge of each amino acid was then determined individually using the Henderson-Hasselbalch equation:

$$pH = pK_a + \log \frac{c(A^-)}{c(HA)} \quad (2)$$

and assigned to the residues using the LEAP tool (also part of the AMBER 9 package). Before the protein structure was used, a short energy minimization (1500 iteration steps) was performed with a continuum solvent model (generalized Born solvation model, Amber parameter: igb = 5, for details read [28]) to avoid general problems with the energetics of the protein structure, such as close contacts between atoms or abnormal torsion angles, etc.

2.4 Ensemble construction and simulation design

To get the final ensemble of adsorbent surface and protein molecule, the protein structure was added onto the surface, with the center of mass of the protein being above the center of the surface. The distance between the surface and the protein was adjusted to 5 Å between the protein and the closest SO₃⁻ group (which in most cases belonged to one of the ligands in the center of the surface). This was done to keep the distance of the protein to the surface equal in all simulations independent of the orientation of the protein. The adjusted distance was large enough to account for the formation of a hydration shell around the protein. For each protein, 62 different orientations in respect to the adsorbent

surface were sampled. This was achieved by stepwise rotating the protein by 30° around the y - (x - and y -axis lie in the surface plane) and the z -axis (perpendicular to the surface plane) to screen the whole surface of the protein for possible interaction sites. After each rotation step, the protein was centered and adjusted to the correct distance. To avoid a change of the orientation during the simulation and to avoid a protein movement away from the surface, the coordinates of the protein backbone (imido-N, C_α and carbonyl-C) were restrained with the same energy as the ligand base atoms (see above), and thus the protein was kept at its position, but still having flexible side chains. Prior to the actual simulation run, the energy of the whole ensemble was minimized for another 1500 steps by using a continuum model (generalized Born solvation model, Amber parameter: `igb = 5`, for details read [28]) to avoid close contacts between the side chains and the ligands which might lead to atypically high energies in the simulation.

2.5 Simulation parameters and computational equipment

The calculations were all done on 64 cores of a HP XC6000 parallel computing cluster with Intel Itanium2 processors with the SANDER tool (also part of the AMBER 9 package).

The force-field used was the *ff03* force-field developed by Duan *et al.* [26], which is a modified version of the *ff99* force-field by Wang *et al.* [27]. All performed MD simulations were of the NVT type, meaning that the number of atoms, the volume and the temperature were kept constant in each simulation run. A Langevin temperature control was used [36, 37] which uses imaginary atom collisions to control the velocities of the atoms in the system. The collision frequency was set to 1 ps^{-1} . Bond interactions including hydrogen atoms were omitted to reduce the computational cost. All simulations were performed using a generalized Born continuum solvent model initially implemented by Onufriev *et al.* [28]. The salt concentration of the continuum was set to 20 mM which influences the dielectric constant of the continuum. If not stated differently, the simulation time was 20 ps with time steps of 0.002 ps. Periodic boundaries were not used, which means that the surface had a fixed size and was not periodically repeated. The cut-off distance was set to 60 Å to include long-ranged electrostatic interactions, and no correction term was added for interactions beyond the cut-off range. The following energies were calculated in each MD run: bond-, angle-, dihedral-, van der Waals-, electrostatic- and restraint-energy. As mentioned above, part of the ligand atoms and the protein backbone were restrained with a harmonic potential of $+1 \text{ kcal}/(\text{mol}\cdot\text{Å})$.

2.6 Snapshot sampling and averaging

All simulations were performed in triplicates. For MD simulations, the course of the simulation may depend on the starting conformation of the system (see results section) and thus for the evolution of the different energies throughout the simulation. To evaluate the effect of the starting structure on the energies calculated during the simulation, three different starting structures for each ensemble were generated. A dynamic simulation of only the surface was done first with a total time of 100 ps starting with a highly ordered surface model (see fig. 1). Three different snapshots of the surface were taken between after 20, 60 and 100 ps simulation time to generate three different sets of ligand coordinates (with a maximum period of simulation time between the snapshots to allow

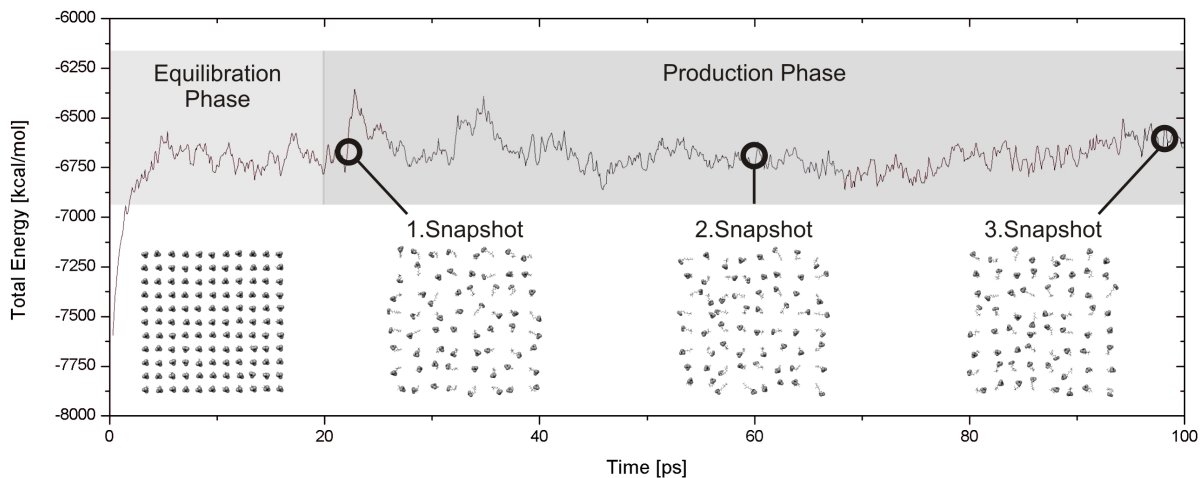


Figure 1: Plot of the total energy over simulation time for the initial simulation used to generate snapshots for the ensemble generation for the surface with 10 Å ligand spacing.

for a bigger difference between the structures) for different conformational states of the surface. These different surfaces were used to generate the starting structure of three different ensembles per protein orientation, and the energies of all three simulations were averaged later. In some cases, the restraint energy (the energy actually needed to keep the ligands and the protein at their position) for the ensemble simulation for one snapshot was significantly higher for all 62 orientations than for the other two snapshots. As this is a strong indicator for deeper problems with the energy of the system (e.g. close contacts between protein and ligands to the ensemble construction procedure). In this case, only the other two corresponding snapshots were used to calculate the average energies. To calculate the interaction energies, reference runs with only the surface and only the protein at the distinct pH were performed in triplicates and averaged. These reference energies were then subtracted from the energies of the ensemble simulation according to:

$$E_{Adsorption} = E_{Ensemble} - E_{Protein} - E_{Surface} \quad (3)$$

The first 10 ps of each simulation were considered to be an equilibration phase, and were thus not used in the calculation of the average energies.

For the correlation of electrostatic interaction energies with retention behaviour, a few assumptions were made:

1. Each protein orientation showing a negative electrostatic interaction energy (which means that there is a net attraction between protein and adsorbent) contributes to protein binding and thus needs to be considered when calculating the average interaction energy.
2. Each protein orientation showing a positive electrostatic interaction energy and thus a net repulsion between protein and surface does not contribute to the average interaction energy.
3. The more negative the interaction energy is of an orientation, the stronger is the contribution the average interaction energy. The general idea behind this is, that

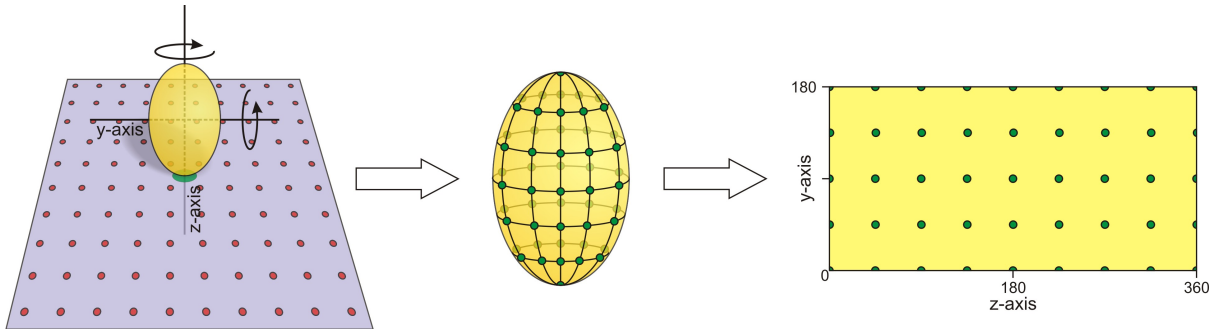


Figure 2: Scheme of the data flow. By rotating the molecule consecutively around the y and z-axis the complete protein surface is sampled. Each orientation is specified by a y and z-angle. These coordinates are then used to plot the energies gathered in the simulations.

a protein with one strong binding site, which is superior to all other binding sites shows a stronger binding than a protein with many weak binding sites, even if the non-weighted average interaction energy is the same. Thus the interaction energies for the individual orientations need to be weighted before averaging.

The MATLAB 4 grid data method was used to interpolate energies with a stepsize of 5° which were then plotted according to fig. 2. The weighting factor for a given orientation can be calculated according to:

$$p_{y,z} = \frac{1}{Z} * e^{-\beta * E_{y,z}^{elec}} \quad (4)$$

where $p_{y,z}$ is the probability for a given orientation defined by the two rotation angles y and z , Z is a normalizing factor, $E_{y,z}^{elec}$ is the electrostatic interaction energy of this orientation and β is a constant:

$$\beta = \frac{1}{k_B * T} \quad (5)$$

where k_B is the Boltzman constant and T is the temperature. Z can be calculated according to:

$$Z = \sum e^{-\beta * E_{y,z}} \quad (6)$$

Then an average electrostatic interaction energy $\bar{E}_{y,z}^{elec}$ would be the sum of the weighted electrostatic interaction energies over all orientations that show $E_{y,z}^{elec} < 0$:

$$\bar{E}^{elec} = \sum p_{y,z} * E_{y,z}^{elec} \quad (7)$$

3 Results and discussion

3.1 Experimentally determined binding orientations

In a previous publication dealing with binding orientations of lysozyme on different adsorbent surfaces under varying experimental conditions [12] a binding mechanism for lysozyme on SP Sepharose FF was proposed. This binding mechanism is illustrated in fig. 3. For low pH the main binding site for lysozyme was located between lysine 1 and

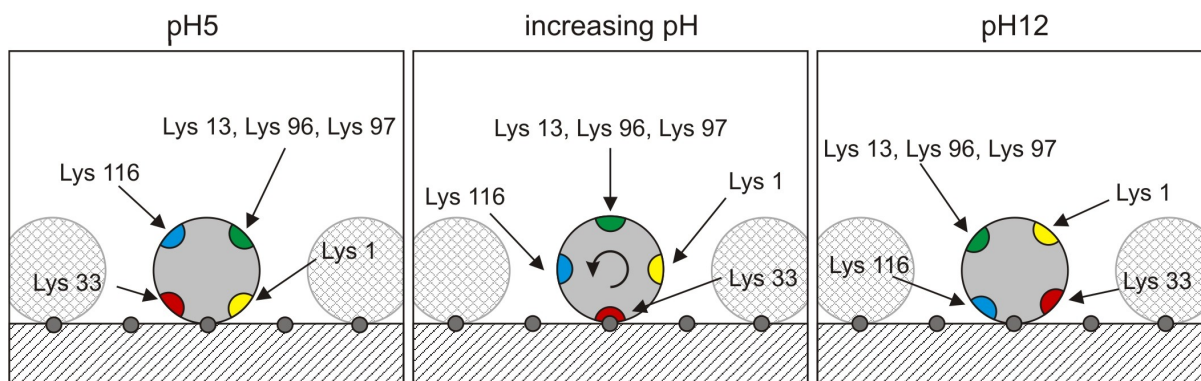


Figure 3: Changes in the binding orientation of lysozyme on SP Sepharose FF based on experimental data taken from Dismer *et al.* [12]. At low pH the main binding site was located between lysine 1 and lysine 33. With increasing pH, the molecule turned towards a second binding site between lysine 33 and lysine 116.

lysine 33, including altogether 4 positively and 1 negatively charged amino acid. With increasing pH the lysozyme molecule turned towards a second binding site located between lysine 33 and lysine 116 also consisting of 4 positively and 1 negatively charged amino acid. The driving force for this re-orientation was the change of charge distribution on the surface of the protein. All amino acids located in the binding site have slightly different intrinsic pK_a values and are thus losing their charge at different pH. Also the N-Terminus is located in the first binding site and is the first amino acid that is deprotonated (already below pH 7). For a detailed explanation please refer to [12]. In the present paper these experimental findings are correlated to the dynamic simulation results and subsequently used to determine the most realistic ligand spacing for the investigated systems.

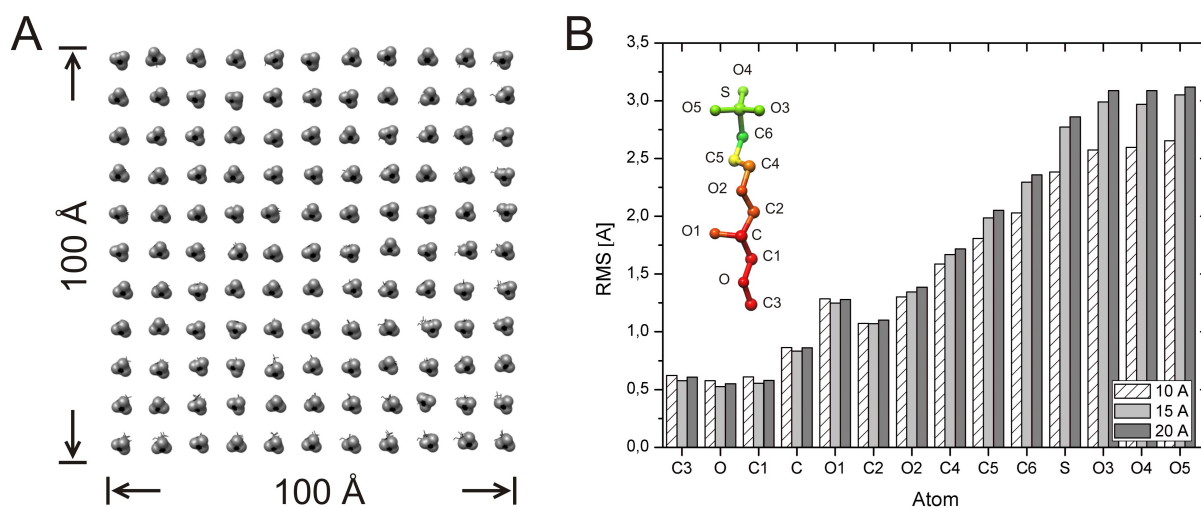


Figure 4: **A.** Model of a SP Sepharose FF surface with a ligand spacing of 10 Å and a total size of 100 Å. SO_3^- groups are colored in gray. **B.** RMS values for ligand atoms for three different ligand densities showing their flexibility during a simulation run (green = high flexibility, red = low flexibility).

3.2 Surface design and snapshot generation

Fig. 4A shows a model of the surface with a spacing of 10 Å. This structure was used for the generation of three snapshots for the ensemble construction and for reference simulations. The ligands in the simulation are actually not bound to a surface, they are rather just fixed in space and kept at their position by applying a restraint energy. Fig. 4B shows RMS values for the ligand atoms which represent the average distance of an atom relative to its mean position throughout a complete simulation, thus the higher the RMS value, the more movement an atom made during the simulation. The first three atoms (C₃, O and C₁) are the atoms that were restrained at their starting Cartesian coordinates by the harmonic potential, representing a covalent attachment to the surface. These three atoms had the lowest RMS value of all (~0.5 Å). With increasing distance to these atoms, the RMS value increased. There was an obvious connection between the ligand density and the flexibility of the ligands. For the 10 Å ligand spacing, the ligands slightly stabilized each other, resulting in lower RMS values. This stabilization was less prominent for increasing ligand spacing. The main reason for restraining three atoms in space rather than one was to avoid a 180 ° rotation of the ligand facing into the 'surface'.

Fig. 4 shows the proceeding for the generation of three different sets of coordinates for the finale protein-surface ensemble. The first 20 ps of the simulation are considered to be an equilibration phase, in which kinetic energy is added to the system to bring the simulation to a temperature of 300 K. After the equilibration phase the data generation phase follows. In this phase three different sets of coordinates of the surface were being extracted. The pictures below the energy curve in Fig. 1 show that the three snapshots actually represent the same surface only with different conformations and that the surface remained intact throughout the whole simulation.

3.3 Snapshot averaging

Fig. 5A shows the total energy for three different simulation runs performed with three different snapshots (starting conformations) of the same system (10 Å ligand spacing, pH7, y=0°, z=0°). The data production phase begins after 10 ps. It was obvious that all three simulations fluctuate around a similar average total energy: -9257 kcal/mol, -9222 kcal/mol and -9134 kcal/mol, although the course of the simulation was different due to the different starting structures. The materials and methods section describes, that the restraint energy of a simulation can be used as a measure for the quality of the simulation. Fig. 5B shows a typical restraint energy profile for 62 different orientations (on a surface with a ligand spacing of 15 Å at pH5). The profile was calculated by using reference simulations with the protein and the surface only as described earlier (see eq. 3). For most of the simulations, the restraint energy of the 2-component system was lower than for individual 1-component systems. Fig. 5C shows the restraint energy profile for the third snapshot under the same conditions, revealing significant problems with the energies of the system such as close contacts between two or more atoms. Simulation runs with such a high restraint energy profile were not considered in the averaging procedure.

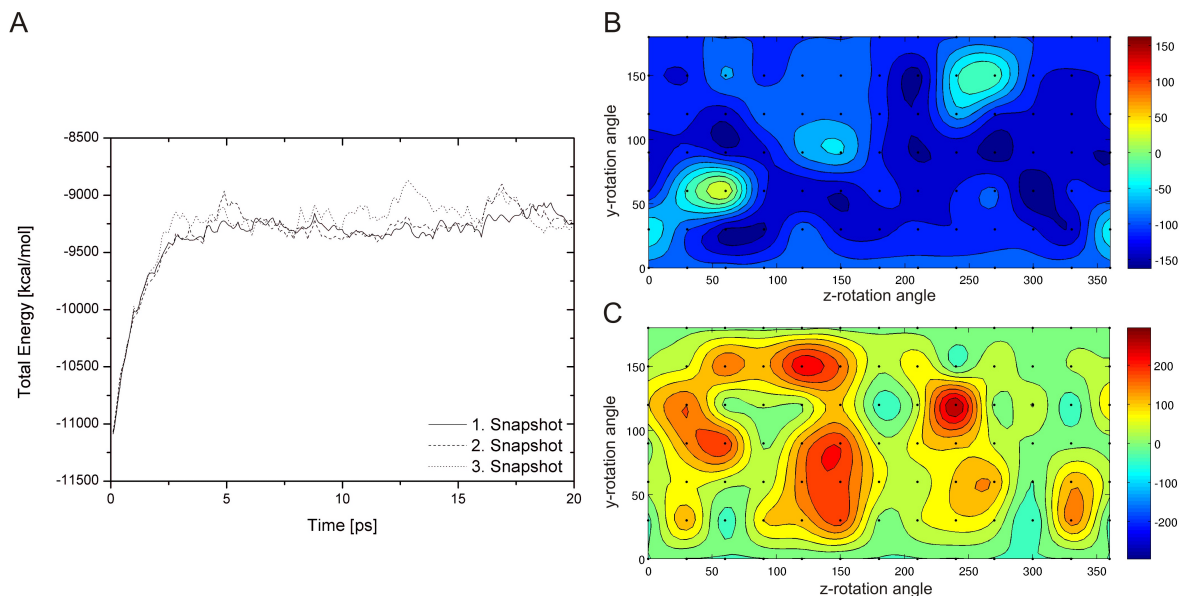


Figure 5: **A.** Total energy for three independent simulations with three different starting structures (10 Å spacing, pH7, $y = 0^\circ$, $z = 0^\circ$). **B.** Restraint energy profiles for the first and the third Snapshot of three individual simulations (15 Å spacing, pH5). The restraint energy profile of the third snapshot reveals problems with the energetics of the third simulation.

3.4 Simulation results for 10 Å ligand spacing

The simulation results for the surface with 10 Å ligand spacing and pH values between 5 and 12 are shown in fig. 6A-E. The first noticeable finding at pH5 was, that the electrostatic energy strongly depended on the orientation of the protein: the difference between the lowest energy (-7588 kcal/mol) and the highest energy (-5321 kcal/mol) was roughly 2300 kcal/mol. The second finding was, that there are apparently two sets of orientations, that were unfavourable for a binding event: one set of orientations around $y = 75^\circ$, $z = 100^\circ$ and one set around $y = 115^\circ$, $z = 220^\circ$.

Although these orientations are unfavourable, the electrostatic energy for the interaction was still negative and these orientations had to be considered to reveal possible binding sites. Binding orientations 1 and 2 were the ones with the lowest energy. Note that the orientation 1 was almost exactly the orientation that was proposed from the experimental data [12] (see fig.5). With increasing pH to pH7, the total electrostatic energy increased by approximately +1400 kcal/mol, but the difference between the lowest and the highest energy remained at roughly 2400 kcal/mol. The first unfavourable binding site became less prominent due to a loss of negative charges at asparagine 52 and 101 located close to the surface at this orientation. At pH11, new unfavourable binding sites occurred due to changes in the charge distribution. At pH12 areas of electrostatic repulsion appeared as expected. Nevertheless, there were still regions in the plot showing a negative electrostatic energy, correlating well with the experimental finding that lysozyme showed significant retention beyond its pI at pH11.3 [12].

Note again, that the most prominent binding orientations (no. 4+5) were close to the ones that were proposed from experimental data [12] (see fig. 5).

The key message of this section is, that a whole variety of potential binding sites exist, some with a higher probability than others. Clearly, the binding orientation greatly

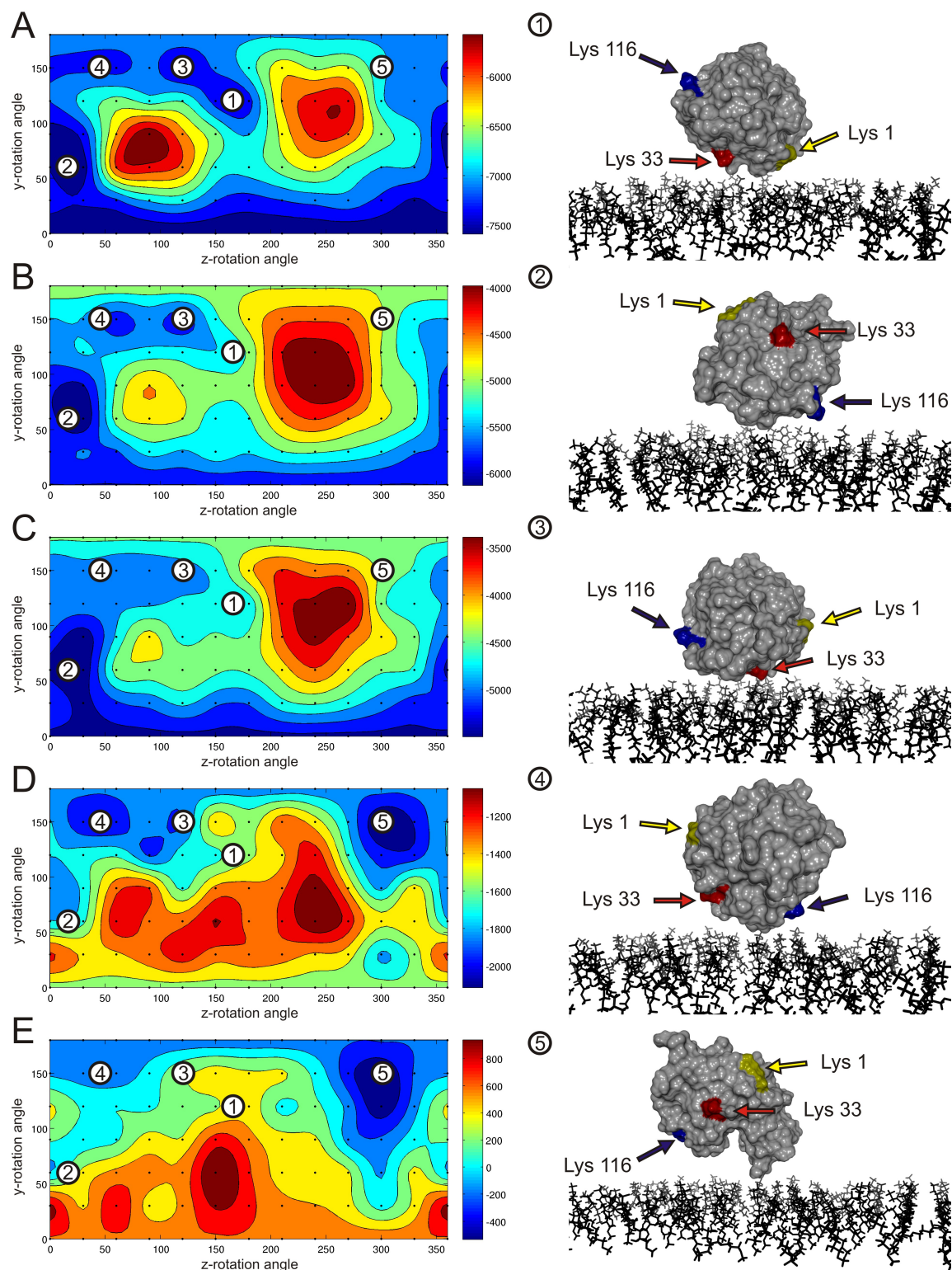


Figure 6: Electrostatic energy profiles for different pH A. pH5 B. pH7 C. pH9 D. pH11 and E. pH12 and a selection of the most favourable binding orientations (1-5).

influences the energy for the adsorption governing the probability of orientation. The simulation results showed that the binding is to be far more complex than the experimentally determined data suggested, but a good correlation of both data sets could be found.

3.5 Correlation with elution studies

In the previous section it was discussed that there are numerous possible binding sites differing in their electrostatic energies. The question arises if these electrostatic energies correlate not only with the adsorption behaviour but can also be used to predict desorption behaviour. In order to predict the retention of a protein two prerequisites would be needed: 1) a general approach to calculate an energy of adsorption from the simulation results and 2) a correlation between this interaction energy and the retention of a protein. In order to calculate an average electrostatic energy of interaction the assumptions were made, that each orientation with a negative energy can possibly bind and lead to retention, while orientations showing a positive energy would not contribute, and that the lower the energy is, the higher the contribution to the retention (for details see the materials and methods section). To account for both, weighted average energies were calculated as described in the materials and methods section. The resulting correlation is shown in fig. 7. As also discussed earlier, in the course of this study simulations with three surfaces differing in their ligand spacing were performed. Fig. 7 showed correlations for all three surface types with experimental data. The experimental data were obtained by eluting lysozyme in a linear gradient over 30 column volumes from 0 to 500 mM NaCl in a 1ml SP Sepharose FF column. The conductivity on the y-axis refers to the conductivity at point of elution as a measure for the affinity between protein and adsorbent. The stronger the binding, the later the elution in the linear gradient and

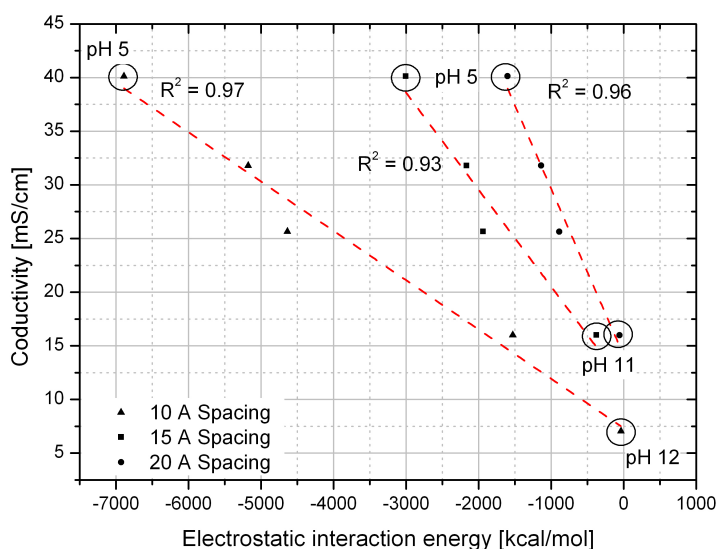


Figure 7: Correlation of the electrostatic energy for three different ligand spacings and the conductivity at point of elution taken from elution studies at different pH.

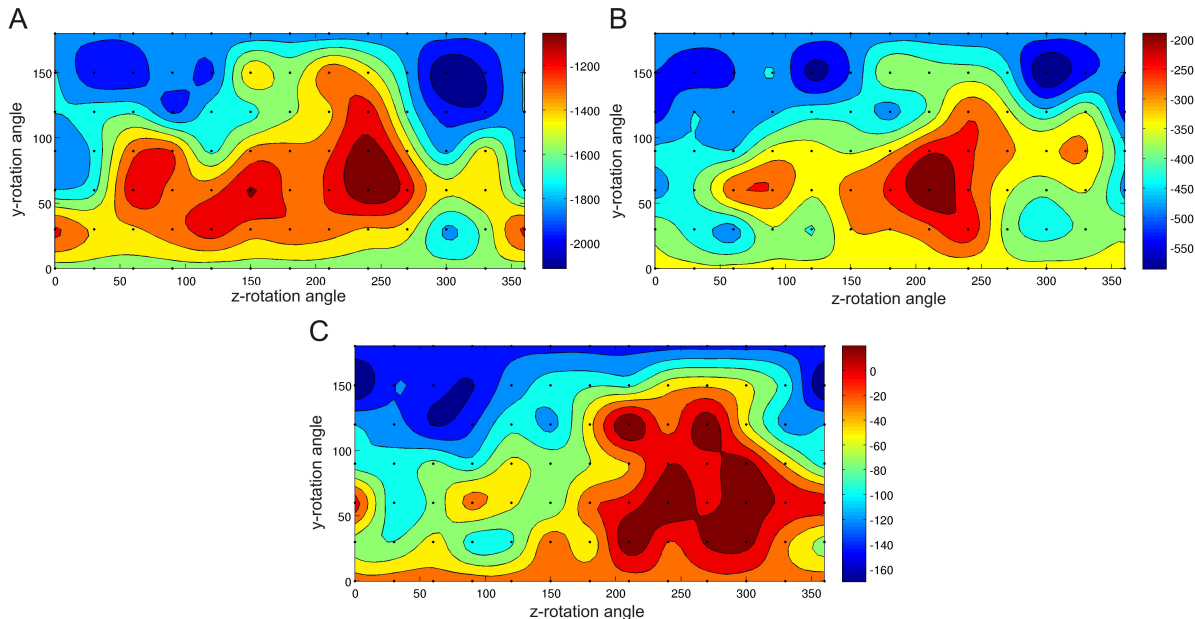


Figure 8: Effects of **A.** 10 Å **B.** 15 Å **C.** 20 Å ligand spacing on the binding orientation of lysozyme here shown at pH11.

thus the higher the conductivity. These experiments were done for different pH values (same pH values that were used for the MD simulations). Note, that for 15 Å and 20 Å spacing no negative electrostatic energies were found for pH12 during the simulations, failing to explain lysozyme retention at this pH on SP Sepharose FF (which has been observed before [12] but also indicating, that protein retention on ion exchange materials beyond the isoelectric point might only occur for adsorbent materials with a sufficiently high ligand density. Besides the results for the surface with 10 Å spacing showed the best correlation ($R^2 = 0.97$).

Fig. 8A-C shows the effects of the ligand spacing on both, the binding orientation and the electrostatic energy for the interaction between lysozyme and the surface at pH11. With increasing ligand spacing, the average electrostatic energy increased from about -1530 kcal/mol to about -40 kcal/mol. Apparently the electrostatic binding becomes also less selective to the charge distribution as the difference between the lowest and the highest energy is reduced from about ~ 1000 kcal/mol to ~ 150 kcal/mol. This finding corresponds and explains reports claiming that ligand density influences not only the maximum binding capacity but the selectivity of adsorbent materials. Wu *et al.* [38] have shown, that with changing ligand density on a silica based material, the elution order of lysozyme and cytochrome changes.

Interestingly the correlation in fig. 7 revealed, that at zero electrostatic energy protein retention still occurred, resulting in an offset of 6.6 mS/cm. The average base conductivity of the loading buffer was ~ 2.5 mS/cm and thus an offset of 2.5 mS/cm would have made sense for a purely electrostatic interaction. One explanation for the offset is that there were other forces contributing to retention of lysozyme: short ranged van der Waals forces as well as hydrophobic effects. The van der Waals forces were considerably low in our simulations (in the range of -25 to -60 kcal/mol), did not show an obvious trend and did also not significantly reduce the offset. To calculate reliable energies for the

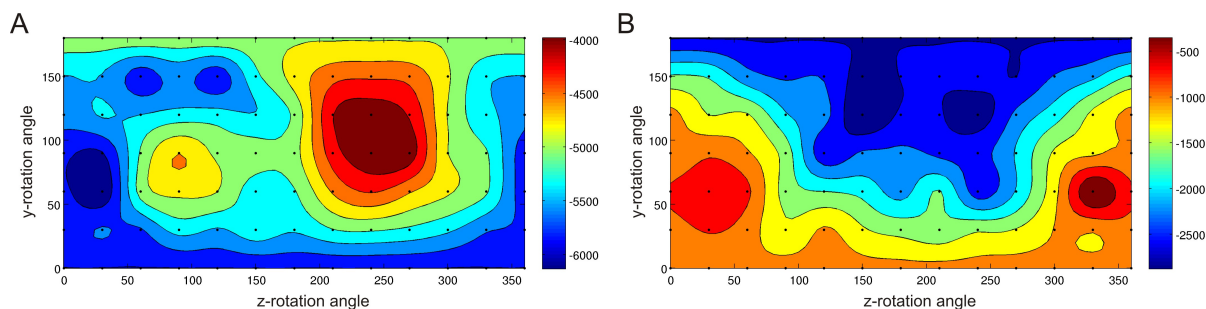


Figure 9: Simulation results for **A.** lysozyme and **B.** ribonuclease A on a surface with 10 Å ligand spacing at pH7.

hydrophobic effects, simulations with implicit water molecules would be necessary. These kind of simulations are very cost intensive in terms of computational time and were not performed in this study. A third explanation could be, that the surface used for the simulations was too small to account for all electrostatic interactions, although apparently is was big enough to show a good trend. A larger surface would lead to more negative electrostatic energies at least for the favourable binding orientations which would lower the offset but which would also drastically increase the computational time. An indication supporting this theory might be, that all three correlations (for 10 Å, 15 Å and 20 Å) show approximately the same y-axis offset (5.9 mS/cm for 15 Å and 6.7 Å for 20 Å).

3.6 Retention volume prediction for ribonuclease A

To evaluate the predictive power for the MD simulations ribonuclease A was used, a protein with a similar size (124 residues) and an estimated pI of 9.5 resulting in a positive net charge at pH7. For the simulations the surface with a 10 Å ligand spacing of the same size as the surface used for the simulations with lysozyme was chosen, representing the system with the best correlation. 62 different orientations were analyzed and the results were interpolated as described in the materials and methods section. The results are shown in fig. 9 in comparison to simulations for lysozyme at pH7.

The calculated average electrostatic energy was -1950 kcal/mol compared to -5164 kcal/mol for lysozyme, so just by looking at this energy, a significantly lower retention volume was expected. By using the linear correlation from fig. 8, a conductivity at point of elution of 15.9 mS/cm was calculated, which referred to an elution volume of 10.9 ml. Performing the same gradient elution used for lysozyme at different pH, a conductivity at point of elution of 16.7 mS/cm was obtained corresponding to a retention volume of 11.3 ml (see fig 10). The predicted retention of ribonuclease A is also overlaid in fig. 10, showing just a slight shift of the elution peak to a lower elution volume.

4 Conclusion and outlook

In this paper, a mechanistical model was introduced to describe protein retention based on the calculation of electrostatic energies from molecular mechanics simulations although it should be mentioned, that the relation of the electrostatic interaction energy to the retention volume was made on an empirical basis. The binding of lysozyme to a SP Sepharose

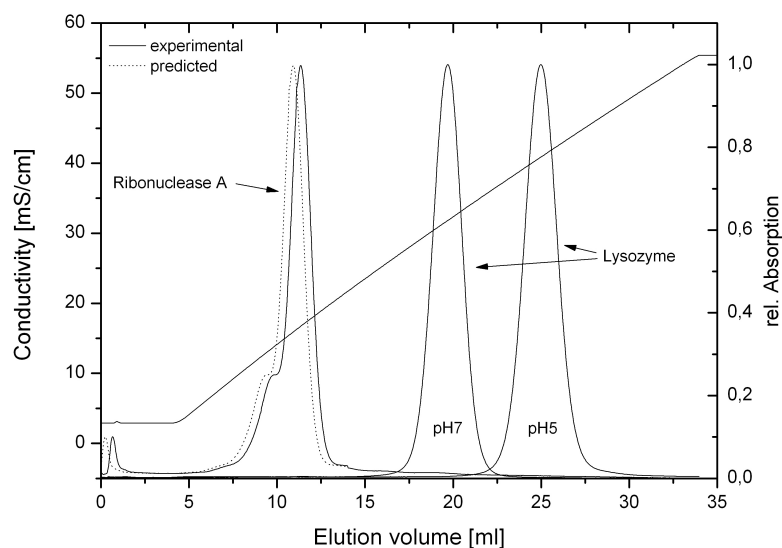


Figure 10: Comparison between experimental results for the gradient elution of ribonuclease A and lysozyme with the predicted retention behaviour of ribonuclease A. The predicted peak was generated by simply shifting the center of the peak to an elution conductivity of 15.9 mS/cm as predicted.

FF matrix was simulated at 5 different pH values for 3 different ligand spacings. A surface with a ligand spacing of 10 Å was most suitable to describe the adsorption of lysozyme. A set of possible binding orientations at different pH was in good agreement with experimental data obtained earlier. The electrostatic energy for the interaction between the surface and the protein was found to be strongly dependent on both, the binding orientation and the ligand density of the surface. The average electrostatic energies calculated from 62 different lysozyme orientations were correlated with the conductivity at point of elution for each individual pH obtained by gradient elution experiments. The correlation was best for the 10 Å ligand spacing which was also the only ligand spacing that showed negative electrostatic potentials for the interaction with lysozyme at pH12. All three correlations for the different ligand spacings revealed a y-axis intercept of 6.6 mS/cm (at zero electrostatic energy) which indicates, that there are other forces contributing to protein retention on SP Sepharose FF (possibly a small contribution of hydrophobic interactions) and that the electrostatic energies were maybe underestimated due to the limited size of the surface used for the simulations (~ 100 Å). Nevertheless, the resulting correlation was good enough to successfully predict the retention behaviour of ribonuclease A with a deviation of 0.8 mS/cm which related to a retention volume difference of 0.4 ml. Future work aims at the evaluation of the model using a set of other proteins, especially larger ones to show its predictive power. Furthermore it needs to be improved to account for hydrophobic interactions more precisely than it does at the moment.

References

- [1] C. A. Brooks, S. M. Cramer, Steric mass-action ion-exchange - displacement profiles and induced salt gradients, *Aiche Journal* 38 (12) (1992) 1969–1978.
- [2] J. C. Bosma, J. A. Wesselingh, pH dependence of ion-exchange equilibrium of pro-

-
- teins, *Aiche Journal* 44 (11) (1998) 2399–2409.
- [3] J. C. Bosma, J. A. Wesselingh, Available area isotherm, *Aiche Journal* 50 (4) (2004) 848–853.
- [4] M. A. Rounds, F. E. Regnier, Evaluation of a retention model for high-performance ion-exchange chromatography using 2 different displacing salts, *Journal of Chromatography* 283 (Jan) (1984) 37–45.
- [5] R. R. Drager, F. E. Regnier, Application of the stoichiometric displacement model of retention to anion-exchange chromatography of nucleic-acids, *Journal of Chromatography* 359 (1986) 147–155.
- [6] R. R. Drager, F. E. Regnier, Retention mechanism of lactate-dehydrogenase in anion-exchange chromatography, *Journal of Chromatography* 406 (1987) 237–246.
- [7] M. Vossoughi, I. Alemzadeh, A. Zarrabi, A. Bahari, R. Roostaazad, Parametric optimization of the purification of restriction enzymes with low concentration using cation-exchange chromatography: Model-based approach (2007) 7–17.
- [8] C. Frerick, P. Kreis, A. Gorak, A. Tappe, D. Melzner, Simulation of a human serum albumin downstream process incorporating ion-exchange membrane adsorbents, *Chemical Engineering and Processing* 47 (7) (2008) 1128–1138.
- [9] T. Vicente, M. F. Q. Sousa, C. Peixoto, J. P. B. Mota, P. M. Alves, M. J. T. Carrondo, Anion-exchange membrane chromatography for purification of rotavirus-like particles, *Journal of Membrane Science* 311 (1-2) (2008) 270–283.
- [10] N. Jakobsson, M. Degerman, E. Stenborg, B. Nilsson, Model based robustness analysis of an ion-exchange chromatography step, *Journal of Chromatography A* 1138 (1-2) (2007) 109–119.
- [11] W. D. Chen, H. H. Hu, Y. D. Wang, Analysis of steric mass-action model for protein adsorption equilibrium onto porous anion-exchange adsorbent, *Chemical Engineering Science* 61 (21) (2006) 7068–7076.
- [12] F. Dimer, M. Petzold, J. Hubbuch, Effects of ionic strength and mobile phase pH on the binding orientation of lysozyme on different ion-exchange adsorbents, *Journal of Chromatography A* 1194 (1) (2008) 11–21.
- [13] T. Yang, M. C. Sundling, A. S. Freed, C. M. Breneman, S. M. Cramer, Prediction of pH-dependent chromatographic behavior in ion-exchange systems, *Analytical Chemistry* 79 (23) (2007) 8927–8939.
- [14] G. Malmquist, U. H. Nilsson, M. Norrman, U. Skarp, M. Stromgren, E. Carredano, Electrostatic calculations and quantitative protein retention models for ion exchange chromatography, *Journal of Chromatography A* 1115 (1-2) (2006) 164–186.

- [15] A. Ladiwala, K. Rege, C. M. Breneman, S. M. Cramer, A priori prediction of adsorption isotherm parameters and chromatographic behavior in ion-exchange systems, *Proceedings of the National Academy of Sciences of the United States of America* 102 (33) (2005) 11710–11715.
- [16] C. M. Roth, A. M. Lenhoff, Electrostatic and vanderwaals contributions to protein adsorption - computation of equilibrium-constants, *Langmuir* 9 (4) (1993) 962–972.
- [17] J. Stahlberg, B. Jonsson, C. Horvath, Theory for electrostatic interaction chromatography of proteins, *Analytical Chemistry* 63 (17) (1991) 1867–1874.
- [18] J. Stahlberg, B. Jonsson, C. Horvath, Combined effect of coulombic and van der waals interactions in the chromatography of proteins, *Analytical Chemistry* 64 (1992) 3118–3124.
- [19] J. Stahlberg, Retention models for ions in chromatography, *Journal of Chromatography A* 855 (1) (1999) 3–55.
- [20] G. Raffaini, F. Ganazzoli, Understanding the performance of biomaterials through molecular modeling: Crossing the bridge between their intrinsic properties and the surface adsorption of proteins, *Macromolecular Bioscience* 7 (5) (2007) 552–566.
- [21] H. O. Johansson, J. M. Van Alstine, Modeling of protein interactions with surface-grafted charged polymers. correlations between statistical molecular modeling and a mean field approach, *Langmuir* 22 (21) (2006) 8920–8930.
- [22] C. Ruggiero, M. Mantelli, A. Curtis, P. Rolfe, Protein-surface interactions - an energy-based mathematical model, *Cell Biochemistry and Biophysics* 43 (3) (2005) 407–417.
- [23] P. M. Biesheuvel, M. van der Veen, W. Norde, A modified poisson-boltzmann model including charge regulation for the adsorption of ionizable polyelectrolytes to charged interfaces, applied to lysozyme adsorption on silica, *Journal of Physical Chemistry B* 109 (9) (—2005—) 4172–4180.
- [24] J. Zhou, J. Zheng, S. Y. Jiang, Molecular simulation studies of the orientation and conformation of cytochrome c adsorbed on self-assembled monolayers, *Journal of Physical Chemistry B* 108 (45) (2004) 17418–17424.
- [25] F. Dimer, J. Hubbuch, A novel approach to characterize the binding orientation of lysozyme on ion-exchange resins, *Journal of Chromatography A* 1149 (2) (2007) 312–320.
- [26] Y. Duan, C. Wu, S. Chowdhury, M. C. Lee, G. M. Xiong, W. Zhang, R. Yang, P. Cieplak, R. Luo, T. Lee, J. Caldwell, J. M. Wang, P. Kollman, A point-charge force field for molecular mechanics simulations of proteins based on condensed-phase quantum mechanical calculations, *Journal of Computational Chemistry* 24 (16) (2003) 1999–2012.

-
- [27] J. M. Wang, P. Cieplak, P. A. Kollman, How well does a restrained electrostatic potential (resp) model perform in calculating conformational energies of organic and biological molecules?, *Journal of Computational Chemistry* 21 (12) (2000) 1049–1074.
- [28] A. Onufriev, D. Bashford, D. A. Case, Exploring protein native states and large-scale conformational changes with a modified generalized born model, *Proteins-Structure Function and Bioinformatics* 55 (2) (2004) 383–394.
- [29] P. DePhillips, I. Lagerlund, J. Farenmark, A. M. Lenhoff, Effect of spacer arm length on protein retention on a strong cation exchange adsorbent, *Analytical Chemistry* 76 (19) (2004) 5816–5822.
- [30] D. A. Pearlman, D. A. Case, J. W. Caldwell, W. S. Ross, T. E. Cheatham, S. Debolt, D. Ferguson, G. Seibel, P. Kollman, Amber, a package of computer-programs for applying molecular mechanics, normal-mode analysis, molecular-dynamics and free-energy calculations to simulate the structural and energetic properties of molecules, *Computer Physics Communications* 91 (1-3) (1995) 1–41.
- [31] D. A. Case, T. E. Cheatham, T. Darden, H. Gohlke, R. Luo, K. M. Merz, A. Onufriev, C. Simmerling, B. Wang, R. J. Woods, The amber biomolecular simulation programs, *Journal of Computational Chemistry* 26 (16) (2005) 1668–1688.
- [32] W. R. Rypniewski, H. M. Holden, I. Rayment, Structural consequences of reductive methylation of lysine residues in hen egg-white lysozyme - an x-ray-analysis at 1.8-angstrom resolution, *Biochemistry* 32 (37) (1993) 9851–9858.
- [33] H. M. Berman, J. Westbrook, Z. Feng, G. Gilliland, T. N. Bhat, H. Weissig, I. N. Shindyalov, P. E. Bourne, The protein data bank, *Nucleic Acids Research* 28 (1) (2000) 235–242.
- [34] E. Chatani, R. Hayashi, H. Moriyama, T. Ueki, Conformational strictness required for maximum activity and stability of bovine pancreatic ribonuclease a as revealed by crystallographic study of three phe 120 mutants at 1.4 angstrom resolution, *Protein Science* 11 (1) (2002) 72–81.
- [35] D. Bashford, Macroscopic electrostatic models for protonation states in proteins, *Front Biosci* 9 (2004) 1082–99.
- [36] R. J. Loncharich, B. R. Brooks, R. W. Pastor, Langevin dynamics of peptides - the frictional dependence of isomerization rates of n-acetylalanyl-n'-methylamide, *Biopolymers* 32 (5) (1992) 523–535.
- [37] R. W. Pastor, B. R. Brooks, A. Szabo, An analysis of the accuracy of langevin and molecular-dynamics algorithms, *Molecular Physics* 65 (6) (1988) 1409–1419.
- [38] D. L. Wu, R. R. Walters, Effects of stationary phase ligand density on high-performance ion-exchange chromatography of proteins, *Journal of Chromatography* 598 (1) (1992) 7–13.

DETAILED ANALYSIS OF MEMBRANE ADSORBER PORE STRUCTURE AND PROTEIN BINDING BY ADVANCED MICROSCOPY

Jun Wang^a, Florian Dismer^b, Juergen Hubbuch^b, Mathias
Ulbricht^{a*}

^a *Lehrstuhl fuer Technische Chemie II, Universitaet Duisburg-Essen, 45117 Essen, Germany*

^b *Institut fuer Biotechnologie, Forschungszentrum Juelich, 52425 Juelich, Germany*

* *Corresponding author. Tel.: +49 201 1833151; fax: +49 201 1833147. E-mail address: mathias.ulbricht@uni-due.de (M. Ulbricht).*

Abstract

Commercial Sartobind[®] porous cation exchanger membranes, based on stabilized regenerated cellulose and with sulfonic acid (S) or carboxylic acid groups (C), were analyzed with respect to their pore structure in dry, slightly swollen and wet state by three microscopic methods, conventional scanning electron microscopy (SEM), environmental SEM (ESEM), and confocal laser scanning microscopy (CLSM). The dehydration behaviour of the membranes was in situ observed at varied vapour pressure in the chamber of the ESEM, indicating some deformations of the macropore structure (largest pore diameters up to 20 μm) and significant changes in dimension and mobility of smaller cellulose fibers within these macropores, both as function of water content of the membrane. The binding of mono-Cy5-labelled lysozyme inside fluoresceine-labelled and unlabelled Sartobind[®] membranes was monitored by CLSM. The characteristic fluorescence intensity distributions in areas of (146 μm 146 μm) indicated that protein binding takes place predominately in a layer which is anchored to a fine cellulose fiber network and, to a lower degree, directly to thick cellulose fibers. Due to the limited thickness of this binding layer, a significant fraction of the macropores remained free of protein. Protein binding as function of concentration and incubation times was also monitored by CLSM and discussed related to the binding isotherms for the membrane Sartobind[®] S and C. Further, a flow-through cell for the in situ monitoring with CLSM of protein binding during the binding step was built, and the results obtained for binding of lysozyme in membranes Sartobind[®] S indicate this experiment can give very important information on the dynamic behaviour of porous membrane adsorbers during separation: the lateral microscopic resolution in the x, y plane enables the identification of different breakthrough times as function of the location (pore structure), and this information can help to explain possible reasons for axial dispersion (in z-direction) observed in breakthrough analyses of the same separation in a chromatography system. The combination of advanced microscopy with detailed investigations of static and dynamic protein binding will provide a better understanding of the coupling between mass transfer and reversible binding in membrane adsorbers onto separation performance, and it will provide valuable guide-lines for the development of improved membrane adsorbers.

Keywords: Membrane adsorber, Ion-exchange, Protein binding, Breakthrough curve, Electron microscopy, Confocal laser scanning microscopy

1 Introduction

Separations with membrane adsorbers (membrane chromatography, solid phase extraction) are a very attractive and rapidly growing field of application for functional macroporous membranes [1]. The key advantages in comparison with conventional porous adsorbers (particles, typically having a diameter of $50\mu\text{m}$) result from the pore structure of the membrane which allows a directional convective flow through the majority of the pores. Thus, the characteristic distances (i.e. times) for pore diffusion will be drastically reduced [2–4]. The separation of substances is based on their reversible binding on the functionalized pore walls. The most frequently used interactions are ion-exchange and various types of affinity binding. Hence, the internal surface area of the membrane and its accessibility is most important for the (dynamic) binding capacity. Typical specific surface areas of macroporous membranes (otherwise used for microfiltration or conventional filtration, or as solid supports) are only moderate. Consequently, the development of high-performance membrane adsorbers should proceed via an independent optimization of pore structure and surface layer functionality, providing a maximum amount of binding sites with optimum accessibility [5]. The most relevant commercial membrane adsorbers are indeed based on macroporous supports from established membrane formation process technology and subsequent chemical modification for the attachment of functional groups acting as binding sites. High binding capacities can be achieved by three-dimensional functional polymer layers on the pore wall. An example is the Sartobind[®] cation exchange membranes, consisting of a macroporous support from cross-linked regenerated cellulose and a grafted synthetic polymer containing sulfonic acid or carboxylic acid groups [6].

Typical characterization methods for membrane adsorbers are focussed on their functionality, i.e. the binding performance for various target solutes or nanoparticles, especially under flowthrough conditions. Break-through curves give information about the influences of convective flow, pore diffusion and binding kinetics. Various mathematical models of membrane adsorption have also been developed [7–10]. However, even the most sophisticated state-of-the-art models use only average parameters (such as binding constant, binding capacity per membrane volume, flowrate and pore diameter) for the porous membrane with their functional pore surface.

In a real membrane adsorber, the pore structure can be quite heterogeneous (including pore shape and size distribution, tortuosity and dead-ended pores), binding can occur in relatively thick functional hydrogel layers extending into the pore space, and this structure may be dynamic due to swelling/shrinking of the basematerial and/or the functional layer under separation conditions, or deformation by mobile phase flow.

The environmental scanning electron microscope (ESEM) allows investigation of wet and insulating samples without prior specimen preparation. It has been used to study the swelling behaviour of cellulose fibers *in situ* [11] and the wetting properties of macroporous polymer membranes [12]. By controlling sample temperature and the pressure of water vapour surrounding it, the water content of the sample can be adjusted *in situ*.

Confocal laser scanning microscopy (CLSM) provides the possibility of measuring the fluorescence emission of tracer fluorophores within three-dimensional objects with high local resolution and depth discrimination. The method had also been proposed for the characterization of porous membrane adsorbers [13–15]. The use of two different fluorescence dyes for labelled membrane and protein which can be detected independently

enables simultaneous visualization of membrane pore structure and protein binding to the membrane functional layer by CLSM.

In this work, pore structure including morphology and dynamics in pore structure, as well as protein binding of commercial Sartobind[®] cation exchanger membranes were investigated by using conventional SEM and ESEM as well as CLSM. Further, the static binding patterns of protein in the membranes after various incubation conditions were investigated. As model protein, Cy5-labelled lysozyme was separated from unlabelled native protein to eliminate artefacts of non-specific interactions and ensure that all proteins are visible under the CLSM conditions [16, 17]. In situ monitoring with CLSM of protein binding in the membranes was done with help of a special flow cell. In combination with the static and dynamic protein binding data, this work provides a better understanding of the coupling between mass transfer and reversible binding in membrane adsorbers onto separation performance.

2 Experimental materials and methods

2.1 Membranes and chemicals

The used membrane adsorbers were flat-sheet materials made from stabilized regenerated cellulose (Sartorius-Stedim Biotech, Goettingen, Germany): a strong cation-exchanger (Sartobind S; batch #2229) with sulfonic acid groups, a weak cation-exchanger (Sartobind C; batch #2231) with carboxylic acid groups and the unmodified base membrane as reference, all nominal pore size of 35 μm . Membrane thickness was 200-250 μm . The thickness of individual samples used for characterization was measured using digimatic micrometer (Mitutoyo Corporation, Japan). Static binding capacity for lysozyme according to the manufacturer are 0.8 mg/cm² (29 mg/ml) for Sartobind S and 0.6 mg/cm² (22 mg/ml) for Sartobind C [6]. The membranes were washed with Milli-Q water (from a system of Millipak[®]-40, Millipore) and equilibrated with buffer before the characterizations.

Lysozyme from hen egg (either "crystalline, powder, 85,400 units/mg" from Fluka, or "~95% protein, ~50,000 units/mg" from Sigma) was used as model protein for this work. The fluorescence dyes were 5-(4,6-dichlorotriazinyl) aminofluorescein (5-DTAF isoform, excitation/emission wavelengths of 492/516nm) from Invitrogen and Cy5 mono-reactive NHS ester (excitation/ emission wavelengths of 633/654nm) from GE Healthcare. Sodium chloride (99.7%) was from VWR International, France. Potassium hydrogenphosphate and potassium dihydrogenphosphate (98.0-100.5%) was from Applichem. Sodium carbonate (99%) and potassium chloride ($\geq 99.0\%$) were from Fluka.

Buffers were prepared using Milli-Q water. 10 mM potassium phosphate buffer, pH 7.0 (buffer A) and 10 mM potassium phosphate buffer with 1 M sodium chloride, pH 7.0 (buffer B) were used for the measurements of binding isotherm and breakthrough curves. Sodium carbonate buffer (100 mM, pH 9.3) was used for labelling. Sodium phosphate buffer (variable ionic strength, pH 7.0) was used in the separation of labelled protein from native protein, and also in CLSM experiments.

Table 1: ESEM relative humidity isobar chart at 2 .C [18]

Vapour pressure (Torr)	4.2	4.0	3.7	3.4	3.2	2.9	2.6	2.4	2.1	1.8	1.6	1.3
Rel. humidity (%)	80	75	70	65	60	55	50	45	40	35	30	25

2.2 Methods for SEM and measuring of wet samples using ESEM

Standard SEM images were recorded at high vacuum using an environmental scanning electron microscope (QUANTA FEG 400, FEI, Eindhoven, The Netherlands). The samples were pre-coated with silver DAG 1415 (Plano GmbH, Wetzlar, Germany) for 1min. The wet samples for ESEM images were equilibrated in 10mM phosphate buffer for 24h, after slightly drying with fine paper they were directly put into the ESEM chamber pre-set at a vapour pressure of 3.4 Torr, representing a relative humidity of 60%.

2.3 Membrane dehydration/hydration investigations

In situ study with ESEM was performed at 2 .C with help of a Peltier chip-controlled cooling stage (table 1) using the same ESEM with modest humidity in chamber. Original Sartobind and gold-coated Sartobind membranes were used. The gold coating on the membrane resulted from step-wise current-less metallization using the solutions PD 11, SLOTONIP 61 and SLOTOGOLD 10 (Schloetter Galvanotechnik, Geislingen, Germany), respectively, for surface activation by deposition of catalytic amounts of palladium, nickel deposition and nickel exchange to gold, respectively, under conditions where an incomplete surface coverage with metal can be achieved.

The membrane sample was pre-equilibrated to relative humidity of approximately 80% in a desiccator (containing a potassium chloride) at room temperature. At the beginning, a pump down sequence described by Cameron and Donald [18] was carried out. The sample was quickly put into the ESEM chamber pre-set at a vapour pressure of 2.9 Torr, representing a relative humidity of 55%. By following this procedure, condensation of water on the membrane surface was prevented. It must be noticed, the pressure in chamber in this way consists of water vapour and the rest of air. In the rest of the paper, data will be reported assuming that the atmosphere in the chamber contains only water vapour. Depending on membrane type and image magnification, the beam voltage was set at 10 or 15 keV and a working distance ≤ 6 mm was used. A reduction of water vapour pressure until to 1.3 Torr followed, and the time to equilibrium for each condition was set to 5min for the original membranes, and to 10 min for the gold-coated membranes. The measurement was performed by using of image analysis software "Scandium 3.2" (soft imaging system).

2.4 Visualization of membrane morphology and protein binding by means of CLSM

2.4.1 Staining of the membrane

The membranes were stained with the hydroxyl-reactive fluorescence dye 5-DTAF. The incubation with dye solution and the following washing steps were performed using a

filter holder (Swinnex, Millipore) with three membrane samples (diameter 13mm) under continuous circulation at a flow rate of 1ml/min. In each case, 20 ml DTAF solution in 100mM sodium carbonate, pH 9.3, with an adapted concentration (15 $\mu\text{g}/\text{ml}$ plus 100 mM NaCl for Sartobind S and 10 $\mu\text{g}/\text{ml}$ for Sartobind C) was used. After circulation for approximately 18 h, the membranes were washed successively with 20% ethanol, 1 M NaCl and 200 mM sodium phosphate buffer, pH 7.0.

2.4.2 Protein labelling and purification

Lysozyme (from Sigma, cf. above) was labelled using a procedure described by Dimer and Hubbuch [19], with the amino-reactive fluorescence dye Cy5 mono-reactive NHS ester. After reaction in sodium carbonate buffer, pH 9.3, the protein was purified with gel filtration and then with HP ion-exchange chromatography. Only mono-labelled lysozyme fractions were pooled and subsequently concentrated using ultrafiltration to the concentration required for binding experiments. UVvis spectroscopy (Cary 50, Varian) was used for determination of lysozyme concentration.

2.5 Membrane incubation with protein

Membrane samples (diameter 5mm) were incubated with labelled lysozyme for 15 min, 4 h and overnight. The used concentrations were 0.03, 0.12 and 0.57 mg/ml (in 200 mM sodium phosphate buffer, pH 7.0, plus 50 mM NaCl) with a defined volume leading to a two fold excess of protein relative to the respective membrane static binding capacity according to the manufacturer (cf. Section 2.1) to minimize both the used amount of labelled protein and the depletion of protein solution. The samples were subsequently washed with buffer for 15 min.

2.6 CLSM analysis

The analysis was carried out using the CLSM system Zeiss LSM510 equipped with a water immersion 63x/NA1.2 CApochromat objective lens. The system is provided with laser excitation sources at 488, 533 and 633 nm. Followed the identification of the beginning of the membrane (scanning depth $z = 0$) and characteristic membrane pore morphology at different z positions, detailed xy scans were performed for both emission wavelengths at gain settings where non-specific fluorescence (i.e., by auto-fluorescence of the membrane material, or due to non-specific interaction of Cy5 with unstained membranes) could not be detected. The obtained images were stored as 8-bit scans and 4 scans were always averaged to reduce noise, data reported have a dimension of $512 \cdot 512$ pixel representing an area of $146.2 \mu\text{m} \cdot 146.2 \mu\text{m}$.

2.6.1 Experimental setup for in situ monitoring of protein binding with CLSM

A self-designed membrane module was used for the in situ monitoring of protein binding using the inverse microscope (fig. 1). Main considerations for module design were a homogeneous flow distribution into the membrane and a small back pressure. The latter

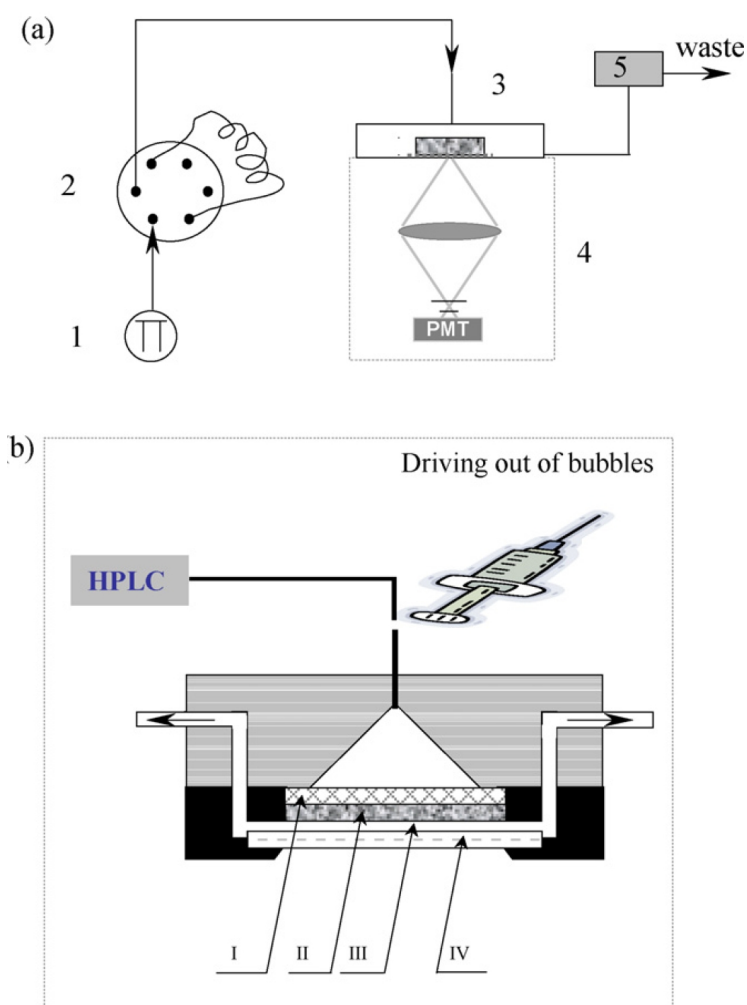


Figure 1: (a) Setup for in situ monitoring of protein binding: 1, pump of HPLC; 2, seven port injection valve; 3, membrane module; 4, confocal laser scanning microscope; 5, high position reservoir. (b) Construction of membrane module: I, distributor; II, membrane; III, channel for outlet liquid; IV, observation glass.

aspect was crucial because the distance between the objective of the microscope and z-position in the membrane could not be larger than 0.07 mm, and the thickness of the glass should provide sufficient mechanical strength to withstand the pressure built-up by the flow through the thin channel into the liquid outlet. The membrane module was directly connected to a HPLC pump (LC-10ADVP Shimadzu) in order to minimize dead volumes of the system. The module was equipped with an additional outlet connected to an elevated buffer reservoir together with a syringe for driving air bubbles out of the system before the start of an experiment.

A dye-stained Sartobind S membrane sample (diameter 12 mm) was installed in the module with the "bottom" side toward the observation glass. A droplet of Milli-Q water was used between the observation glass and objective. The flowrate was set to 0.3 ml/min, and the system was first equilibrated with buffer for 10 membrane volumes. A solution of a mixture of labelled and native lysozyme was used (protein concentration 1.7 mg/ml, 30% labelled protein). The protein solution was given in a 1 ml loop and injected to the module

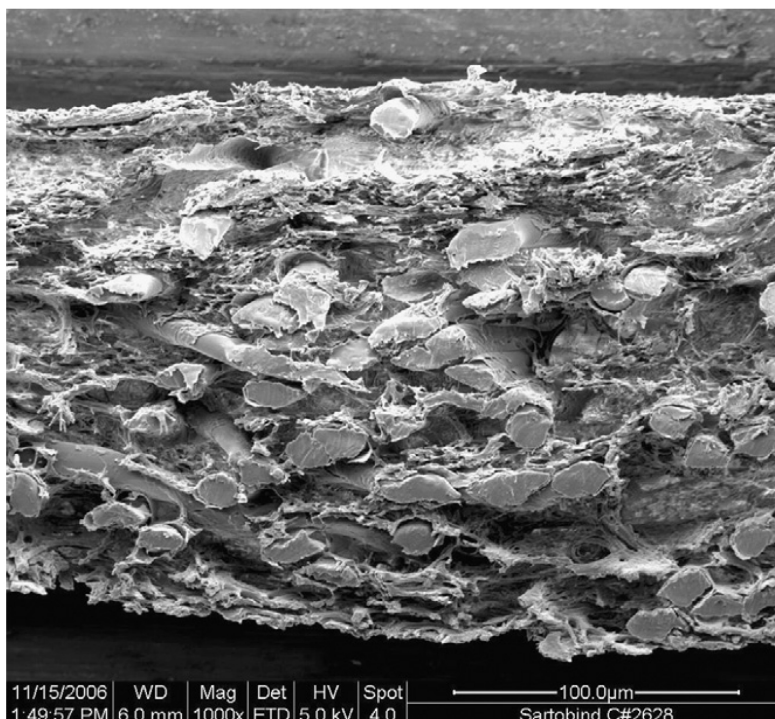


Figure 2: SEM image of a cross-section of membrane Sartobind C: the sample was embedded in paraffin, cut with a microtome, washed with ether and ethanol, and dried.

with a seven-port injection valve (7725i, Rheodyne). Simultaneously with the injection, image acquisition was started at the pre-chosen position of interest (at a distance of $\sim 10\mu\text{m}$ from the outer surface of the membrane), selected using an excitation wavelength of 488 nm, corresponding to the membrane bound dye. The x-y intensity profile for both emission wavelengths (488 and 633 nm) was measured with a time resolution of every 2 s and saved as an 8-bit single scan.

2.7 Protein binding isotherms

Protein binding isotherm was determined via batch adsorption experiments with different initial protein concentration for lysozyme (from Fluka), using the procedure described in detail in [20]. Langmuir adsorption parameters were estimated by fitting eluted protein amount from membranes using non-linear least-square regression with K as Langmuir constant and q_{max} as maximum binding capacity.

2.8 Breakthrough curves

Breakthrough curves were recorded using an Akta Purifier (GE Healthcare Life Sciences) with a UV detector set at 280 nm. One piece (diameter 12 mm) of Sartobind S or unmodified base membrane was stacked in a CIM module (BIA Separations, Ljubljana, Slovenia). Experiments were performed at room temperature and a flow rate of 0.3 ml/min using 2 mg/ml lysozyme (from Fluka).

3 Results and discussion

3.1 Morphology

The SEM cross-section image (fig. 2) illustrates that the Sartobind membranes have an anisotropic macroporous structure. The mechanical stability of the membrane is mainly connected to thick fibers with a diameter of about 10 μm . The occurrence of these fibers is concentrated to the middle section of the membrane. However, few fibers are also seen directly beneath the outer surface. Therefore, the pore morphology in the regions close to outer surface is slightly different from the rest of the membrane. In general, the morphology of Sartobind membranes is very diverse, irregular and complex when compared to typical microfiltration membranes.

The typical morphology for the bottom side of Sartobind S and C membrane in dry (fig. 3a) and wet state (fig. 3c) is a very coarse structure, consisting of relatively thick cellulose-based fibers connected to a network of fine fibers and clustered membrane material, together forming the macropores on the outer surface. The CLSM image in buffer of a fluorescence-stained membrane, ~ 10 μm from the outer surface, reveals that the very coarse structure containing the macroporous cellulose fiber network is characteristic also for the inner structure of the membranes (fig. 3b). The diameter of the larger pores is larger than 15 μm . It had been found that membrane morphology in buffer can be visualized using CLSM only to ~ 20 μm depth, i.e. a complete profile cannot be obtained under those conditions. Overall, SEM, ESEM and CLSM show similar and complementary morphologies at different depths of membrane, and the morphology of CLSM image for the dye-stained wet membrane is similar to that in wet state measured using ESEM (however, under the experimental conditions in ESEM, the scanned outer membrane surface does presumably not contain anymore water in the pore volume, so that only the image of a hydrated membrane matrix is obtained). When scanning the "top" side of the membrane significant differences in the pore morphology have been observed, the consistency between the three methods however remained. The typical morphology of the "top" side region is a more narrow network of the thick cellulose-based fibers connected to the fine fibers and clusters forming the macropores; i.e. the apparent porosity is lower than for the "bottom" side (data not shown).¹

The lateral resolution achieved for Sartobind membranes at a relative humidity of 50% was about 100 nm, far away from 5 to 10nm for standard SEM under ideal conditions [21]. The main reason for this is the chemical structure of the regenerated cellulose membrane, i.e. its non-conductivity (release of excessive charge built-up due to electron beam is by absorbed water only) and its pronounced sensitivity to heating by the electron beam during scanning.

CLSM allows noninvasive image scanning at variable depth within the membrane; i.e. it has the potential for visualization of pore structure in three dimensions under wet conditions. However, lateral resolution and sensitivity depend critically on the fluorophor which is essential for detection and on the intensities of excitation and emitted light within

¹All results presented in this paper are for the "bottom" sides of Sartobind S and C membranes, because this surface and the layer underneath are more uniform and more porous than the "top" sides, and consequently there is a larger fraction of area for protein binding per image. However, analogous results with respect to correlations between pore morphology and protein binding have been obtained for the "top" sides as well.

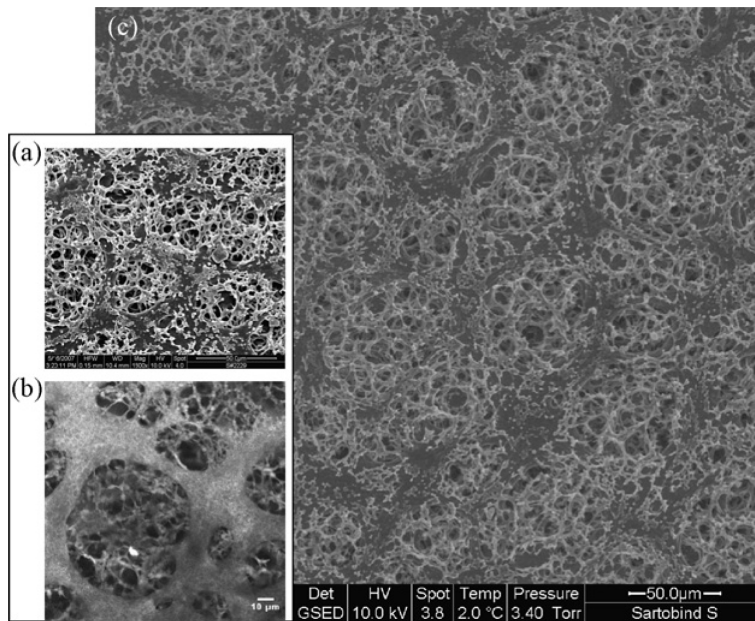


Figure 3: Morphology of membrane Sartobind S, bottom side: (a) SEM image of outer surface in dry state; (b) CLSM image in a depth of $10\ \mu\text{m}$ in $50\ \text{mM}$ phosphate buffer; (c) ESEM image of outer surface at $2\ ^\circ\text{C}$ and $3.4\ \text{Torr}$ after equilibration in $10\ \text{mM}$ phosphate buffer for 24 h.

the three-dimensional object. For a material with no intrinsic fluorescence, staining with a fluorescence dye is necessary.

During this study, it had been observed that the efficiency of the labelling reaction of the cellulose matrix with the hydroxyl reactive dye was lower for the S than for the C membrane. This can be explained by electrostatic repulsion between the dye derivative, carrying a negative charge under labelling conditions, and the sulfonic acid groups of the S membrane, and this problem had been reduced by using a higher salt concentration during staining of the S membranes (cf. Section 2.4). The staining intensity and its variation in different depths within the specimen can result in different attenuation of excitation or emitted light. This problem is less relevant in this study because the sampling depth was limited due to other reasons discussed below. Photo-bleaching can cause an irreversible decay of fluorescence with time. This problem is more pronounced for the fluorescein derivative used for membrane staining than for the Cy5 dye used for the protein labelling (cf. Section 3.3), and the scanning times had been adapted accordingly. The morphology of the Sartobind membranes, a random network of irregularly shaped elements of varied size, is crucial for the correct description of light attenuation in the CLSM experiments of this work. The limit of lateral resolution of a CLSM can be estimated using the point objects method of Inoué [22] (cf. [13]) and is about $1\ \mu\text{m}$ for the used CLSM system. The accuracy in z direction is due to the focus of the excitation light which is also larger than $1\ \mu\text{m}$. Therefore, objects are resolved if their dimensions are larger than $1\ \mu\text{m}^3$. Consequently, using CLSM only macropores larger than $1\ \mu\text{m}$ can be separately identified in the stained membranes. Furthermore, the differences in refractive index between cellulose (1.45) and aqueous buffer (1.33), cause a steep decay of excitation intensity over thickness, and are considered the main reason for the limited sampling depth of $\sim 20\ \mu\text{m}$.

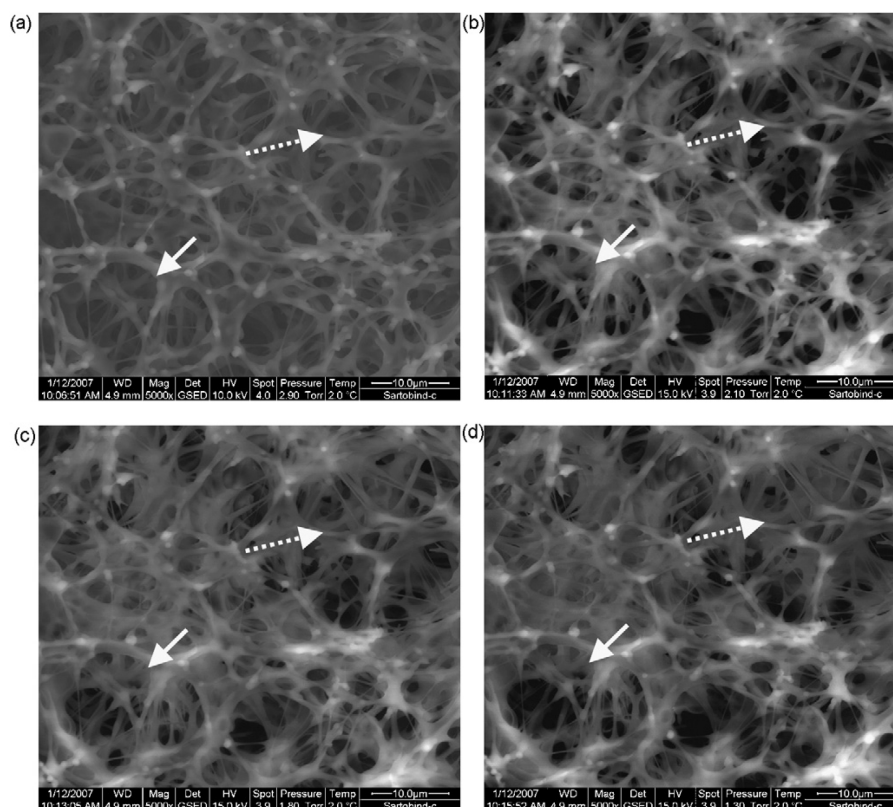


Figure 4: Dehydration of membrane Sartobind C[®], bottom side, in ESEM chamber at 2 °C (magnification 5000x): the vapour pressure was (a) 2.9 Torr (~55% rel. humidity), (b) 2.1 Torr (~44% rel. humidity), (c) 1.8 Torr (~35% rel. humidity), (d) 1.3 Torr (~25% rel. humidity); the scale bar of images is 10 μm .

3.2 Membrane hydration/dehydration

ESEM was used to study how the membrane pore geometry would change upon uptake or release of water from/to the gas phase. This compromise had been chosen because the investigation of water-wet sample did not yield images where the pore structure could be clearly resolved (cf. Section 3.1). Data for in situ dehydration of water vapour saturated Sartobind C membrane is shown in fig. 4.

After reducing relative humidity from 55% (fig. 4a) to 40% (fig. 4b), the small cellulose fibers became thinner than in the saturated state. Overall, the apparent porosity increased slightly with decreasing vapour pressure in the chamber (fig. 4bd), but the most pronounced changes (exemplary regions indicated by arrows in the images) occurred at the pressure of 2.1 Torr. The shape of the macropore network defined by the strongest fibers did not change much.

Because of the sensitivity to the electron beam and the non-conductivity of the material itself, the untreated Sartobind membrane did not allow larger magnification in ESEM (cf. Section 3.1). A Sartobind membrane, coated with gold from solution (cf. Section 2.3), was therefore used for visualization of thick and thin fibers forming the macropores at a magnification of 20,000-fold (fig. 5). The few particular agglomerates in the images are gold particles as proven by EDX analysis. With decreasing vapour pressure, significant dehydration of fibers with diameters in the sub- μm range was observed. The

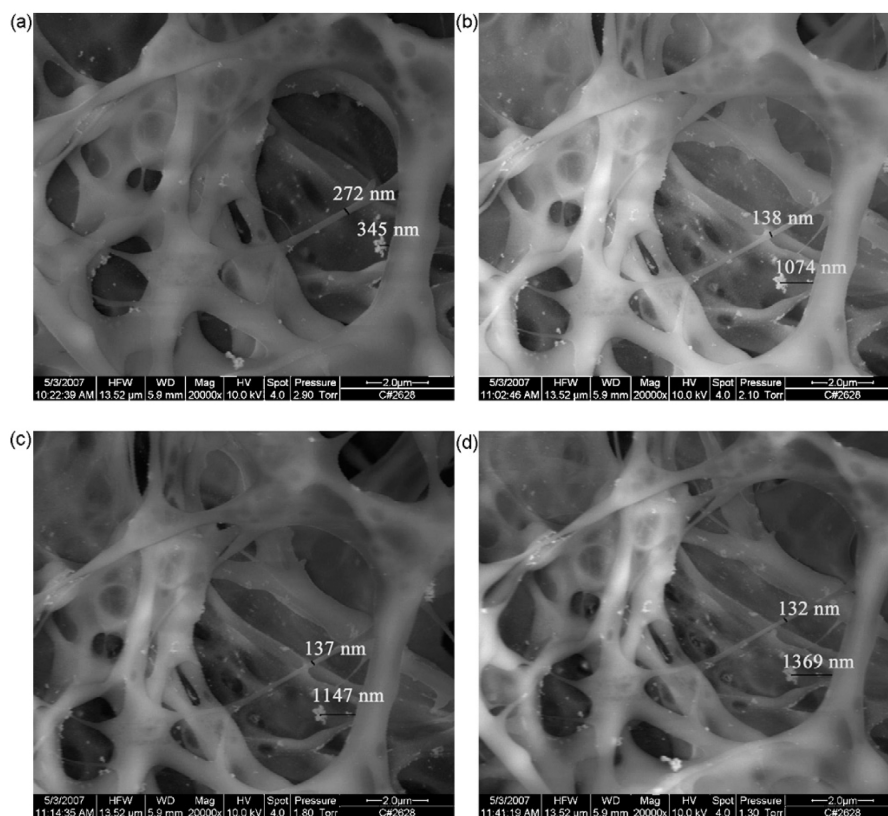


Figure 5: Dehydration of gold-coated membrane Sartobind® C, bottom side, in ESEM chamber at 2 °C (magnification 20,000x): the vapour pressure was data were measured using "Scandium 3.2, soft imaging system" and the image was produced using "Photoshop element 3.0".

reduction in area was maximal 30% (fig. 5a and d). The distance between the thick fiber and the largest gold agglomerate, which seems to be sticking to other fibers, increased about three fold (fig. 5a and d). The maximum enlargement of the large pore (left side in fig. 5) was 34%. Similar to the data for the original membrane (cf. fig. 4), the most pronounced changes occurred at a relative humidity of 40%. If the pressure reduced from 2.9 to 2.1 Torr, the area of the large pore increased by about 25% increase of pore diameter might be caused by a deformation of pore shape through the dehydration. The partial gold coating increased the image resolution while the swelling/shrinking properties of the cellulose fibers remained essentially unchanged. Similar morphology changes upon reducing the water vapour pressure had been observed for Sartobind S membranes.

3.3 Batch protein binding and static visualization by CLSM

Lysozyme from hen egg, consisting of 129 amino acids, has a molecular weight of 14.3 kg/mol and a pI of 11.3. Amino acids carrying positive charge are 6 lysines and 11 arginines. Along with the nine negatively charged amino acids, a positive net charge of lysozyme at pH7.0 is observed [23]. Lysozyme has a shape similar to an ellipsoid, with a length of about 5 nm and a width of about 3 nm. During protein labelling, the fluorescence dye Cy5, having a molecular weight of 789 g/mol, will be covalently attached to the primary amino group of a lysine residue. Only 1 or 2 Cy5 molecules will be bound

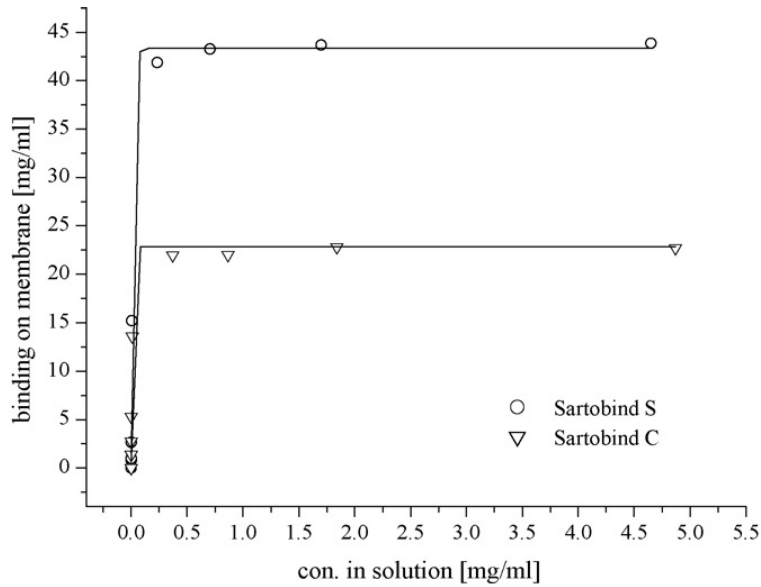


Figure 6: Binding isotherm for lysozyme on membranes Sartobind S and C measured by batch incubation; the fit to the data was calculated using nonlinear least-square regression.

to one lysozyme molecule under the used labelling conditions. A mixture of all the six isoforms of mono-labelled lysozyme was used in this work (cf. Section 2.4).

Binding isotherms for native lysozyme were measured to characterize the interactions of the model protein with the adsorbers (fig. 6), however only for the native lysozyme due to cost of the dye-labelled derivative. With membrane thickness of $230 \mu\text{m}$, the q_{max} for Sartobind S is 44 mg/ml , and the K is 76 ml/mg , while the q_{max} for Sartobind C is 23 mg/ml and the respective K is 62 ml/mg . The measured maximal binding capacity for the used Sartobind S membrane is much larger than the data of manufacturer. The concentrations of Cy5-labelled lysozyme in the CLSM experiments were 0.03 , 0.12 and 0.57 mg/ml , corresponding to the linear and near plateau region of the binding isotherms for Sartobind S and C (cf. Fig. 6), under the assumption that the interaction of unlabelled protein to the membrane is similar to that of the labelled protein isoform. As the used amount of protein was calculated according to the data of manufacturer, the initial concentration of 0.57 mg/ml for Sartobind S was shifted to the left, the beginning of the plateau region (fig. 6).

The subtle, but significant effects of labelling onto ion-exchange binding, which had been recently studied and discussed in detail for lysozyme [16], were considered by not using a mixture of labelled and unlabelled protein (as done in many other studies, cf. [14, 15]). By this means, fractionation between labelled and unlabelled protein within the adsorber according to different affinities can be avoided. It is important to keep in mind that the protein dimension is smaller than the lateral resolution of the method. Consequently, protein visualization is based on a fluorescence intensity beyond the detection limit in a volume larger $\geq 1 \mu\text{m}^3$, and the determination of the detection limit and an exact quantitative correlation between fluorescence intensity and protein amount do not yet exist for the used system due to the complex pore morphology (cf. Section 3.1).

Figs. 7 and 8 show results of simultaneous visualization of pore morphology and protein binding pattern for Sartobind S and C membranes, obtained after binding of

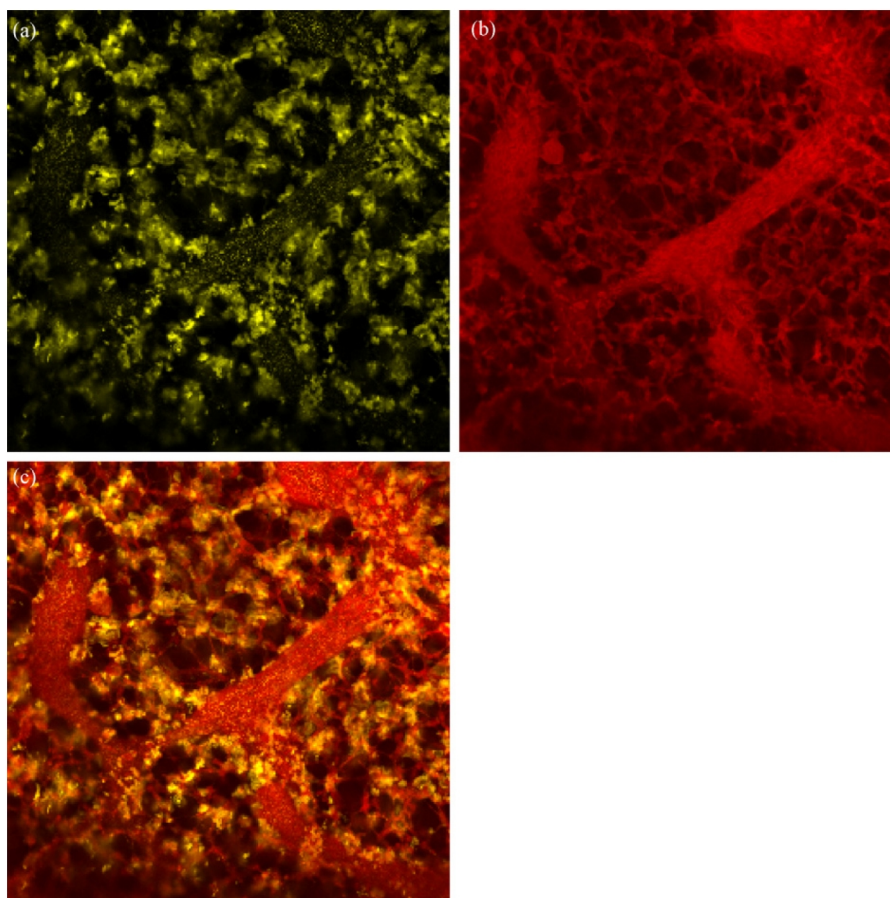


Figure 7: CLSM images of membrane Sartobind[®] C, bottom side, 7 μm from the outer surface: (a) bound lysozyme from 0.43 mg/ml (633 nm); (b) stained membrane (488 nm); (c) overlap of labelled protein binding to stained membrane.

labelled protein from a concentration of 0.43 mg/ml for 4 h to fluorescence-stained membranes. The control experiments with unmodified cellulose membranes had proven that the fluorescence-labelling of the membrane did not increase lysozyme binding capacity. Figs. 7a and 8a show the bound protein detected at 633 nm, Figs. 7b and 8b show the stained matrix detected at 488 nm, and the overlap of images at both wavelengths is given in figs. 7c and 8c. For the Sartobind S membranes, the protein binding pattern was similar to the pore morphology, and the protein filled in a relatively thick and homogeneous layer significant fraction of the macropores leaving the interior of the pore empty, while the bound protein density was much lower in the region of the thick cellulose fibers (fig. 8a). For the Sartobind C membranes, a more clustered protein pattern in the macropore space was observed, again with very little detectable protein on the thick cellulose fibers (fig. 7a). The overlap of the bound protein to stained membrane indicated that for both membranes the protein binding proceeds mainly in a layer which is anchored to the cellulose fiber network, and to a lower degree directly on the cellulose. Because of the limited thickness of this functional layer containing the ion-exchange groups, significant fractions of the pore volume remained dark. The differences in binding patterns between Sartobind S and Sartobind C membranes might be introduced by differences in the grafted functional polymer layers, the nature of ion-exchange group or the porous

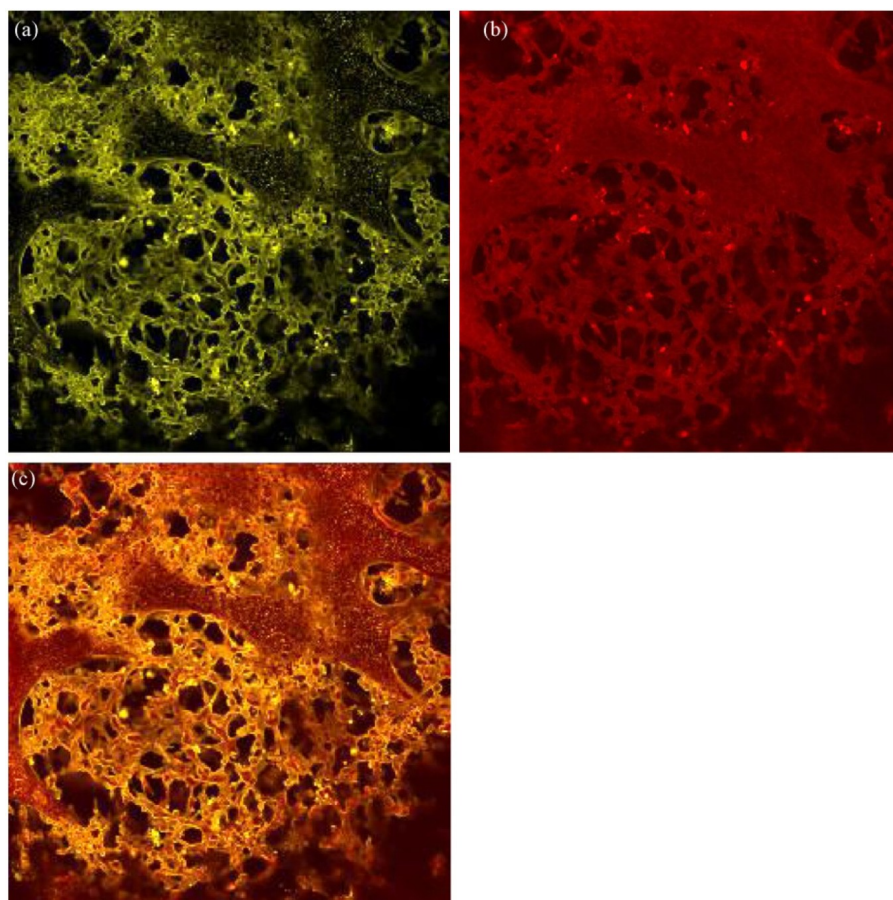


Figure 8: CLSM images of membrane Sartobind[®] S, bottom side, 7 μm from the outer surface: (a) bound lysozyme from 0.43 mg/ml (633 nm); (b) stained membrane (488 nm); (c) overlap of labelled protein binding to stained membrane.

base materials. The protein binding patterns within the pore structure of Sartobind membranes were also visualized after batch incubation with Cy5-labelled lysozyme for different times and at varied concentrations. In control experiments with an unmodified cellulose-based membrane of the same pore structure either stained or unstained membrane did not exhibit significant non-specific binding of the labelled protein at the used gain. Fig. 9 presents data obtained by CLSM for the bottom side of the Sartobind S membranes.² While the protein binding patterns were similar to that in figs. 7 and 8, the intensity distribution was significantly different. The coverage of all fine pores with protein was laterally quite homogeneous after binding from 0.03 mg/ml for 15 min (fig. 9a). However, an increase in time and concentration yielded a more clustered protein binding pattern (cf. Fig. 9b and c). Such apparent differences became even smaller with increasing protein concentration and for the experiments with a protein concentration of 0.57 mg/ml no significant difference as function of incubation time could be identified (cf. Fig. 9e and f). Also, the binding patterns did not exhibit differences after incubation overnight for all concentrations (cf. fig. 9a, d, and f). It was found that the protein binding capacity had been saturated after 4 h (data not shown).

Those subtle dependences of protein binding pattern, mainly on protein concentration,

²Cf. footnote 1.

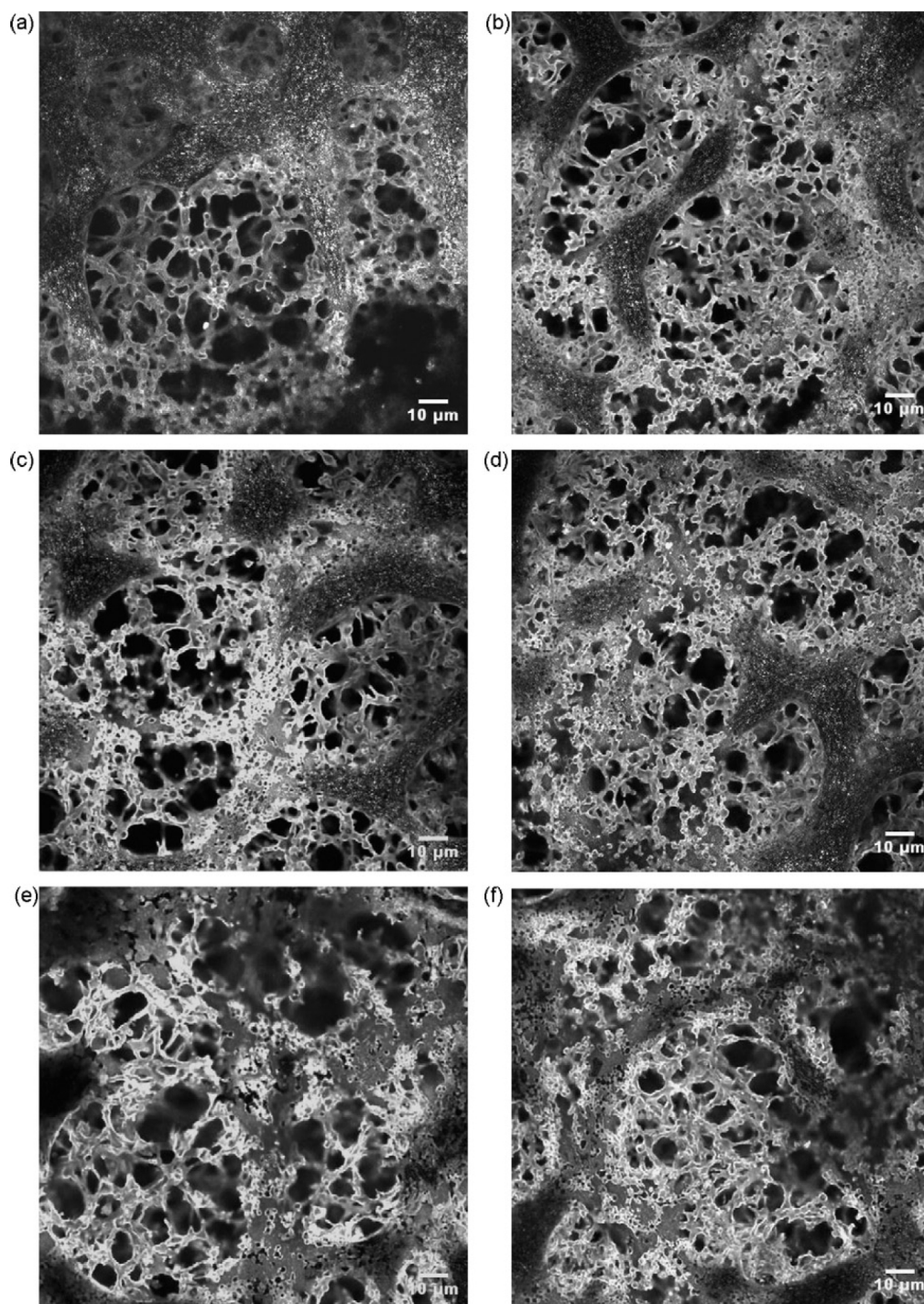


Figure 9: CLSM image (633 nm) of unstained membrane Sartobind[®] S, bottom side, 6 μm from the outer surface, after binding of Cy5-labelled lysozyme isoform: (a) from 0.03 mg/ml for 15 min, (b) from 0.03 mg/ml overnight, (c) from 0.12 mg/ml for 15 min, (d) from 0.12 mg/ml overnight, (e) from 0.57 mg/ml for 15 min, (f) from 0.57 mg/ml overnight in phosphate buffer.

may be explained by differences in driving force and kinetic influences onto diffusion and binding processes, both presumably also a function of the accessibility of binding sites in the macroporous membrane adsorber.

Irrespective the technical problems with CLSM in the highly irregular pore structures making exact quantitative estimations very complicated (cf. Section 3.1 and above), all results can be discussed with respect to the protein distribution in the system of membrane macropores as well as the relative bound protein amount in the x-y plane, indicated by the light intensity acquired at same CLSM z-position and gain setting.

3.4 Protein binding under flow-through and in situ monitoring by CLSM

The protein binding in the porous membrane adsorber was in situ monitored using a special flow-through membrane module (cf. fig. 1). An excess of a mixture of labelled and native lysozyme was injected as step function. Exemplary results for the Sartobind S membrane, in a distance of $\sim 10 \mu\text{m}$ from the bottom surface, are shown in fig. 10. In the right panel, the morphology of the stained membrane has been observed at 488 nm. In the left panel labelled lysozyme has been monitored at 633 nm. The gain to acquire the membrane images was set higher than in the previous experiments (cf. figs. 3b and 8b), in order to identify eventual changes of pore structure. After a time delay of 60 s following the injection of the protein solution, the first trace of protein appeared as small spot on the left panel. The area of protein binding increased within the subsequent ~ 20 s and trended to become stable after 80 s. The image for bound lysozyme distribution at 84 s (cf. fig. 10) was essentially identical to data obtained for the same membrane after batch adsorption for at least 15 min (cf. fig. 9). Protein was preferentially bound in a layer on the fine distributed cellulose fibers forming the macropores. Also, it should be noted that the protein in solution and in the pore volume was not visible. This can be well explained by a significant increase of local protein concentration upon binding to the adsorber surface.

However, the images of the membrane in the right panels changed notably during the process. Consistently between 72 and 80 s after protein injection, the membrane moved out of the previous z focus of the CLSM objective. This might have been caused by the applied flow and the slightly altered viscosity of the protein solution compared to pure buffer, or, most probably, by a morphology change imparted by the protein binding to the functional layers (cf. [24]) occurring exactly in this time interval.

The elution of bound protein using a high salt concentration was also monitored. It was clearly observed that the protein signal disappeared within few seconds to about 1 min depending on the concentration of salt. However, images for labelled protein showed very high intensity fluctuations, which can be explained by high local concentrations of protein in the elution peak, but also additional influences of refractive index change or change of membrane swelling, both due to change of salt concentration. Therefore, these images are not shown and further discussed in this work.

The in situ membrane module can be simplified according to a system model as shown in fig. 11, consisting of PFR (V_1 : the total volume of the capillaries, $88 \mu\text{l}$), CSTR (V_2 : the hold-up volume of the membrane module in front of the membrane, $105 \mu\text{l}$), and the membrane volume (V_3 : $17 \mu\text{l}$). For the flow rate of 0.3 ml/min, the first protein

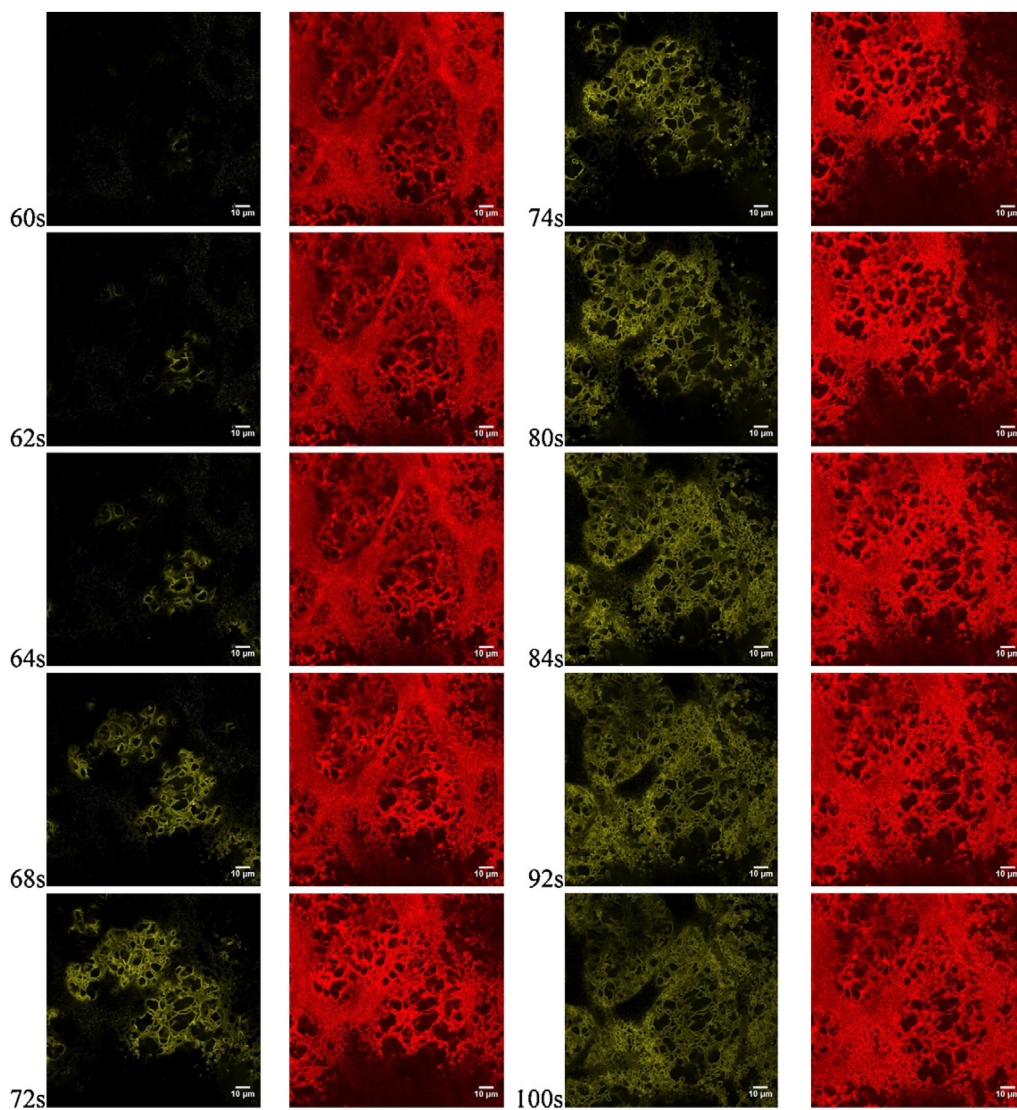


Figure 10: Time-resolved images for lysozyme binding from a 1.7 mg/ml (30% labelled isoform) solution in membrane Sartobind[®] S, ~10 µm from the outer surface. Left: Cy5-labelled lysozyme (633 nm); right: stained membrane (488 nm).

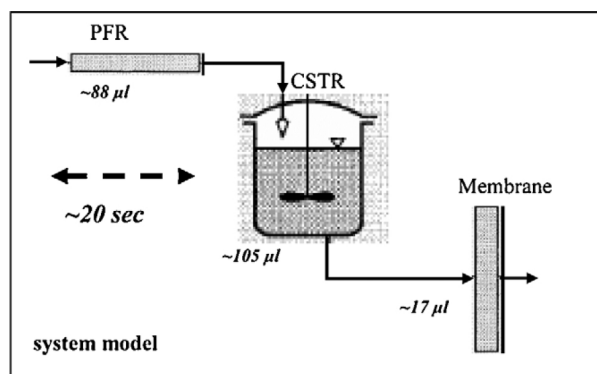


Figure 11: Simplified system model of in situ membrane module for CLSM, consisting of the HPLC capillary (considered as plug flow reactor/PFR/) and the flow distributor before the membrane (considered as continuous stirred tank reactor/CSTR/; cf. fig. 1).

would enter the hold-up volume of the membrane module ~ 20 s after injection. Due to mixing in volume V2, the protein would start to enter the membrane from this moment. The time to reach complete saturation of all binding sites in the membrane volume (V3, reduced by the volume of the $10 \mu\text{m}$ thick layer below the CLSM focus) after a step injection (which is not the case in practice, cf. above), without axial dispersion and at no kinetic hindrance by the binding would be ~ 110 s.

That axial dispersion in the Sartobind membranes is much larger, is demonstrated by the breakthrough curve measured at the same linear flow rate in a chromatography module (fig. 12). The time to saturation for the Sartobind S membrane at 10% breakthrough was indeed ~ 70 s when compared with the unmodified base membrane having the same pore structure. Therefore, the observed time delay until first protein detection in the in situ CLSM experiments can be quite well understood. On the other hand, the significant dispersion of breakthrough curve observed in chromatography (400 s to 100%)

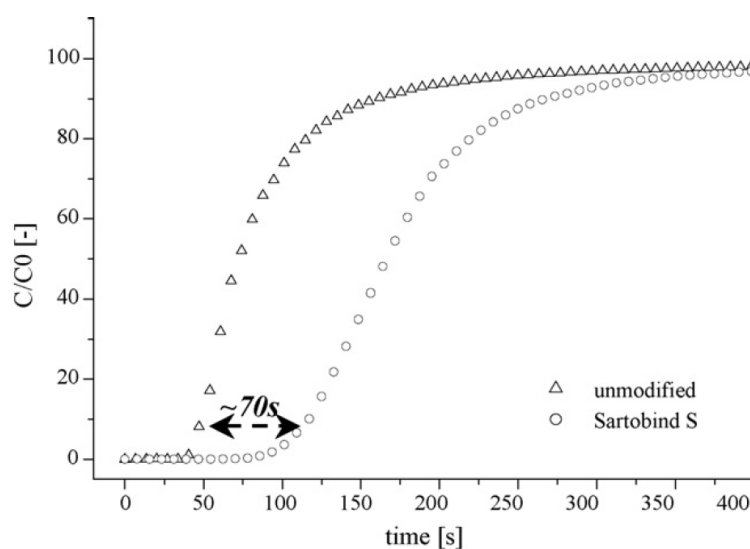


Figure 12: Breakthrough curves at a flow rate of 0.3 mg/ml for 1 layer of membrane Sartobind[®] S and unmodified cellulose base membrane, measured using 2 mg/ml lysozyme.

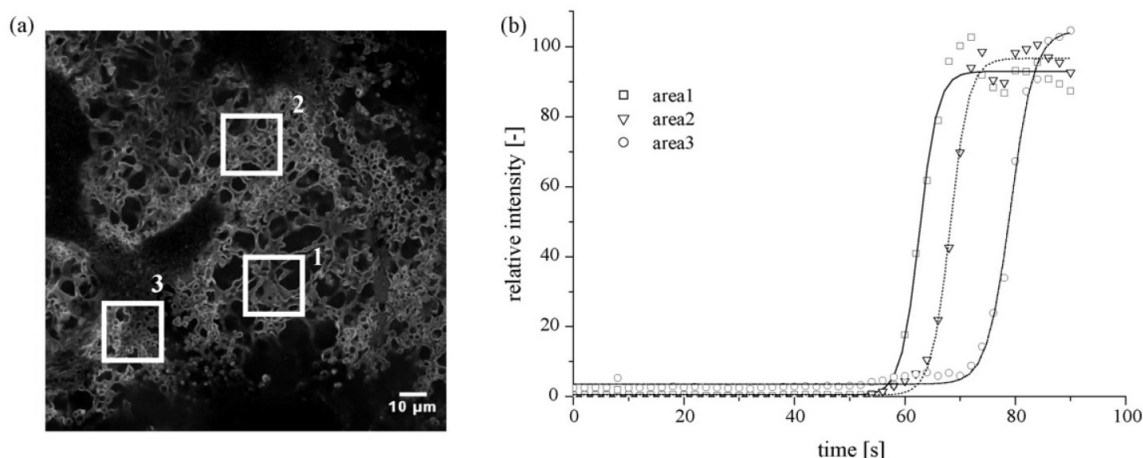


Figure 13: (a) Image of bound lysozyme (633 nm) in membrane Sartobind S after 84 s (cf. fig. 10): the highlighted areas ($2.2 \mu\text{m} \cdot 2.2 \mu\text{m}$) were selected for construction of breakthrough curves from complete data set; (b) breakthrough curves of the areas shown in (a); the intensity of protein fluorescence was normalized by the fluorescence intensity of the labelled membrane in the same area.

saturation) seems to be largely underestimated in the CLSM experiment (20 s to saturation after appearance of the first trace of protein). This, however, can be explained by the not yet established quantitative relationships between fluorescence intensity and protein concentration. It should be noted that in chromatography the time between 10 and 80% breakthrough (100 s) is also much shorter than reaching complete saturation (time between 80 and 100% are additional 300 s), and especially the latter changes are hardly distinguished by fluorescence imaging.

Using the time-resolved data from in situ CLSM, breakthrough curves can also be established for the labelled protein. The fluorescence image intensity of bound protein in three selected areas (size of $2.2 \mu\text{m} \cdot 2.2 \mu\text{m}$) as function of time was normalized by the fluorescence intensity of the labelled membrane in the same area (fig. 13). In all cases, the intensities showed a relatively large fluctuation after a relatively steep increase (fig. 13b). Because the relationship between intensity and concentration is not known (cf. above), the steepness cannot be discussed quantitatively. However, the breakthrough times were significantly different. The fastest breakthrough occurred in a region with fine fibers in a macropore (area 1), while late breakthrough was seen in an area close to a very thick cellulose fiber (area 3). One should keep in mind that the plane of observation was $\sim 220 \mu\text{m}$ behind the outer surface where the protein had entered. Nevertheless, it may be conceived that the very heterogeneous morphology of membrane causes uneven flow distribution, e.g. channeling.

Therefore, the most important conclusion from this experiment is that in addition to the information from conventional chromatography evaluation with respect to (average) axial dispersion, the lateral microscopic resolution in the x-y plane can give much additional information about possible reasons of such loss in chromatographic resolution.

4 Conclusion

Commercial macroporous membrane adsorbers have been characterized with help of different microscopic techniques in combination with static and dynamic protein binding experiment. Due to intrinsic difficulties with investigations of the porous membranes in completely wet state in the ESEM, the effects of water uptake and release from the gas phase have been investigated: while the macropore network remained unchanged, smaller fibers within the macropores showed a significant volume change and mobility. Using staining of the membrane matrix in combination with CLSM, the pore morphology in completely wet state and also inside the membrane volume can be imaged. However, the three dimensional resolution ($\leq 1 \mu\text{m}^3$) and depth of penetration in the sample (up to $20 \mu\text{m}$) are limited. The visualization of protein binding was possible, and significant binding in the pore volume but not extending throughout the entire diameter of the macropores has been confirmed. For the first time, the dynamic protein binding in macroporous membrane adsorbers has been monitored in situ using CLSM and qualitatively analyzed. This method will be further developed. Based on the knowledge obtained from advanced microscopy in combination with more conventional binding experiments, a new generation of membrane adsorbers is currently prepared via UV-initiated grafting of tailored functional polymeric ion-exchange layers (cf. [25]) on macroporous supports made from stabilized regenerated cellulose, and their improved separation performance will be related to the key parameters such as matrix pore structure and architecture of grafted functional polymer layers [18].

5 Acknowledgments

The authors are grateful for the technical support by Smail Boukercha, Universiteit Duisburg-Essen (UDE), during the work using ESEM. The skilled technical support for the manufacture of the in situ membrane module by Frank Matthes, UDE, is also acknowledged. The gold coating of membrane was performed by student Feng Yu, UDE. The Sartobind membranes were kindly provided by Dr. Rene Faber, Sartorius Stedim Biotech GmbH, Goettingen, Germany.

References

- [1] H. L. Knudsen, R. L. Fahrner, Y. Xu, L. A. Norling, G. S. Blank, Membrane ion-exchange chromatography for process-scale antibody purification, *J Chromatogr A* 907 (1-2) (2001) 145–54.
- [2] J. X. Zhou, T. Tressel, Basic concepts in q membrane chromatography for large-scale antibody production, *Biotechnol Prog* 22 (2) (2006) 341–9.
- [3] D. K. Roper, E. N. Lightfoot, Comparing steady counterflow separation with differential chromatography, *J Chromatogr A* 654 (1) (1993) 1–16.
- [4] R. Ghosh, Protein separation using membrane chromatography: opportunities and challenges, *J Chromatogr A* 952 (1-2) (2002) 13–27.

-
- [5] M. Ulbricht, Advanced functional polymer membranes, *Polymer* 47 (7) (2006) 2217–2262.
- [6] Sartorius, Sartobind membrane adsorbers for rapid purification of proteins, Sartorius brochure.
- [7] K. H. Gebauer, J. Thommes, M. R. Kula, Breakthrough performance of high-capacity membrane adsorbers in protein chromatography, *Chemical Engineering Science* 52 (3) (1997) 405–419.
- [8] S. Y. Suen, M. R. Etzel, A mathematical-analysis of affinity membrane bioseparations, *Chemical Engineering Science* 47 (6) (1992) 1355–1364.
- [9] H. W. Yang, M. Bitzer, M. R. Etzel, Analysis of protein purification using ion-exchange membranes, *Industrial & Engineering Chemistry Research* 38 (10) (1999) 4044–4050.
- [10] C. Boi, S. Dimartino, G. C. Sarti, Modelling and simulation of affinity membrane adsorption, *Journal of Chromatography A* 1162 (1) (2007) 24–33.
- [11] L. M. Jenkins, A. M. Donald, Use of the environmental scanning electron microscope for the observation of the swelling behaviour of cellulosic fibres, *Scanning* 19 (2) (1997) 92–97.
- [12] R. E. Delaparra, A method to detect variations in the wetting properties of microporous polymer membranes, *Microscopy Research and Technique* 25 (5-6) (1993) 362–373.
- [13] C. Charcosset, A. Cherfi, J. C. Bernengo, Characterization of microporous membrane morphology using confocal scanning laser microscopy, *Chemical Engineering Science* 55 (22) (2000) 5351–5358.
- [14] U. Reichert, T. Linden, G. Belfort, M. R. Kula, J. Thommes, Visualising protein adsorption to ion-exchange membranes by confocal microscopy, *Journal of Membrane Science* 199 (1-2) (2002) 161–166.
- [15] S. R. Wickramasinghe, J. O. Carlson, C. Teske, J. Hubbuch, M. Ulbricht, Characterizing solute binding to macroporous ion exchange membrane adsorbers using confocal laser scanning microscopy, *Journal of Membrane Science* 281 (1-2) (2006) 609–618.
- [16] C. A. Teske, M. Schroeder, R. Simon, J. Hubbuch, Protein-labeling effects in confocal laser scanning microscopy, *Journal of Physical Chemistry B* 109 (28) (2005) 13811–13817.
- [17] M. Schroeder, E. von Lieres, J. Hubbuch, Direct quantification of intraparticle protein diffusion in chromatographic media, *Journal of Physical Chemistry B* 110 (3) (2006) 1429–1436.

- [18] J. Wang, M. Ulbricht, Influence of pore size distribution and architecture of functional layers on separation performance of flow-through macroporous membrane adsorbers, *J. Chromatogr. A* submitted.
- [19] F. Dismer, J. Hubbuch, A novel approach to characterize the binding orientation of lysozyme on ion-exchange resins, *Journal of Chromatography A* 1149 (2) (2007) 312–320.
- [20] N. Singh, J. Wang, M. Ulbricht, S. R. Wickramasinghe, S. M. Husson, Surface-initiated atom transfer radical polymerization: A new method for preparation of polymeric membrane adsorbers, *Journal of Membrane Science* 309 (1-2) (2008) 64–72.
- [21] A. McDonald, Environmental scanning electron microscopy - esem, *Materials World* 6 (7) (1998) 399–401.
- [22] Inou, *Handbook of biological confocal microscopy* (2006).
- [23] D. E. Kuehner, J. Engmann, F. Fergg, M. Wernick, H. W. Blanch, J. M. Prausnitz, Lysozyme net charge and ion binding in concentrated aqueous electrolyte solutions, *Journal of Physical Chemistry B* 103 (8) (1999) 1368–1374.
- [24] T. Kawai, K. Sugita, K. Saito, T. Sugo, Extension and shrinkage of polymer brush grafted onto porous membrane induced by protein binding, *Macromolecules* 33 (4) (2000) 1306–1309.
- [25] M. Ulbricht, H. Yang, Porous polypropylene membranes with different carboxyl polymer brush layers for reversible protein binding via surface-initiated graft copolymerization, *Chemistry of Materials* 17 (10) (2005) 2622–2631.

A NOVEL TWO-ZONE PROTEIN UPTAKE
MODEL FOR AFFINITY
CHROMATOGRAPHY AND ITS
APPLICATION TO THE DESCRIPTION OF
ELUTION BAND PROFILES OF PROTEINS
FUSED TO A FAMILY 9 CELLULOSE
BINDING MODULE AFFINITY TAG

Mojgan Kavooosi^a, Nooshafarin Sanaie^a, Florian Dimer^b, Juergen
Hubbuch^b, Douglas G. Kilburn^a, Charles A. Haynes^{a,*}

^a Michael Smith Laboratories and the Department of Chemical and Biological Engineering, The University of British Columbia, Vancouver, BC, Canada V6T 1Z4

^b Bioseparations Group, Institute of Biotechnology 2, Research Centre Juelich, 52425 Juelich, Germany

* Corresponding author at: The University of British Columbia, Department of Chemical Engineering, 6174 University Blvd, Room 237, Vancouver, BC V6T 1Z3, Canada. Tel.: +1 604 822 5136; fax: +1 604 822 2114. E-mail address: israel@chml.ubc.ca (C.A. Haynes).

Abstract

A novel two-zone model (TZM) is presented to describe the rate of solute uptake by the stationary phase of a sorption-type chromatography column. The TZM divides the porous stationary-phase particle into an inner protein-free core and an outer protein-containing zone where intraparticle transport is limited by pore diffusion and binding follows Langmuir theory. The TZM and the classic pore-diffusion model (PDM) of chromatography are applied to the prediction of stationary-phase uptake and elution bands within a cellulose-based affinity chromatography column designed to selectively purify proteins genetically labelled with a CBM9 (family 9 cellulose binding module) affinity tag. Under both linear and nonlinear loading conditions, the TZM closely matches rates of protein uptake within the stationary phase particles as measured by confocal laser scanning microscopy, while the PDM deviates from experiment in the linear-binding region. As a result, the TZM is shown to provide improved predictions of product breakthrough, including elution behavior from a bacterial lysate feed.

Keywords: Protein purification, Affinity chromatography, Fusion tag, Cellulose binding module, Pore diffusion model, Confocal laser scanning microscopy

1 Introduction

Due to its exquisite binding selectivity, affinity chromatography is finding increasingly widespread use in the purification of natural and recombinant protein products at the manufacturing scale [1]. The large-scale capture and affinity purification of monoclonal antibodies on immobilized protein A columns is the most widely used and thoroughly studied application of industrial affinity chromatography [2], but many other important applications exist, including the purification of human tissue plasminogen from blood plasma using immobilized lysine [3] and the purification of ATP-dependent kinases and NAD⁺-dependent dehydrogenases using immobilized 5'-AMP [4].

The power of affinity separations can be extended to proteins with no known binding partner through recombinant DNA technology, which enables production of a target protein as a recombinant fusion to an N- or C-terminal affinity tag possessing a highly specific binding partner that can be immobilized to form a stable affinity chromatography media. A number of affinity tag technologies are commercially available, including the glutathione S-transferase (GST) tag [5, 6], the calmodulin binding peptide tag [7–9], the streptavidin tag [10, 11], the FLAG peptide tag [12, 13] and the polyhistidine tag, which permits selective capture and purification of the fusion protein on an immobilized metal affinity chromatography column [13–15].

Intraparticle mass transport, most notably the rate of diffusion within the pore liquid of the stationary phase, typically limits protein uptake and controls band broadening in adsorptive modes of protein chromatography, including affinity chromatography, where the binding interaction with the stationary phase is strong [16, 17]. A number of models have therefore been developed to describe intraparticle mass transport inside sorbent particles, with the pore diffusion model (PDM) finding the most widespread use (e.g. [18]). The PDM assumes that the overall rate of protein uptake is proportional to the concentration gradient in the pore liquid, permitting simplification of the general rate model of chromatography by eliminating concentration gradients in the hydrodynamic film surrounding each sorbent particle and by establishing local equilibrium of the sorbate at each radial position within the sorbent particle. Assuming for the moment that surface diffusion effects are negligible, the rate of protein uptake within the porous sorbent particle is given by the PDM through the relation

$$\epsilon \frac{dc_i}{dt} = \frac{1}{r^2} \frac{d}{dr} \left(\epsilon_p D_p r^2 \frac{dc_i}{dt} \right) - \frac{dq_i}{dt} \quad (1)$$

where when sorbate equilibrium is described by the Langmuir isotherm,

$$\frac{dq_i}{dt} = \frac{dq_i}{dc_i} \frac{dc_i}{dt} = \frac{q_i^{sat} K_{ai}}{(1 + K_{ai}c_i)^2} \frac{dc_i}{dt} \quad (2)$$

Thus knowledge of the stationary phase porosity ϵ_p , the saturation capacity of the sorbent q_{sat} (kg m³), and the Langmuir equilibrium binding constant K_{ai} (M⁻¹), permits estimation of solute c_i and sorbate q_i concentration profiles within the stationary phase as a function of time. Mass transfer within an interstitial volume element of the column is given by the column continuity equation

$$\frac{dC_i}{dt} = D_L \frac{d^2 C_i}{dz^2} - u_0 \frac{dC_i}{dz} - \frac{(1 - \epsilon)}{\epsilon} \frac{d\bar{s}_i}{dt} \quad (3)$$

where C_i is the concentration of protein i in the interstitial mobile-phase liquid, ϵ is the interstitial void fraction of the column, D_L is the axial dispersion coefficient ($\text{m}^2 \text{s}^{-1}$), u_0 is the interstitial velocity of the mobile phase (m s^{-1}), z is the axial positional vector, and \bar{s}_i is the average protein concentration within the stationary phase particles of uniform radius r_p , given by

$$\bar{s}_i = \frac{3}{r_p^3} \int_0^{r_p} (\epsilon_p c_i + q_i) r^2 dr = \frac{3}{r_p^3} \int_0^{r_p} s_i(r, t) r^2 dr \quad (4)$$

The boundary conditions for solving Eq. (1) of the PDM are given by

$$c_i(r = r_p, t) = C_i \quad (5)$$

$$\frac{dc_i(r = 0, t)}{dr} = 0 \quad (6)$$

where C_i is given by solution of Eq. (3) at time t . The boundary condition at $r = 0$ given by Eq. (6) is generally applied in all continuous models of chromatography. However, the full implications of its use are not always appreciated. In particular, since c_i and q_i are both specified by Eq. (1) to be continuous functions of r and t , the application of Eq. (6) necessarily leads to a physically improbable model prediction that both $c_i(r=0, t)$ and $q_i(r = 0, t)$ become nonzero immediately upon contact of the stationary phase particle with the mobile phase liquid, where $c_i(r_p, t = 0) = C_i^0$. Eq. (6) has nevertheless been extensively applied to the modeling of many different forms of adsorptive chromatography [19–21], including various forms of affinity chromatography [16, 22–26].

A more general and physically realistic model for protein uptake within a porous stationary phase would predict for sufficiently short contact times a region within the interior of the sorbent particle that contains no protein, while both c_i and q_i would be nonzero and increase with r in the outer shell of the particle. The protein-containing zone would then be predicted to increase with time at the expense of the protein-free zone. This two-zone behavior has been observed in confocal laser scanning microscopy (CLSM) studies of protein uptake in porous chromatography particles, particularly when there is strong interaction between the sorbate and the sorbent, as is typically observed in the affinity chromatography systems [27–30]. It is reminiscent of the classic shrinking-core model of diffusion controlled chemical reaction engineering first proposed by Weisz and Goodwin [31]. However, that model assumes that local sorbate equilibrium is defined by the rectangular isotherm and thereby predicts an infinitely steep concentration gradient at the core radius r_c separating the protein-free inner core from the sorbent-saturated outer shell of the porous particle [32].

Here we describe a generalized two-zone model for protein uptake in a porous sorbent particle that relaxes the rectangular isotherm approximation of the traditional shrinking-core model to allow for simultaneous intraparticle mass transport and sorbent loading within the outer zone of the porous particle and thus, the presence of concentration gradients within the shell region. The model is applied to the description of elution band profiles for fusion proteins tagged at their N-terminus with TmXyn10ACBM9-2 (henceforth referred to as CBM9), the C-terminal family 9 carbohydrate-binding module of xylanase 10A from *Thermotoga maritima* [33]. In a previous paper [34], we introduced the CBM9 affinity tag and demonstrated its application in the affinity purification of

recombinant proteins from *E. coli* using an inexpensive, commercially available cellulosic resin, PerlozaTM MT100. CBM9 binds specifically and tightly to the reducing ends of both insoluble cellulose and simple soluble sugars, including glucose [35]. These unique binding properties allow for selective binding of CBM9-tagged fusion proteins to a porous cellulose sorbent particle and quantitative elution using 1M glucose. PerlozaTM MT100, a highly porous, beaded cellulosic resin sells for ca. \$35 per liter of resin. The extraordinary low cost of this matrix, combined with its high static binding capacity for CBM9-tagged fusion proteins (10 $\mu\text{mol g}^{-1}$ dry resin), offer considerable economic advantages over other commercially available affinity tag technologies. In this work, we fuse CBM9 to the N-terminus of the green fluorescent protein (GFP) from the jellyfish *Aequorea victoria* [35, 36], and use the natural fluorescence of GFP as a direct and convenient means to track our fusion protein and validate our model. CLSM is used to measure temporally and radially resolved CBM9-GFP concentration profiles inside the PerlozaTM MT100 sorbent particle, permitting tracking of radial and intraparticle mass transport of protein in the outer zone of the particle. Because GFP of CBM9-GFP fluoresces naturally, uptake artifacts associated with competition between unlabelled and chemically labelled protein are eliminated, greatly simplifying data analysis [37, 38].

2 A proposed generalized two-zone model of affinity chromatography

As with the PDM, the derivation of our generalized two-zone model (TZM) of adsorptive chromatography is based on the condition that both protein adsorption kinetics and protein transport through the hydrodynamic fluid film surrounding the porous particle are rapid compared to solute diffusion processes within the spherical particles of uniform radius r_p and porosity ϵ_p . We may therefore apply the well-known parallel pore diffusion model for spherical sorbent particles [39], given by

$$\frac{ds_i}{dt} = \frac{1}{r^2} \frac{d}{dr} \left[r^2 (\epsilon_p D_p \frac{dc_i}{dr} + D_s \frac{dq_i}{dr}) \right] \quad (7)$$

where D_s is the surface diffusivity of the sorbate and the driving force for diffusion in the adsorbed phase is assumed to be given by the sorbate concentration gradient. Surface diffusion is ignored in most chromatography model developments as D_s is generally thought to be at least two orders of magnitude smaller than D_p . It will not be explicitly accounted for in this study either as independent measurement of D_s was not possible. However, we note that in high capacity chromatography media loaded in the nonlinear region, the surface concentration gradient may be higher than the solute concentration gradient within the pore liquid, thereby resulting in a sorbate flux contribution to intraparticle protein transport despite the significantly lower value of D_s . Extension of the model described here to that situation is straightforward.

The parallel flux term in Eq. (7) has therefore been simplified to

$$\frac{ds_i}{dt} = \frac{1}{r^2} \frac{d}{dr} \left[r^2 \epsilon_p D_p \frac{dc_i}{dr} \right] \quad (8)$$

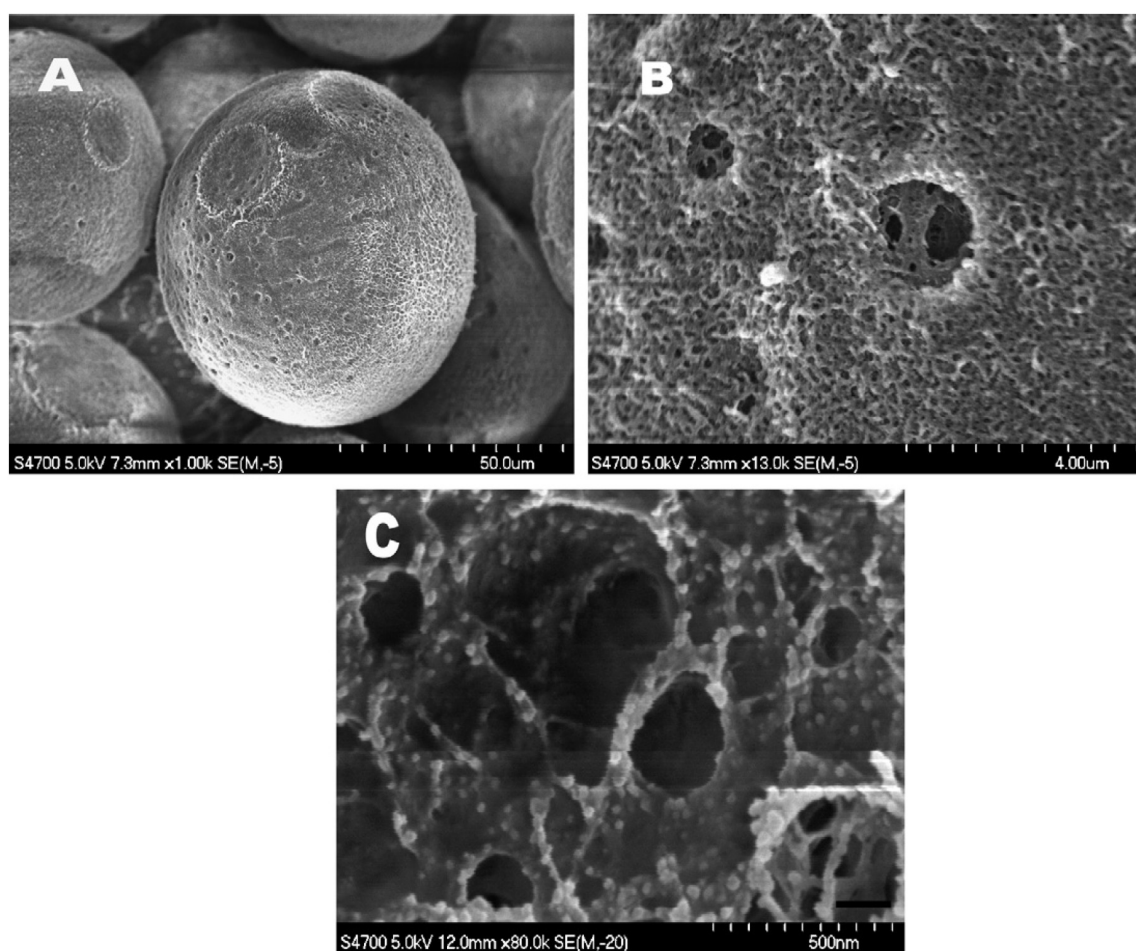


Figure 1: Scanning electron micrographs of PerlozaTM MT100 beaded media. (A)(C) show an MT100 particle at 1.0 k, 13.0 k and 80.0 k magnification, respectively. The pore structure shown at the center of (B) is further magnified and shown in (C).

As shown in Fig. 1, the TZM divides the porous sorbent particle into two zones that meet at r_c , the core radius, which decreases as a function of time due to intraparticle mass transport of the protein. Protein uptake in the outer shell extending from r_c to r_p is defined by Eq. (8) and the adsorption isotherm model selected. The inner core from $r = 0$ to r_c contains no protein. Thus, an inner boundary condition of $c_i = 0$ at $r = r_c$ may be used to solve Eq. (8) to determine protein $c_i(r, t)$ and sorbate $q_i(r, t)$ concentration profiles in the outer shell provided the value of $r_c(t)$ is known. An estimate of $r_c(t)$ can be obtained by numerical iteration. To illustrate the strategy used, which is based on an iterative solution scheme developed by Pritzker [40], we consider the simple case where C_i remains equal to C_i^0 at all times.

The rate of sorbate uptake into the porous particle equals the flux of sorbate across the external surface of the particle

$$\frac{4}{3}\pi r_p^3 \frac{d\bar{s}_i}{dt} = 4\pi r_p^2 \left(\epsilon_p D_p \frac{dc_i}{dr} \Big|_{r=r_p} \right) \quad (9)$$

The right-hand side of this equation may be evaluated by applying the steady-state approximation (i.e., $d\bar{s}_i/dt = 0$) to Eq. (8) to permit its analytical integration within the outer zone. Since $r = r_c(t)$ marks the position of the advancing front of the adsorbate, it requires that $c_i(r_c, t) = 0$, which automatically sets $q_i(r, t) = 0$. The boundary conditions at $r = r_0$ remains the same as in the homogeneous model, giving

$$c_i(r, t) = C_i^0 \left(\frac{1/r_c - 1/r}{1/r_c - 1/r_p} \right) \quad (10)$$

and then differentiating with respect to r and evaluating the result at $r = r_p$ to give

$$\frac{d\bar{s}_i}{dt} = \frac{3}{r_p^3} C_i^0 \frac{1}{1/r_c(t) - 1/r_p} \quad (11)$$

For a given time t , an assumed value of r_c therefore allows estimation of $\bar{s}_i(t)$ based on the initial condition $\bar{s}_i(t = 0) = 0$. The value of $\bar{s}_i(t)$ for an assumed value of $r_c(t)$ may also be determined from Eq. (4), which upon insertion of Eq. (10) may be written as

$$\bar{s}_i = \frac{3}{r_p^3} \int_0^{r_p} \left[\epsilon_p C_i^0 \frac{1/r_c - 1/r}{1/r_c - 1/r_p} + q_i(r, t) \right] r^2 dr \quad (12)$$

Solution of Eq. (12) requires knowledge of $q_i(r, t)$, which may be determined for the assumed value of $r_c(t)$ through insertion of Eq. (10) into the chosen adsorption isotherm relation. If the adsorption process follows the one-component Langmuir adsorption isotherm, we obtain

$$q_i(r, t) = \frac{q_i^{sat} K_{ai} C_i^0 \frac{(1/r_c - 1/r)}{(1/r_c - 1/r_p)}}{\left[1 + K_{ai} C_i^0 \frac{1/r_c - 1/r}{1/r_c - 1/r_p} \right]} \quad (13)$$

A self-consistent estimate of $r_c(t)$ can therefore be obtained by using a NewtonRaphson algorithm to minimize the difference in the value of $\bar{s}_i(t)$ calculated from Eqs. (11) and (12). It is important to note that this estimate of $r_c(t)$ is not exact since we have

invoked the steady-state approximation to derive Eq. (10). However, as we will show, the estimated values of $r_c(t)$ are quantitatively consistent with CLSM data for CBM9-GFP uptake in the stationary-phase media, indicating that the steady-state approximation, though clearly inexact, is sufficiently reliable to permit accurate model predictions.

3 Two-zone model solution algorithm

The set of coupled transport Eqs. (3), (4) and (8) were solved numerically by a finite-difference iteration scheme written in FORTRAN 90. Initial and boundary conditions for the column continuity equation are:

$$\begin{aligned} C_i &= 0 & t &= 0, & 0 \leq z \leq L \\ C_i &= C_i^{feed} + \frac{D_L}{u_0} \frac{dC_i}{dz} & z &= 0 & \text{all } t > 0 \\ \frac{\delta C_i}{\delta z} &= 0 & z &= L & \text{all } t > 0 \end{aligned} \quad (14)$$

Time and space domains were discretized by a Crank-Nicolson scheme [41] to approximate differentials by a central difference in time and an average central difference in space. The column was meshed in the z dimension into N (at least 400) volume elements to match (or slightly exceed) the number of theoretical units (NTUs) within the column, and the number of radial volume elements within the stationary phase particle was set equal to 30. Finer meshing within the stationary phase increased computational time without a noticeable improvement in model accuracy. This discretization of the model equations yields a set of tridiagonal linear algebraic equations that were solved by the Thomas algorithm [42] and the application of a first-order upwind-corrected power-law scheme [43] to ensure diagonal dominant matrices. Time increments for solution of Eqs. (3) and (8) were set at $0.01 L/\text{Nu}$ and $0.002 L/\text{Nu}$, respectively, where L is the column length and u is the superficial velocity.

4 Materials and Methods

4.1 Chromatographic media and reagents

PerlozaTM MT100 was purchased from Iontosorb Inc. (Czech Republic). PerlozaTM MT100 is a porous, spherical media derived from regenerated cellulose. The particle diameter (d_p) distribution of PerlozaTM MT100 as well as the average d_p was determined by light scattering using a Malvern Mastersizer 2000 (Malvern Instruments, UK). The average particle volume was calculated assuming a spherical geometry from which the mean particle diameter of the sphere was obtained using MIE theory [44]. PerlozaTM MT100 has a particle diameter (d_p) distribution of 56 to 159 μm with a mean value of $84 \pm 0.6 \mu\text{m}$.

Sephadex G15 and Ni²⁺-Sepharose IMAC media were obtained from Sigma-Aldrich (Mississauga, ON, Canada) and Novagen (Milwaukee, MI), respectively.

4.2 Scanning electron micrographs

Scanning electron micrographs of PerlozaTM MT100 media and its associated pore structure were obtained using a Hitachi S-4700 Field Emission scanning electron microscope operating at an accelerating voltage of 5 kV with a working distance of 5 to 15 mm. Samples were prepared by loading a high-pressure freezing hat with approximately 3 μ L of concentrated PerlozaTM MT100 in nano-pure water. The hat was immersed for 5.7 s in subcooled liquid nitrogen (-210 °C), then fractured open by microtome cleavage. The exposed resin surface was mounted and then sputter coated with gold for 30 s to generate the appropriate phase contrast for imaging.

The cloning of CBM9 and CBM9-GFP is reported elsewhere [34]. CBM9 or CBM9-GFP was produced in a 60 L fermentation as follows. BL21 (DE3) cells containing the pET28-CBM9-GFP expression vector were grown at 37 °C in Luria broth (LB) to a cell density (OD₆₀₀ nm) between 1.0 and 2.0. Protein expression was induced with isopropyl-1-thio- β -D-galactoside (IPTG) to a final concentration of 0.1 mM and the cells allowed to incubate for a further 10.12 h at 30 °C. The cells pellet was resuspended in high salt buffer (1M NaCl, 50mM potassium phosphate, pH 7.0), ruptured by two passages through a French pressure cell (21,000 lb in⁻²), and the cell debris was removed by centrifugation (27,000 \times g) for 30 min at 4 °C. Highly pure CBM9 or CBM9-GFP was obtained by first passing the clarified cell extract over a Pharmacia XK-16 column (10 cm \times 1.6 cm i.d.) packed with the PerlozaTM MT100-based composite media. Contaminating proteins were removed by washing the column with 10 column volumes (CV) of high salt buffer, followed by 5 CV of low salt buffer (150 mM NaCl, 50 mM potassium phosphate, pH 7.0). CBM9 or CBM9-GFP was then eluted from the column with 2 CV of 1 M glucose in TBS8 (15 mM NaCl, 10 mM Tris-HCl, pH 8.0) and the eluent peak was injected into a column packed with Ni⁺²-Sepharose IMAC media and purified according to the manufacturer's instructions. The protein eluted from the IMAC column was buffer exchanged into low salt buffer, concentrated in a stirred ultrafiltration (UF) unit (Amicon, Beverly MA) and stored at 4 °C until use. The concentration of the purified protein was determined by UV absorbance (280 nm) using a calculated molar extinction coefficient of 43100 M⁻¹ cm⁻¹ (CBM9) or 62870 M⁻¹ cm⁻¹ (CBM9-GFP) [45].

4.3 Equilibrium binding isotherms

Equilibrium isotherms for binding of CBM9 and CBM9-GFP to PerlozaTM MT100 and to the PerlozaTM MT100/G15 composite media were measured at pH 7.0 and 4 °C. Purified protein at concentrations ranging from 1 to 30 μ M was mixed with stationary phase media (1 mg dry weight) in low salt buffer to a final volume of 1 ml. Samples were then incubated overnight under continuous end-over-end rotation. The media was removed by centrifugation (27,000 \times g) for 16 min. The supernatant was collected and the concentration of free protein was determined by UV absorbance (280 nm) using a Cary 100 Spectrophotometer (Varian).

The resulting isotherm was generated by plotting the concentration of bound protein (μ mol g⁻¹ dry resin), determined by total mass balance, against the concentration of free protein (mol L⁻¹). Binding parameters were then determined by nonlinear regression of the Langmuir adsorption isotherm equation to the experimental data using GraphPad Prism 3.0 software.

4.4 Confocal laser scanning microscopy

Time-course fluorescence intensity profiles for uptake of CBM9-GFP into PerlozaTM MT100 media packed into an optically transparent two-dimensional chromatography column were measured according to the procedures described in [46] using an inverted Zeiss LSM 510 confocal laser scanning microscope equipped with a water immersion 63×/NA1.2 C-Apochromat (Zeiss) objective and an argon laser. The GFP chromophore has an absorbance maximum at 475 nm. Excitation was conducted at 488 nm, on the red-shifted shoulder of the absorbance peak, to attenuate the resulting fluorescence emission at 505 nm to avoid saturation of the signal. The laser intensity was kept constant for all experiments. Slight adjustments (± 20 V) of the photomultiplier (PMT) detector gain were necessary to account for signal attenuation effects from neighboring particles in the packed bed. An 80/20 filter and no-band or long-pass filter before the PMT were used to improve signal-to-noise. The fluorescence intensity profile within the central particle was measured every second with 300500 frames in total. All profiles were stored as eight-bit single scans with a resolution of 512×512 pixels representing an area of 146.2×146.2 m. The chosen time interval allowed monitoring of the diffusion both into and out of the particle in one run. Bleaching of GFP was not observed. Before each individual run, the reflection mode of the microscope was used to verify that the focal plane went through the center of the particle. The image frame consisted of the particle of interest, other particles (focal plane not necessarily through particle center), and interstitial areas between the particles, from which the average bulk protein concentration was determined.

4.5 Characterization and application of PerlozaTM MT100/G15 composite media column

A Pharmacia Inc. (GE Healthcare) FPLC system with two P- 500 reciprocating pumps, an 8-port mixing and injection valve, a UV-MII flow spectrophotometer (monitoring absorbance at 280 nm), and a Frac-200 fraction collector was used to measure all chromatograms. Columns 710mL in volume (Pharmacia Inc. HR-10 column (1.0 cm i.d.)) were packed with either degassed PerlozaTM MT100 or a 50% PerlozaTM MT100 (by mass)/50% Sephadex G15 degassed slurry under a superficial velocity u of $4.25 \times 10^{-4} \text{ ms}^{-1}$ and then equilibrated with degassed loading buffer (50m M potassium phosphate, 150 mM NaCl, 0.02% NaN₃, pH 7.0) prior to use. In all columns used, the column length L to diameter d_c ratio (L/d_c) was maintained well above 2 to minimize end effects [47]. In addition, the volume of solute pulses used for moment analysis was kept well below 0.5% of the column void to minimize any precolumn solute dispersion effects [48]. Wall effects could be ignored since the column diameter to particle diameter ratio was much higher than 30 [49].

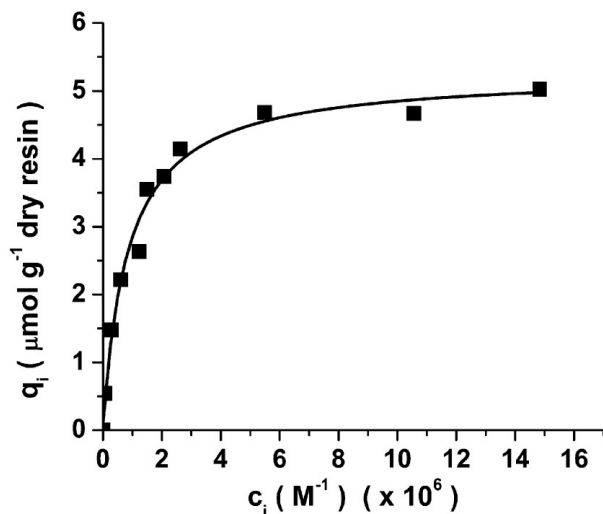


Figure 2: Equilibrium adsorption isotherm for batch binding of CBM9-GFP to PerlozaTM MT100/G15 composite media at 4 °C. The solvent consisted of 50 mM potassium phosphate, 150 mM NaCl, pH 7. The solid curve represents the best fit of the experimental data to the Langmuir isotherm equation.

5 Results and discussion

5.1 Geometric and sorption properties of PerlozaTM MT100/Sephadex G15 composite media

PerlozaTM MT100 is a highly porous, hydrophilic media derived from regenerated cellulose with its structural elements comprised of partially microcrystalline regions stabilized by interchain hydrogen bonds (Iontosorb, CZ). Scanning electron micrographs (SEM) of the spherical MT100 particles (Fig. 1A) show that this media offers a network of primarily submicron pores with a small percentage of larger pores up to 2 μm in nominal diameter (Fig. 1B and C). Simple hydrodynamic calculations proposed by Liapis [50] predict for the 80 μm particles and range of linear solvent velocities used in this work that intraparticle convective flow requires pores greater than ca. 45 μm in nominal diameter. Thus, diffusion is the primary solute transport process within this stationary phase media. Adsorption of CBM9 and CBM9-tagged fusion proteins to PerlozaTM MT100 has previously been shown to follow Langmuir-type adsorption behavior [34]. Efficient purification from clarified *E. coli* cell lysates of CBM9-tagged fusion proteins on analytical-scale MT100 columns (i.e. less than 5 ml in volume) has also been demonstrated [24]. Due to the compressible gel-like nature of the MT100 matrix, scale-up of a packed MT100 column to a volume above ca. 10 to 15 mL is compromised by stationary-phase compression effects that degrade column performance. Mechanical stabilization of the stationary phase is therefore required and can be achieved through addition of an inert support media, in this case Sephadex G15, that provides a rigid mechanical scaffold stabilizing the active stationary phase to allow stable columns to be prepared on the semi-preparative to preparative scale as will be documented in a technology scale-up paper to follow. Here, however, our focus is on validation of our proposed generalized two-zone model of adsorptive chromatography.

Equilibrium isotherms for pure CBM9-GFP binding to a 50/50 (by dry mass) compos-

3 PUBLICATIONS & MANUSCRIPTS

Table 1: Measured Langmuir isotherm parameters for binding of CBM9-GFP and each of its fusion partners to Perloza MT100, Sephadex G15, and the composite MT100/G15 media at 4 °C

Protein	Perloza MT100		MT100/G15 composite		Sephadex G15	
	$K_a \times 10^6$ (M^{-1})	q_i^{sat} ($\mu\text{mol/g}$)	$K_a \times 10^6$ (M^{-1})	q_i^{sat} ($\mu\text{mol/g}$)	$K_a \times 10^6$ (M^{-1})	q_i^{sat} ($\mu\text{mol/g}$)
CBM9-GFP	0.72 (± 0.07)	9.54 (± 0.22)	1.2 (± 0.15)	5.27 (± 0.18)	NB	NB
CBM9	1.1 (± 0.08)	11.2 (± 0.14)	0.85 (± 0.15)	5.67 (± 0.32)		
GFP	NB	NB				

The solvent consisted of 50 mM potassium phosphate, 150 mM NaCl, pH 7. NB indicates that no binding was observed.

ite media of MT100/G15 (Fig. 2), and regression of the Langmuir isotherm parameters (Table 1) to those data show that the addition of the G15 mechanical support does not affect the equilibrium association constant (K_a) for CBM9-GFP binding to MT100 but reduces the static capacity of the composite media (q_i^{sat}) to half its value when the stationary phase consists of pure PerlozaTM MT100. This is expected since q_i^{sat} is reported in terms of the total volume of the stationary phase, only half of which is MT100 in the composite media suitable for scale-up. Nevertheless, due to the extraordinarily high binding capacity of MT100 for CBM9 tagged fusion proteins (ca. 1112 $\mu\text{mol g}^{-1}$ dry resin), the MT100/G15 composite column is capable of binding 4570 mg of CBM9-GFP per column milliliter, making it highly competitive with popular commercial affinity chromatography media. Finally, control experiments confirm that the binding interaction is between CBM9 and cellulose (Table 1). Interactions between CBM9-GFP and Sephadex G15 and between untagged GFP and PerlozaTM MT100 are insignificant.

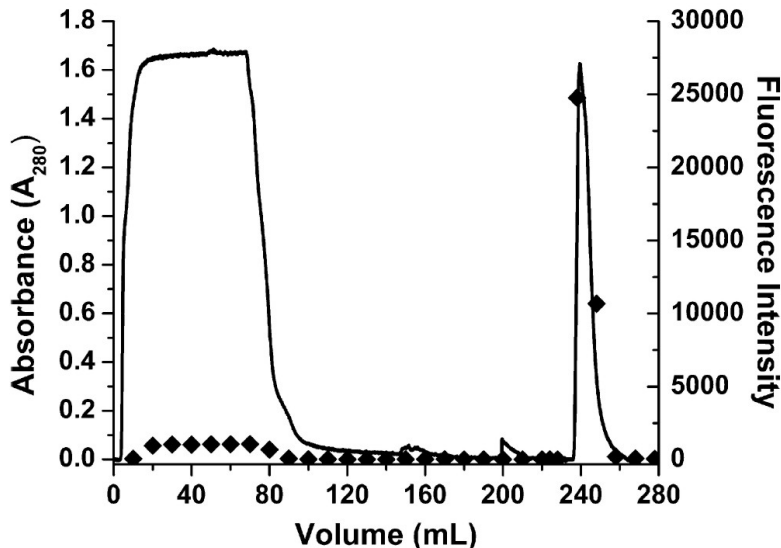


Figure 3: Chromatogram for CBM9-GFP purification on PerlozaTM MT100/G15 composite media. Clarified *E. coli* cell lysate containing CBM9-GFP was loaded at a superficial velocity of 4.25×10^{-3} cm s^{-1} onto a 10 mL column. Fractions were collected and analyzed both by absorbance at 280 nm (line) and by fluorescence intensity (solid diamond) as shown.

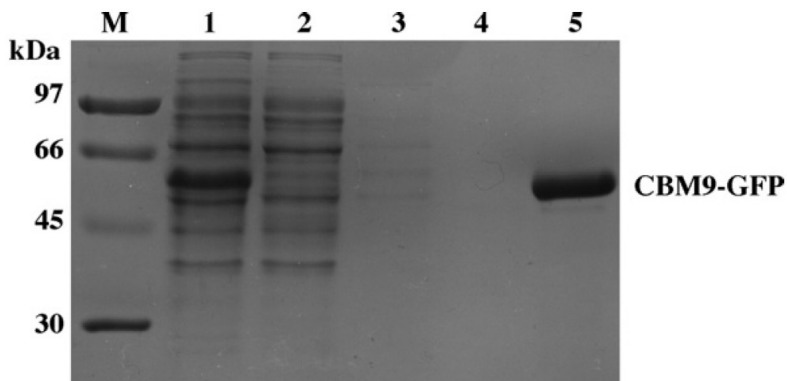


Figure 4: SDS-PAGE documentation of CBM9-GFP purification on a 10 mL PerlozaTM MT100/G15 column. All samples were dissolved in sample buffer containing 10% SDS. Lane M: molecular mass markers; Lane 1: clarified cell lysate prior to column loading; Lane 2: column flow through; Lane 3: high salt wash; Lane 4: low salt wash; Lane 5: CBM9-GFP eluted in low salt buffer containing 1M glucose.

5.2 Purification of CBM9-GFP on PerlozaTM MT100/G15 composite media column

The chromatogram and gel documentation for purification of CBM9-GFP from a clarified cell lysate are shown in Figs. 3 and 4, respectively. Eluent from the column was continuously monitored both for total protein using absorbance at 280 nm (A_{280}) and for CBM9-GFP using the intrinsic fluorescence of GFP (excitation at 395 nm and emission at 509 nm). Initial breakthrough of contaminating proteins was observed just after 1 column void volume. The small fluorescence peak observed within the contaminant breakthrough peak is due to the presence in the feed mixture of free GFP, released as a result of a small amount of degradation (no protease inhibitors were used during the purification) within the linker region connecting CBM9 to GFP [51]. Two wash steps were used to effectively remove most of the contaminating proteins present in the column. As evident by the overlapping A_{280} and fluorescent signals (Fig. 3), addition of 1 M glucose to the mobile phase elutes CBM9-GFP as a single sharp peak.

Table 2 compares the yield, purity and concentration factor for the affinity purification of CBM9-GFP on the MT100/G15 composite column relative to that achieved on the pure MT100 column [34]. The performance of the two columns is very similar at the relatively small column scales used in this study (10 mL composite column, 7 mL pure MT100 column).

5.3 Characterization of solute mass transfer within PerlozaTM MT100/G15 composite columns

Measured solute (CBM9-GFP) mass-transfer and column geometry parameters for our proposed generalized two-zone model for mass transport in a PerlozaTM MT100/G15 composite media column are listed in Table 3. Good column packing uniformity, defined according to the guidelines proposed by Bristow and Knox [52], is indicated both by a peak asymmetry factor (A_s) close to unity and a reduced plate height value (h) close to 3 for pulse injection of 100 μL at a superficial velocity of $2.1 \times 10^{-3} \text{ cm s}^{-1}$.

The column void fraction ϵ was determined by pulse injection of blue dextran (MW

3 PUBLICATIONS & MANUSCRIPTS

Table 2: Yield, purity and concentration factor for the affinity purification of CBM9-GFP on a MT100/G15 composite column and on a pure MT100 column

	MT100/G15 column	MT100 column
Purity*	>95%	>95%
Yield	85 ±3%	82 ±3%
Concentration factor (C_i/C_i^0)	29 ±2	31 ±2

Clarified *E. coli* cell lysate containing CBM9-GFP was loaded onto each column at a superficial velocity of $4.25 \times 10^{-3} \text{ cm s}^{-1}$. Fractions were collected and analyzed both by absorbance at 280 nm and by fluorescence intensity to obtain reported data. The total lysate volume loaded was 65mL and contained a CBM9- GFP concentration of $5.7 \mu\text{M}$.

* Determined from SDS-PAGE analysis.

(= 2,000,000 Da) as a function of the superficial velocity, u (ms^{-1}). Elution peaks for this large non binding solute were Gaussian or very nearly Gaussian in shape. Direct computation of the first moment (μ_1) of each elution peak and application of the theory of Haynes and Sarma [53]

$$\mu_1 = \frac{L}{u} [\epsilon + (-\epsilon) \epsilon_p] \quad (15)$$

yielded ϵ from the slope of a plot of μ_1 versus u^{-1} (Fig. 5) under the approximation that $\epsilon_p = 0$. The estimated value of ϵ is in close agreement with the value expected for a column packed

uniformly with spherical beads [48], as well as with an independent measure of ϵ obtained from application of the Blake, Kozeny and Carmen [54] equation

$$\Delta P = 36k \frac{u L \eta (1 - \epsilon)^2}{\epsilon d_p^2 \epsilon^3} \quad (16)$$

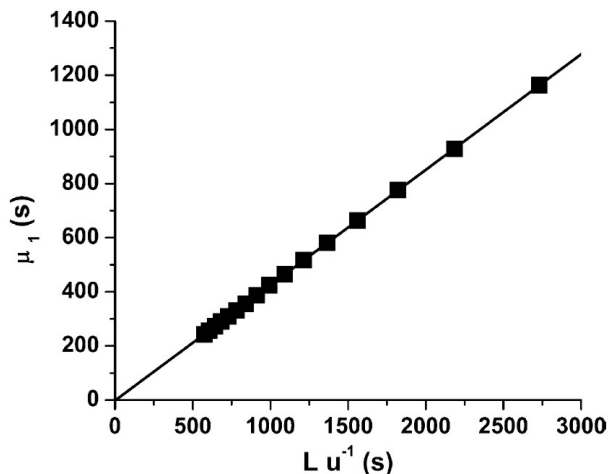


Figure 5: First moment (μ_1) analysis for a 10 mL column packed with PerlozaTM MT100/G15. Integrated μ_1 values are reported for pulse injections of a $50 \mu\text{L}$ solution of blue dextran (MW 2000 kDa) over the interstitial velocity range 4.25×10.3 to $2.02 \times 10.2 \text{ cm s}^{-1}$. The mobile phase consisted of 50 mM phosphate buffer, 150 mM NaCl (pH 7, 4 °C).

Table 3: Measured mass-transfer and column-geometry parameters for CBM9-GFP transport in a PerlozaTM MT100/G15 composite media column

Column property	Value	Units
L	7.9-11.4	cm
d_c	1.0	cm
$\langle d_p \rangle$	83.7 ± 0.6	μm
ρ_p	1.33 ± 0.73	kg m^{-3}
ϵ	0.425 ± 0.015	
ϵ_p	0.65 ± 0.03	
h (reduced plate height)	2.9 ± 0.3	
A_s (peak symmetry factor)	1.20 ± 0.03	
D_L	3.0 ± 10^{-5}	$\text{m}^2 \text{s}^{-1}$
k_f	8.45 ± 10^{-6}	m s^{-1}
D_M	1.54 ± 10^{-11}	$\text{m}^2 \text{s}^{-1}$
D_p	7.17 ± 10^{-12}	$\text{m}^2 \text{s}^{-1}$
Pe	500 - 2000	
Bi	16.4	
Da	≥ 100	

for pressure drop data across the column measured as a function of u , where η is the fluid viscosity ($\text{g m}^{-1} \text{s}^{-1}$). For spherical packing, the aspect factor k is assumed equal to 5 [55].

Nonbinding protein-based probes were used to determine the effective porosity ϵ_p of the MT100/G15 composite media as a function of protein molecular mass (Fig. 6). Each data point in the figure was determined by measuring μ_1 as a function of u for the respective marker and application of Eq. (15) using the measured void fraction of 0.425. Interpolation between measured ϵ_p data was facilitated by fitting to an exponential decay type equation of the form:

$$\epsilon_p = \alpha e^{-M/\gamma} - \delta \quad (17)$$

where α , δ and γ are fitted parameters and M is the protein molecular weight (kg mol^{-1}). The solid curve in Fig. 6 represents the best fit, for which $\alpha = 0.815$, $\delta = 0.033$ and $\gamma = 207.8$.

Numerical determination of the second moment (σ^2) of the elution peak as a function of the interstitial velocity, u_0 was combined with the Laplace transform results of Haynes and Sarma [53] for operation within the linear region of the adsorption isotherm

$$\frac{u_0 \sigma^2 L}{2\mu_1^2} = D_L + u_0^2 \frac{1}{K_M} \left(\frac{\epsilon}{1-\epsilon} \right) \left[1 + \frac{\epsilon}{(1-\epsilon)\epsilon_p} \right]^{-2} \quad (18)$$

to obtain values for the parameters characterizing mass transfer of the CBM9-GFP fusion protein within the PerlozaTM MT100/G15 composite media column. In Eq. (18), which has been used in many similar parameter estimation studies (e.g. [56–58]), K_M is the overall solute mass transfer coefficient, given by

$$\frac{1}{K_M} = R_M = \frac{r_p}{3k_f} + \frac{r_p^2}{15\epsilon_p D_p} + \frac{1}{k_a ds} \left(1 + \frac{\epsilon_p}{(1-\epsilon_p)K_{ai}} \right)^{-2} \quad (19)$$

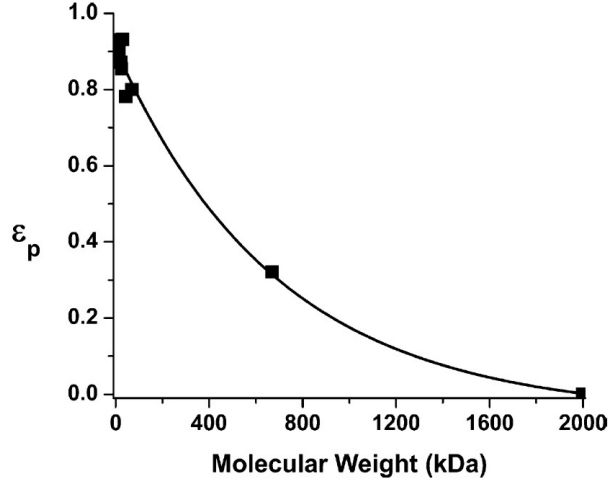


Figure 6: Measured average porosity ϵ_p of composite media as a function of molecular weight of standard proteins. Pulse injections of standard molecular weight protein markers were used over the interstitial velocity range 2.1×10^{-3} to 8.5×10^{-3} cm s $^{-1}$. The porosity was determined from Eq. (15) using the measured void fraction of 0.425.

where R_M is the overall resistance to solute mass transfer, k_f is the film mass-transfer coefficient (m s $^{-2}$) and k_{ads} is the sorption rate constant (M $^{-1}$ s $^{-1}$). Eqs. (18) and (19) can be applied under both binding and non binding conditions to estimate the axial dispersion coefficient (D_L) (m 2 s $^{-1}$) and the overall mass transfer coefficient (K_M) from the y-intercept and slope, respectively, of a plot of $u_0 \sigma^2 L / (2\mu_1^2)$ versus u_0^2 . Results for CBM9-GFP under non binding conditions (i.e., in the presence of 2 M glucose) are shown in Fig. 7, from which the parameters in Table 3 were determined following estimation of the film mass transfer coefficient using the correlation of Wilson and Greankoplis [59]

$$Sh = \frac{2r_p k_f}{D_M} = \left(\frac{1.09}{\epsilon} \right) Re^{1/3} Sc^{1/3} \quad (20)$$

for solute mass transfer in a packed bed of porous, spherical particles at conditions where $0.0016 < Re < 55$ and $165 < Sc < 70600$. The correlation of Young et al. [60] was used to estimate the bulk molecular diffusivity D_M (m 2 s $^{-1}$) of CBM9-GFP

$$D_M = 0 \frac{8.34 \times 10^{-8} T}{\eta M^{1/3}} \quad (21)$$

where T is the temperature (K) and M is the molecular mass of the solute in units of g mol $^{-1}$. The estimate of k_f using this approach is in close agreement (within 10% of) with that estimated using either the correlation of Wakao et al. [61] or of Goto et al. [62]. First and second moments analysis of the first derivative of breakthrough curve data for frontal loading of pure CBM9-GFP under binding conditions indicates that the last term on the right hand side of Eq. (19) makes less than a 1% contribution to R_M . This indicates that $k_{ads} < 0.33$ m 3 mol $^{-1}$ s $^{-1}$, which is consistent with the value of k_{ads} determined by Jervis et al. [63]

for the binding of the family 2a carbohydrate binding module (CBM2a) to the surface of crystalline cellulose. The measured mass-transfer and adsorption-kinetics parameters allow calculation of the column Peclet ($Pe = 2r_p u_0 / D_p$), Biot ($Bi = k_f r_p / 3D_p$) and the

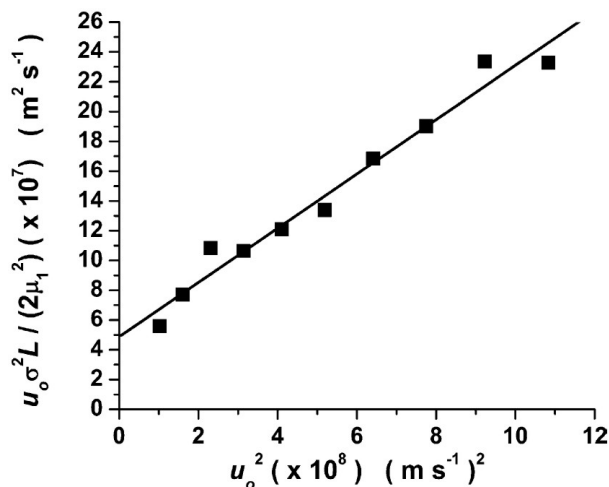


Figure 7: Determination of axial dispersion coefficient D_L and overall solute mass transfer coefficient K_M for injection of CBM-GFP under non binding conditions onto a 10 mL column packed with PerlozaTM MT100/G15. Pulse injections of a 50 μL solution of CBM9-GFP was used over the interstitial velocity range 4.25×10.3 to 1.38×10.2 cm s^{-1} . The mobile phase consisted of 50 mM potassium phosphate, 150 mM NaCl (pH 7, 4 $^\circ\text{C}$) with 2 M glucose added to achieve non binding conditions.

Damkoehler ($Da = k_{ads}r_p^2/D_p$) numbers (Table 3), which together indicate that pore diffusion limits CBM9-GFP mass transport within the composite media column. As a result, the local equilibria approximation can be invoked for the column loading process, with elution band profiles and the rate of solute uptake within the stationary phase best described by an appropriately formulated pore diffusion model of chromatography. As noted previously, relatively slow rates of intraparticle diffusion often limit affinity chromatography processes as well as other forms of adsorptive chromatography [58, 64], particularly under conditions where the concentration of solute in the feed is significantly greater than $1/K_a$ [65], as was the case in our experiments. The CBM9-GFP affinity capture process therefore provides a suitable system for investigating the advantages of treating intraparticle solute uptake in pore-diffusion-limited adsorptive chromatography processes using the proposed generalized two-zone model of affinity chromatography relative to using the traditional PDM for spherical sorbent particles encoded in Eqs. (1)-(6).

5.4 CLSM-Derived rates of CBM9-GFP uptake

Time-course fluorescence-intensity profiles (Fig. 8) for batch uptake of CBM9-GFP into a PerlozaTM MT100 particle show a two-zone behavior characterized by a region within the interior of the sorbent particle containing no protein, and a second region in which s_i is nonzero and increases with r . In this experiment, the interstitial volume of the 100 μL viewing chamber was rapidly flooded with CBM9-GFP feed solution to an initial concentration of 5.4 μM to permit fluorescence intensities both within the central particle and within the surrounding

interstitial volume to be monitored as a function of time. Fluorescence intensities in the outer protein-containing shell of the stationary phase particle do not exhibit the square-wave characteristics predicted by the traditional shrinking-core model, where adsorption equilibrium is described by the rectangular isotherm. Instead, finite concen-

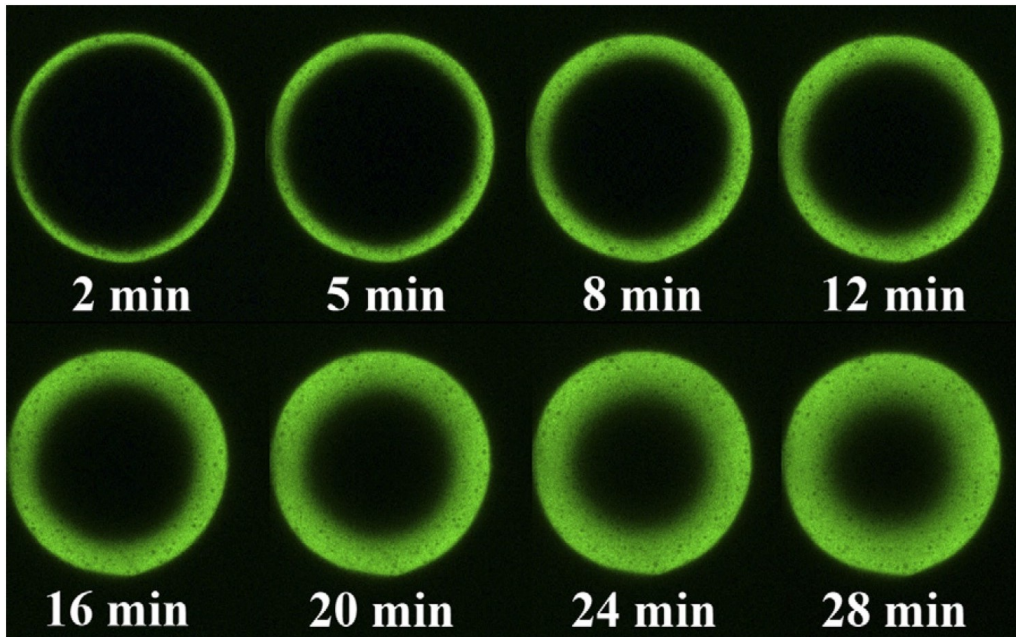


Figure 8: Time course fluorescent intensity profile of CBM9-GFP uptake into PerlozaTM MT100 particle. Protein uptake monitored by an inverted Zeiss LSM 510 confocal laser scanning microscope with the center of the particle used as the focal plane. Excitation and emission wavelengths were 488 and 505 nm, respectively. The initial CBM9-GFP concentration C_i^0 outside the particle was $5.4 \mu\text{M}$.

tration gradients within the shell region are observed, whose description is better described through use of a more realistic equilibrium relationship such as the Langmuirtype isotherm used in the traditional PDM and the two-zone model proposed here.

Time-dependent radial profiles of CBM9-GFP uptake within a PerlozaTM MT100 particle predicted by the PDM (Fig. 9A) and by the new TZM (Fig. 9B) are compared with normalized fluorescence intensities measured by CLSM for an interstitial feed concentration (C_i^0) of $5.4 \mu\text{M}$. This feed concentration represents conditions within the linear portion of the adsorption isotherm, and both models accurately capture initial rates and profiles of CBM9-GFP uptake under this moderate loading condition. Divergence of the traditional PDM from the measured solute uptake profiles is observed after ca. 1018 min of exposure, with that model predicting a faster rate of protein uptake due to an unrealistically rapid accumulation of solute near the center to the stationary phase particle error created by the continuous nature of the model that requires both $c_i(r=0, t)$ and $q_i(r=0, t)$ to become nonzero immediately upon contact of the stationary phase particle with the mobile phase liquid. By eliminating this approximation and incorporating a realistic isotherm model (relative to the traditional shrinking core model), the TZM accurately predicts the experimentally observed rates and profiles of solute uptake within the PerlozaTM MT100 particle throughout the loading process. This includes model predictions of $r_c(t)$, which agree with CLSM estimated values to within experimental error (Fig. 10).

Errors in rates of CBM9-GFP uptake predicted by the PDM decrease with increasing protein load in the feed. When C_i^0 is increased to $49 \mu\text{M}$, adsorption equilibrium lies in the nonlinear region of the isotherm, resulting in a more rapid penetration of solute into the sorbent particle and improved agreement of PDM predictions with both experiment

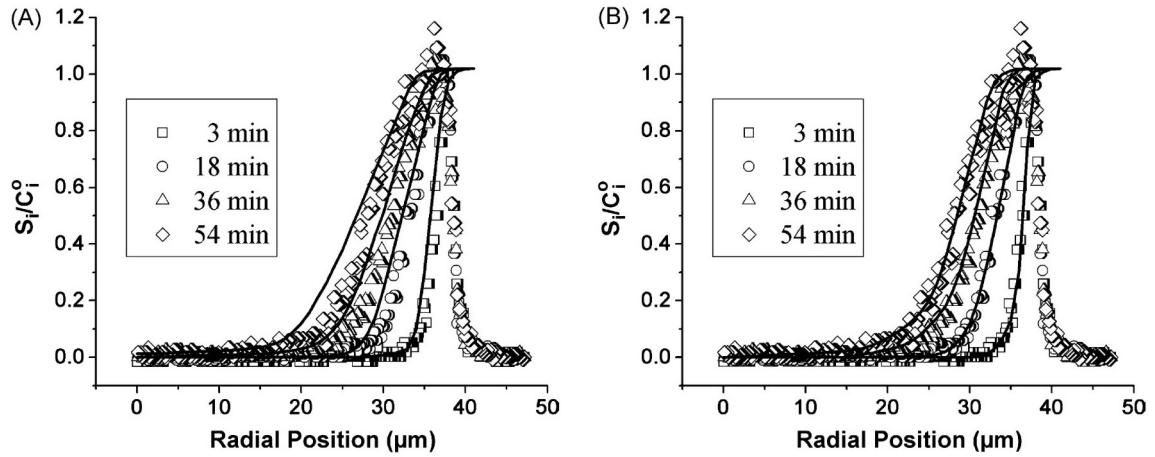


Figure 9: Time dependent radial profiles of CBM9-GFP uptake into a PerlozaTM MT100 particle for a feed concentration of 5.4 μM . Predicted uptake rates using (A) pore-diffusion model and (B) two-zone model are compared with experiment. The rapid drop in fluorescence intensity at radial positions above ca. 39 μm indicates the position of the outer radius of the bead.

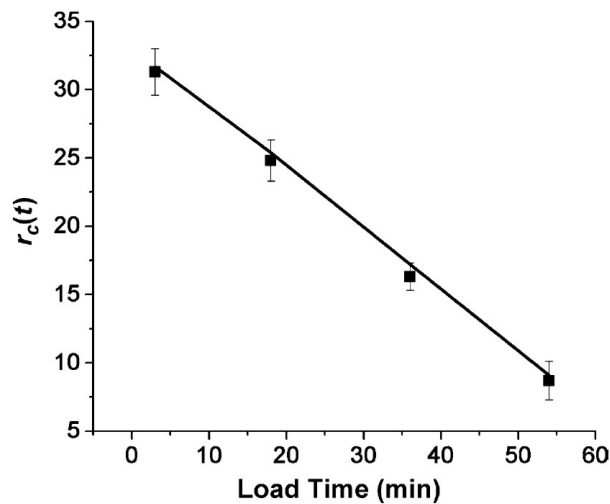


Figure 10: Comparison of TZM model predictions of $r_c(t)$ with values computed from CLSM data. CLSM determined core radius reported as the radius at which the measured fluorescence intensity falls below $3\times$ the standard deviation of the background fluorescence. Load conditions same as stated in Fig. 9.

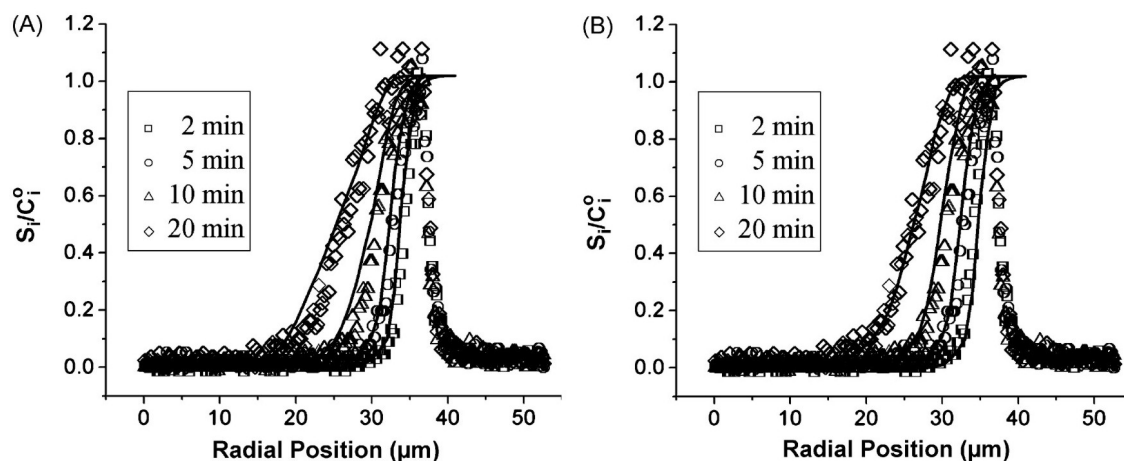


Figure 11: Time dependent radial profiles of CBM9-GFP uptake into a PerlozaTM MT100 particle for a feed concentration of 49 μM . Predicted uptake rates using (A) pore-diffusion model and (B) two-zone model are compared with experiment.

and TZM predictions (Fig. 11). Indeed, under nonlinear or overload conditions, model predictions are more sensitive to the choice of isotherm model than to improvements provided by the TZM.

5.5 Simulation of breakthrough curves

Fig. 12A and B compare model predictions to normalized breakthrough curve data for the cases where binding equilibrium is within the linear and non-linear regions of the isotherm, respectively. Under linear binding conditions, the TZM agrees with experiment while the traditional PDM over-predicts the dynamic capacity of the column, resulting in a significant delay in the predicted onset of breakthrough. Both models provide a reliable prediction of breakthrough behavior when the concentration of CBM9-GFP in the feed is increased to nonlinear loading conditions due to the more rapid rate of protein uptake in the stationary phase. Model agreement, however, is not exact. The experimental breakthrough curve is slightly asymmetric, such that the leading edge of the breakthrough transition is a bit sharper than the approach to saturation. This slight asymmetry, present in the other breakthrough curves measured at low linear velocities, could be due to a number of factors not fully captured in either of the two models, including non-uniform mixing in some regions of the bed, non-specific adsorption, or conformational changes in the adsorbed protein [66].

TZM predictions are compared in Fig. 13 to raw breakthrough data to show that the model captures changes in elution band profiles and dynamic capacity over a wide range of feed concentrations. The TZM also predicts the dependence of the elution band profile on u (Fig. 14) and thus the expected changes in solute dispersion and dynamic capacity [67, 68].

Figs. 12-14 present breakthrough data for a binary buffer solution containing pure CBM9-GFP. We have previously shown that our custom expression vectors for expression of CBM9- tagged fusion proteins direct high-level production of the chimeric protein, typically yielding concentrations of soluble product between 0.4 to 5 g L^{-1} [34]. This high

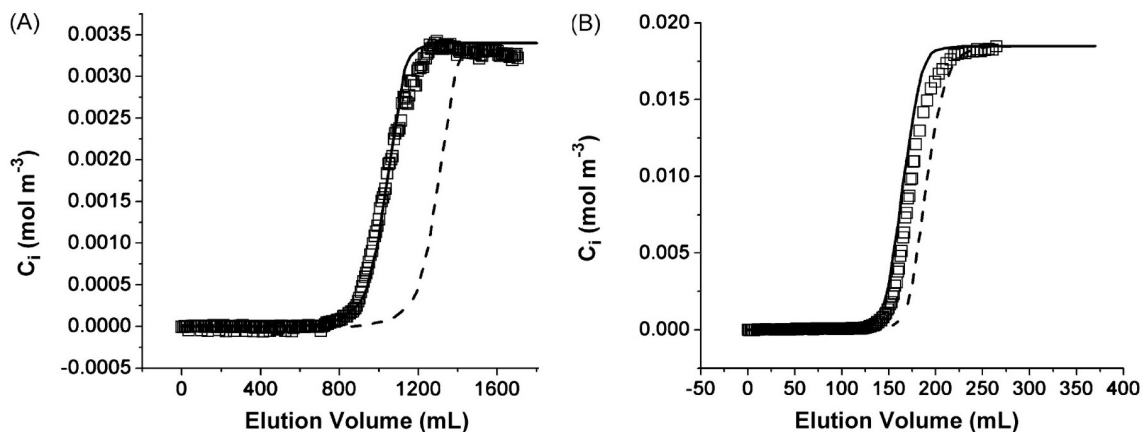


Figure 12: Comparison of TQM (solid curve) and PDM (dashed curve) predictions with experimental (points) breakthrough curves. Pure CBM9-GFP loaded at a superficial velocity of $8.5 \times 10^{-3} \text{ cm s}^{-1}$ onto a PerlozaTM MT100/G15 composite media column: (A) frontal load of $3.4 \times 10^{-3} \text{ mol m}^{-3}$ CBM9-GFP and (B) frontal load of $1.85 \times 10^{-2} \text{ mol m}^{-3}$ CBM9-GFP.

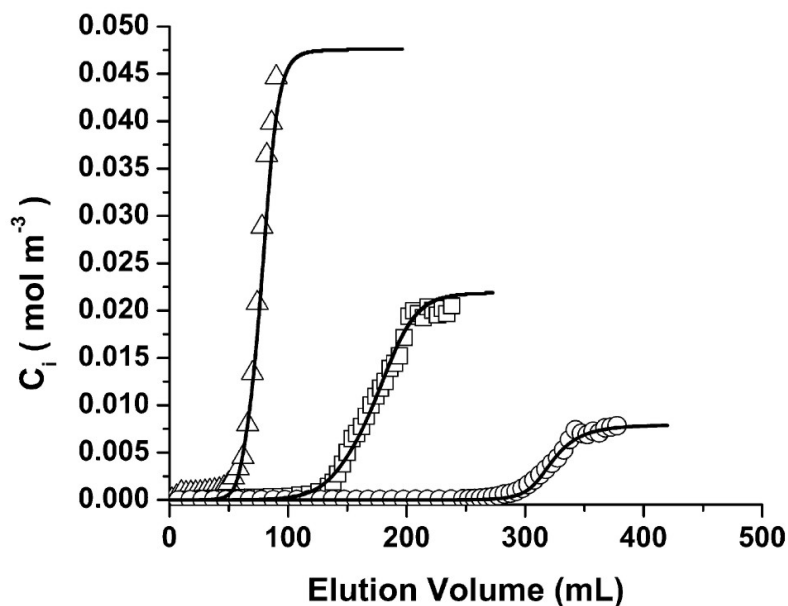


Figure 13: TQM predicted (line) and experimental (points) breakthrough curves for pure CBM9-GFP loaded onto a PerlozaTM MT100/G15 composite media column at three different feed concentrations: $C_i^0 = 4.77 \times 10^{-2} \text{ mol m}^{-3}$ (triangles), $2.2 \times 10^{-2} \text{ mol m}^{-3}$ (squares), and $8.0 \times 10^{-3} \text{ mol m}^{-3}$ (circles). Mobile phase loaded at a flow rate of 0.4 mL min^{-1} .

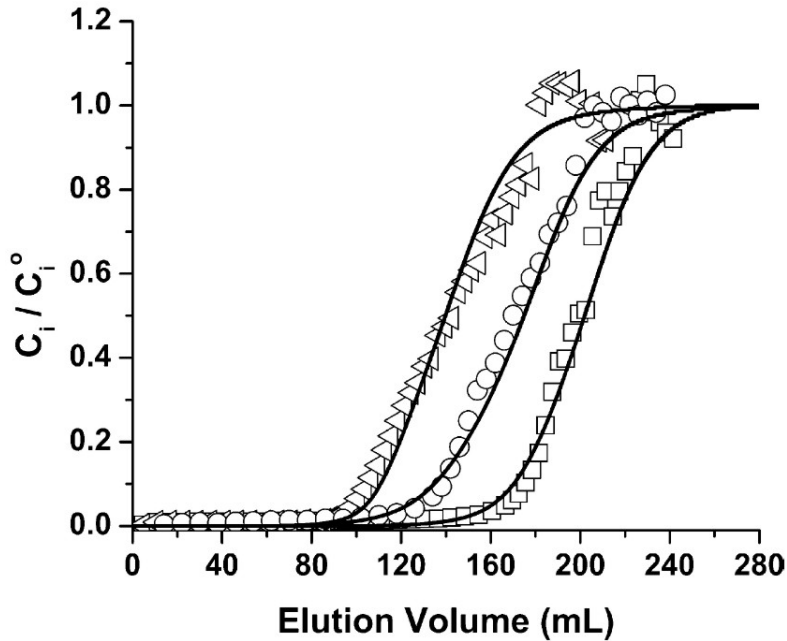


Figure 14: TZM predicted (line) and experimental (points) breakthrough curves as a function of interstitial velocity. Pure CBM9-GFP loaded onto a PerlozaTM MT100/G15 composite media column: $u = 1.7 \times 10^{-2} \text{ cm s}^{-1}$ (triangles), $8.5 \times 10^{-3} \text{ cm s}^{-1}$ (circles), and $4.2 \times 10^{-3} \text{ cm s}^{-1}$ (squares).

level expression is exemplified in Fig. 4, where soluble CBM9-GFP comprises approximately half of the total protein within the clarified cell extract. Nonbinding contaminant effects on mass transport and affinity binding of the target protein are therefore likely to be relatively minor, suggesting that TZM predictions using the one component Langmuir isotherm and pure-component transport parameters (Table 3) may be sufficient to predict product elution bands for a clarified cell extract feed containing CBM9-GFP.

Fig. 15 compares predictions of this simplified TZM to breakthrough data for frontal loading of a clarified cell extract containing $25 \pm 0.7 \mu\text{M}$ CBM9-GFP onto a 7.5 ml PerlozaTM MT100/G15 composite column at a superficial velocity of $8.5 \times 10^{-3} \text{ cm s}^{-1}$. The breakthrough of CBM9-GFP was continuously monitored using the intrinsic fluorescence of GFP (excitation at 395 nm, emission at 510 nm). The results confirm that our pseudo-binary solution assumption is accurate provided the fusion-protein makes up a high percentage of the total protein in the feed and the total protein load in the feed is not greater than ca. 3 g L^{-1} .

6 Conclusions

We have introduced a novel generalized two-zone model for adsorptive chromatography and compared it to the traditional pore-diffusion model for protein uptake within a porous stationary phase. The TZM divides each stationary phase particle into two zones, an inner protein-free core and an outer zone into which a finite mass of protein has penetrated. The TZM replaces the rectangular isotherm of the traditional shrinking-core model with Langmuir theory, thereby allowing for simultaneous intraparticle mass transport and sorbent loading within the outer region of the porous particle by accounting for the presence

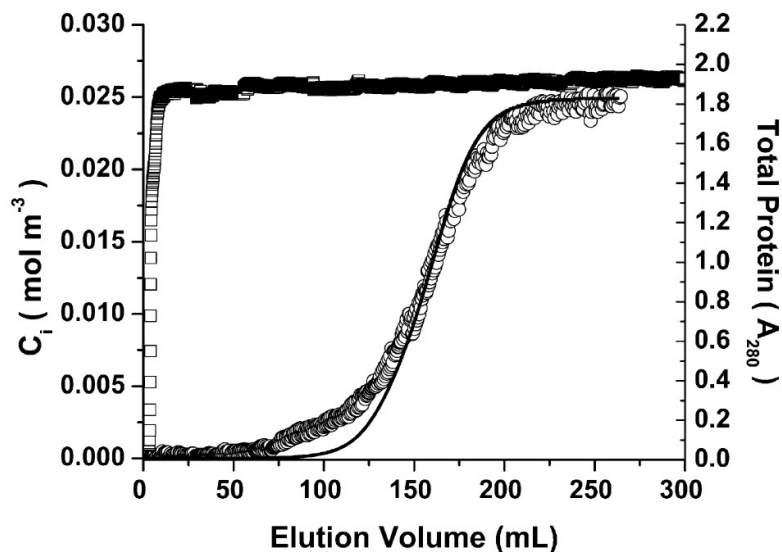


Figure 15: Predicted (line) and experimental (points) breakthrough curves for frontal loading of a clarified cell extract onto a PerlozaTM MT100/G15 composite media column. The clarified cell extract contained 25 μM CBM9-GFP and was loaded at a superficial velocity of $8.5 \times 10^{-3} \text{ cm s}^{-1}$. Eluent absorbance data at 280 nm (open squares) are also shown to indicate total protein as a function of time.

of a protein concentration gradient within this outer region. The model therefore improves upon the PDM by eliminating a boundary condition that forces the unrealistic prediction of a nonzero protein concentration at the center of the particle immediately upon contact of the empty particle with a protein containing mobile phase. Confocal laser scanning microscopy results indicate that under linear loading conditions, both models accurately predict the initial rate of solute uptake. As loading time increases, the PDM deviates from experimental results due to errors associated with the continuous nature of the model, while the TZM continues to accurately predict experimental data. Under nonlinear loading conditions, both models performed well, with the choice of isotherm model becoming the more critical factor in determining the accuracy of the prediction. Finally, the TZM was able to predict product breakthrough over a range of feed concentrations and superficial velocities, including accurate prediction of product breakthrough during frontal loading of a clarified cell extract.

Acknowledgments

The authors would like to thank Professor Tony Warren for helpful discussions and use of his laboratory space and equipment. This work was supported by grants from Protein Engineering Network of Centres of Excellence (PENCE) and NSERC.

References

- [1] C. R. Lowe, A. R. Lowe, G. Gupta, New developments in affinity chromatography with potential application in the production of biopharmaceuticals, *Journal of Biochemical and Biophysical Methods* 49 (1-3) (2001) 561–574.

- [2] A. Jungbauer, R. Hahn, Engineering protein a affinity chromatography, *Current Opinion in Drug Discovery & Development* 7 (2) (2004) 248–256.
- [3] D. G. Deutsch, E. T. Mertz, Plasminogen - purification from human plasma by affinity chromatography, *Science* 170 (3962) (1970) 1095.
- [4] P. Mulcahy, M. O’Flaherty, L. Jennings, T. Griffin, Application of kinetic-based biospecific affinity chromatographic systems to atp-dependent enzymes: studies with yeast hexokinase, *Analytical Biochemistry* 309 (2) (2002) 279–292.
- [5] K. L. Guan, J. E. Dixon, Eukaryotic proteins expressed in escherichia-coli - an improved thrombin cleavage and purification procedure of fusion proteins with glutathione-s-transferase, *Analytical Biochemistry* 192 (2) (1991) 262–267.
- [6] D. B. Smith, K. S. Johnson, Single-step purification of polypeptides expressed in escherichia-coli as fusions with glutathione s-transferase, *Gene* 67 (1) (1988) 31–40.
- [7] R. E. Stofkohahn, D. W. Carr, J. D. Scott, A single step purification for recombinant proteins - characterization of a microtubule associated protein (map-2) fragment which associates with the type-ii camp-dependent protein-kinase, *Febs Letters* 302 (3) (1992) 274–278.
- [8] P. Vaillancourt, T. G. Simcox, C. F. Zheng, Recovery of polypeptides cleaved from purified calmodulin-binding peptide fusion proteins, *Biotechniques* 22 (3) (1997) 451–453.
- [9] C. F. Zheng, T. Simcox, L. Xu, P. Vaillancourt, A new expression vector for high level protein production, one step purification and direct isotopic labeling of calmodulin-binding peptide fusion proteins, *Gene* 186 (1) (1997) 55–60.
- [10] A. D. Keefe, D. S. Wilson, B. Seelig, J. W. Szostak, One-step purification of recombinant proteins using a nanomolar-affinity streptavidin-binding peptide, the sbp-tag, *Protein Expression and Purification* 23 (3) (2001) 440–446.
- [11] D. S. Wilson, A. D. Keefe, J. W. Szostak, The use of mrna display to select high-affinity protein-binding peptides, *Proceedings of the National Academy of Sciences of the United States of America* 98 (7) (2001) 3750–3755.
- [12] A. Einhauer, A. Jungbauer, The flag (tm) peptide, a versatile fusion tag for the purification of recombinant proteins, *Journal of Biochemical and Biophysical Methods* 49 (1-3) (2001) 455–465.
- [13] T. P. Hopp, K. S. Prickett, V. L. Price, R. T. Libby, C. J. March, D. P. Cerretti, D. L. Urdal, P. J. Conlon, A short polypeptide marker sequence useful for recombinant protein identification and purification, *Bio-Technology* 6 (10) (1988) 1204–1210.
- [14] J. Crowe, H. Dobeli, R. Gentz, E. Hochuli, D. Stuber, K. Henco, 6xhis-ni-nta chromatography as a superior technique in recombinant protein expression/purification, *Methods Mol Biol* 31 (1994) 371–87.

-
- [15] J. Porath, J. Carlsson, I. Olsson, G. Belfrage, Metal chelate affinity chromatography, a new approach to protein fractionation, *Nature* 258 (5536) (1975) 598–9.
- [16] F. H. Arnold, H. W. Blanch, C. R. Wilke, Analysis of affinity separations .1. predicting the performance of affinity adsorbers, *Chemical Engineering Journal and the Biochemical Engineering Journal* 30 (2) (1985) B9–B23.
- [17] D. Farnan, D. D. Frey, C. Horvath, Intraparticle mass transfer in high-speed chromatography of proteins, *Biotechnology Progress* 13 (4) (1997) 429–439.
- [18] D. Farnan, D. D. Frey, C. Horvath, Surface and pore diffusion in macroporous and gel-filled gigaporous stationary phases for protein chromatography, *Journal of Chromatography A* 959 (1-2) (2002) 65–73.
- [19] G. L. Skidmore, B. J. Horstmann, H. A. Chase, Modeling single-component protein adsorption to the cation exchanger s sepharose ff, *Journal of Chromatography* 498 (1) (1990) 113–128.
- [20] G. Guiochon, Preparative liquid chromatography, *Journal of Chromatography A* 965 (1-2) (2002) 129–161.
- [21] A. Johnston, M. T. W. Hearn, High-performance liquid-chromatography of amino-acids, peptides and proteins .114. protein interactions with porous coulombic sorbents - comparison of experimental findings with predictions of several adsorption models, *Journal of Chromatography* 557 (1-2) (1991) 335–358.
- [22] A. V. Patwardhan, M. M. Ataii, M. Zenouzi, *Htd* 322 (1995).
- [23] F. H. Arnold, H. W. Blanch, C. R. Wilke, Analysis of affinity separations .2. the characterization of affinity columns by pulse techniques, *Chemical Engineering Journal and the Biochemical Engineering Journal* 30 (2) (1985) B25–B36.
- [24] B. H. Arve, A. I. Liapis, The modeling and analysis of the elution stage of biospecific adsorption in fixed-beds, *Biotechnology and Bioengineering* 30 (5) (1987) 638–649.
- [25] S. Katoh, T. Kambayashi, R. Deguchi, F. Yoshida, Performance of affinity chromatography columns, *Biotechnology and Bioengineering* 20 (2) (1978) 267–280.
- [26] D. A. Sirotti, A. Emery, Mass-transfer parameters in an immobilized glucoamylase column by pulse response analysis, *Biotechnology and Bioengineering* 25 (7) (1983) 1773–1779.
- [27] P. Li, G. H. Xiu, A. E. Rodrigues, Modeling separation of proteins by inert core adsorbent in a batch adsorber, *Chemical Engineering Science* 58 (15) (2003) 3361–3371.
- [28] J. Hubbuch, T. Linden, E. Knieps, A. Ljunglof, J. Thommes, M. R. Kula, Mechanism and kinetics of protein transport in chromatographic media studied by confocal laser scanning microscopy - part i. the interplay of sorbent structure and fluid phase conditions, *Journal of Chromatography A* 1021 (1-2) (2003) 93–104.

- [29] T. Linden, A. Ljunglof, L. Hagel, M. R. Kula, J. Thommes, Visualizing patterns of protein uptake to porous media using confocal scanning laser microscopy, *Separation Science and Technology* 37 (1) (2002) 1–32.
- [30] A. Ljunglof, R. Hjorth, Confocal microscopy as a tool for studying protein adsorption to chromatographic matrices, *Journal of Chromatography A* 743 (1) (1996) 75–83.
- [31] P. B. Weisz, R. D. Goodwin, Combustion of carbonaceous deposits within porous catalyst particles .1. diffusion-controlled kinetics, *Journal of Catalysis* 2 (5) (1963) 397–404.
- [32] E. E. Graham, N. D. Pinto, A predictive model for ion-exchange of proteins, *Reactive Polymers* 6 (1) (1987) 53–53.
- [33] C. Winterhalter, P. Heinrich, A. Candussio, G. Wich, W. Liebl, Identification of a novel cellulose-binding domain within the multidomain 120-kda xylanase xyna of the hyperthermophilic bacterium *thermotoga-maritima*, *Molecular Microbiology* 15 (3) (1995) 431–444.
- [34] M. Kavooosi, J. Meijer, E. Kwan, A. L. Creagh, D. G. Kilburn, C. A. Haynes, Inexpensive one-step purification of polypeptides expressed in *escherichia coli* as fusions with the family 9 carbohydrate-binding module of xylanase 10a from *t-maritima*, *Journal of Chromatography B-Analytical Technologies in the Biomedical and Life Sciences* 807 (1) (2004) 87–94.
- [35] O. Shimomura, F. H. Johnson, Y. Saiga, Extraction, purification and properties of aequorin, a bioluminescent protein from luminous hydromedusan, *aequorea*, *Journal of Cellular and Comparative Physiology* 59 (3) (1962) 223.
- [36] A. Cramer, E. A. Whitehorn, E. Tate, W. P. C. Stemmer, Improved green fluorescent protein by molecular evolution using dna shuffling, *Nature Biotechnology* 14 (3) (1996) 315–319.
- [37] C. Martin, G. Iberer, A. Ubiera, G. Carta, Two-component protein adsorption kinetics in porous ion exchange media, *Journal of Chromatography A* 1079 (1-2) (2005) 105–115.
- [38] G. Carta, A. R. Ubiera, T. M. Pabst, Protein mass transfer kinetics in ion exchange media: Measurements and interpretations, *Chemical Engineering & Technology* 28 (11) (2005) 1252–1264.
- [39] Z. Ma, R. D. Whitley, N. H. L. Wang, Pore and surface diffusion in multicomponent adsorption and liquid chromatography systems, *Aiche Journal* 42 (5) (1996) 1244–1262.
- [40] M. D. Pritzker, Model for parallel surface and pore diffusion of an adsorbate in a spherical adsorbent particle, *Chemical Engineering Science* 58 (2) (2003) 473–478.
- [41] J. Crank, P. Nicolson, A practical method for numerical evaluation of solutions of partial differential equations of the heat-conduction type, *Proceedings of the Cambridge Philosophical Society* 43 (1) (1947) 50–67.

-
- [42] C. D. Holland, A. I. Liapis, Computer methods for solving dynamic separation problems (1983).
- [43] S. V. Patankar, Numerical heat transfer and fluid flow (1980).
- [44] P. W. Barber, S. C. Hill, Light scattering by particles: Computational methods (1983).
- [45] H. Mach, C. R. Middaugh, R. V. Lewis, Statistical determination of the average values of the extinction coefficients of tryptophan and tyrosine in native proteins, *Analytical Biochemistry* 200 (1) (1992) 74–80.
- [46] J. Hubbuch, T. Linden, E. Knieps, J. Thommes, M. R. Kula, Dynamics of protein uptake within the adsorbent particle during packed bed chromatography, *Biotechnology and Bioengineering* 80 (4) (2002) 359–368.
- [47] A. Jungbauer, Preparative chromatography of biomolecules, *Journal of Chromatography* 639 (1) (1993) 3–16.
- [48] M. R. Ladisch, M. Voloch, J. Hong, P. Bienkowski, G. T. Tsao, Cornmeal adsorber for dehydrating ethanol vapors, *Industrial & Engineering Chemistry Process Design and Development* 23 (3) (—1984) 437–443.
- [49] J. H. Knox, G. R. Laird, P. A. Raven, Interaction of radial and axial-dispersion in liquid-chromatography in relation to infinite diameter effect, *Journal of Chromatography* 122 (Jul7) (1976) 129–145.
- [50] G. A. Heeter, A. I. Liapis, Affinity adsorption of adsorbates into spherical monodisperse and bidisperse porous perfusive and purely diffusive adsorbent particles packed in a column - parameter estimation in the laplace transform domain, *Journal of Chromatography A* 760 (1) (1997) 55–69.
- [51] M. Kavooosi, A. L. Creagh, D. G. Kilburn, C. A. Haynes, Strategy for selecting and characterizing linker peptides for cbm9-tagged fusion proteins expressed in *escherichia coli*, *Biotechnology and Bioengineering* 98 (3) (2007) 599–610.
- [52] P. A. Bristow, J. H. Knox, Standardization of test conditions for high-performance liquid-chromatography columns, *Chromatographia* 10 (6) (1977) 279–289.
- [53] H. W. Haynes, P. N. Sarma, Model for application of gas-chromatography to measurements of diffusion in bidisperse structured catalysts, *Aiche Journal* 19 (5) (1973) 1043–1046.
- [54] T. Allen, Powder sampling and particle size measurement (1997).
- [55] J. C. Janson, L. Ryden, Protein purification: Principles, high-resolution methods and applications (1998).
- [56] J. C. Giddings, Dynamics of chromatography (1965).

- [57] G. Gouichon, S. G. Shirazi, A. M. Katti, *Fundamentals of preparative and nonlinear chromatography* (1994).
- [58] M. R. Ladisch, *Bioseparations engineering: Principles, practice and economics* (2001).
- [59] E. J. Wilson, Geankopl.Cj, Liquid mass transfer at very low reynolds numbers in packed beds, *Industrial & Engineering Chemistry Fundamentals* 5 (1) (1966) 9.
- [60] M. E. Young, P. A. Carroad, R. L. Bell, Estimation of diffusion-coefficients of proteins, *Biotechnology and Bioengineering* 22 (5) (1980) 947–955.
- [61]
- [62] M. Goto, N. Hayashi, S. Goto, Separation of electrolyte and non-electrolyte by an ion retardation resin, *Separation Science and Technology* 18 (5) (1983) 475–484.
- [63] E. J. Jervis, C. A. Haynes, D. G. Kilburn, Surface diffusion of cellulases and their isolated binding domains on cellulose, *Journal of Biological Chemistry* 272 (38) (1997) 24016–24023.
- [64] A. Jungbauer, Insights into the chromatography of proteins provided by mathematical modeling, *Current Opinion in Biotechnology* 7 (2) (1996) 210–218.
- [65] K. R. Hall, L. C. Eagleton, A. Acrivos, Vermeule.T, Pore- and solid-diffusion kinetics in fixed-bed adsorption under constant-pattern conditions, *Industrial & Engineering Chemistry Fundamentals* 5 (2) (1966) 212.
- [66] A. Johnston, M. T. W. Hearn, High-performance liquid-chromatography of amino-acids, peptides and proteins .103. mass-transfer resistances in ion-exchange and dye-affinity chromatography of proteins, *Journal of Chromatography* 512 (1990) 101–114.
- [67] Q. M. Mao, A. Johnston, I. G. Prince, M. T. W. Hearn, High-performance liquid-chromatography of amino-acids, peptides and proteins .113. predicting the performance of nonporous particles in affinity-chromatography of proteins, *Journal of Chromatography* 548 (1-2) (1991) 147–163.
- [68] Q. M. Mao, I. G. Prince, M. T. W. Hearn, High-performance liquid-chromatography of amino-acids, peptides and proteins .139. impact of operating parameters in large-scale chromatography of proteins, *Journal of Chromatography A* 691 (1-2) (1995) 273–283.

4 Conclusion & Outlook

This work shows that it is possible to establish mechanistical models for ion-exchange chromatography that have a certain predictive power with regard to retention behaviour of different proteins. In the course of this work we actually used two different approaches:

1. **Patch based approach:** This approach was used to model protein retention of different isoforms of lysozyme, all carrying a dye molecule at a different position. Electrostatic potentials were calculated for patches with a radius of 5 Å around the charge carrying groups. Modelling of isoforms is a rather simple task compared to completely different proteins, because the overall size, shape and surface properties are very similar on most parts of the surface. For that reason, this straight forward approach proofed to be suitable only for isoforms but failed to predict the elution order of different proteins.
2. **Molecular Dynamics (MD) approach:** This is a rather complex approach that allows for the calculation of the binding energies between a protein and an adsorber surface. Because it includes complete protein molecules rather than just patches and because it accounts for different possible binding orientations, its predictive power is not limited to isoforms. Nevertheless, this model is computationally more demanding and has to be set up very carefully. It also allows the investigation of the influence of adsorber chemistry and geometry on the adsorption and thus can help to improve adsorber materials more efficiently.

During the development of the models we gathered a large amount of data about protein adsorption to charged surfaces. In general it can be said, that protein adsorption is a rather complex process which can depend on many parameter:

- Polymer backbone of the adsorber material
- Geometry of the attached ligands
- Density of the ligands on the surface
- pH of the mobile phase

The MD approach also gave rise to the question, why many adsorbers differ significantly in their selectivity, although the above mentioned parameters are very similar and their ligand chemistry is exactly the same: the ligand density. We could show that with increasing ligand density the selectivity of the adsorber increases because it becomes more sensitive to the charge distribution on the protein surface (and thus to the protein orientation on the surface) and less sensitive to the net charge. This means, that proteins with the same net charge can be separated, if the ligand density of the material is high enough.

For this modelling approach to become useful for process development, a few things need to be done. Its predictive power has to be further evaluated especially to show that it also works for bigger proteins. It is also necessary to develop 3D structures of different adsorber materials and to include hydrophobic interaction energies.

In the second part we could show, that confocal laser-scanning microscopy is still a useful tool to visualize and characterize protein transport even in unconventional media. The design of a flow-cell for membrane adsorbers made it possible to study transport and adsorption in several types of membrane adsorbers, indicating that the flow rate is not homogeneously distributed over the complete membrane, which offers a way to explain peak broadening in these materials. We also identified areas where no protein adsorption was found, namely the structure giving cellulose fibers, and this offers a good starting point for increasing the maximum binding capacity, which is often very limited for membrane adsorbers. In a second project we helped to develop a new transport model for spherical particles proteins that makes a more precise modelling of chromatographic column experiments possible by splitting the particle into two regions: a protein filled outer shell and an empty particle core. Together with an improved term for a concentration dependent protein adsorption equilibrium, this model was able to describe experimental data better than the common model. The final step would be to combine both kinds of models, the adsorption models and the transport models to achieve a reasonable simulation of complete chromatographic processes. This would lead to a new *in silico* platform for the optimization of chromatographic downstream processes by reducing experimental screening efforts, and by finding process conditions closer to the real optimal conditions.

References

- AGUILAR, M. I., CLAYTON, D. J., HOLT, P., KRONINA, V., BOYSEN, R. I., PURCELL, A. W. and HEARN, M. T. W. (1998). *Rp hplc binding domains of proteins*. Analytical Chemistry, 70(23):5010.
- ALLEN, T. (1997). *Powder sampling and particle size measurement*.
- ARNOLD, F. H., BLANCH, H. W. and WILKE, C. R. (1985a). *Analysis of affinity separations .1. predicting the performance of affinity adsorbers*. Chemical Engineering Journal and the Biochemical Engineering Journal, 30(2):B9.
- ARNOLD, F. H., BLANCH, H. W. and WILKE, C. R. (1985b). *Analysis of affinity separations .2. the characterization of affinity columns by pulse techniques*. Chemical Engineering Journal and the Biochemical Engineering Journal, 30(2):B25.
- ARVE, B. H. and LIAPIS, A. I. (1987). *The modeling and analysis of the elution stage of biospecific adsorption in fixed-beds*. Biotechnology and Bioengineering, 30(5):638.
- ASTHAGIRI, D. and LENHOFF, A. M. (1997). *Influence of structural details in modeling electrostatically driven protein adsorption*. Langmuir, 13(25):6761.
- BARBER, P. W. and HILL, S. C. (1983). *Light scattering by particles: Computational methods*.
- BARLOW, D. J. and THORNTON, J. M. (1986). *The distribution of charged groups in proteins*. Biopolymers, 25(9):1717.
- BASHFORD, D. (2004). *Macroscopic electrostatic models for protonation states in proteins*. Front Biosci, 9:1082.
- BERMAN, H. M., WESTBROOK, J., FENG, Z., GILLILAND, G., BHAT, T. N., WEISSIG, H., SHINDYALOV, I. N. and BOURNE, P. E. (2000). *The protein data bank*. Nucleic Acids Research, 28(1):235.
- BIESHEUVEL, P. M., VAN DER VEEN, M. and NORDE, W. (—2005—). *A modified poisson-boltzmann model including charge regulation for the adsorption of ionizable polyelectrolytes to charged interfaces, applied to lysozyme adsorption on silica*. Journal of Physical Chemistry B, 109(9):4172.
- BOI, C. (2007). *Membrane adsorbers as purification tools for monoclonal antibody purification*. Journal of Chromatography B-Analytical Technologies in the Biomedical and Life Sciences, 848(1):19.
- BOI, C., DIMARTINO, S. and SARTI, G. C. (2007). *Modelling and simulation of affinity membrane adsorption*. Journal of Chromatography A, 1162(1):24.
- BORASTON, A. B., CREAGH, A. L., ALAM, M. M., KORMOS, J. M., TOMME, P., HAYNES, C. A., WARREN, R. A. J. and KILBURN, D. G. (2001). *Binding specificity and thermodynamics of a family 9 carbohydrate-binding module from thermotoga maritima xy lanase 10a*. Biochemistry, 40(21):6240.

REFERENCES

- BOSCHETTI, E., GIROT, P., GUERRIER, L. and ANDRE, B. (1993). *[chromatographic sorbents for the preparative separation of proteins]*. Ann Pharm Fr, 51(6):299.
- BOSMA, J. C. and WESSELINGH, J. A. (1998a). *ph dependence of ion-exchange equilibrium of proteins*. Aiche Journal, 44(11):2399.
- BOSMA, J. C. and WESSELINGH, J. A. (1998b). *ph dependence of ion-exchange equilibrium of proteins*. Aiche Journal, 44(11):2399.
- BOSMA, J. C. and WESSELINGH, J. A. (2004). *Available area isotherm*. Aiche Journal, 50(4):848.
- BOUHALLAB, S., HENRY, G. and BOSCHETTI, E. (1996). *Separation of small cationic bioactive peptides by strong ion-exchange chromatography*. Journal of Chromatography A, 724(1-2):137.
- BRISTOW, P. A. and KNOX, J. H. (1977). *Standardization of test conditions for high-performance liquid-chromatography columns*. Chromatographia, 10(6):279.
- BROOKS, C. A. and CRAMER, S. M. (1992). *Steric mass-action ion-exchange - displacement profiles and induced salt gradients*. Aiche Journal, 38(12):1969.
- CAMERON, R. E. and DONALD, A. M. (1994). *Minimizing sample evaporation in the environmental scanning electron-microscope*. Journal of Microscopy-Oxford, 173:227.
- CANO, T., OFFRINGA, N. and WILLSON, R. C. (2007). *The effectiveness of three multi-component binding models in describing the binary competitive equilibrium adsorption of two cytochrome b(5) mutants*. Journal of Chromatography A, 1144(2):197.
- CARLSSON, F., HYLTER, E., ARNEBRANT, T., MALMSTEN, M. and LINSE, P. (2004). *Lysozyme adsorption to charged surfaces. a monte carlo study*. Journal of Physical Chemistry B, 108(28):9871.
- CARTA, G., UBIERA, A. R. and PABST, T. M. (2005). *Protein mass transfer kinetics in ion exchange media: Measurements and interpretations*. Chemical Engineering & Technology, 28(11):1252.
- CASE, D. A., CHEATHAM, T. E., DARDEN, T., GOHLKE, H., LUO, R., MERZ, K. M., ONUFRIEV, A., SIMMERLING, C., WANG, B. and WOODS, R. J. (2005). *The amber biomolecular simulation programs*. Journal of Computational Chemistry, 26(16):1668.
- CHANG, C. and LENHOFF, A. M. (1998). *Comparison of protein adsorption isotherms and uptake rates in preparative cation-exchange materials*. J Chromatogr A, 827(2):281.
- CHARCOSSET, C., CHERFI, A. and BERNENGO, J. C. (2000). *Characterization of microporous membrane morphology using confocal scanning laser microscopy*. Chemical Engineering Science, 55(22):5351.
- CHEN, H. and HORVATH, C. (1995). *High-speed high-performance liquid chromatography of peptides and proteins*. J Chromatogr A, 705(1):3.

- CHEN, W. D., HU, H. H. and WANG, Y. D. (2006). *Analysis of steric mass-action model for protein adsorption equilibrium onto porous anion-exchange adsorbent*. Chemical Engineering Science, 61(21):7068.
- CHICZ, R. M. and REGNIER, F. E. (1989). *Single amino-acid contributions to protein retention in cation-exchange chromatography - resolution of genetically engineered subtilisin variants*. Analytical Chemistry, 61(18):2059.
- CHICZ, R. M. and REGNIER, F. E. (1990). *Microenvironmental contributions to the chromatographic behavior of subtilisin in hydrophobic-interaction and reversed-phase chromatography*. Journal of Chromatography, 500:503.
- CRAMERI, A., WHITEHORN, E. A., TATE, E. and STEMMER, W. P. C. (1996). *Improved green fluorescent protein by molecular evolution using dna shuffling*. Nature Biotechnology, 14(3):315.
- CRANK, J. and NICOLSON, P. (1947). *A practical method for numerical evaluation of solutions of partial differential equations of the heat-conduction type*. Proceedings of the Cambridge Philosophical Society, 43(1):50.
- CROWE, J., DOBELI, H., GENTZ, R., HOCHULI, E., STUBER, D. and HENCO, K. (1994). *6xhis-ni-nta chromatography as a superior technique in recombinant protein expression/purification*. Methods Mol Biol, 31:371.
- CURLING, J. (2007). *History of chromatography: Process chromatography: Five decades of innovation*. BioPharm International, February(2).
- DALY, S. M., PRZYBYCIEN, T. M. and TILTON, R. D. (2003). *Coverage-dependent orientation of lysozyme adsorbed on silica*. Langmuir, 19(9):3848.
- DELAPARRA, R. E. (1993). *A method to detect variations in the wetting properties of microporous polymer membranes*. Microscopy Research and Technique, 25(5-6):362.
- DEPHILLIPS, P., LAGERLUND, I., FARENMARK, J. and LENHOFF, A. M. (2004). *Effect of spacer arm length on protein retention on a strong cation exchange adsorbent*. Anal Chem, 76(19):5816.
- DEPHILLIPS, P. and LENHOFF, A. M. (2001). *Determinants of protein retention characteristics on cation-exchange adsorbents*. J Chromatogr A, 933(1-2):57.
- DEUTSCH, D. G. and MERTZ, E. T. (1970). *Plasminogen - purification from human plasma by affinity chromatography*. Science, 170(3962):1095.
- DISMER, F. and HUBBUCH, J. (2007). *A novel approach to characterize the binding orientation of lysozyme on ion-exchange resins*. Journal of Chromatography A, 1149(2):312.
- DISMER, F., PETZOLD, M. and HUBBUCH, J. (2008). *Effects of ionic strength and mobile phase ph on the binding orientation of lysozyme on different ion-exchange adsorbents*. Journal of Chromatography A, 1194(1):11.

REFERENCES

- DRAGER, R. R. and REGNIER, F. E. (1986). *Application of the stoichiometric displacement model of retention to anion-exchange chromatography of nucleic-acids*. Journal of Chromatography, 359:147.
- DRAGER, R. R. and REGNIER, F. E. (1987). *Retention mechanism of lactate-dehydrogenase in anion-exchange chromatography*. Journal of Chromatography, 406:237.
- EINHAEUER, A. and JUNGBAUER, A. (2001). *The flag (tm) peptide, a versatile fusion tag for the purification of recombinant proteins*. Journal of Biochemical and Biophysical Methods, 49(1-3):455.
- FANG, F. W., AGUILAR, M. I. and HEARN, M. T. W. (1996a). *High-performance liquid chromatography of amino acids, peptides and proteins .93. influence of temperature on the retention behaviour of proteins in cation-exchange chromatography*. Journal of Chromatography A, 729(1-2):49.
- FANG, F. W., AGUILAR, M. I. and HEARN, M. T. W. (1996b). *High-performance liquid chromatography of amino acids, peptides and proteins .96. temperature-induced changes in the bandwidth behaviour of proteins separated with cation-exchange adsorbents*. Journal of Chromatography A, 729(1-2):67.
- FARNAN, D., FREY, D. D. and HORVATH, C. (1997). *Intraparticle mass transfer in high-speed chromatography of proteins*. Biotechnology Progress, 13(4):429.
- FARNAN, D., FREY, D. D. and HORVATH, C. (2002). *Surface and pore diffusion in macroporous and gel-filled gigaporous stationary phases for protein chromatography*. Journal of Chromatography A, 959(1-2):65.
- FAUSNAUGHPOLLITT, J., THEVENON, G., JANIS, L. and REGNIER, F. E. (1988). *Chromatographic resolution of lysozyme variants*. Journal of Chromatography, 443:221.
- FELINGER, A. and GUIOCHON, G. (1992a). *Optimization of the experimental conditions and the column design parameters in displacement chromatography*. Journal of Chromatography, 609(1-2):35.
- FELINGER, A. and GUIOCHON, G. (1992b). *Optimization of the experimental conditions and the column design parameters in overloaded elution chromatography*. Journal of Chromatography, 591(1-2):31.
- FREERICK, C., KREIS, P., GORAK, A., TAPPE, A. and MELZNER, D. (2008). *Simulation of a human serum albumin downstream process incorporating ion-exchange membrane adsorbents*. Chemical Engineering and Processing, 47(7):1128.
- FRITZ, J. S. (2004). *Early milestones in the development of ion-exchange chromatography: a personal account*. Journal of Chromatography A, 1039(1-2):3.
- GEBAUER, K. H., THOMMES, J. and KULA, M. R. (1997). *Breakthrough performance of high-capacity membrane adsorbents in protein chromatography*. Chemical Engineering Science, 52(3):405.

- GHOSH, R. (2002). *Protein separation using membrane chromatography: opportunities and challenges*. J Chromatogr A, 952(1-2):13.
- GIDDINGS, J. C. (1965). *Dynamics of chromatography*.
- GILL, C. O. and BRYANT, J. (1993). *The presence of escherichia-coli, salmonella and campylobacter in pig carcass dehairing equipment*. Food Microbiology, 10(4):337.
- GILL, D. S., ROUSH, D. J., SHICK, K. A. and WILLSON, R. C. (1995). *Microcalorimetric characterization of the anion-exchange adsorption of recombinant cytochrome b(5) and its surface-charge mutants*. Journal of Chromatography A, 715(1):81.
- GILL, D. S., ROUSH, D. J. and WILLSON, R. C. (1994). *Adsorption heterogeneity and thermodynamic driving forces in anion-exchange equilibria of cytochrome-b(5)*. Journal of Colloid and Interface Science, 167(1):1.
- GOTO, M., HAYASHI, N. and GOTO, S. (1983). *Separation of electrolyte and non-electrolyte by an ion retardation resin*. Separation Science and Technology, 18(5):475.
- GOUCHON, G., SHIRAZI, S. G. and KATTI, A. M. (1994). *Fundamentals of preparative and nonlinear chromatography*.
- GRAHAM, E. E. and PINTO, N. D. (1987). *A predictive model for ion-exchange of proteins*. Reactive Polymers, 6(1):53.
- GUAN, K. L. and DIXON, J. E. (1991). *Eukaryotic proteins expressed in escherichia-coli - an improved thrombin cleavage and purification procedure of fusion proteins with glutathione-s-transferase*. Analytical Biochemistry, 192(2):262.
- GUIOCHON, G. (2002). *Preparative liquid chromatography*. Journal of Chromatography A, 965(1-2):129.
- HAFF, L. A., FAGERSTAM, L. G. and BARRY, A. R. (1983). *Use of electrophoretic titration curves for predicting optimal chromatographic conditions for fast ion-exchange chromatography of proteins*. Journal of Chromatography, 266(AUG):409.
- HAGGERTY, L. and LENHOFF, A. M. (1991). *Relation of protein electrostatics computations to ion-exchange and electrophoretic behavior*. Journal of Physical Chemistry, 95(3):1472.
- HALL, K. R., EAGLETON, L. C., ACRIVOS, A. and VERMEULE, T. (1966). *Pore- and solid-diffusion kinetics in fixed-bed adsorption under constant-pattern conditions*. Industrial & Engineering Chemistry Fundamentals, 5(2):212.
- HALLGREN, E., KALMAN, F., FARNAN, D., HORVATH, C. and STAHLBERG, J. (2000). *Protein retention in ion-exchange chromatography: effect of net charge and charge distribution*. Journal of Chromatography A, 877(1-2):13.
- HASHIM, M. A., CHU, K. H. and TSAN, P. S. (1995). *Effects of ionic-strength and pH on the adsorption equilibria of lysozyme on ion-exchangers*. Journal of Chemical Technology and Biotechnology, 62(3):253.

REFERENCES

- HAYNES, H. W. and SARMA, P. N. (1973). *Model for application of gas-chromatography to measurements of diffusion in bidisperse structured catalysts*. Aiche Journal, 19(5):1043.
- HEETER, G. A. and LIAPIS, A. I. (1997). *Affinity adsorption of adsorbates into spherical monodisperse and bidisperse porous perfusive and purely diffusive adsorbent particles packed in a column - parameter estimation in the laplace transform domain*. Journal of Chromatography A, 760(1):55.
- HELFFERICH, F. G. and WHITLEY, R. D. (1996). *Non-linear waves in chromatography .2. wave interference and coherence in multicomponent*. Journal of Chromatography A, 734(1):7.
- HERRMANN, T., SCHRODER, M. and HUBBUCH, J. (2006). *Generation of equally sized particle plaques using solid-liquid suspensions*. Biotechnology Progress, 22(3):914.
- HIGNETT, T. P. and HUBBUCH, T. N. (1946). *Fused tricalcium phosphate production by defluorination of rock phosphate in a shaft furnace*. Industrial and Engineering Chemistry, 38(12):1208.
- HODDER, A. N., AGUILAR, M. I. and HEARN, M. T. (1989). *High-performance liquid chromatography of amino acids, peptides and proteins. lxxxix. the influence of different displacer salts on the retention properties of proteins separated by gradient anion-exchange chromatography*. J Chromatogr, 476:391.
- HODDER, A. N., MACHIN, K. J., AGUILAR, M. I. and HEARN, M. T. W. (1990). *High-performance liquid-chromatography of amino-acids, peptides and proteins .101. identification and characterization of coulombic interactive regions on sperm whale myoglobin by high-performance anion-exchange chromatography and computer-graphic analysis*. Journal of Chromatography, 507:33.
- HOLLAND, C. D. and LIAPIS, A. I. (1983). *Computer methods for solving dynamic separation problems*.
- HOPP, T. P., PRICKETT, K. S., PRICE, V. L., LIBBY, R. T., MARCH, C. J., CERRETTI, D. P., URDAL, D. L. and CONLON, P. J. (1988). *A short polypeptide marker sequence useful for recombinant protein identification and purification*. Bio-Technology, 6(10):1204.
- HUBBUCH, J., LINDEN, T., KNIEPS, E., LJUNGLOF, A., THOMMES, J. and KULA, M. R. (2003). *Mechanism and kinetics of protein transport in chromatographic media studied by confocal laser scanning microscopy - part i. the interplay of sorbent structure and fluid phase conditions*. Journal of Chromatography A, 1021(1-2):93.
- HUBBUCH, J., LINDEN, T., KNIEPS, E., THOMMES, J. and KULA, M. R. (2002). *Dynamics of protein uptake within the adsorbent particle during packed bed chromatography*. Biotechnology and Bioengineering, 80(4):359.
- INOUE (2006). *Handbook of biological confocal microscopy*.

- JACOBSON, S. C., FELINGER, A. and GUIOCHON, G. (1992a). *Optimizing the sample-size and the reduced velocity to achieve maximum production-rates of enantiomers*. Biotechnology Progress, 8(6):533.
- JACOBSON, S. C., FELINGER, A. and GUIOCHON, G. (1992b). *Optimizing the sample-size and the retention parameters to achieve maximum production-rates for enantiomers in chiral chromatography*. Biotechnology and Bioengineering, 40(10):1210.
- JAKOBSSON, N., DEGERMAN, M., STENBORG, E. and NILSSON, B. (2007). *Model based robustness analysis of an ion-exchange chromatography step*. Journal of Chromatography A, 1138(1-2):109.
- JANSON, J. C. and RYDEN, L. (1998). *Protein purification: Principles, high-resolution methods and applications*.
- JANZEN, R., UNGER, K. K., MULLER, W. and HEARN, M. T. W. (1990). *Adsorption of proteins on porous and nonporous poly(ethyleneimine) and tentacle-type anion-exchangers*. Journal of Chromatography, 522:77.
- JENKINS, L. M. and DONALD, A. M. (1997). *Use of the environmental scanning electron microscope for the observation of the swelling behaviour of cellulosic fibres*. Scanning, 19(2):92.
- JERVIS, E. J., HAYNES, C. A. and KILBURN, D. G. (1997). *Surface diffusion of cellulases and their isolated binding domains on cellulose*. Journal of Biological Chemistry, 272(38):24016.
- JOHANSSON, H. O. and VAN ALSTINE, J. M. (2006). *Modeling of protein interactions with surface-grafted charged polymers. correlations between statistical molecular modeling and a mean field approach*. Langmuir, 22(21):8920.
- JOHNSTON, A. and HEARN, M. T. W. (1990). *High-performance liquid-chromatography of amino-acids, peptides and proteins .103. mass-transfer resistances in ion-exchange and dye-affinity chromatography of proteins*. Journal of Chromatography, 512:101.
- JOHNSTON, A. and HEARN, M. T. W. (1991). *High-performance liquid-chromatography of amino-acids, peptides and proteins .114. protein interactions with porous coulombic sorbents - comparison of experimental findings with predictions of several adsorption models*. Journal of Chromatography, 557(1-2):335.
- JUNGBAUER, A. (1993). *Preparative chromatography of biomolecules*. Journal of Chromatography, 639(1):3.
- JUNGBAUER, A. (1996). *Insights into the chromatography of proteins provided by mathematical modeling*. Current Opinion in Biotechnology, 7(2):210.
- JUNGBAUER, A. and HAHN, R. (2004). *Engineering protein a affinity chromatography*. Current Opinion in Drug Discovery & Development, 7(2):248.
- KATOH, S., KAMBAYASHI, T., DEGUCHI, R. and YOSHIDA, F. (1978). *Performance of affinity chromatography columns*. Biotechnology and Bioengineering, 20(2):267.

REFERENCES

- KAVOOSI, M., CREAGH, A. L., KILBURN, D. G. and HAYNES, C. A. (2007). *Strategy for selecting and characterizing linker peptides for cbm9-tagged fusion proteins expressed in escherichia coli*. *Biotechnology and Bioengineering*, 98(3):599.
- KAVOOSI, M., MEIJER, J., KWAN, E., CREAGH, A. L., KILBURN, D. G. and HAYNES, C. A. (2004). *Inexpensive one-step purification of polypeptides expressed in escherichia coli as fusions with the family 9 carbohydrate-binding module of xylanase 10a from t-maritima*. *Journal of Chromatography B-Analytical Technologies in the Biomedical and Life Sciences*, 807(1):87.
- KAWAI, T., SUGITA, K., SAITO, K. and SUGO, T. (2000). *Extension and shrinkage of polymer brush grafted onto porous membrane induced by protein binding*. *Macromolecules*, 33(4):1306.
- KEEFE, A. D., WILSON, D. S., SEELIG, B. and SZOSTAK, J. W. (2001). *One-step purification of recombinant proteins using a nanomolar-affinity streptavidin-binding peptide, the sbp-tag*. *Protein Expression and Purification*, 23(3):440.
- KIM, J. and SOMORJAI, G. A. (2003). *Molecular packing of lysozyme, fibrinogen, and bovine serum albumin on hydrophilic and hydrophobic surfaces studied by infrared-visible sum frequency generation and fluorescence microscopy*. *J Am Chem Soc*, 125(10):3150.
- KNOX, J. H., LAIRD, G. R. and RAVEN, P. A. (1976). *Interaction of radial and axial-dispersion in liquid-chromatography in relation to infinite diameter effect*. *Journal of Chromatography*, 122(Jul7):129.
- KNUDSEN, H. L., FAHRNER, R. L., XU, Y., NORLING, L. A. and BLANK, G. S. (2001). *Membrane ion-exchange chromatography for process-scale antibody purification*. *J Chromatogr A*, 907(1-2):145.
- KOPACIEWICZ, W. and REGNIER, F. E. (1983a). *Mobile phase selection for the high-performance ion-exchange chromatography of proteins*. *Anal Biochem*, 133(1):251.
- KOPACIEWICZ, W. and REGNIER, F. E. (1983b). *A system for coupled multiple-column separation of proteins*. *Anal Biochem*, 129(2):472.
- KOPACIEWICZ, W., ROUNDS, M. A. and REGNIER, F. E. (1985). *Stationary phase contributions to retention in high-performance anion-exchange protein chromatography - ligand density and mixed-mode effects*. *J. Chromatogr.*, 318(2):157.
- KUEHNER, D. E., ENGMANN, J., FERGG, F., WERNICK, M., BLANCH, H. W. and PRAUSNITZ, J. M. (1999). *Lysozyme net charge and ion binding in concentrated aqueous electrolyte solutions*. *Journal of Physical Chemistry B*, 103(8):1368.
- KYTE, J. and DOOLITTLE, R. F. (1982). *A simple method for displaying the hydropathic character of a protein*. *Journal of Molecular Biology*, 157(1):105.
- LADISCH, M. R. (2001). *Bioseparations engineering: Principles, practice and economics*.

- LADISCH, M. R., VOLOCH, M., HONG, J., BIENKOWSKI, P. and TSAO, G. T. (—1984). *Cornmeal adsorber for dehydrating ethanol vapors*. *Industrial & Engineering Chemistry Process Design and Development*, 23(3):437.
- LADIWALA, A., REGE, K., BRENEMAN, C. M. and CRAMER, S. M. (2005). *A priori prediction of adsorption isotherm parameters and chromatographic behavior in ion-exchange systems*. *Proceedings of the National Academy of Sciences of the United States of America*, 102(33):11710.
- LAPIDUS, L. and AMUNDSON, N. R. (1952). *Mathematics of adsorption in beds .6. the effect of longitudinal diffusion in ion exchange and chromatographic columns*. *Journal of Physical Chemistry*, 56(8):984.
- LEE, B. and RICHARDS, F. M. (1971). *Interpretation of protein structures - estimation of static accessibility*. *Journal of Molecular Biology*, 55(3):379.
- LENHOFF, A. M. (1994). *Contributions of surface-features to the electrostatic properties of rough colloidal particles*. *Colloids and Surfaces A*, 87(1):49.
- LI, P., XIU, G. H. and RODRIGUES, A. E. (2003). *Modeling separation of proteins by inert core adsorbent in a batch adsorber*. *Chemical Engineering Science*, 58(15):3361.
- LINDEN, T., LJUNGLOF, A., HAGEL, L., KULA, M. R. and THOMMES, J. (2002). *Visualizing patterns of protein uptake to porous media using confocal scanning laser microscopy*. *Separation Science and Technology*, 37(1):1.
- LJUNGLOF, A. and HJORTH, R. (1996). *Confocal microscopy as a tool for studying protein adsorption to chromatographic matrices*. *Journal of Chromatography A*, 743(1):75.
- LOWE, C. R., LOWE, A. R. and GUPTA, G. (2001). *New developments in affinity chromatography with potential application in the production of biopharmaceuticals*. *Journal of Biochemical and Biophysical Methods*, 49(1-3):561.
- MA, Z., WHITLEY, R. D. and WANG, N. H. L. (1996). *Pore and surface diffusion in multicomponent adsorption and liquid chromatography systems*. *Aiche Journal*, 42(5):1244.
- MACH, H., MIDDAGH, C. R. and LEWIS, R. V. (1992). *Statistical determination of the average values of the extinction coefficients of tryptophan and tyrosine in native proteins*. *Analytical Biochemistry*, 200(1):74.
- MALMQUIST, G., NILSSON, U. H., NORRMAN, M., SKARP, U., STROMGREN, M. and CARREDANO, E. (2006). *Electrostatic calculations and quantitative protein retention models for ion exchange chromatography*. *Journal of Chromatography A*, 1115(1-2):164.
- MAO, Q. M., JOHNSTON, A., PRINCE, I. G. and HEARN, M. T. W. (1991). *High-performance liquid-chromatography of amino-acids, peptides and proteins .113. predicting the performance of nonporous particles in affinity-chromatography of proteins*. *Journal of Chromatography*, 548(1-2):147.

REFERENCES

- MAO, Q. M., PRINCE, I. G. and HEARN, M. T. W. (1995). *High-performance liquid-chromatography of amino-acids, peptides and proteins .139. impact of operating parameters in large-scale chromatography of proteins*. Journal of Chromatography A, 691(1-2):273.
- MARTIN, C., IBERER, G., UBIERA, A. and CARTA, G. (2005). *Two-component protein adsorption kinetics in porous ion exchange media*. Journal of Chromatography A, 1079(1-2):105.
- MAZSAROFF, I., VARADY, L., MOUCHAWAR, G. A. and REGNIER, F. E. (1990). *Thermodynamic model for electrostatic-interaction chromatography of proteins*. Journal of Chromatography, 499:63.
- MCDONALD, A. (1998). *Environmental scanning electron microscopy - esem*. Materials World, 6(7):399.
- MELANDER, W. R., ELRASSI, Z. and HORVATH, C. (1989). *Interplay of hydrophobic and electrostatic interactions in bio-polymer chromatography - effect of salts on the retention of proteins*. Journal of Chromatography, 469:3.
- MITEVA, M. A., TUFFERY, P. and VILLOUTREIX, B. O. (2005). *Pce: web tools to compute protein continuum electrostatics*. Nucleic Acids Res, 33(Web Server issue):W372.
- MULCAHY, P., O'FLAHERTY, M., JENNINGS, L. and GRIFFIN, T. (2002). *Application of kinetic-based biospecific affinity chromatographic systems to atp-dependent enzymes: studies with yeast hexokinase*. Analytical Biochemistry, 309(2):279.
- NOINVILLE, V., CRAESCU, C. T., VIDALMADJAR, C. and SEBILLE, B. (1995a). *Molecular approach to protein polymer interactions in ion-exchange chromatography*. Journal of Chromatography B-Biomedical Applications, 664(1):33.
- NOINVILLE, V., VIDALMADJAR, C. and SEBILLE, B. (1995b). *Modeling of protein adsorption on polymer surfaces - computation of adsorption potential*. Journal of Physical Chemistry, 99(5):1516.
- NOINVILLE, V., VIDALMADJAR, C. and SEBILLE, B. (1995c). *Simulation of protein adsorption on anion-exchanger synthetic-polymers*. Journal of Trace and Microprobe Techniques, 13(3):341.
- ONUFRIEV, A., BASHFORD, D. and CASE, D. A. (2004). *Exploring protein native states and large-scale conformational changes with a modified generalized born model*. Proteins-Structure Function and Bioinformatics, 55(2):383.
- PATANKAR, S. V. (1980). *Numerical heat transfer and fluid flow*.
- PATWARDHAN, A. V., ATAANI, M. M. and ZENOUI, M. (1995). *Htd 322*.
- PEARLMAN, D. A., CASE, D. A., CALDWELL, J. W., ROSS, W. S., CHEATHAM, T. E., DEBOLT, S., FERGUSON, D., SEIBEL, G. and KOLLMAN, P. (1995). *Amber*,

- a package of computer-programs for applying molecular mechanics, normal-mode analysis, molecular-dynamics and free-energy calculations to simulate the structural and energetic properties of molecules.* Computer Physics Communications, 91(1-3):1.
- PETTERSEN, E. F., GODDARD, T. D., HUANG, C. C., COUCH, G. S., GREENBLATT, D. M., MENG, E. C. and FERRIN, T. E. (2004). *Ucsf chimera - a visualization system for exploratory research and analysis.* Journal of Computational Chemistry, 25(13):1605.
- PORATH, J., CARLSSON, J., OLSSON, I. and BELFRAGE, G. (1975). *Metal chelate affinity chromatography, a new approach to protein fractionation.* Nature, 258(5536):598.
- PRITZKER, M. D. (2003). *Model for parallel surface and pore diffusion of an adsorbate in a spherical adsorbent particle.* Chemical Engineering Science, 58(2):473.
- RAFFAINI, G. and GANAZZOLI, F. (2007). *Understanding the performance of biomaterials through molecular modeling: Crossing the bridge between their intrinsic properties and the surface adsorption of proteins.* Macromolecular Bioscience, 7(5):552.
- REICHERT, U., LINDEN, T., BELFORT, G., KULA, M. R. and THOMMES, J. (2002). *Visualising protein adsorption to ion-exchange membranes by confocal microscopy.* Journal of Membrane Science, 199(1-2):161.
- RHEE, H. K., ARIS, R. and AMUNDSON, N. R. (1970). *Theory of multicomponent chromatography.* Philosophical Transactions of the Royal Society of London Series a - Mathematical and Physical Sciences, 267(1182):419.
- RIGHETTI, P. G., TUDOR, G. and EK, K. (1981). *Isoelectric points and molecular-weights of proteins - a new table.* Journal of Chromatography, 220(2):115.
- ROPER, D. K. and LIGHTFOOT, E. N. (1993). *Comparing steady counterflow separation with differential chromatography.* J Chromatogr A, 654(1):1.
- ROTH, C. M. and LENHOFF, A. M. (1993). *Electrostatic and vanderwaals contributions to protein adsorption - computation of equilibrium-constants.* Langmuir, 9(4):962.
- ROTH, C. M., SADER, J. E. and LENHOFF, A. M. (1998). *Electrostatic contribution to the energy and entropy of protein adsorption.* Journal of Colloid and Interface Science, 203(1):218.
- ROTH, C. M., UNGER, K. K. and LENHOFF, A. M. (1996). *Mechanistic model of retention in protein ion-exchange chromatography.* Journal of Chromatography A, 726(1-2):45.
- ROUNDS, M. A. and REGNIER, F. E. (1984). *Evaluation of a retention model for high-performance ion-exchange chromatography using 2 different displacing salts.* Journal of Chromatography, 283(Jan):37.
- ROUSH, D. J., GILL, D. S. and WILLSON, R. C. (1994). *Electrostatic potentials and electrostatic interaction energies of rat cytochrome b(5) and a simulated anion-exchange adsorbent surface.* Biophysical Journal, 66(5):1290.

REFERENCES

- RUGGIERO, C., MANTELLI, M., CURTIS, A. and ROLFE, P. (2005). *Protein-surface interactions - an energy-based mathematical model*. Cell Biochemistry and Biophysics, 43(3):407.
- RUTTAN, V. W. and HUBBUCH, T. N. (1953). *The changing industrial molasses market*. Journal of Agricultural and Food Chemistry, 1(9):602.
- SARTORIUS (2006). *Sartobind membrane adsorbers for rapid purification of proteins*. Sartorius brochure.
- SCHMIDT-TRAUB, H. (2005). *Preparative Chromatography of Fine Chemicals and Pharmaceutical Agents*. Wiley-VCH, first edition.
- SCHRODER, M., VON LIERES, E. and HUBBUCH, J. (2006). *Direct quantification of intraparticle protein diffusion in chromatographic media*. Journal of Physical Chemistry B, 110(3):1429.
- SHI, Q. S., ZHOU, Y. and SUN, Y. (2005). *Influence of pH and ionic strength on the steric mass-action model parameters around the isoelectric point of protein*. Biotechnology Progress, 21(2):516.
- SHIMOMURA, O., JOHNSON, F. H. and SAIGA, Y. (1962). *Extraction, purification and properties of aequorin, a bioluminescent protein from luminous hydromedusan, aequorea*. Journal of Cellular and Comparative Physiology, 59(3):223.
- SINGH, N., WANG, J., ULBRICHT, M., WICKRAMASINGHE, S. R. and HUSSON, S. M. (2008). *Surface-initiated atom transfer radical polymerization: A new method for preparation of polymeric membrane adsorbers*. Journal of Membrane Science, 309(1-2):64.
- SIROTTI, D. A. and EMERY, A. (1983). *Mass-transfer parameters in an immobilized glucoamylase column by pulse response analysis*. Biotechnology and Bioengineering, 25(7):1773.
- SKIDMORE, G. L., HORSTMANN, B. J. and CHASE, H. A. (1990). *Modeling single-component protein adsorption to the cation exchanger s sepharose ff*. Journal of Chromatography, 498(1):113.
- SMITH, D. B. and JOHNSON, K. S. (1988). *Single-step purification of polypeptides expressed in escherichia-coli as fusions with glutathione s-transferase*. Gene, 67(1):31.
- STAHLBERG, J. (1999). *Retention models for ions in chromatography*. Journal of Chromatography A, 855(1):3.
- STAHLBERG, J., JONSSON, B. and HORVATH, C. (1991). *Theory for electrostatic interaction chromatography of proteins*. Analytical Chemistry, 63(17):1867.
- STEELS, B. M., KOSKA, J. and HAYNES, C. A. (2000). *Analysis of brush-particle interactions using self-consistent-field theory*. Journal of Chromatography B, 743(1-2):41.
- STEUDLE, A. (2007). *Personal communication*.

- STOFKOHAIN, R. E., CARR, D. W. and SCOTT, J. D. (1992). *A single step purification for recombinant proteins - characterization of a microtubule associated protein (map-2) fragment which associates with the type-ii camp-dependent protein-kinase*. Febs Letters, 302(3):274.
- SUEN, S. Y. and ETZEL, M. R. (1992). *A mathematical-analysis of affinity membrane bioseparations*. Chemical Engineering Science, 47(6):1355.
- SUN, Y., WELSH, W. J. and LATOUR, R. A. (2005). *Prediction of the orientations of adsorbed protein using an empirical energy function with implicit solvation*. Langmuir, 21(12):5616.
- SUSANTO, A., HERRMANN, T. and HUBBUCH, J. (2006). *Short-cut method for the correction of light attenuation influences in the experimental data obtained from confocal laser scanning microscopy*. Journal of Chromatography A, 1136(1):29.
- TANAKA, N. and KOBAYASHI, H. (2003). *Monolithic columns for liquid chromatography*. Anal Bioanal Chem, 376:298.
- TESKE, C., SIMON, R., NIEBISCH, A. and HUBBUCH, J. (2006). *Changes in retention behaviour of fluorescently labeled proteins during ion-exchange chromatography caused by different protein surface labeling positions*. Biotechnology and Bioengineering, accepted.
- TESKE, C. A., SCHROEDER, M., SIMON, R. and HUBBUCH, J. (2005). *Protein-labeling effects in confocal laser scanning microscopy*. Journal of Physical Chemistry B, 109(28):13811.
- TESKE, C. A., SIMON, R., NIEBISCH, A. and HUBBUCH, J. (2007). *Changes in retention behavior of fluorescently labeled proteins during ion-exchange chromatography caused by different protein surface labeling positions*. Biotechnology and Bioengineering, 98(1):193.
- TSWETT, M. S. (1989). *About a new category of adsorption phenomena and their application for biochemical-analysis*. Chemical Reviews, 89(2):281.
- TUGCU, N. and CRAMER, S. M. (2005). *The effect of multi-component adsorption on selectivity in ion exchange displacement systems*. Journal of Chromatography A, 1063(1-2):15.
- ULBRICHT, M. (2006). *Advanced functional polymer membranes*. Polymer, 47(7):2217.
- ULBRICHT, M. and YANG, H. (2005). *Porous polypropylene membranes with different carboxyl polymer brush layers for reversible protein binding via surface-initiated graft copolymerization*. Chemistry of Materials, 17(10):2622.
- VAILLANCOURT, P., SIMCOX, T. G. and ZHENG, C. F. (1997). *Recovery of polypeptides cleaved from purified calmodulin-binding peptide fusion proteins*. Biotechniques, 22(3):451.

REFERENCES

- VANDEEMTER, J. J., ZUIDERWEG, F. J. and KLINKENBERG, A. (1956). *Longitudinal diffusion and resistance to mass transfer as causes of nonideality in chromatography*. Chemical Engineering Science, 5(6):271.
- VICENTE, T., SOUSA, M. F. Q., PEIXOTO, C., MOTA, J. P. B., ALVES, P. M. and CARRONDO, M. J. T. (2008). *Anion-exchange membrane chromatography for purification of rotavirus-like particles*. Journal of Membrane Science, 311(1-2):270.
- VOLOCH, M., LADISCH, M. R., CANTARELLA, M. and TSAO, G. T. (1984). *Preparation of cellodextrins using sulfuric-acid*. Biotechnology and Bioengineering, 26(5):557.
- VOSSOUGH, M., ALEMZADEH, I., ZARRABI, A., BAHARI, A. and ROOSTAAZAD, R. (2007). *Parametric optimization of the purification of restriction enzymes with low concentration using cation-exchange chromatography: Model-based approach*. pages 7–17.
- WAKAO, N., OSHIMA, T. and YAGI, S. (1983).
- WALSH, G. (2003a). *Biopharmaceutical benchmarks - 2003 (vol 21, pg 865, 2003)*. Nature Biotechnology, 21(11):1396.
- WALSH, G. (2003b). *Pharmaceutical biotechnology products approved within the european union*. European Journal of Pharmaceutics and Biopharmaceutics, 55(1):3. 647.
- WALSH, G. (2005). *Biopharmaceuticals: recent approvals and likely directions*. Trends in Biotechnology, 23(11):553.
- WALSH, G. (2006). *Biopharmaceutical benchmarks 2006*. Nature Biotechnology, 24(7):769.
- WANG, J. and ULBRICHT, M. (). *Influence of pore size distribution and architecture of functional layers on separation performance of flow-through macroporous membrane adsorbers*.
- WEISZ, P. B. and GOODWIN, R. D. (1963). *Combustion of carbonaceous deposits within porous catalyst particles .1. diffusion-controlled kinetics*. Journal of Catalysis, 2(5):397.
- WICKRAMASINGHE, S. R., CARLSON, J. O., TESKE, C., HUBBUCH, J. and ULBRICHT, M. (2006). *Characterizing solute binding to macroporous ion exchange membrane adsorbers using confocal laser scanning microscopy*. Journal of Membrane Science, 281(1-2):609.
- WILSON, D. S., KEEFE, A. D. and SZOSTAK, J. W. (2001). *The use of mrna display to select high-affinity protein-binding peptides*. Proceedings of the National Academy of Sciences of the United States of America, 98(7):3750.
- WILSON, E. J. and GEANKOPL.CJ (1966). *Liquid mass transfer at very low reynolds numbers in packed beds*. Industrial & Engineering Chemistry Fundamentals, 5(1):9.

- WINTERHALTER, C., HEINRICH, P., CANDUSSIO, A., WICH, G. and LIEBL, W. (1995). *Identification of a novel cellulose-binding domain within the multidomain 120-kda xy-lanase xyna of the hyperthermophilic bacterium thermotoga-maritima*. *Molecular Microbiology*, 15(3):431.
- WU, D. L. and WALTERS, R. R. (1992a). *Effects of stationary phase ligand density on high-performance ion-exchange chromatography of proteins*. *Journal of Chromatography*, 598(1):7.
- WU, D. L. and WALTERS, R. R. (1992b). *Effects of stationary phase ligand density on high-performance ion-exchange chromatography of proteins*. *Journal of Chromatography*, 598(1):7.
- XIE, J. R., AGUILAR, M. I. and HEARN, M. T. W. (1995a). *High-performance liquid-chromatography of amino-acids, peptides and proteins .138. adsorption of horse heart cytochrome-c onto a tentacle-type cation-exchanger*. *Journal of Chromatography A*, 691(1-2):263.
- XIE, J. R., AGUILAR, M. I. and HEARN, M. T. W. (1995b). *Studies on the adsorption capacities of proteins with a tentacle-type ion-exchanger and their relationship to the stoichiometric retention parameter $z(c)$* . *Journal of Chromatography A*, 711(1):43.
- YAMAMOTO, S. and ISHIHARA, T. (2000). *Resolution and retention of proteins near isoelectric points in ion-exchange chromatography. molecular recognition in electrostatic interaction chromatography*. *Separation Science and Technology*, 35(11):1707.
- YANG, H. W., BITZER, M. and ETZEL, M. R. (1999). *Analysis of protein purification using ion-exchange membranes*. *Industrial & Engineering Chemistry Research*, 38(10):4044.
- YANG, T., SUNDLING, M. C., FREED, A. S., BRENNEMAN, C. M. and CRAMER, S. M. (2007). *Prediction of ph-dependent chromatographic behavior in ion-exchange systems*. *Analytical Chemistry*, 79(23):8927.
- YAO, Y. and LENHOFF, A. M. (2004). *Electrostatic contributions to protein retention in ion-exchange chromatography. 1. cytochrome c variants*. *Anal Chem*, 76(22):6743.
- YAO, Y. and LENHOFF, A. M. (2005). *Electrostatic contributions to protein retention in ion-exchange chromatography. 2. proteins with various degrees of structural differences*. *Analytical Chemistry*, 77(7):2157.
- YOON, B. J. and LENHOFF, A. M. (1992). *Computation of the electrostatic interaction energy between a protein and a charged surface*. *Journal of Physical Chemistry*, 96(7):3130.
- YOUNG, M. E., CARROAD, P. A. and BELL, R. L. (1980). *Estimation of diffusion-coefficients of proteins*. *Biotechnology and Bioengineering*, 22(5):947.
- ZHENG, C. F., SIMCOX, T., XU, L. and VAILLANCOURT, P. (1997). *A new expression vector for high level protein production, one step purification and direct isotopic labeling of calmodulin-binding peptide fusion proteins*. *Gene*, 186(1):55.

REFERENCES

- ZHOU, J., CHEN, S. F. and JIANG, S. Y. (2003). *Orientation of adsorbed antibodies on charged surfaces by computer simulation based on a united-residue model*. *Langmuir*, 19(8):3472.
- ZHOU, J., ZHENG, J. and JIANG, S. Y. (2004). *Molecular simulation studies of the orientation and conformation of cytochrome c adsorbed on self-assembled monolayers*. *Journal of Physical Chemistry B*, 108(45):17418.
- ZHOU, J. X. and TRESSEL, T. (2006). *Basic concepts in q membrane chromatography for large-scale antibody production*. *Biotechnol Prog*, 22(2):341.

Education

- Mar 2008 to now **Graduate student** at the Institute of engineering in Life Sciences, TU Karlsruhe (relocation of the group)
- Nov 2005 to Feb 2008 **Graduate student** at the Institute of Biotechnology 2, Research Centre Juelich
Aug 2005 **Diploma** in Biology (technical oriented) at the University of Stuttgart
overall mark: excellent
- Dec 2004 to Aug 2005 **Thesis** at the Drug Design and Development Center (DDDC) in Shanghai, China
"Nuclear receptor families LXR and PPAR: A thermodynamic approach to characterize their interaction"
mark: 1.5 (excellent)
- May 2002 to Jul 2003 **Student Research Project** at Roche Pharmaceuticals in Shanghai, China
"Optimisation of the sterilization- and filling-procedure of an interferon α -2a based drug"
mark: 1.0 (excellent)
- Dec 2001 **Intermediate Diploma** with exams in Physics, Chemistry, Mathematics, Biophysics, Molecular Biology, Biochemistry, Zoology and Genetics.
mark: 1.7 (good)
- Oct 1999 to Aug 2008 **Studies of Technical Biology** at the University of Stuttgart
- May 1999 to Sep 1999 **Studies of Chemistry** at the University of Wuerzburg
-

Work Experience

- Oct 2003 to Jul 2004 Student assistant at the Department of Biotechnology, University of Stuttgart
- Dec 2002 to Jul 2003 Internship at Roche Pharmaceutical, Shanghai, China
- Jul 2001 to Nov 2002 Student assistant at the Department of Zoology, University of Stuttgart
- Jun 2000 to Jun 2001 Student assistant at the Department of Biophysics, University of Stuttgart
-

Scientific Publications

- Posters Florian Dismer, Jürgen Hubbuch
Determination of lysozyme binding orientation on different adsorber materials
ISPPP (International Symposium on Separation of Proteins, Peptides and Polynucleotides), 22.-24. September 2008, Baden-Baden
- Florian Dismer, Esther Knieps-Grünhagen, Jürgen Hubbuch
Confocal Laser-Scanning Microscopy: Pore Accessibility Determination with Single Adsorber Particles
ISPPP (International Symposium on Separation of Proteins, Peptides and Polynucleotides), 17.-20. October 2006, Innsbruck

Scientific Publications (continued)

Florian Dimer, Chris Teske, Jürgen Hubbuch

Effects of Alterations in Protein Surface Composition on the Retention Behavior in Ion Exchange Chromatography

GVC/Dechema-Congress "Industrielle Biotechnologie und Gewinnung von Produkten", 22.-24. May 2006, Würzburg

Talks

Florian Dimer, Martin Petzold, Jürgen Hubbuch

Einfluss von pH und Ionenstärke auf die Bindungsorientierung von Lysozym auf verschiedenen chromatographischen Adsorberoberflächen

ProcessNet, 07.-09. October 2008, Karlsruhe

Florian Dimer, Eric Willmann, Jürgen Hubbuch

High throughput screening in process development - a novel approach

Purification of Biological Products, 08.-10. September 2008, Philadelphia, USA

Florian Dimer, Martin Petzold, Jürgen Hubbuch

Lysozyme binding Orientation on different Adsorber Materials with varying pH and Ionic Strength

ISPPP (International Symposium on Separation of Proteins, Peptides and Polynucleotides), September 2007, Orlando, USA

Florian Dimer, Martin Petzold, Jürgen Hubbuch

Bindungsorientierung von Lysozym in Abhängigkeit von der Oberflächenstruktur verschiedener Ionenaustausch-Materialien

DECHEMA/GVC Tagung, "Aufarbeitung biotechnologischer Produkte", May 2007, Osnabrück

Florian Dimer, Martin Petzold, Jürgen Hubbuch

A novel approach to determine the binding orientation of lysozyme on chromatographic adsorber surfaces

EFB-DSP, "International Workshop on Downstream Processing", May 2007, Delft, Netherlands

Papers

Jun Wang, Florian Dimer, Jürgen Hubbuch, Mathias Ulbricht

Detailed analysis of membrane adsorber pore structure and protein binding by advanced microscopy

Journal of Membrane Science 320 (2008) 456-467

Florian Dimer, Martin Petzold, Jürgen Hubbuch

Effects of ionic strength and mobile phase pH on the binding orientation of lysozyme on different ion-exchange adsorbents

Journal of Chromatography A, 1194 (2008) 11-21

Mojgan Kavooosi, Nooshafarin Sanaie, Florian Dimer, Jürgen Hubbuch, Douglas G. Kilburn, Charles A. Haynes

A Novel Two-Zone Protein Uptake Model for Affinity Chromatography and Its Application to the Description of Elution Band Profiles of Proteins Fused to a Family 9 Cellulose Binding Module Affinity Tag

Journal of Chromatography A, 1160 (2007) 137-149

Florian Dimer, Jürgen Hubbuch

A novel approach to characterize the binding orientation of lysozyme on ion-exchange resins

Journal of Chromatography A, 1149 (2007) 312-320